Shape-Specific Hydrogel Nanoparticles with Defined Composition and Surface Properties for Gene Silencing

Stuart Scott Dunn

A dissertation submitted to the faculty of the University of North Carolina at Chapel Hill in partial fulfillment of the requirements for the degree of Doctor of Philosophy in the Department of Chemistry

Chapel Hill
2012

Approved by

Joseph M. DeSimone

Wei You

Maurice S. Brookhart

Sergei S. Sheiko

Leaf Huang

Abstract

STUART SCOTT DUNN: Shape-Specific Hydrogel Nanoparticles with Defined Composition and Surface Properties for Gene Silencing
(under the direction of Prof. Joseph M. DeSimone)

Diseases and disorders may be treated through RNA interference (RNAi), a natural post-transcriptional gene silencing event. Synthetic small interfering RNAs (siRNAs) may be designed to target specific genes for down-regulation in RNAi therapies. In the delivery of siRNA to target cells *in vivo*, numerous challenges are encountered such as susceptibility to degradation by RNases, clearance by the reticuloendothelial system, low internalization by cells, and endosomal escape. siRNA may be chemically modified or associated with lipid- or polymer-based particulate vehicles to enhance *in vivo* stability, increase bioavailability, improve transfection, facilitate accumulation in particular tissues, and enable cell-specific gene silencing. Independent control over the physicochemical properties of nanoparticles in the delivery of siRNA was enabled through a particle molding process that is a unique off-shoot of soft lithography known as PRINT® (Particle Replication in Non-wetting Templates) technology. Cationic hydrogel nanoparticles were tested using biocompatible poly(vinyl pyrrolidone)- and poly(ethylene glycol) (PEG)-based matrices for their ability to physically encapsulate and deliver siRNA to target cells. Effective gene silencing was observed *in vitro* using PEGylated hydrogel nanoparticles without inducing cytotoxicity. Functionalization of particles with maleic anhydride-derivatized ligands was pursued to produce a wholly acid-

labile system capable of targeting the transferrin receptor, endosomal escape, and delivery of siRNA.

To maximize retention of siRNA within hydrogel nanoparticles during systemic administration or functionalization with ligands, a pro-drug strategy was sought for covalent incorporation and triggered intracellular release of siRNA. Gene silencing efficiency and biocompatibility were optimized in the pro-drug siRNA system by screening the amine content of nanoparticles. When control cargos were implemented in the preparation of hydrogels, only target-specific, releasable siRNA cargo elicited gene knockdown. In effort to treat liver diseases, nanoparticles were functionalized with ligands targeting hepatocytes, cells of liver parenchyma implicated in diseases. Ligand-decorated nanoparticles were selectively internalized by hepatocytes *in vitro* and accumulated in hepatocytes *in vivo*. Hydrogel nanoparticles coated with ligands reduced target liver gene expression after administration to mice. Further investigation and exploration of this system will hopefully enable efficacious *in vivo* RNAi therapies in the treatment of numerous diseases.

ACKNOWLEDGEMENTS

The author acknowledges those who contributed to and assisted with the work herein: Dr. Shaomin Tian for providing essential input into data analysis and planning siRNA experiments such that the entire project could have not been pursued without her skilled expertise in conducting all *in vitro* and *in vivo* work; Dr. Warefta Hasan for conversing about the siRNA projects and research directions in general; Dr. J. Christopher Luft for his insightful contributions to research discussions, *in vitro* work, and collaboration on additional endeavors; Dr. Steve Blake for his great contribution to the project and for synthesizing acid-labile PEGs; other group members who have been part of the siRNA team, including Dr. Jing Xu, Dr. Jin Wang, Luke Roode, Dr. Dorian Canelas, Xin Gao, and Dr. Charlie Bowerman; Liquidia siRNA team members aided significantly in the development of PRINT nanoparticles described herein for RNAi therapies.

The professors from my undergraduate institution (Virginia Tech) who nurtured my interest in chemistry, polymers, and research played a crucial role in developing an appreciation for the potential of science. Most notably, my advisor at Virginia Tech, Prof. James E. McGrath, fostered my interest in research and pursuing applied polymer science. While at Virginia Tech, I had the opportunity to be taught by great mentors like Dr. Abhishek Roy and Dr. Harry Lee in the McGrath Group. Prof. Timothy and Vicki Long, Prof. Riffle, Prof. Esker, and Prof. Ward fueled my affinity toward physical chemistry and polymer

science. Prof. T. Daniel Crawford delightfully taught Physical Chemistry and provided excellent mentorship on computational quantum chemistry research.

Professors at UNC who supplemented knowledge in organic and polymer chemistry as well as advances in drug delivery are much appreciated. Facilities and training for chemical and particle analysis were provided by Dr. Sohrab Habibi (mass spectrometry), Dr. Marc ter Horst (NMR), and Drs. Carrie Donley, Amar Kumbhar, and Wallace Ambrose (CHANL).

I highly value the extracurricular times at Chapel Hill, playing basketball, Frisbee, softball, and flag football with peers. It has been a privilege to sit next to Tammy Shen who made the past years such a pleasurable time while providing essential energy sources at the snack shack. Cathy Fromen continually made lab entertaining and had a pumpkin always filled with lovely goodies. Vicki Haithcock and Crista Farrell were very helpful, resourceful, and pleasant in enabling group operations. I would like to especially thank everyone in the Chemistry Department and DeSimone Lab for their kindness and hospitality in providing an enjoyable place to conduct research over the years.

This exciting experience would not have been possible without the wonderful guidance, support, inspiration, and teachings from my exceptional advisor, Prof. Joseph DeSimone. Without significant biological knowledge or bio-related research experience, I was shown by Prof. DeSimone how to venture into uncharted terrain, establish concrete research aims, develop new approaches to realize goals, and keep the big picture in mind. The opportunity to work on different applications of PRINT technology has been an invigorating honor for which I sincerely thank Prof. DeSimone. I would like to say many

thanks to Prof. Mary Napier as well for always being open, understanding, and extremely insightful in discussing research and directions. Prof. Mary Napier was essential in pushing research forward, exploring new ideas, and staying focused on attainable paths.

My entire experience definitely would not have been made possible without continued support from my unconditionally loving family: mother and father, Linda and Scott; brother and friend, Trevor; and close members, Nana, Tim, Trisha, and The Shriders.

Table of Contents

List of Tables

List of Figures

List of abbreviations

ACN – acetonitrile

AEM – 2-aminoethylmethacrylate hydrochloride

AON – antisense oligonucleotide

DCM – dichloromethane

DMF – *N,N*-dimethylformamide

DLS – dynamic light scattering

DMSO – dimethylsulfoxide

DNA – deoxyribonucleic acid

DOPE – 1,2-dioleoyl-sn-Glycero-3-Phosphoethanolamine

DOTAP – *N*-[1-(2,3-Dioleoyloxy)propyl]-*N,N,N*-trimethylammonium chloride

D_z – *Z*-average diameter

EC_{50} – half maximal effective concentration

EDC – 1-ethyl-3-(3-dimethylaminopropyl) carbodiimide

EtOAc – ethyl acetate

HeLa – human cervical adenocarcinoma cell line

HPLC – high performance liquid chromatography

kDa – kilodaltons (1,000 g/mol)

NHS – *N*-hydroxysuccinimide

NIPAM – *N*-isopropylacrylamide

PBS – phosphate buffered saline

PEG – poly(ethylene glycol)

PFPE – perfluoropolyether

PLGA – poly(lactic-co-glycolic acid)

PRINT – Particle Replication In Non-wetting Templates

PVA – poly(vinyl alcohol)

RES – reticuloendothelial system

RISC – RNA-induced silencing complex

RNAi – ribonucleic acid interference

siRNA – small interfering ribonucleic acid

SEM – scanning electron microscopy

CHAPTER 1

INTRODUCTION TO GENE THERAPY AND RNA INTEFERENCE

1.1 Introduction to gene therapy and RNA interference

1.1.1 Gene therapy and background on nucleic acids

Diseases and cancers may be treated with gene therapy through the introduction of nucleic acids into target cells to modulate gene expression and remedy cellular malfunctioning. When errors arise in the production or processing of nucleic acids, propagation of genetic mutations can lead to diseases that pose serious threats to health. Cancer has received the most attention in clinical trials worldwide, comprising 64.7% of all trials while the next most commonly treated diseases are monogenic (8.5%) and cardiovascular (8.4%).[1] Examples of monogenic diseases include cystic fibrosis, haemophilia, and severe combined immunodeficiency disorder. In addition to monogenic and polygenic (e.g. cancer) diseases, gene therapy efforts have been focused on infectious diseases (HIV/AIDS), Alzheimer's disease, and Parkinson's disease in clinical trials.

Before delving into gene therapy endeavors in detail, an overview of basic biological processes should provide a foundation for understanding the mechanisms and motivations behind different therapeutic nucleic acids. To begin, nucleic acids are the fundamental building blocks of living organisms that provide the blueprints for protein production and cellular functions through genetic sequences. Instructions for the development and operations of inherited and environmentally influenced traits are contained within the code. Nucleic

acids are polynucleotides (linear polymers of nucleotides) linked 3' to 5' *via* phosphodiester bridges (Figure 1.1). There are five bases present in nucleic acids, where one is unique to DNA (thymine) and the other to RNA (uracil). The bases provide inter-chain hydrogen bonding that dictate structure, e.g. the double helix. DNA and RNA are the two natural forms of nucleic acids that are responsible for information storage (due to greater stability) and expression of the code (due to catalytic capabilities), respectively. An exception to this statement can be noted in some viruses that store their genetic information as RNA.

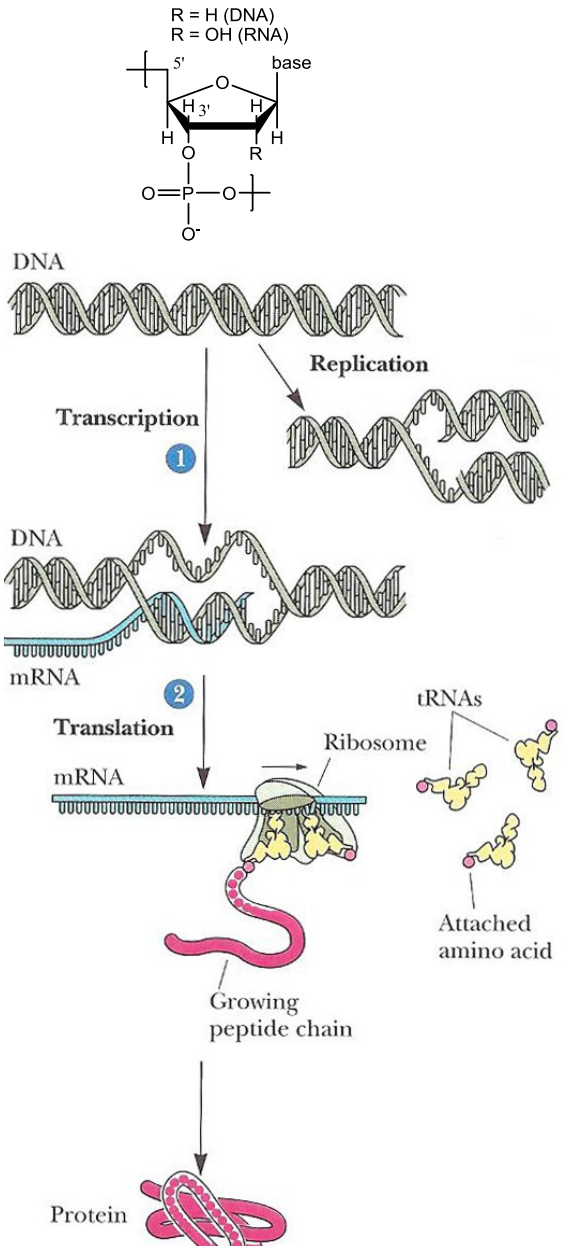

Figure 1.1 Biological processes for the synthesis of proteins from DNA.[1]

DNA has one critical biological role: carry and protect genetic code in chromosomes to provide information for generating all biofunctional macromolecules. Conversely, RNA can be seen in multiple copies, forms, and functions with one crucial role being the transfer of DNA to protein. Nucleic acid processing involves intricate pathways (Figure 1.1),[1] which play a role in essentially all cellular metabolic processes. DNA replication may yield an identical molecule, e.g. during cell division, while transcription is carried out by RNA polymerase to create complementary

base sequences to DNA in a single-stranded messenger RNA (mRNA). Three-base codons on mRNA define a particular amino acid and the sequence of a protein through translation. Transfer RNAs carry amino acids and recognize the mRNA codons for synthesis of proteins in the ribosome. Biological processes proceed through the transfer of information, starting from DNA, moving to mRNA, and then to protein, that governs biological behaviors and functions.

1.1.2 Nucleic acids for gene therapy

To fix malfunctions in genetic processing, nucleic acids may be delivered to restore normal cellular behavior that alleviates the disease. Currently, some of the most commonly delivered nucleic acids are plasmid DNA (pDNA), antisense oligonucleotides (AONs), and small interfering RNA (siRNA), each with unique repairing mechanisms. First, pDNA is an extrachromosomal form of DNA that generally exists as double stranded and ranges from 1-200 kilobase pairs, adopting open circular, linear, or supercoiled conformations. Once inside the cytoplasm, pDNA must travel to the nucleus by crossing the nuclear pore membrane for its expression. In therapeutic applications, pDNA must efficiently insert the critical genes to be expressed at specific chromosome locations within the genome to ultimately produce desired proteins. Several gene therapies based on plasmids have been approved and are in clinical trials, some designed to cure severe combined immunodeficiency, neuroblastoma, or cystic fibrosis by replacing or repairing defective genes while cancer may be treated through expression of tumor suppressing genes.[2]

Expression of genes may also be directly modified by introducing exogenous nucleic acids with the first example dating back to 1977 where single-stranded DNA was found to inhibit translation of a complementary RNA in a cell-free system.[3] Work continued in this

area with the discovery of the natural role of antisense RNA in gene regulation and modification, thereby promoting its potential to be harnessed for therapeutics.[4] Antisense therapies can be envisioned to take action at the gene or mRNA level. Single stranded triple-helix-forming oligodeoxynucleotides (TFOs) are an example of gene level regulators: they halt transcription by binding to the major groove of duplex DNA through Hoogsteen bonds (Figure 1.2) in purine- or pyrimidine-rich sequences, ultimately preventing the unwinding of DNA. TFOs can also induce mutations that repair an inherited or acquired defective gene by activating the cellular nucleotide excision repair system.[5,6] A requirement for successful TFO targeting and hybridization is that 10-30 nucleotide stretches of pyridines on one strand with pyrimidines on the other must be present, which makes TFO methods less appealing.

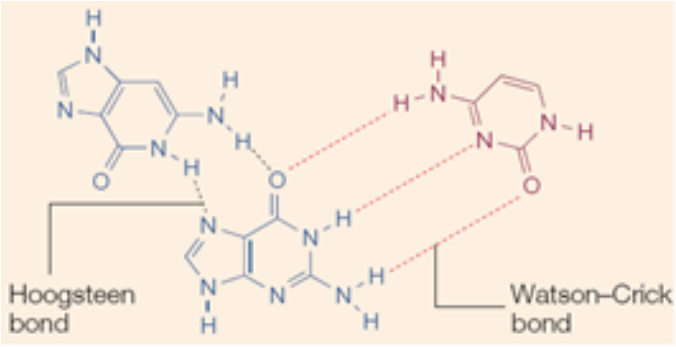

Figure 1.2 Gene level triple-helix formation to impede transcription through introduction of TFO, which binds to a Watson-Crick paired duplex.[7]

Another approach to take action at the gene level is to use short DNA or RNA decoy molecules that compete for transcription factor complexes.[8] In sequestering the transcription factors, the production of undesired mRNA may be arrested. Aptamers are a common example of RNA decoy molecules (25–40 nucleotides long) that display highly organized tertiary structures and provide specific, high-affinity binding to their target.[9] With many attractive features such as ease of production, low immunogenicity, and long-term storage,[10] aptamers are a very promising therapeutic with many potential targets like transcription

factors or proteins[11] involved in diseases. However, aptamers are sometimes limited by the requirement for local administration: systemic *in vivo* delivery would impair proteins in untargeted organs; still, there is hope with new delivery technologies.

Now, therapeutics working at the mRNA level will be addressed: stoichiometrically, it seems less effective than attacking the genetic "source" (DNA); however, mRNA is more susceptible to attack since it is single-stranded and unprotected in transcription, transport from nucleus to cytoplasm, and translation. Once again, decoys (RNA now) may be employed to compete with protein binding sites that serve as translational activators or mRNA stabilizers.[12,13] Consequently, decoys can prevent translation or induce mRNA instability, leading to its degradation. More commonly, antisense approaches are taken to interfere with gene expression by providing a nucleic acid with a complementary sequence to the mRNA of interest for hybridization and subsequent treatment. Direct sequence-specific cleavage of transcripts may be achieved with ribozymes or DNAzymes that bind to target RNA through Watson-Crick base pairing and contain a catalytic moiety that cleaves the hybrid.[14,15]

Still targeting mRNA, AONs have evolved from generation to generation, enhancing stability and efficiency. First, the backbone of AONs was modified by replacing one of the free oxygen atoms on the phosphate group with sulfur, leading to the name phosphorothioate deoxyoligonucleotide. Stable to nuclease degradation and effective in targeting mRNA for cleavage by RNAse H (a ribonuclease that cleaves the phosphodiester bond), these phosphorothioate oligonucleotides showed success;[16] however, they can bind nonspecifically to serum proteins, leading to toxicity and side effects.[17] Next, alkyl modification were made to the ribose ring at the 2' position to yield 2'-*O*-methyl or 2'-*O*-methoxy-ethyl RNA that are

less toxic and show high targeting specificity.[18] Nevertheless, degradation of mRNA through RNAse H cannot be triggered and translation of mRNA is generally blocked by duplex formation; therefore, silencing efficiency is relatively low. Not directly binding mRNA, antisense 2'-*O*-methylribooligonucleotides can be targeted against specific mutated sequences in pre-mRNAs to restore correct splicing of RNAs *in vitro*; this has been seen in targeting β-globin pre-mRNA to treat β-thalassemia and prevent anemia.[19]

micro RNA have only limited complementarity (in the seed region) to the target mRNA, resulting in repression of translation and non-sequence-specific mRNA degradation.[20] Design of AONs is constantly improving as can be seen with recent developments of peptide nucleic acids[21] and morpholino deoxynucleotides,[22] which have significant modifications to the backbone and nucleotide structures (bases are maintained). These highly derivatized AONs exhibit complete nuclease resistance and a translation-blocking mechanism of the target instead of activating RNAse H for target degradation.

Direct gene silencing may be achieved efficiently with siRNA, which are short (20–25 nucleotides), double-stranded RNA, that play crucial biological roles, especially in RNAi. Phase I clinical trials for treating age-related macular degeneration have shown that siRNA is well tolerated and has desirable pharmacokinetic properties for gene therapy.[23] Naturally or synthetically produced, the antisense strand of siRNA is targeted to a specific gene, which has a complementary sequence. Once recognized by the RNA-induced silencing complex (RISC), a ribonucleoprotein complex in the cytoplasm, siRNA is unwound and incorporated into RISC to locate and bind to its target mRNA sequence. After siRNA binds to the complementary mRNA strand, RISC activates a ribonuclease that cleaves and degrades the duplex; thus, expression of the target gene is prevented using the natural pathway of RNAi.

Regardless of the therapeutic nucleic acid identity and function, the cargo must be delivered to the cells of interest, which often proves to be a challenge. To facilitate delivery of therapeutic payloads into target tissues, cells, and intracellular compartments, delivery vehicles or external devices are often implemented.

External devices that utilize electric currents include electroporation, which involves applying an electric field to permeabilize cell membranes, and iontophoresis, which uses a small electric current to deliver charged molecules through skin and tissue. Ultrasound therapy has been used along with microbubbles in sonoporation to permeabilize membranes for gene delivery. The gene gun was invented to transfect DNA-coated nanoparticles into cells to express genes, which has been used in vaccine and plasmid delivery.

Delivery vehicles may include viruses or nanoparticles for encapsulating the cargo, protecting it from degradation, targeting receptors on cells of interest, and releasing the cargo in specific extracellular or intracellular locations. Viral vectors are the most commonly used delivery vehicle as they demonstrate extremely high transfection efficiency since the nanoparticle assembly has evolved over time to transfect genetic material efficiently. The process of delivering nucleic acids to target cells, known as transfection, faces challenges *in vivo* and *in vitro*. When nucleic acids are administered systemically *via* intravenous injection, nucleic acids (in particular, RNAs) are subject to degradation by nucleases, clearance by the reticuloendothelial system, and protein fouling. Internalization of nucleic acids by cells may not proceed efficiently since the highly charged nucleic acid is generally repelled by the negatively charged cell membrane. After uptake of nucleic acids by cells, they must travel to specific intracellular locations, such as the cytoplasm or endocytic vesicles for oligonucleotides and the nucleus for plasmid DNAs.

1.1.3 RNAi for silencing expression of genes in cells

After covering different therapeutic nucleic acids and their functions for regulating gene expression, notable highlights for siRNA include simple delivery to the cytoplasm (instead of the nucleus), harnessing the natural pathway of RNA interference (RNAi), high potency with catalytic activity, minimization of adverse side effects (that could be caused with drugs), and the ability to theoretically target any gene of interest. Avoiding delivery to specific intracellular compartments (e.g. vesicles or the nucleus) enables rather facile intracellular delivery of siRNA. The post-transcriptional gene regulating phenomenon known as RNAi provides innate defense against invading viruses and transposable elements.[24] In 1998, Fire and Mello discovered RNAi in the nematode *Caenorhabditis elegans*[25] for which they received the Nobel Prize in Physiology or Medicine in 2006. Next, Tuschl and coworkers demonstrated that synthetic, 21- to 22-nucleotide long double-stranded RNAs are sequence-specific mediators for RNAi.[26]

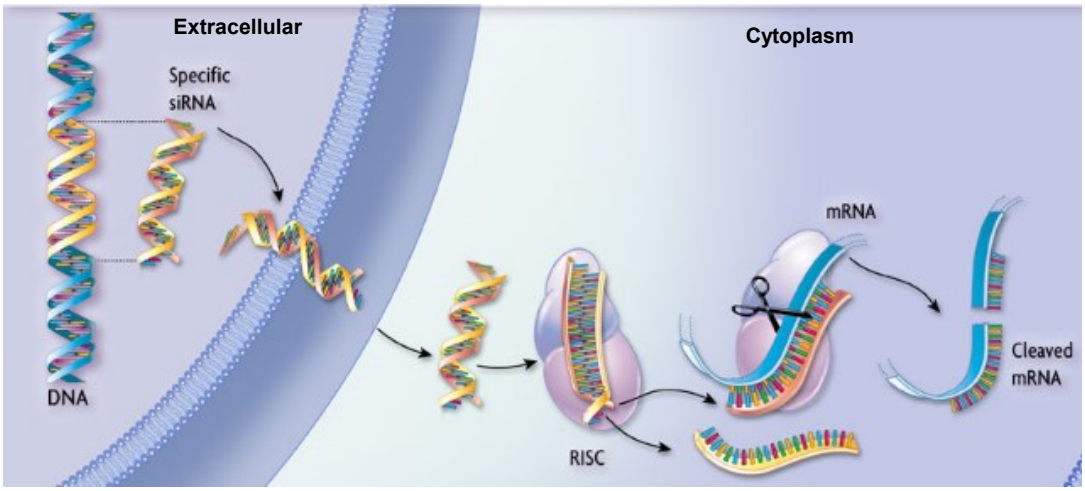

Figure 1.3 Illustration of intracellular gene silencing mechanism mediated by exogenously introduced synthetic siRNAs incorporated into the RNA-Induced Silencing Complex (RISC). Adapted from Alnylam, Inc.

Synthetic siRNAs can be designed to target a specific gene with minimal off-targeting effects. After introduction into the cytoplasm of a cell, siRNA becomes incorporated into the

RNA Induced Silencing Complex (RISC), which unwinds the double-stranded siRNA such that the antisense strands then targets its complementary mRNA sequence (Figure 1.3). Once the antisense strand of siRNA binds to mRNA in the RISC, the mRNA is degraded in the cell, preventing its translation and the expression of a target protein. siRNA acts catalytically by incorporating into the RISC, whose endonuclease activity is directed by the siRNA, and should minimally shutdown off-target genes due to the extensive complementarity required between the mRNA and siRNA.[27] Multiple siRNA libraries exist in literature and industry for addressing different gene families and functions.

1.2 RNAi for therapeutic applications and targeting diseases

1.2.1 Design of siRNA for effective gene knockdown

Antisense siRNA sequences may be systematically screened for triggering degradation of mRNA from target genes. Characteristics of the siRNA have been shown to influence potency for gene silencing. For example, low G/C content, lack of inverted repeats, and sense strand preferences were identified to play key roles in siRNA functionality as determined in a comprehensive analysis of 180 siRNAs targeting mRNA of two genes.[28] Establishing siRNA candidates is a multi-step process, taking into account roles in functionality such as single nucleotide polymorphisms as well as mismatch target site tolerance and discrimination to produce allele-specific siRNAs.[29] Dharmacon, Inc., a leader in RNAi technology, offers SMARTselection, which is an 8-step process that identifies ideal sequences for siRNAs targeting specific genes. Minimizing off-targeting effects and expanding knowledge of silencing specificity will further the evolution of effective RNAi therapies with increased potency.

Modifications to siRNA and antisense oligonucleotides have been explored to alter bioavailability, serum stability, and transfection. Chemical structures of different oligonucleotide chemistries focus on backbone and substituent modifications (Figure 1.4). For example, phosphorothioate (PS) backbones and 2'-*O*-methyl substituents increase resistance to degradation by nucleases and enhance binding to target RNAs.[30] Locked nucleic acids (LNA) also increase binding to target mRNA and phosphorodiamidate morpholino oligomers (PMO) yield neutral oligonucleotide analogs that are extremely stable in the presence of nucleases. Positively charged piperazine, amino, and arginine-containing PMOs offer enhanced cellular internalization and transfection. Modifications to siRNA that enhance resistance to nuclease stability may not increase the duration of gene silencing, but rather protect siRNA from degradation in the extracellular environment.

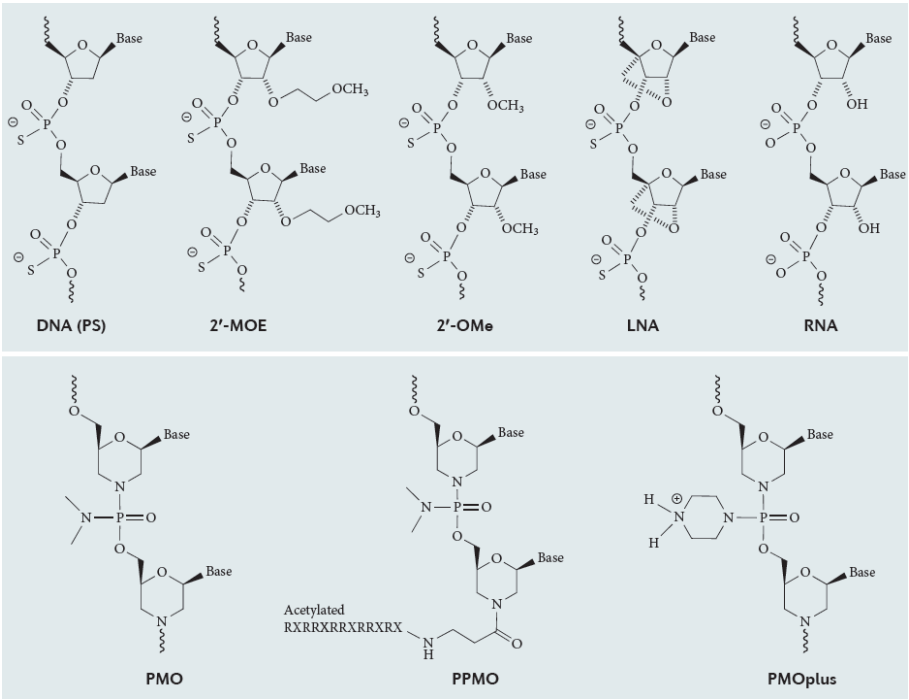

Figure 1.4 Structures of oligonucleotide derivatives for enhanced stability, mRNA binding, and intracellular delivery.[30]

Unmodified siRNAs exhibit intracellular stability in living cells, suggesting that siRNAs are largely degraded in the extracellular environment.[31] Kinetics of gene silencing

really depend on cell division: unmodified siRNA achieved gene silencing that lasted roughly a week in rapidly dividing cells while knockdown persisted for a month in slowly dividing fibroblast cells.[32] To confirm gene silencing kinetic mechanisms, cells with low proliferation were investigated: prolonged RNAi was observed in primary macrophages[33] and mammalian cells.[34] After optimizing sequence specificity and stability of siRNAs, *in vivo* efficacy mainly depends on effective delivery to the target tissue and cell. Design of delivery vectors and devices plays a crucial role in influencing biodistribution, cell uptake, and delivery to the cytoplasm. First, one must begin with the disease at hand to develop delivery systems before determining the best route of administration.

1.2.2 Targeted diseases in the clinic for RNAi

Since RNAi offers the ability to theoretically target any gene by using the appropriate sequence to silence translation of a given mRNA, several types of diseases have been investigated in the clinic with RNAi such as ocular and retinal disorders, cancer, kidney disorders, infectious diseases, and liver diseases. Select clinical trials utilizing siRNA for different applications are listed in Table 1.1.[35] For example, in collaboration with siRNA therapeutics, Allergan pursued intravitreal injection of siRNA targeting vascular endothelial growth factor receptor 1 (VEGF1) to treat age-related macular degeneration choroidal neovascularization. Administered siRNA was well-tolerated without dose-limiting toxicity. Stabilization and improvement in visual acuity and foveal thickness was noted for patients treated with RNAi therapy.[36] Chronic myeloid leukemia (CML) was tackled by Hadassah and the Department of Defense with a S40 lentiviral vector encapsulating siRNA targeting one of the two fusion genes in CML patients. The S40 pseudoviral vector was noted to be

efficient in gene transmission into human hematopoietic cells, resulting in inhibited cell growth and increased sensitivity to imatinib, a tyrosine kinase inhibitor.[35]

For the injury of kidney acute renal failure, Quark Pharmaceuticals intravenously injected naked siRNA (I5NP) to inhibit the expression of the pro-apoptotic protein, p53. Dose-dependent attenuation of apoptotic signal was observed where analysis of renal histology and apoptosis revealed improved injury scores in both cortical and corticomedullary regions. Furthermore, this siRNA to p53 was also effective in a model of cisplatin-induced kidney injury.[37]

Table 1.1 Clinical trials for RNAi therapies.[35]

Disease	Sponsor	Drug	Target	Status
Macular degeneration	Opko Health, Inc.	Bevasiranib	VEGF	Phase II
Glaucoma	Sylentis	SYL040012	β2 adrenergic receptor	Phase II
Solid tumor	Calando Pharm.	CALAA-01	RRM2	Phase I
Metastatic melanoma	Duke University	NCT00672542	LMP2, LMP7, and MECL1	Phase I
Liver cancer	NCI	TKM-080301	PLK1 gene product	Phase I
Hepatitis B virus	Nucleonics, Alnylam Pharm.	NUC B1000	HBV mRNA	Phase I
Hepatitis C virus	Santaris Pharma	SPC3649	miR-122	Phase II
Respiratory syncytial virus	Alnylam Pharm.	ALN-RSV01	RSV N-gene	Phase II
Kidney injury	Quark Pharm, Inc.	QPI-1002/I5NP	p53	Phase I

Opko Health, Inc. sought to treat diabetic macular edema through intravitreal injection of Cand5, a siRNA that targets VEGF. At multiple dose levels in patients with wet age-related macular degeneration, Cand5 was found to be well-tolerated, but the siRNA only blocked production of new VEGF (not pre-existing forms); therefore, desirable efficacy was

not attained. Baseline treatment with VEGF may be required first to take care of pre-existing VEGF to realize therapeutic value for Cand5.[38] To attain RNAi efficacy in clinical trials, platform technologies are under development to enhance delivery of siRNA.

1.3 Platforms for RNAi therapies

1.3.1 Route of administration for delivery of RNAi therapeutics

Accessibility to diseased tissue by siRNA determines the route of administration, which broadly includes local, topical, and systemic. Localized delivery of siRNA involves direct application to the accessible tissue of interest. Administration of siRNA to the skin comprises topical modes of delivery. In tissues which are not accessible directly or through topical application of RNAi therapies, systemic administration becomes necessary. Systemic delivery concerns the intravenous injection of therapeutics, which take on the intravascular journey, encountering *in vivo* barriers *en route* to the target tissue and cell. Select *in vivo* studies implementing local, topical, and systemic delivery approaches are outlined as therapeutic interventions in Table 1.2.

Table 1.2 Different routes of administration for RNAi therapies.

Route of administration	Disease	Organ	siRNA target
Electroporation[39]	Cancer	Prostate	VEGF
Iontophoresis[40]	Atopic dermatitis	Epidermis	IL-10
Ultrasound[41]	Yolk sac carcinoma	Tumor	MDR1
Topical[42]	Inflammatory bowel	Rectum	CCR5
Inhalation[43]	Cancer	Lung	PI 3-kinase, NF-κB
Topical[44]	Angiogensis	Eye	TLR3
Intracranial[45]	Alzheimer	Brain	BACE1
Systemic[46]	Ewing's sarcoma	Metastasized tumors	EWS-FLI1

As a form of local delivery, electroporation involves application of controlled electric fields to permeabilize cells for the introduction of siRNA. Implementing "plate and fork" electrodes, efficient delivery of siRNA *in vivo* through electroporation was achieved to suppress growth of prostate cancer tumors.[39] Application of ultrasound to gas-encapsulated microbubbles enables sonoporation (permeabilization of cells with sound), which can be harnessed for gene therapy. Perfluoropropane gas-encapsulated, PEGylated bubble liposomes were combined with siRNA and ultrasound was applied to enable gene silencing *in vitro* and *in vivo*.[47] Inhalation of RNAi therapies offers a unique way to reach previously untreatable respiratory conditions. Inflammatory and immune conditions, cystic fibrosis, infectious diseases, and cancer may be tackled with RNAi therapies through inhalation.[48]

Alnylam has completed Phase 2b clinical trials on a novel RNAi antiviral therapeutic directed against respiratory syncytial virus. Developing systemically-administrable siRNA delivery platforms that enable tissue- and cell-targeting capabilities without immunogenicity or toxicity should offer translation to other routes of administration. In search of robust RNAi delivery platforms, nanoparticles present opportunities to enhance stability, increase bioavailability, target tissues and cells, and optimize transfection through combinatorial material screening.

1.3.2 *In vivo* barriers to systemic delivery of siRNA

Although nanoparticles may offer beneficial features to enhance RNAi therapies, several challenges are still encountered during the *in vivo* journey after systemic injection. Delivery is the key challenge to successful RNAi *in vivo*. As illustrated in Figure 1.3, systemic delivery begins with intravenous injection of an aqueous dispersion containing nanoparticles. Hurdles encountered in effective systemic delivery of siRNA include (A)

filtration, phagocytosis, and degradation in the bloodstream, (B) extracellular matrix diffusion, (C) cellular receptor targeting and uptake, (D) endosomal escape, (E) siRNA release or dissociation from the carrier, and (F) intracellular trafficking to the RISC to degrade mRNA as illustrated in Figure 1.5. Delivery of naked siRNA may be performed; yet, it is highly susceptible to rapid clearance and nuclease degradation, showing low cell uptake in systemic delivery.

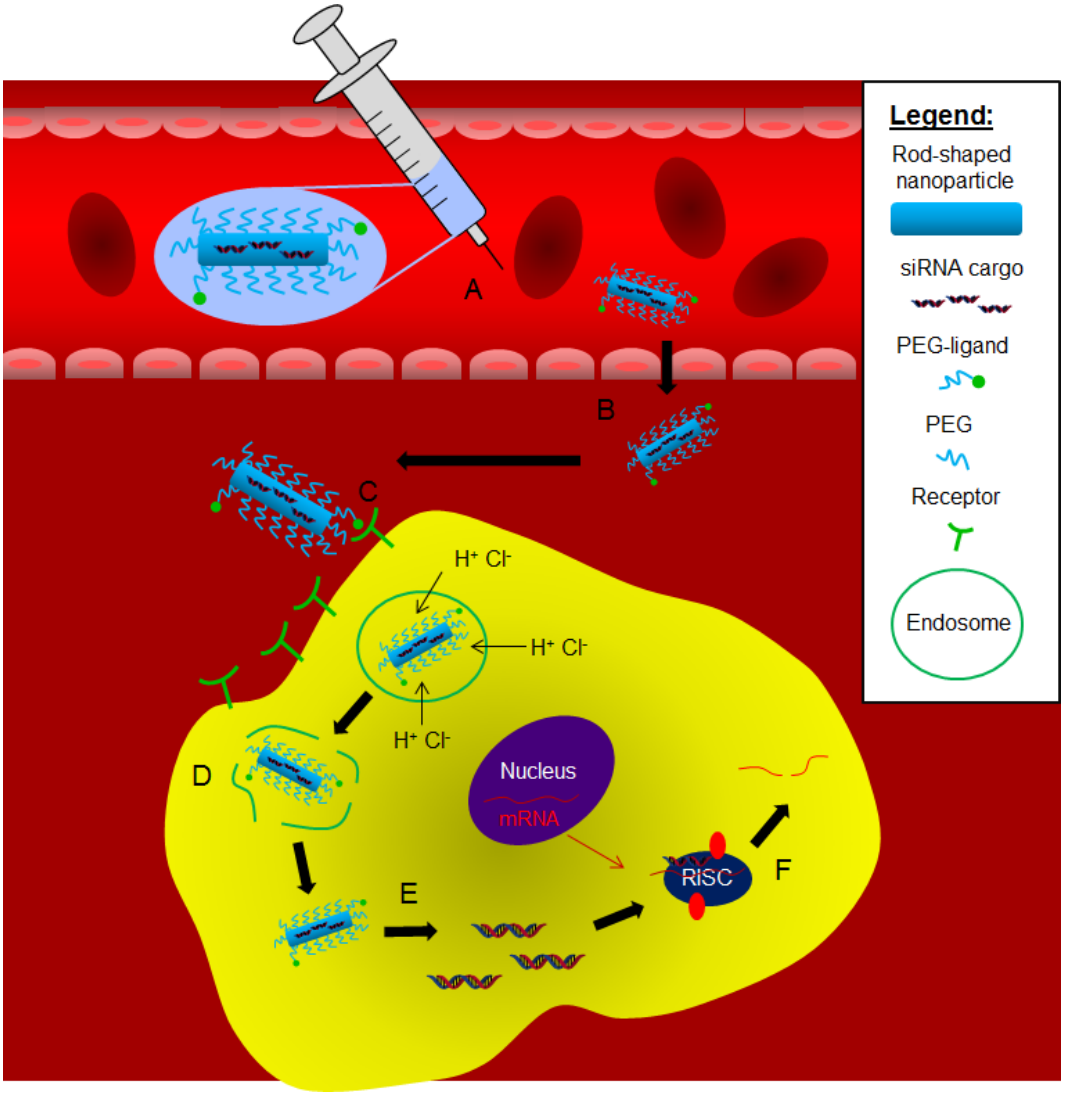

Figure 1.5 *In vivo* barriers to systemic delivery of siRNA-containing nanoparticles. Administration of nanoparticles, which must: A, avoid clearance and degradation in serum; B, travel across the vascular endothelium; C, diffuse in the extracellular matrix to target cells for receptor-mediated endocytosis; D, escape endosomal vesicles; E, release siRNA in the cytoplasm; F, halt expression of target proteins and degrade mRNA.

Hydrodynamic injection of naked nucleic acids may overcome some barriers by using a large volume of high pressure solution; however, potential side effects like high blood pressure, low heart rate, and death tarnish the appeal. Encapsulation of siRNA in delivery vehicles may allow for improved efficiency, stability, and cell specificity while avoiding immune responses. Methods to obtain proper packaging of siRNAs, stability, resistance to nuclease degradation, and efficient transfections are constantly being developed. Ideal nanoparticle features for RNAi in liver or tumor targets include small size (< 150 nm), effective siRNA loading and stability, surface decorations like PEG and targeting ligands, dispersion stability in serum, endosomolytic (endosome lysing) behavior, and effective unpackaging of siRNA cargo in the intracellular environment.

In the first step of the journey, siRNA may avoid degradation by nucleases through appropriate chemical conjugation and/or inclusion within a protective delivery vector. Prolonged serum circulation may be achieved by mimicking biological features of red blood cells such as with low modulus hydrogel microparticles.[49] To minimize filtration, nanovectors should be greater than 5-10 nm in diameter to avoid kidneys. PEGylation of nanoparticles has been demonstrated to play a crucial role in minimizing clearance by the immune system, specifically phagocytic cells of the mononuclear phagocytic system, which excels in clearing foreign entities, providing immunity, and clearing nanoparticles. PEG provides a stealth-like hydration layer around particles to prevent absorption of serum proteins and opsins, which would trigger clearance from the bloodstream. Given appropriate time and nanoparticle sizes, diffusion across the extracellular milieu to the target cell may be governed by biophysical properties of the delivery vehicle. For instance, liver parenchyma (Figure 1.6) consist of 150 nm fenestrations in their sinusoids that present a size restriction

upon nanoparticles, which must be below the size of fenestrations to effectively reach liver parenchymal cells (hepatocytes).

After diffusing through extracellular space to the target cell, ligand-conjugated nanoparticles may bind to receptors to undergo receptor-mediated endocytosis whereby the cell internalizes the vector into an endocytic vesicle. Depending on the cell line and individual species, approximately a thirty minute window exists for the nanoparticle to escape the endocytic vesicle before lysosomal fusion occurs in which degradation of contents by proteases and nucleases will occur. Often amine-containing materials are implemented in nanoparticle formulations to escape the endosome by harnessing the so-called "proton sponge effect". Progression of the endosomal vesicle over time is accompanied by decreasing pH, proceeding from physiological values to ca. pH 5.5 at the late-stage of the endosome's lifetime. Ionizable groups that have pKa values ranging from physiological to endosomal values are capable of buffering the decreasing pH of the endosome, resulting in an influx of protons and chloride ions to maintain the pH of the endosome. Resulting, osmotic pressure may increase such that the endosome becomes unstable and ruptures, releasing its contents into the cytoplasm. Alternatives to exploiting the "proton sponge effect" include use of membrane-lysing or -fusing species as well as pore-forming peptides. In the process of or after endosomal escape, nanoparticles may release siRNA into the cytoplasm where it incorporates into the RISC to silence gene expression by binding to and triggering degradation of target mRNA.

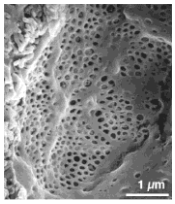

Figure 1.6 Hepatic liver sinusoids with ca. 150 nm fenestrations.[50]

1.3.3 Viral vectors for gene therapy *in vivo*

Produced by nature, viruses are highly evolved nanoparticles of uniform size that are coated by a protein shell and contain RNA- or DNA-based genes, which are responsible for diseases ranging from minor afflictions such as chickenpox or cold sores to major ones like acquired immune deficiency syndrome or severe acute respiratory syndrome. The distinct shapes (e.g. icosahedral, helical, or enveloped) and sizes of viruses provide superior abilities to infect organisms. Noting their efficiency for inducing disease, viruses may be captured and modified to create viral vectors or studied to design synthetic vectors, both aimed in opposition to the purpose of viruses: curing disease.

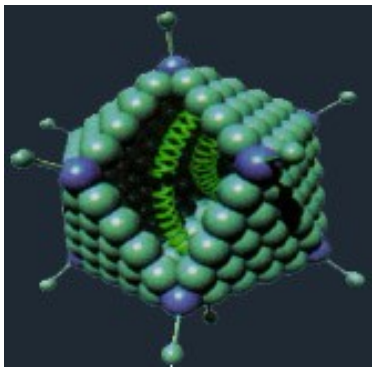

Figure 1.7 Structure of adenovirus with knobs as cell receptor binding agents, spheres as proteins, and duplexes as nucleic acids inside.[51]

Viral vectors are self-assembled particles (~ 100 nm in diameter) and are generally composed of lipids, proteins, and nucleic acids. Several types of these vectors exist: one is the retrovirus, which protects nucleic acids in a lipid bilayer, while an adenovirus (Figure 1.7) separates nucleic acids from the environment by a set of tightly packed coat proteins. Crucial viral proteins are (a) capsids for nucleic acid condensation, (b) envelopes for cell receptor binding, and (c) enzymes for releasing and integrating their cargo into the cell.[52] Interestingly, retroviruses can only enter the cell nucleus during mitosis whereas adenoviruses bear nuclear localization signals on surface proteins that facilitate their entry

through the nuclear pore complex.[53] A lentiviral vector was created for delivery of siRNA targeting BACE1 in a transgenic model that ameliorated Alzheimer disease neuropathy.[45]

Considering the aforementioned viral characteristics, viral vectors can overcome the major biological hurdles; however, significant drawbacks still are present. Specifically, they can be difficult to mass-produce, immunogenic (toxic), and limited to low cargo capacity.[54] Some have been noted for their potential to induce mutagenic integration.[55] Tragically, viral vector gene therapies have resulted in death: the first was in 1999 with a patient suffering from the inability to metabolize ammonia where the vector triggered an immune response that led to multiple organ failure and brain death;[56] another involved the treatment of a healthy patient for rheumatoid arthritis in 2007.[57] Serious risks are present in gene therapy; still, instead of these tragedies being research deterrents, they may be viewed as warnings to proceed with extreme caution before implementing a system that has not been rigorously tested. Furthermore, viral vectors may be investigated to understand how tragedy may be prevented while extracting their features for delivery. An alternative to viral vectors for delivery of therapeutics involves synthetic vectors.

1.3.4 Non-viral, synthetic vectors for RNAi

For synthetic delivery vehicles, immune responses may be avoided while repeated administration, large-scale production at low cost, and complete control over composition may be realized.[58] Since synthetic vehicles may not be composed entirely of biological molecules, the first assessment of efficacy resides in biocompatibility, which has been broadly defined as "the ability of a material to perform with an appropriate host response in a specific application".[59] Evaluating toxicity is crucial in determining the applicability of a material for *in vivo* delivery, which has been extensively reviewed[59,60] and will be discussed

later. Some of the most common carrier molecules for condensing and protecting siRNA are cationic lipids and polymers, which yield lipoplexes and polyplexes, respectively. One of the most commonly employed polycations for nucleic acid delivery is poly(ethylene imine) (PEI), illustrated in Figure 1.8, due to its high gene transfection activity. Molecular weight and structure (linear or branched) of PEI substantially impact toxicity and transfection.[61] The mechanism for transfection by PEI has been attributed to the 'proton sponge effect': amine groups provide pH buffering in the endosome to maintain neutrality and the influx of ions causes osmotic swelling and bursting of the endosome, resulting in a release of its contents into the cytosol. Thereafter, the polyplex may dissociate so that the polymer may be processed while siRNA incorporates into the RISC.

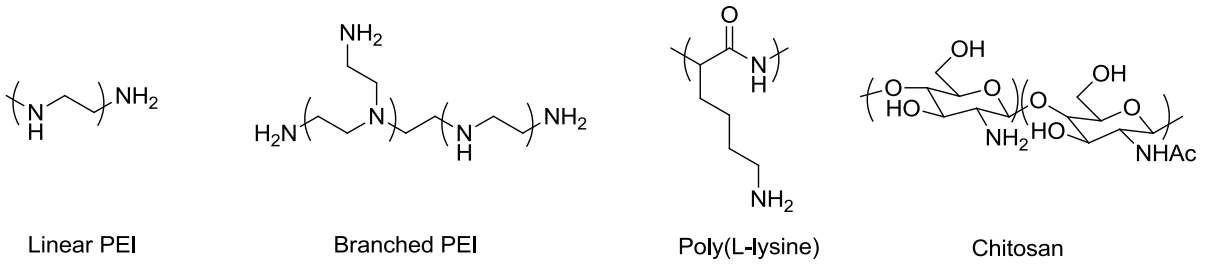

Figure 1.8 Chemical structures of cationic polymers used for siRNA delivery.

Nucleic acid condensation (or compaction), protection, and transfection may be optimized with polycations using computer simulations. For example, considering DNA as a semiflexible polymer, a coil-globule transition exists between the elongated and "liquid-drop-like" compact states. With condensing agents like polyethyleneimine (PEI), the nature of the folding transition of DNA governs the final state: a continuous transition yields a globule whereas a nano-ordered crystalline state is produced in a discrete transition. The globule size is larger, more swollen, and loosely-packed than the ordered crystal.[62] Consequently, unique shapes may be observed such as toroids and rods, which can be harnessed for effective nucleic acid delivery. The degree of packing may heavily influence

protection of the nucleic acid and dissociation of the polyplex in systemic delivery. Studies may be performed to identify the best-suited polycation structure for delivering a particular nucleic acid or siRNA as a polyplex. Commonly used cationic polymers for transfection are illustrated in Figure 1.9 where amine functionality seems to be a common feature, providing complexation to nucleic acids, cellular uptake, and endosomal escape.

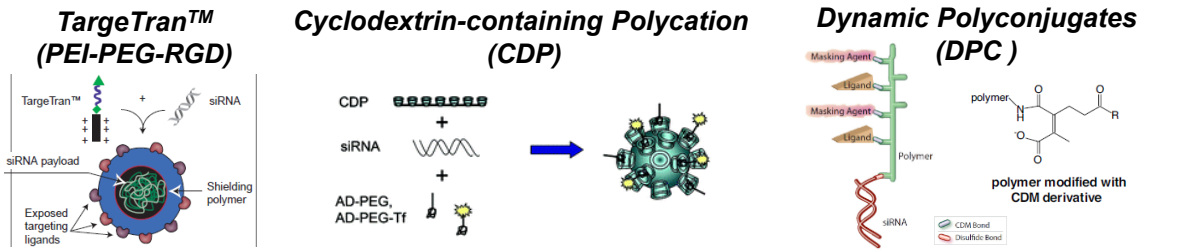

System	Group	Materials	Targeting	Approach	Properties	siRNA	Model	Efficacy
TargeTran	Intradigm	Branched polyethylene-imine 25 kDa	PEG-Cyclic RGD	Functionalization of PEI	$D \approx 100$ nm $\zeta \approx +6$ mV	VEGFs	Neuro2A	Inhibition of angiogenesis
CDP	Calando, M. E. Davis	Amidine and imidazole CDP	PEG-Transferrin	Adamatne – CD inclusion complex	$D \approx 70$ nm $-10 < \zeta < +10$ mV	RRM2	Melanoma	First RNAi elicited in humans
DPC	Mirus, J. A. Wolff	Poly(butyl-amino vinyl ether)	PEG-Galactose	Maleamate mask; disulfide conjugate	$D \approx 10$ nm $-20 < \zeta < 0$ mV	apoB	Liver	Reduction in serum cholesterol

Figure 1.9 Non-viral polycation systems for effective *in vivo* RNAi.

Notable cationic polymer-based delivery vehicles are illustrated in Figure 1.7 along with details regarding the nanoparticle characteristics, *in vivo* models, and efficacy. PEI was functionalized an RGD ligand, targeting integrins on tumor endothelium, through a PEG spacer to provide a functional cationic polymer capable of condensing, protecting, and delivering siRNA to target cells while exhibiting colloidal stability and reduction of surface charge and aspecific cellular uptake.[63] Cyclodextrin-containing polycations featuring amidine and imidazole ionizable groups were mixed with adamantane-terminated PEG, PEG-transferrin, and siRNA to produce nanoparticles capable of effective RNAi *in vivo*, demonstrating the first gene silencing in human subjects with melanoma.[64] A series of

amphipathic amino poly(alkyl vinyl ether)s were pursued for establishing endosomolytic materials capable of transfection.[65] After determining the ideal alkyl chain length in amphipathic polycations, an approach to mask the membrane-lytic behavior was established by reversibly conjugating maleic anhydride derivatives.[66] Subsequently, conjugation of siRNA through a labile bond to amphipathic polycations functionalized with PEG and ligand-functionalized PEG enabled *in vivo* RNAi in mice liver toward the reduction of serum cholesterol.[66]

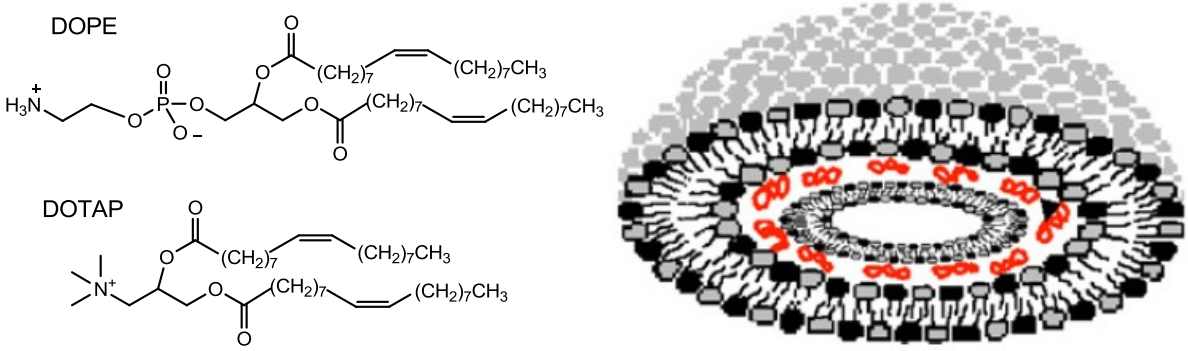

Figure 1.10 Structures of DOPE and DOTAP lipids as well as an illustration of a multilamellar lipoplex with nucleic acid sandwiched between bilayers.[67]

Lipoplexes are generally prepared from cationic liposomes to obtain desirable encapsulation efficiency of the siRNA. Cationic liposomes can be generated by dispersing cationic and neutral lipids, which contain a polar headgroup and hydrophobic tail, in aqueous solution, resulting in the formation of spherical bilayered liposomes. Common cationic and neutral lipids employed are *N*-(1-(2,3-dioleoyloxy)propyl)-*N,N,N*-trimethyl-ammoniumchloride (DOTAP) and dioleoylphosphatidylethanolamine (DOPE), shown in Figure 1.10. Here, DOTAP serves to bind the negatively charged nucleic acid while DOPE, a cone-like lipid, promotes endosomal escape by adopting a hexagonal phase that disrupts the membrane.[68] Lipoplexes are spontaneously formed through electrostatic interactions between

the nucleic acid and cationic liposome, leading to self-assembly of lipid bilayers between which the nucleic acid is present for multilamellar lipoplexes (Figure 1.10).[69]

Lipid-like materials have been most commonly pursued for the effective *in vivo* delivery of siRNA. In Figure 1.11, efficacious *in vivo* RNAi therapies using lipid-based delivery vehicles are illustrated. Cationic or neutral lipids are often formulated with cholesterol to enhance bilayer stability and PEGylated lipids to provide the hydrophilic stealth-like qualities for prolonged circulation. The rational design of lipids involved pursuit of liposomal structures that would undergo an inverted hexagonal phase in the endosome to fuse with endosomal membranes in a flip-flop manner to release cargo into the cytosol.[70] Ionizable cationic lipids with secondary amine functionality were screened with different linkers to observe the influence on RNAi *in vivo*. An acid-sensitive acetal linker in 1,2-dilinoleyloxy-3-dimethylaminopropane (DLinDMA)-based lipids was found to enable low dose activity in rodents and non-human primates.[71] A novel lipid (DSGLA) containing guanidinium, primary amine, and quaternary ammonium functionality was incorporated into lipid-polycation-DNA nanoparticles grafted with an anisamide ligand to facilitate effective gene silencing in non-small cell lung adenocarcinoma *in vivo*.[72] Stable nucleic acid lipid particles were formulated with DLinDMA, cholesterol, PEGylated lipid, and 1,2-distearoyl-sn-glycero-3-phosphocholine to enable RNAi-mediated liver target gene silencing in non-human primates.[73] Combinatorial libraries of lipid-like materials have been synthesized using robotic automation to produce lipidoids by reacting alkyl epoxides or acrylics with amines.[74–77] Lipid-like materials, when formulated with cholesterol and PEGylated lipids, have demonstrated the ability to silence multiple genes simultaneously *in vivo* at unprecedentedly low doses.[75] The formation of polyplex and lipoplex nanoparticles proceeds through self-

assembly, which can depend on several factors such as siRNA content, material identity, and concentrations. Conversely, top-down approaches to the fabrication of nanoparticles defines biophysical and dimensional properties, which may be tuned to provide efficacious siRNA delivery vehicles.

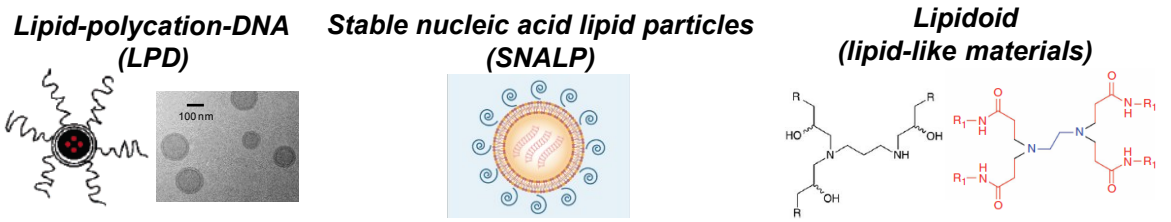

System	Group	Materials	Targeting	Approach	Properties	siRNA	Model	Efficacy
LPD	L. Huang	Cholesterol, DSGLA, protamine-DNA	PEG-Anisamide	Novel DSGLA lipid with amine functionalities	*D* ≈ 100 nm	EGFR	Non-small cell lung cancer	Tumor growth inhibition
SNALP	Tekmira	Cholesterol, DLinDMA, DSPC	PEG	Stealthed SNALP for delivery to liver	*D* ≈ 80 nm	apoB	Liver	First RNAi in non-human primates
Lipidoid	Alnylam, R. Langer	Alkyl epoxides or acrylics with amines, cholesterol	PEG	Combinatorial libraries for screening	*D* ≈ 140 nm	FVII, etc.	Liver	Multiple gene silencing at *low* doses

Figure 1.11 Lipid-based delivery vectors for effective RNAi *in vivo*.

1.4 PRINT technology and application to RNAi

1.4.1 Background to PRINT technology and applications in materials and life sciences

Adapting lithographic techniques from the semiconductor industry, PRINT is a top-down, versatile technology that allows for the preparation of monodisperse particles of distinct size, shape, and composition.[78] PRINT was developed in the DeSimone Lab, from which a start-up company was spun-out, namely Liquidia Technologies, to commercialize the technology. Depicted in Figure 1.12, a silicon wafer is etched with micro- or nano-scale features through traditional photolithography to which a photocurable perfluoropolyether (PFPE) resin (Fluorcur^{TM}) is applied, completely wetting the surface. The low surface energy of PFPE enables complete wetting of the template, after which it is photochemically cured to

yield a crosslinked elastomeric mold with shape- and size-specific cavities. Furthermore, the low interfacial tension of PFPE provides direct filling of micro- or nano-scale cavities using organic liquids without wetting area around the features. As a result, distinct particle are fabricated without an interconnecting "scum layer". Chemical resistance of PFPE also prevents its swelling by the liquid precursor, unlike with poly(dimethyl siloxane) molds,[79] maintaining the cavity features and allowing virtually any composition to be used.

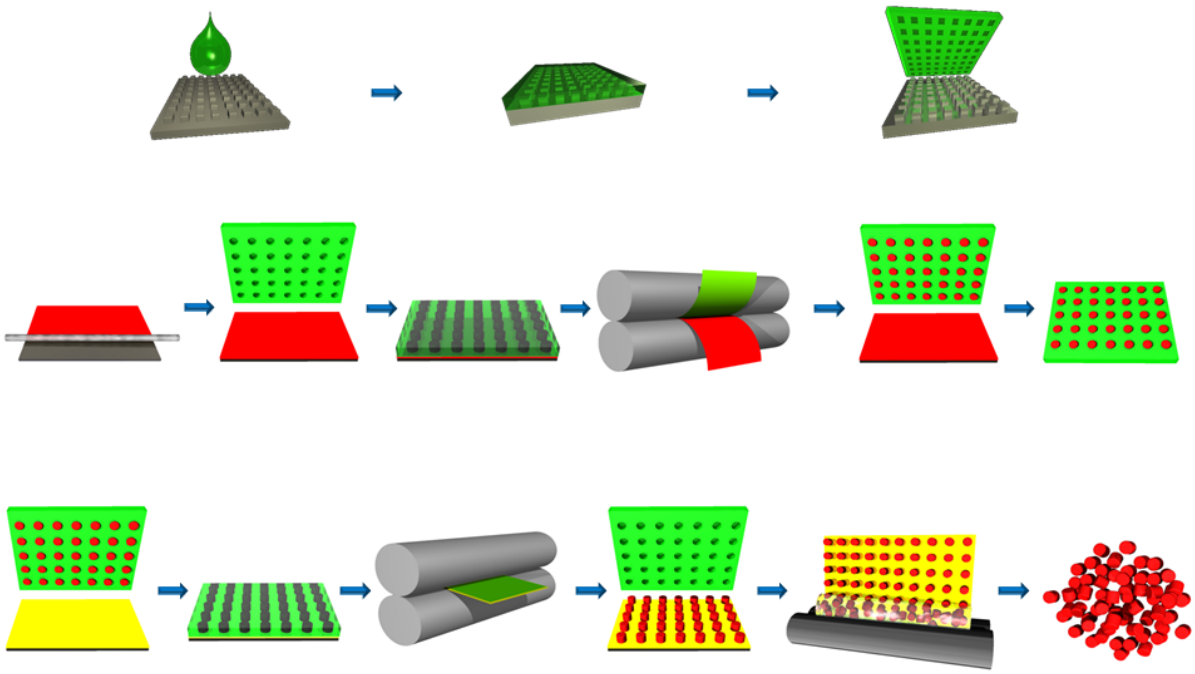

Figure 1.12 Illustration of PRINT process: a nano- or micro-patterned silicon wafer is fabricated through traditional photolithography; PFPE (green) is spread on the template and photochemically cured to yield an elastomeric mold; a film (red) may be prepared from a pre-particle solution containing various materials; the mold is married to the film through a laminator nip, using elevated temperatures if necessary to fill the mold cavities, which are then solidified; filled molds may be laminated against a sacrificial harvesting layer (yellow) to adhere the harvesting film to the particles; after adhesion, particles may be removed, yielding an array of monodisperse particles that may be harvested by passing the particle array-covered film through a nip containing a bead of solvent that will dissolve the sacrificial polymer to yield a dispersion of monodisperse particles.

The mold cavities may be filled with a monomer liquid precursor through capillary forces or a variety of materials through melt-fill processes. For materials below their glass

transition or melting temperature, a film of material may be prepared, married to the mold, and passed through a heated laminator to flow material into mold cavities. Subsequently, particles may be solidified through photochemical crosslinking, vitrification, or crystallization. Particles in the mold may be extracted by laminating the mold to a sacrificial harvesting layer, using heat if necessary, to promote adhesion. The harvesting film may be delaminated from the mold, revealing an array of particles on a sacrificial layer. The particle array-covered harvesting layer may be passed through a laminating nip containing a bead of appropriate solvent to dissolve the adhesive and yield a dispersion of monodisperse PRINT particles.

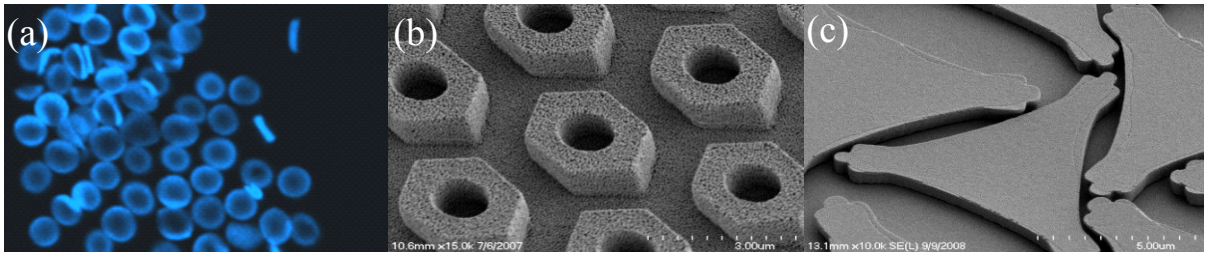

Figure 1.13 Range of particle shapes, sizes, and compositions accessible with PRINT. (a) Low modulus hydrogel microparticles; (b) 3x1 μm silver particles; (c) 7 μm pollen particles.

Examples of particles with different dimensions, compositions, and deformability produced *via* PRINT illustrate the versatility of the technology (Figure 1.13). Biologically-relevant cargos may be incorporated in the liquid precursor ranging from nucleic acids and proteins to magnetic resonance contrast agents for life science applications. The preparation of particles with controlled composition, shape, size, and surface functionalization[80] enables exploration in life sciences and materials science endeavors. For example, application of electric fields to anisotropic PRINT particles with unique shapes resulted in alignment of particles and crystallization.[81] Superparamagnetic and ferromagnetic magnetite nanoparticles were incorporated into PRINT particles to yield unique magneto-polymer composite particles

with a range of geometries.[82] Multiphasic and regio-specifically functionalized particles were prepared to enable two compositionally different chemistries for Janus particles with particle end-labeling *via* post-functionalization.[83] By geometrically controlling the chemical composition distribution during the fabrication process, amphiphilic block microparticles were prepared with high aspect ratio (Figure 1.14). Resulting, a series of di-block, tri-block, and multi-block particles were synthesized, exhibiting end-to-end assembly when dry or self-assembly at oil-water interfaces.[84] Amphiphilic high aspect ratio particles may find applications in the P-N junctions of semiconductors for electronics.

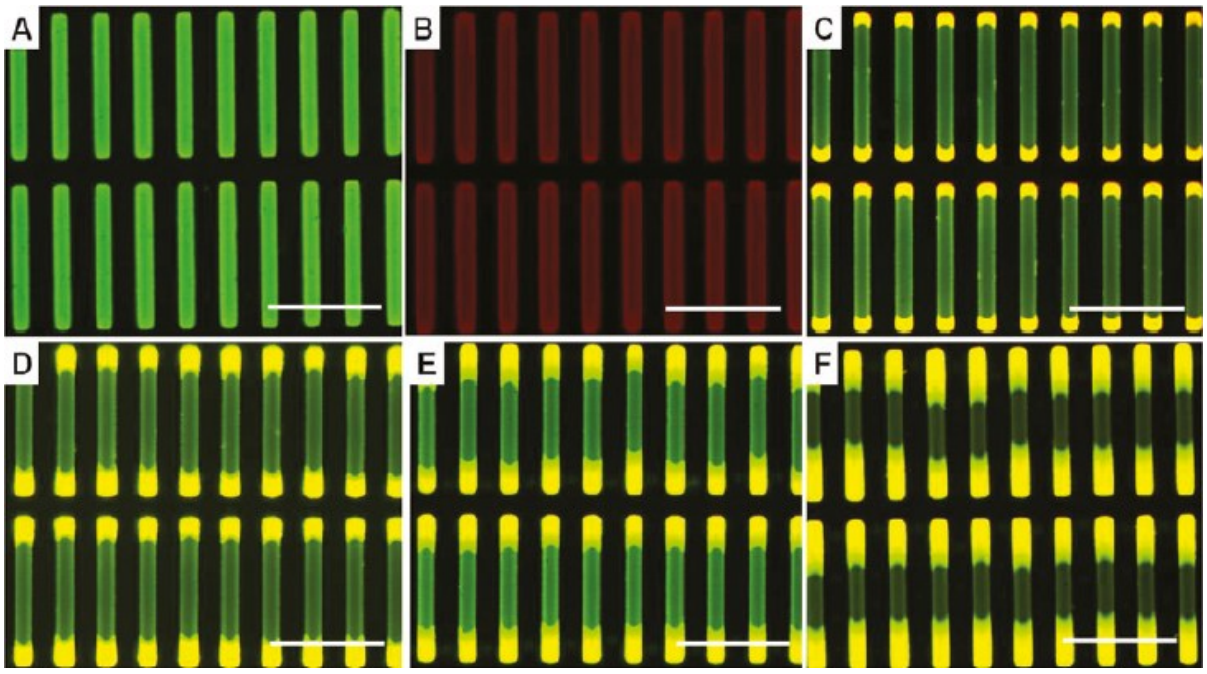

Figure 1.14. Array of 20 x 20 x 240 μm rod particles on harvesting film with tunable dimensions in ABA triblock structures. (A) One component hydrophobic particles. (B) One component hydrophilic particles. (C-F) ABA triblock particles with different hydrophilic/hydrophobic/ hydrophilic ratios corresponding to the four HP_4MA concentrations of (C): 10, (D): 20, (E): 30, and (F): 50 wt %. C-F were captured by overlaying the images under red and green channels.[84]

The physical dimensions of drug delivery vectors have been noted to impact the kinetics and mechanism of cell uptake *via* PRINT technology. For instance, positively charged cylindrical particles (diameter = 150 nm, aspect ratio = 3) were taken up by a cancer

cell line the most rapidly of eight PEG-based hydrogels having different sizes (0.1 – 5 μm) and shapes (cylinders and cubes).[85] Furthermore, the higher aspect ratio particles were internalized through multiple endocytotic routes simultaneously relative to the other particles in the study, accounting for their rapid uptake kinetics. The surface charge of particles has been observed to play a key role in cellular uptake as well. Acetylating primary amines on cationic particles rendered the ζ-potential negative and significantly decreased the amount of particles internalized by HeLa cells. Intravenous administration of highly crosslinked 200 nm PEG particles to mice indicated accumulation notably in the liver and spleen, accompanied by fast clearance (apparent distribution half-life of 17 min followed by slow redistribution with a half-life of 3.3 h). The rapid clearance rate of these particles, which is comparable to that of non-PEGylated liposomes, may be due to a non-ideal steric layer from low molar mass PEG in the particle matrix.

Toward synthetic blood substitutes exhibiting prolonged circulation times, biocompatible red blood cell mimetic (RBCMs) hydrogel microparticles with tunable modulus were explored to match the morphology and deformability of erythrocytes[49] (Figure 1.15). The deformability of RBCMs was evaluated *in vitro* in a microfluidic system containing narrow channels where low-modulus particles were able to deform and pass through slits while high-modulus particles could not effectively translocate. *In vivo* testing of PRINT-based RBCMs demonstrated the impact of RBCM modulus on circulation time, ranging from hours for stiff particles to days (half-life = 93 d) for highly-deformable, soft particles. Furthermore, the biodistribution of these particles following intravenous injection indicated a substantial decrease in lung filtration and a corresponding increase in splenic

accumulation over a 24 h period, which was attributed to the long residence time of these particles in the vasculature.

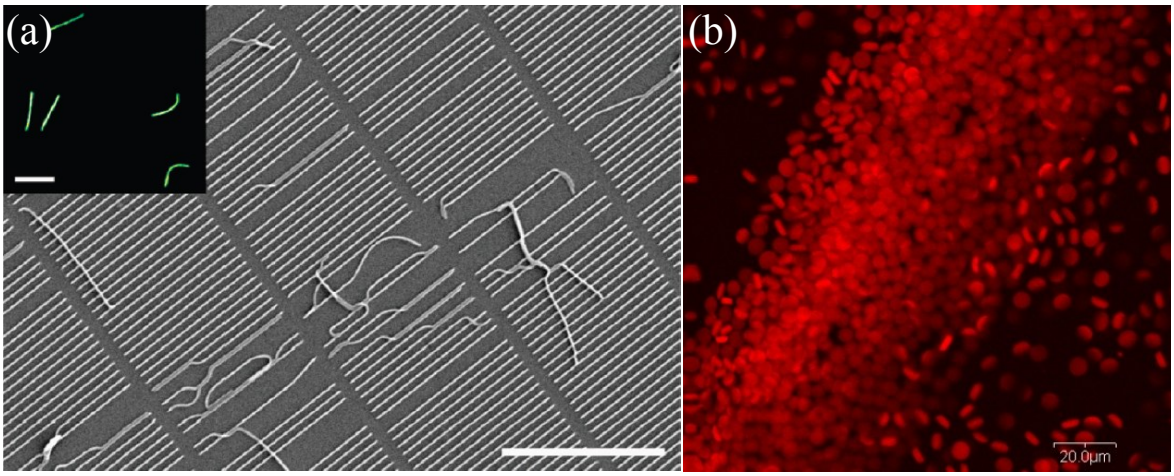

Figure 1.15 (a) Representative SEM image showing 96 wt% PEGDA 80 × 5000 nm particles. Several particles have detached from the PET sheet and display some flexibility. Inset: a fluorescence microscope image of the harvested particles shown in the SEM image. Scale bars for both images are 5 μm.[87] (b) Fluorescent micrograph of a dispersion of RBCM microparticles. Scale bar = 20 μm.[49]

The ability of PRINT particles to extravasate through nanopores was tested using a series of high aspect ratio hydrogel nanoparticles (Figure 1.15).[87] Filamentous particles (except 80 x 5000 nm worms with high cross-link density) were able to translocate across a porous membrane, providing promise for high-aspect ratio particles to extravasate through pores in biological environments under systemic circulation. Looking at another approach to particle delivery, high-performance aerosol particles were pursued for inhalation therapies *via* PRINT technology. Aerodynamic properties were tuned by controlling the size and shape of aerosol microparticles, leading to enhanced aerosolization and differential lung deposition *in vivo*.[88] Different particle compositions were explored for PRINT aerosols using biologics, fillers, and pure drugs. The first demonstration of nano-molding of protein particles was carried out using neat insulin and albumin in the PRINT process along with therapeutic cargos including siRNA and paclitaxel.[89] In addition to controlling the composition of

PRINT particles, the surface density of antibody ligands was investigated through well-defined conjugation chemistries to yield insight on the complex role of multivalency in targeting the transferrin receptor with nanoparticles toward cancer therapies.[90] Particles labeled with transferrin receptor antibody or human transferrin showed minimal toxicity to solid tumor cells lines; however, in Ramos B-cell lymphoma, particles activated apoptotic pathways leading to programmed cell death.

1.4.2 Incorporation of biologically-relevant cargos into PRINT particles for drug delivery

Drugs and biologics have been incorporated into PRINT particles toward therapeutic applications to elicit cellular responses. First, doxorubicin, a DNA-intercalating anthracycline, was encapsulated into reductively-labile PRINT microparticles for triggered intracellular release and induction of cell death in human cervical carcinoma cells.[91] Docetaxel, a taxane chemotherapeutic that interferes with cell division, was charged into poly(lactic-co-glycolic acid) (PLGA) particles with exceptionally high cargo loading. Dose-dependent death of ovarian cancer cells was elicited by docetaxel-loaded PLGA PRINT particles *in vitro*.[92] Controlling the release rate of chemotherapeutics or other biologics could be crucial in minimizing off-targeting effects and induction of cell death in healthy cells as well as achieving sustained release of drugs in relevant diseases for long-term therapy. A family of bifunctional silyl ether crosslinkers were synthesized to produce acid-sensitive PRINT particles with controlled rates of degradation.[93] Varying the size of the alkyl substituent on the silicon atom influenced the rate of degradation since the access of water and acid to the silyl ether linkages will be governed by the degree of hydrophobicity and sterics.

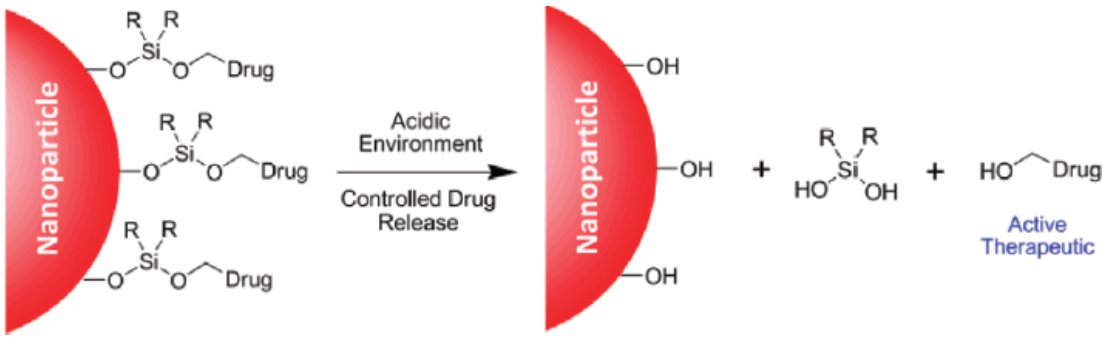

Figure 1.16 Controlled release of drugs from silyl ether prodrug-conjugated nanoparticles.[94]

A series of silyl ether prodrugs derived from chemotherapeutics bearing pendant alcohols were synthesized for controlled release under intracellular acidic conditions from PRINT nanoparticles (Figure 1.16).[94] The release rate of drug from nanoparticles could be controlled by varying the alkyl substituent on the silicon atom. Asymmetric bifunctional silyl ether prodrugs enabled controlled release of chemotherapeutics from particles and induced death in cancer cells *in vitro*. Moving to another set of cargos, the controlled release of biologics from PRINT particles was engineered by transiently rendering protein-based particles insoluble in aqueous environments through crosslinking.[95] A novel disulfide crosslinker was used to render bovine serum albumin (BSA)-based particles insoluble under physiological conditions where controlled dissolution would then occur under the reducing intracellular environment with the rate of dissolution depending on the degree of crosslinking. RNA Replicon, an autonomously replicating RNA, was incorporated into crosslinked BSA particles for intracellular delivery and expression of protein. In contrast to inducing expression of protein, particles encapsulating oligonucleotides have been explored to silence expression of proteins. Multiple siRNAs were encapsulated into PLGA rice-shaped nanoparticles for gene silencing in prostate cancer cells.[96] siRNA-loaded PLGA nanoparticles were coated with cationic lipids to enable gene silencing and induction of cell

death with siRNA targeting KIF11, which is known to cause mitotic arrest and apoptosis in cancer cell lines.

1.4.3 Design of particles for gene silencing

Given the ability to tune particle characteristics with PRINT technology, different particle dimensions with tailored chemical composition, surface functionality, and cargo release profiles may be engineered toward the development of nanoparticles for gene silencing. Shape has been seen to play a role in gene silencing efficiency where high-aspect ratio polystyrene and shape-shifting PLGA nanoneedles enhanced gene knockdown relative to spherical microspheres.[97] The composition of delivery vectors plays one of the most important roles in achieving transfection with siRNA. Features of particles that protect siRNA under physiological conditions and enable cell uptake, efficient endosomal escape, and release of siRNA are essential to an efficacious platform for RNAi. The structures of amine-containing monomers have been explored to optimize gene silencing efficiency in nanoparticles self-assembled from polymers and lipids. Applied to PRINT technology, different amine-containing monomers and endosomolytic species may be incorporated into or coated on particles to bestow gene silencing capabilities.

Functionalization of particle surfaces with stealthing and targeting ligands may enable receptor-mediated endocytosis for transfecting specific cells. Chemical or physical approaches taken in functionalization of particle surfaces may influence corresponding endosomolytic activity of nanoparticles. Reversibly conjugating or coating ligands to nanoparticles, with dissociation of ligands under slightly acidic environments, may enable effective gene silencing activity by revealing bare particles with lytic activity in the

endosome. Controlled release of siRNA from the particle may be pursued by controlling particle charge density, degree of porosity, and method of cargo encapsulation, whether through physical entrapment or chemical conjugation. Aforementioned particle characteristics may be explored in the PRINT process to provide RNAi therapies toward the treatment of diseases.

References

(1) Garrett, R. H.; Grisham, C. M. *Biochemistry,* 3rd ed.; Thomson Brooks/Cole: Belmont, CA, 2005.

(2) Gene Therapy Clinical Trials Worldwide http://www.abedia.com/wiley/indications.php (accessed May 2012).

(3) Paterson, B. M.; Robertst, B. E.; Kuff, E. L. *Proceedings of the National Academy of Sciences of the United States of America* **1977**, *74*, 4370-4374.

(4) Stephenson, M. L.; Zamecnik, P. C. *Proceedings of the National Academy of Sciences of the United States of America* **1978**, *75*, 285-288.

(5) Faruqi, A. F.; Datta, H. J.; Carroll, D.; Michael, M.; Glazer, P. M.; Seidman, M. M. *Molecular and Cellular Biology* **2000**, *20*, 990-1000.

(6) Datta, H. J.; Chan, P. P.; Vasquez, K. M.; Gupta, R. C.; Glazer, P. M. *The Journal of Biological Chemistry* **2001**, *276*, 18018-18023.

(7) Opalinska, J. B.; Gewirtz, A. M. *Nature Reviews Drug Discovery* **2002**, *1*, 503-514.

(8) Sharma, H. W.; Perez, J. R.; Higgins-Sochaski, K.; Hsiao, R.; Narayanan, R. *Anticancer Research* **1996**, *16*, 61-69.

(9) Doudna, J. A.; Cech, T. R.; Sullenger, B. A. *Proceedings of the National Academy of Sciences of the United States of America* **1995**, *92*, 2355-2359.

(10) Fichou, Y.; Férec, C. *Trends in Biotechnology* **2006**, *24*, 563-570.

(11) Nimjee, S. M.; Rusconi, C. P.; Sullenger, B. A. *Annual Review of Medicine* **2005**, *56*, 555-583.

(12) Beelman, C. A.; Parker, R. *Cell* **1995**, *81*, 179-183.

(13) Liebhaber, S. A. *Nucleic Acids Symposium Series* **1997**, *36*, 29-32.

(14) Castanotto, D.; Scherr, M.; Rossi, J. J. *Methods in Enzymology* **2000**, *313*, 401-420.

(15) Santoro, S. W.; Joyce, G. F. *Proceedings of the National Academy of Sciences of the United States of America* **1997**, *94*, 4262-4266.

(16) Crooke, S. T. *Methods in Enzymology* **2000**, *313*, 3-45.

(17) Guvakova, M.A.; Yakubov, L. A.; Vlodavsky, I; Tonkinson, J. L.; Stein, C. A. *Journal of Biological Chemistry* **1995**, *270*, 2620-2627.

(18) Kurreck, J. *Europen Journal of Biochemistry* **2003**, *270*, 1628-1644.

(19) El-Beshlawy, A.; Mostafa, A.; Youssry, I; Gabr, H.; Mansour, I. M.; El-Tablawy, M.; Aziz, M.; Hussein, I. R. *Journal of Pediatric Hematology/Oncology* **2008**, *30*, 281-284.

(20) Castanotto, D; Rossi, J. J. *Nature* **2009**, *457*, 426-433.

(21) Nielsen, P. E. *Annual Review of Biophysics and Biomolecular Structure* **1995**, *24*, 167-183.

(22) Summerton, J.; Weller, D. *Antisense Nucleic Acid Drug Development* **1997**, *7*, 187-195.

(23) Tansey, B. *San Francisco Chronicle*. August 11, 2006, D-1.

(24) Kim, D. H.; Rossi, J. J. *Nature Reviews Genetics* **2007**, *8*, 173-184.

(25) Fire, A.; Xu, S.; Montgomery, M. K.; Kostas, S. A.; Driver, S. E.; Mello, C. C. *Nature* **1998**, *391*, 806-811.

(26) Elbashir, S. M.; Lendeckel, W.; Tuschl, T. *Genes & Development* **2001**, *15*, 188-200.

(27) Hutvágner, G.; Zamore, P. D. *Science* **2002**, *297*, 2056-2060.

(28) Reynolds, A.; Leake, D.; Boese, Q.; Scaringe, S.; Marshall, W. S.; Khvorova, A. *Nature Biotechnology* **2004**, *22*, 326-230.

(29) Huang, H.; Qiao, R.; Zhao, D.; Zhang, T.; Li, Y.; Yi, F.; Lai, F.; Hong, J.; Ding, X.; Yang, Z.; Zhang, L.; Du, Q.; Liang, Z. *Nucleic Acids Research* **2009**, *37*, 7560-2569.

(30) Kole, R.; Krainer, A. R.; Altman, S. *Nature Reviews Drug Discovery* **2012**, *11*, 125-140.

(31) Raemdonck, K.; Remaut, K.; Lucas, B.; Sanders, N. N.; Demeester, J.; De Smedt, S. C. *Biochemistry* **2006**, *45*, 10614-10623.

(32) Bartlett, D. W.; Davis, M. E. *Nucleic Acids Research* **2006**, *34*, 322-333.

(33) Omi, K.; Tokunaga, K.; Hohjoh, H. *FEBS Letters* **2004**, *558*, 89-95.

(34) Song, E.; Lee, S.-K.; Dykxhoorn, D. M.; Novina, C.; Zhang, D.; Crawford, K.; Cerny, J.; Sharp, P. A.; Lieberman, J.; Manjunath, N.; Shankar, P. *Journal of Virology* **2003**, *77*, 7174-7181.

(35) ClinicalTrials. http://clinicaltrials.gov (accessed May, 2012).

(36) Kaiser, P. K.; Symons, R. C. A.; Shah, S. M.; Quinlan, E. J.; Tabandeh, H.; Do, D. V.; Reisen, G.; Lockridge, J. a; Short, B.; Guerciolini, R.; Nguyen, Q. D. *American Journal of Ophthalmology* **2010**, *150*, 33-39.

(37) Molitoris, B. A.; Dagher, P. C.; Sandoval, R. M.; Campos, S. B.; Ashush, H.; Fridman, E.; Brafman, A.; Faerman, A.; Atkinson, S. J.; Thompson, J. D.; Kalinski, H.; Skaliter, R.; Erlich, S.; Feinstein, E. *Journal of the American Society of Nephrology* **2009**, *20*, 1754-1764.

(38) Lim, J. I. *Age-Related Macular Degeneration,* 2nd ed.; Informa Healthcare, 2007.

(39) Takei, Y.; Nemoto, T.; Mu, P.; Fujishima, T.; Ishimoto, T.; Hayakawa, Y.; Yuzawa, Y.; Matsuo, S.; Muramatsu, T.; Kadomatsu, K. *Molecular Cancer Therapeutics* **2008**, *7*, 211-221.

(40) Kigasawa, K.; Kajimoto, K.; Hama, S.; Saito, A.; Kanamura, K.; Kogure, K. *International Journal of Pharmaceutics* **2010**, *383*, 157-160.

(41) He, Y.; Bi, Y.; Hua, Y.; Liu, D.; Wen, S.; Wang, Q.; Li, M.; Zhu, J.; Lin, T.; He, D.; Li, X.; Wang, Z.; Wei, G. *Journal of Experimental & Clinical Cancer Research* **2011**, *30*, 104.

(42) Zhang, Y.; Cristofaro, P.; Silbermann, R.; Pusch, O.; Boden, D.; Konkin, T.; Hovanesian, V.; Monfils, P. R.; Resnick, M.; Moss, S. F.; Ramratnam, B. *Molecular Therapy* **2006**, *14*, 336-342.

(43) Han, S. W.; Roman, J. *Oncogene* **2006**, *25*, 4341-4349.

(44) Kleinman, M. E.; Yamada, K.; Takeda, A.; Chandrasekaran, V.; Nozaki, M.; Baffi, J. Z.; Albuquerque, R. J. C.; Yamasaki, S.; Itaya, M.; Pan, Y.; Appukuttan, B.; Gibbs, D.; Yang, Z.; Karikó, K.; Ambati, B. K.; Wilgus, T. A.; DiPietro, L. A.; Sakurai, E.; Zhang, K.; Smith, J. R.; Taylor, E. W.; Ambati, J. *Nature* **2008**, *452*, 591-597.

(45) Singer, O.; Marr, R. A.; Rockenstein, E.; Crews, L.; Coufal, N. G.; Gage, F. H.; Verma, I. M.; Masliah, E. *Nature Neuroscience* **2005**, *8*, 1343-1349.

(46) Hu-Lieskovan, S.; Heidel, J. D.; Bartlett, D. W.; Davis, M. E.; Triche, T. J. *Cancer Research* **2005**, *65*, 8984-8992.

(47) Negishi, Y.; Endo, Y.; Fukuyama, T.; Suzuki, R.; Takizawa, T.; Omata, D.; Maruyama, K.; Aramaki, Y. *Journal of Controlled Release* **2008**, *132*, 124-130.

(48) Durcan, N.; Murphy, C.; Cryan, S.-A. *Molecular Pharmaceutics* **2008**, *5*, 559-566.

(49) Merkel, T. J.; Jones, S. W.; Herlihy, K. P.; Kersey, F. R.; Shields, A. R.; Napier, M.; Luft, J. C.; Wu, H.; Zamboni, W. C.; Wang, A. Z.; Bear, J. E.; DeSimone, J. M. *Proceedings of the National Academy of Sciences of the United States of America* **2011**, *108*, 586-591.

(50) http://ehp.niehs.nih.gov/members/2000/suppl-5/861-872schwab/schwab-full.html (accessed April, 2011).

(51) Weitzman Lab. http://logw.salk.edu/adresearch.html (accessed May, 2012).

(52) Roth, C. M.; Sundaram, S. *Annual Review of Biomedical Engineering* **2004**, *6*, 397-426.

(53) Escriou, V.; Carriere, M.; Scherman, D.; Wils, P. *Advanced Drug Delivery Reviews* **2003**, *55*, 295-306.

(54) Lv, H.; Zhang, S.; Wang, B.; Cui, S.; Yan, J. J. *Journal of Controlled Release* **2006**, *114*, 100-109.

(55) Daniel, R.; Smith, J. A. *Human Gene Therapy* **2008**, *19*, 557-568.

(56) Stolberg, S. G. *The New York Times*. October 4, 2002. http://www.nytimes.com/2002/10/04/us/trials-are-halted-on-a-gene-therapy.html?ref=jessegelsinger (accessed August, 2012).

(57) Williams, D. A. *Molecular Therapy* **2007**, *15*, 2053-2054.

(58) Zhang, S. B.; Xu, Y. M.; Wang, B.; Qiao, W. H.; Liu, D. L.; Li, Z. S. *Journal of Controlled Release* **2004**, *100*, 165-180.

(59) Zuckerman, S. T.; Kao, W. J. *Nanomaterials and Biocompatibility: BioMEMS and Dendrimers. In Nanotechnology in Drug Delivery*; de Villiers, M. M.; Aramwit, P.; Kwon, G. S.; Springer New York, 2009; pp. 193-228.

(60) Conwell, C. C.; Huang, L. *Recent Progress in Non-viral Gene Delivery. In Non-viral Gene Therapy, Gene Design and Delivery*; Taira, K.; Kataoka, K.; Niidome, T.; Springer Tokyo: Tokyo, Japan, 2005; pp. 3-10.

(61) Kunath, K.; von Harpe, A.; Fischer, D.; Petersen, H.; Bickel, U.; Voigt, K.; Kissel, T. *Journal of Controlled Release* **2003**, *89*, 113-125.

(62) Yoshikawa, K.; Yoshikawa, Y. *Physical Chemistry of DNA-Carrier Complexes. In Non-viral Gene Therapy, Gene Design and Delivery*; Taira, K.; Kataoka, K.; Niidome, T.; Springer Tokyo: Tokyo, Japan, 2005; pp. 11-18.

(63) Schiffelers, R. M.; Storm, G. *Expert Opinion on Drug Delivery* **2006**, *3*, 445-454.

(64) Davis, M. E. *Molecular Pharmaceutics* **2009**, *6*, 659-668.

(65) Wakefield, D. H.; Klein, J. J.; Wolff, J. A.; Rozema, D. B. *Bioconjugate Chemistry* **2005**, *16*, 1204-1208.

(66) Rozema, D. B.; Ekena, K.; Lewis, D. L.; Loomis, A. G.; Wolff, J. A. *Bioconjugate Chemistry* **2003**, *14*, 51-57.

(67) Remaut, K.; Sanders, N. N.; De Geest, B. G.; Braeckmans, K.; Demeester, J.; De Smedt, S. C. *Materials Science and Engineering: R: Reports* **2007**, *58*, 117-161.

(68) Zuhorn, I. S.; Bakowsky, U.; Polushkin, E.; Visser, W. H.; Stuart, M. C. A.; Engberts, J. B. F. N.; Hoekstra, D. *Molecular Therapy* **2005**, *11*, 801-810.

(69) Oberle, V.; Bakowsky, U.; Zuhorn, I. S.; Hoekstra, D. *Biophysical Journal* **2000**, *79*, 1447-1454.

(70) Cullis, P. R.; Hope, M. J. *Nature* **1978**, *271*, 672-674.

(71) Semple, S. C.; Akinc, A.; Chen, J.; Sandhu, A. P.; Mui, B. L.; Cho, C. K.; Sah, D. W. Y.; Stebbing, D.; Crosley, E. J.; Yaworski, E.; Hafez, I. M.; Dorkin, J. R.; Qin, J.; Lam, K.; Rajeev, K. G.; Wong, K. F.; Jeffs, L. B.; Nechev, L.; Eisenhardt, M. L.; Jayaraman, M.; Kazem, M.; Maier, M. A.; Srinivasulu, M.; Weinstein, M. J.; Chen, Q.; Alvarez, R.; Barros, S. A.; De, S.; Klimuk, S. K.; Borland, T.; Kosovrasti, V.; Cantley, W. L.; Tam, Y. K.; Manoharan, M.; Ciufolini, M. A.; Tracy, M. A.; de Fougerolles, A.; MacLachlan, I.; Cullis, P. R.; Madden, T. D.; Hope, M. J. *Nature Biotechnology* **2010**, *28*, 172-176.

(72) Chen, Y.; Sen, J.; Bathula, S. R.; Yang, Q.; Fittipaldi, R.; Huang, L.; Hill, C.; Carolina, N. *Molecular Pharmaceutics* **2009**, *80*, 696-705.

(73) Zimmermann, T. S.; Lee, A. C. H.; Akinc, A.; Bramlage, B.; Bumcrot, D.; Fedoruk, M. N.; Harborth, J.; Heyes, J. A.; Jeffs, L. B.; John, M.; Judge, A. D.; Lam, K.; McClintock, K.; Nechev, L. V.; Palmer, L. R.; Racie, T.; Röhl, I.; Seiffert, S.; Shanmugam, S.; Sood, V.; Soutschek, J.; Toudjarska, I.; Wheat, A. J.; Yaworski, E.; Zedalis, W.; Koteliansky, V.; Manoharan, M.; Vornlocher, H.-P.; MacLachlan, I. *Nature* **2006**, *441*, 111-114.

(74) Akinc, A.; Zumbuehl, A.; Goldberg, M.; Leshchiner, E. S.; Busini, V.; Hossain, N.; Bacallado, S. A.; Nguyen, D. N.; Fuller, J.; Alvarez, R.; Borodovsky, A.; Borland, T.; Constien, R.; de Fougerolles, A.; Dorkin, J. R.; Jayaprakash, K. N.; Jayaraman, M.; John, M.; Koteliansky, V.; Manoharan, M.; Nechev, L.; Qin, J.; Racie, T.; Raitcheva, D.; Rajeev, K. G.; Sah, D. W. Y.; Soutschek, J.; Toudjarska, I.; Vornlocher, H.-P.; Zimmermann, T. S.; Langer, R.; Anderson, D. G. *Nature Biotechnology* **2008**, *26*, 561-569.

(75) Love, K. T.; Mahon, K. P.; Levins, C. G.; Whitehead, K. A.; Querbes, W.; Dorkin, J. R.; Qin, J.; Cantley, W.; Qin, L. L.; Racie, T.; Frank-Kamenetsky, M.; Yip, K. N.; Alvarez, R.; Sah, D. W. Y.; de Fougerolles, A.; Fitzgerald, K.; Koteliansky, V.; Akinc, A.; Langer, R.; Anderson, D. G. *Proceedings of the National Academy of Sciences of the United States of America* **2010**, *107*, 1864-1869.

(76) Goldberg, M. S.; Xing, D.; Ren, Y.; Orsulic, S.; Bhatia, S. N.; Sharp, P. A. *Proceedings of the National Academy of Sciences of the United States of America* **2011**, *108*, 745-750.

(77) Akinc, A.; Goldberg, M.; Qin, J.; Dorkin, J. R.; Gamba-Vitalo, C.; Maier, M.; Jayaprakash, K. N.; Jayaraman, M.; Rajeev, K. G.; Manoharan, M.; Koteliansky, V.; Röhl, I.; Leshchiner, E. S.; Langer, R.; Anderson, D. G. *Molecular Therapy* **2009**, *17*, 872-879.

(78) Rolland, J. P.; Maynor, B. W.; Euliss, L. E.; Exner, A. E.; Denison, G. M.; DeSimone, J. M. *Journal of the American Chemical Society* **2005**, *127*, 10096-10100.

(79) Schmid, H.; Michel, B. *Macromolecules* **2000**, *33*, 3042-3049.

(80) Perry, J. L.; Herlihy, K. P.; Napier, M. E.; DeSimone, J. M. *Accounts of Chemical Research* **2011**, *44*, 990-998.

(81) Herlihy, K. P.; Nunes, J.; DeSimone, J. M. *Langmuir* **2008**, *24*, 8421-8426.

(82) Nunes, J.; Herlihy, K. P.; Mair, L.; Superfine, R.; DeSimone, J. M. *Nano Letters* **2010**, *10*, 1113-1119.

(83) Zhang, H.; Nunes, J. K.; Gratton, S. E. A.; Herlihy, K. P.; Pohlhaus, P. D.; DeSimone, J. M. *New Journal of Physics* **2009**, *11*, 075018.

(84) Wang, J.-Y.; Wang, Y.; Sheiko, S. S.; Betts, D. E.; DeSimone, J. M. *Journal of the American Chemical Society* **2012**, *134*, 5801-5806.

(85) Gratton, S. E. A.; Ropp, P. A.; Pohlhaus, P. D.; Luft, J. C.; Madden, V. J.; Napier, M. E.; DeSimone, J. M. *Proceedings of the National Academy of Sciences of the United States of America* **2008**, *105*, 11613-11618.

(86) Gratton, S. E. A.; Pohlhaus, P. D.; Lee, J.; Guo, J.; Cho, M. J.; DeSimone, J. M. *Journal of Controlled Release* **2007**, *121*, 10-18.

(87) Kersey, F. R.; Merkel, T. J.; Perry, J. L.; Napier, M. E.; DeSimone, J. M. *Langmuir* **2012**, *28*, 8773-8781.

(88) Garcia, A.; Mack, P.; Williams, S.; Fromen, C.; Shen, T.; Tully, J.; Pillai, J.; Kuehl, P.; Napier, M.; DeSimone, J. M.; Maynor, B. W. *Journal of Drug Delivery* **2012**, *2012*, 1-10.

(89) Kelly, J. Y.; DeSimone, J. M. *Journal of the American Chemical Society* **2008**, *130*, 5438-5439.

(90) Wang, J.; Tian, S.; Petros, R. A.; Napier, M. E.; DeSimone, J. M. *Journal of the American Chemical Society* **2010**, *132*, 11306-11313.

(91) Petros, R. A.; Ropp, P. A.; DeSimone, J. M. *Journal of the American Chemical Society* **2008**, *130*, 5008-5009.

(92) Enlow, E. M.; Luft, J. C.; Napier, M. E.; DeSimone, J. M. *Nano Letters* **2011**, *11*, 808-813.

(93) Parrott, M. C.; Luft, J. C.; Byrne, J. D.; Fain, J. H.; Napier, M. E.; DeSimone, J. M. *Journal of the American Chemical Society* **2010**, *132*, 17928-17932.

(94) Parrott, M. C.; Finniss, M.; Luft, J. C.; Pandya, A.; Gullapalli, A.; Napier, M. E.; DeSimone, J. M. *Journal of the American Chemical Society* **2012**, *134*, 7978-7982.

(95) Xu, J.; Wang, J.; Luft, J. C.; Tian, S.; Owens, G.; Pandya, A. a; Berglund, P.; Pohlhaus, P.; Maynor, B. W.; Smith, J.; Hubby, B.; Napier, M. E.; DeSimone, J. M. *Journal of the American Chemical Society* **2012**, *134*, 8774-8777.

(96) Hasan, W.; Chu, K.; Gullapalli, A.; Dunn, S. S.; Enlow, E. M.; Luft, J. C.; Tian, S.; Napier, M. E.; Pohlhaus, P. D.; Rolland, J. P.; DeSimone, J. M. *Nano Letters* **2012**, *12*, 287-292.

(97) Kolhar, P.; Doshi, N.; Mitragotri, S. *Small* **2011**, *7*, 2094-2100.

CHAPTER 2

HYDROGEL NANOPARTICLES FOR TARGETED DELIVERY OF SMALL INTERFERING RNA TO CANCER AND LIVER CELLS

2.1 Introduction to hydrogels for delivery of siRNA

Hydrogel particles, comprised of water-loving materials, can be prepared *via* physical self-assembly through secondary interactions or *via* formation of chemical bonds, leading to covalently crosslinked networks. The affinity of hydrogels for water promotes swelling, which depends on the degree of crosslinking or identity of chemical groups, e.g. ionizable carboxylic acid groups. With desirable features for delivery of siRNA such as biocompatibility and potential for loading cargos, hydrogel nanoparticles are mechanically robust and may allow for facile tuning of particle composition toward gene silencing.

Cationic dextran micro- and nanogels have been pursued as biodegradable particles for loading siRNA post-fabrication to enable time-controlled delivery of siRNA.[1,2] Enhanced Green Fluorescent Protein (EGFP) was used as the reporter gene in a human hepatocellular carcinoma cell line to evaluate gene knockdown efficacy of dextran-based particles. When hepatocytes were dosed with microgels and PEGylated nanogels containing siRNA against EGFP, gene knockdown was achieved, exhibiting efficacy similar to the commercial transfection reagent, RNAiMAX. A straightforward, scalable protocol for preparation of amphiphilic nanogels of poly(*N*-isopropylmethyacrylamide) (NIPAM) as the core component was established for "breathing-in" siRNA where lyophilized nanogels were re-suspended in

an aqueous solution containing the siRNA.[3] Poly(NIPAM) exhibits thermoresponsive behavior, undergoing a coil-to-globule transition around 43 ºC, and may allow for thermally-triggered release of cargo. Bare and peptide-functionalized poly(NIPAM) nanogels silenced EGFR expression in human ovarian carcinoma cells. Cationic core-shell gel particles were prepared for absorption of siRNA post-fabrication and subsequent transfection of African green monkey kidney epithelial (BSC-40) cells.[4] Core-shell particles silenced expression of cyclophilin B at the mRNA level as determined by reverse transcriptase polymerase chain reaction (RT-PCR).

A unique approach to deliver siRNA from biopolymer hydrogel scaffolds containing cells and siRNA was carried out to provide a minimally invasive, injectable administration route.[5] Macroscopic biopolymer hydrogels encapsulating siRNA were fabricated in transwell membranes with 0.4 μm pore size. Ionic- and photo-crosslinking of alginate as well as thermal gelation of collagen were explored to synthesize biodegradable hydrogel matrices. Green fluorescent protein (GFP)-positive human embryonic kidney (HEK 293) cells were cultured with siRNA-loaded alginate and collagen biopolymer hydrogels. Substantial GFP knockdown was observed for cells cultured in hydrogel scaffolds after 72 h incubation.

PRINT technology enables control over the encapsulation of siRNA in hydrogels, either through direct physical entrapment or covalent incorporation of siRNA during particle fabrication. Additionally, post-fabrication loading of siRNA may be pursued through electrostatic attraction; however, the surface properties of particles may be altered and the association of cargo with particles may be dynamic. In addition to allowing for control over the approach to load siRNA in hydrogels, PRINT allows for the incorporation of relevant functional monomers to be carried out in a plug-and-play manner, e.g. implementing

monomers with endosomolytic activity, reactive handles, dyes, and triggered degradation. Many vinyl-based monomers may undergo photoinitiated free-radical polymerization using UV light in a matter of minutes. Rapid production of monodisperse, shape-specific particles with tailored key design features may enable gene silencing for a broad range of applications.

2.2 Cationic poly(vinyl pyrrolidone)-based, degradable hydrogel nanoparticles for delivery of siRNA

As a water-soluble, FDA-approved pharmaceutical excipient with biocompatibility, poly(vinyl pyrrolidone) (PVP) is a non-ionic, neutral polymer that has been explored as a hydrophilic component of nanoparticles for gene therapy. Although PVP may not condense nucleic acids through electrostatics, PVP can interact with DNA base-pairs through hydrogen bonding in the major groove in a mildly acidic environment.[6] DNA plasmids have been formulated with PVP for injection into the muscle of rats for expression of β-galactosidase as a reporter gene.[7] Improved tissue dispersion and cellular uptake of pDNA using PVP and poly(vinyl alcohol) (PVA) after injection into muscle was attributed to potential osmotic effects. For targeted transfection of hepatocytes with plasmid DNA, galactosylated chitosan-*graft*-PVP (GCPVP) was implemented *in vitro*.[8] Negligible cytotoxicity and transfection was encountered for HepG2 cells dosed with GCPVP as noted by minimal cell death and appearance of EGFP expression.

With PVP as the hydrophilic, biocompatible linear polymer of hydrogels, a degradable crosslinker was desired for the triggered release of particle contents under intracellular conditions. Disulfide-based carriers have attractive qualities for the delivery of nucleic acids, which often require localization in the cytoplasm or nucleus of cells for

transfection.[9] The redox gradient that exists between extracellular milieu and the intracellular cytoplasm may be exploited for the triggered degradation of disulfide-based carriers after internalization by cells due to the inherent intracellular reducing environment. Self-assembled polymersomes formed from disulfide-linked poly(ethylene glycol)-poly(propylene sulfide) block copolymers exhibited disruptive properties after internalization by cells,[10] suggesting potential for cytoplasmic delivery of biomacromolecules.

Dissolution of nanogels synthesized *via* atom transfer radical polymerization (ATRP) for a disulfide-containing crosslinker with oligo(ethylene oxide) monomethoxy methacrylate allowed for reductively-triggered degradation (dissolution) and release of a drug (doxorubicin) to invoke cell death in a human cervical carcinoma (HeLa) cell line.[11] Similarly, Trojan horse PRINT microparticles were prepared for the intracellular delivery of doxorubicin using a disulfide-based crosslinker for triggered release of cargo and induction of cell death.[12] Gene transfection was observed for polyplexes prepared from poly(amido amine)s containing bioreducible disulfide units that were complexed with plasmid DNA in African Green Monkey fibroblast-like kidney (COS-7) cells.[13] Core-shell type polyplexes were fabricated from PEG and PEG-poly(L-lysine) block copolymers with disulfide crosslinked cores for effective *in vivo* gene delivery using plasmid DNA[14] to mice livers.

Designing cationic hydrogels has been realized through incorporation of amine-containing monomers. pH-independent, positively charged particles have been developed by incorporating quaternary ammonium-containing monomers, such as 2-[2-(acryloyloxy) ethyl]trimethyl ammonium chloride (AETMAC). Cationic polymeric nanogels were synthesized *via* inverse microemulsion polymerization using PEG diacrylate and AETMAC

for loading oligonucleotides and DNA.[15] Uptake of nanogels by HeLa cells and corresponding biocompatibility was observed at different N/P ratios.

In the first generation of PRINT hydrogels for the delivery of siRNA to cells, PVP was implemented as the primary hydrophilic component of the particle matrix. The precursor monomer to PVP is *N*-vinyl-2-pyrrolidone (VP), which is a liquid monomer that may be polymerized through a photoinitiated free radical mechanism. To provide triggered intracellular degradation of hydrogels for release of siRNA cargo, a disulfide-containing crosslinker was synthesized and incorporated in particles. Disulfide bonds may be cleaved in the intracellular milieu by reducing enzymes while the integrity of disulfide bonds is largely maintained in normal extracellular environments.[16,17] The quaternary ammonium-containing monomer, AETMAC, can instill electrostatic attraction between the cationic nanoparticle matrix and the negatively charged siRNA. Additionally, the positive charge from AETMAC enables non-specific interaction with cells, which have negatively charged membranes, resulting in endocytosis, a pathway by which cells internalize molecules, proteins, or particles. High charge density of nanoparticles can induce lysis of membranes, which is necessary after endocytosis for endosomal escape to effectively deliver siRNA to the cytoplasm of cells and avoid degradation in lysosomal vesicles. Incorporation of fluorescently-tagged monomers (e.g. fluorescein *o*-acrylate, FOA) into the hydrogel matrix allows for evaluation of cell internalization of particles using flow cytometry. PRINT molds filled with pre-particle solutions may be rapidly cured through incorporation of UV-absorbing photoinitiators that will promote quick free radical photopolymerization under exposure to UV light.

2.2.1 Experimental

2.2.1.1 Materials

Monomers and reagents were purchased from Sigma Aldrich. Molecular biology grade solvents (and DEPC-treated water, Ambion, Inc.) were used when mixing components with siRNA and they were obtained from Thermo Fisher Scientific, Inc. siRNA was purchased from Dharmacon, Inc. with anti-firefly luciferase sequence: 5'-GAUUAUGUCCGGUUAUGUAUU-3'; anti-sense: 5'-P-UACAUAACCGGACAUAAUC-UU-3'. The pre-particle solution consisted of dissolving solid and liquid monomers with sparse addition of DMSO to provide a homogenous solution. siRNA was dissolved in DEPC-treated water at 50 mg/mL. The composition of the pre-particle solution was (wt%): *N*-vinyl-2-pyrrolidone (VP) (57), bis(ethylene acrylate) disulfide (30), AETMAC (10), FOA (1), 1-hydroxycyclohexyl phenyl ketone (HCPK) (1), and siRNA (1) with the addition of 10 wt% DMSO. A custom-designed, double-nip laminator was implemented for preparing PVP particles. PRINT molds were graciously supplied by Liquidia Technologies.

2.2.1.2 Synthesis of bis(ethylene acrylate) disulfide

2,2'-dithiodiethanol (1.55 mL, 13 mmol) and triethylamine (5.4 mL, 3 eq) were dissolved in a 100-mL round-bottomed flask containing 40 mL of anhydrous dichloromethane under an argon blanket followed by submerging the flask in an ice-cold water bath. Acryloyl chloride (2.22 mL, 2.5 eq) was added dropwise to the reaction mixture and allowed to react for 2 h. The crude product mixture was washed with 1 M HCl three times and concentrated *via* rotary evaporation. The bis(acrylate) crosslinker was purified by silica gel column chromatography (4:1 hexanes:ethyl acetate), yielding 2.41 g of crosslinker

(71%), and structure was confirmed by ^{1}H NMR (400 MHz, $CDCl_3$) δ = 6.45 (dd, *J* = 17.2 Hz, 2H), δ = 6.15 (dd, *J* = 10.3 Hz, 17.3 Hz, 2H), δ = 5.88 (dd, J = 10.6 Hz, 2H), δ = 4.44 (t, *J* = 7.0, 4H), δ = 2.99 (t, *J* = 7.0 Hz, 4H).

2.2.1.3 Fabrication of PVP-based hydrogel nanoparticles

A double nip laminator was used for filling molds against PET followed by immediate contact with a sheet of poly(ethylene terephthalate), to which the materials would be cured. Filled molds were minimally exposed to air to prevent evaporation of VP monomer due to its volatility. 20 μL of pre-particle solution was evenly distributed at the PET-mold nip for each foot of mold and laminated at 40 psi followed by a split and immediate lamination against corona-treated PET to prevent evaporation of VP. The filled mold-PET sandwich was cured in a UV oven ((λ_{max} = 365 nm, 90 mW/cm^2) for 10 min. The cured mold was delaminated from the PET sheet to reveal an array of particles, which were mechanically collected using DEPC-treated water and a cell scraper. PVP particles were isolated and washed *via* centrifugation (14 krpm, 4 ºC, 10 min).

2.2.1.4 Characterization of hydrogels

ζ-potentials and diameters of particles were determined by light scattering (Brookhaven Instruments Inc., 90Plus Particle Size Analyzer and ZetaPlus Zeta Potential Analyzer) on 20 μg/mL particle dispersions in 1 mM KCl. Particle concentrations were determined *via* thermogravimetric analysis (Pyris 1, PerkinElmer). For scanning electron microscopy, a small volume (5 μL) of particle suspension (1 mg/mL in H_2O) was dispensed on a glass slide, coated with 2 nm of Au/Pd, and imaged (Hitachi model S-4700).

2.2.1.5 Cell culture and assays

Luciferase-expressing HeLa cell line (HeLa/luc) was from Xenogen. HeLa/luc cells were maintained in DMEM high glucose supplemented with 10% FBS, 2 mM L-glutamine, 50 units/mL penicillin and 50 μg/mL streptomycin, 1 mM sodium pyruvate, and non-essential amino acids. All media and supplements were from GIBCO except for FBS which was from Mediatech, Inc. Transfection with Lipofectamine^{TM} 2000 was carried out according to manufacturer instructions.

In vitro cell uptake analysis. HeLa/luc cells were plated in a 96-well plate at 10,000/well and incubated overnight at 37°C. Cells were dosed with particles in OPTI-MEM at 37 °C (5 % CO_2) for 4 h or indicated time for cell uptake studies. After incubation, cells were washed and detached by trypsinization. After centrifugation, cells were re-suspended in a 0.4 % trypan blue (TB) solution in Dulbecco's Phosphate Buffers Saline solution (DPBS) to quench the fluorescein fluorescence from particles associated to the cell surface. Cells were then washed and re-suspended in DPBS or fixed in 1% paraformaldehyde/DPBS, and analyzed by CyAn ADP flowcytometer (Dako). Cell uptake was represented as the percentage of cells that were positive in fluorescein fluorescence.

In vitro cytotoxicity and luciferase expression assays. HeLa/luc cells were plated in a 96-well plate at 10,000/well and incubated overnight at 37°C. Cells were dosed with particles or Lipofectamine^{TM} 2000/siRNA mix in OPTI-MEM at 37 °C (5 % CO_2) for 4 h, then particles were removed, and complete grow medium was added for another 72 h incubation at 37°C. Cell viability was evaluated with Promega CellTiter 96$^{®}$ AQ_{ueous} One Solution Cell Proliferation Assay, and luciferase expression level was evaluated with Promega Bright-Glo™ Luciferase Assay according to manufacturer's instructions. Light

absorption or bioluminescence was measured by a SpectraMax M5 plate reader (Molecular Devices). The viability or luciferase expression of the cells exposed to PRINT particles was expressed as a percentage of that for cells grown in the absence of particles.

2.2.2 Activity of siRNA after exposure to UV light with photoinitiator: compatibility with particle fabrication conditions

Since wavelength-dependent, UV-induced damage (oxidation, dimer formation) has been noted for nucleic acids exposed to irradiation,[18–21] the activity of siRNA was tested before and after exposure to UV light. To ensure that siRNA would retain activity when incorporated into hydrogels prepared *via* UV photocuring, a solution of siRNA and photoinitiator (HCPK) was treated with UV light for 5 min. The activity of siRNA was evaluated through transfection of HeLa cells stably expressing firefly luciferin gene with luciferase-targeting siRNA using Lipofectamine™ 2000 (Figure 2.1). The activity of UV-treated siRNA was retained when compared to an untreated solution of siRNA. Viability of HeLa cells was maintained across all dosing concentrations.

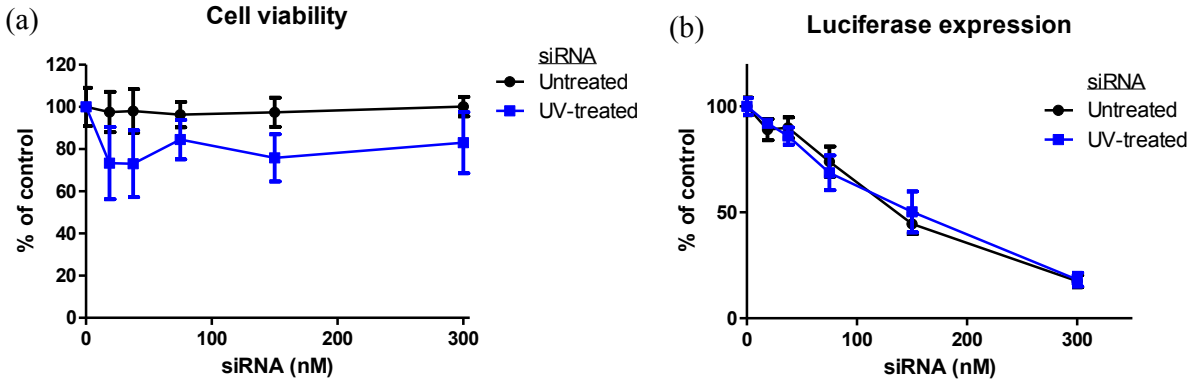

Figure 2.1 (a) Viability and (b) luciferase expression of HeLa cells dosed with Lipofectamine-siRNA complexes for 4 h followed by 72 h incubation.

2.2.3 Physicochemical characteristics of PVP-based hydrogels

Structures of the monomers implemented into the pre-particle solution are illustrated in Figure 2.2a. The morphology of PVP-based hydrogels appeared cylindrical and rigid from the SEM micrographs in Figure 2.2b since these particles have a relatively high crosslink density. The cationic, amine-containing monomer (AETMAC) instilled a highly positive ζ-potential for these particles (+68.2 ± 1.2 mV), which exhibited a diameter of 440.7 ± 9.2 nm.

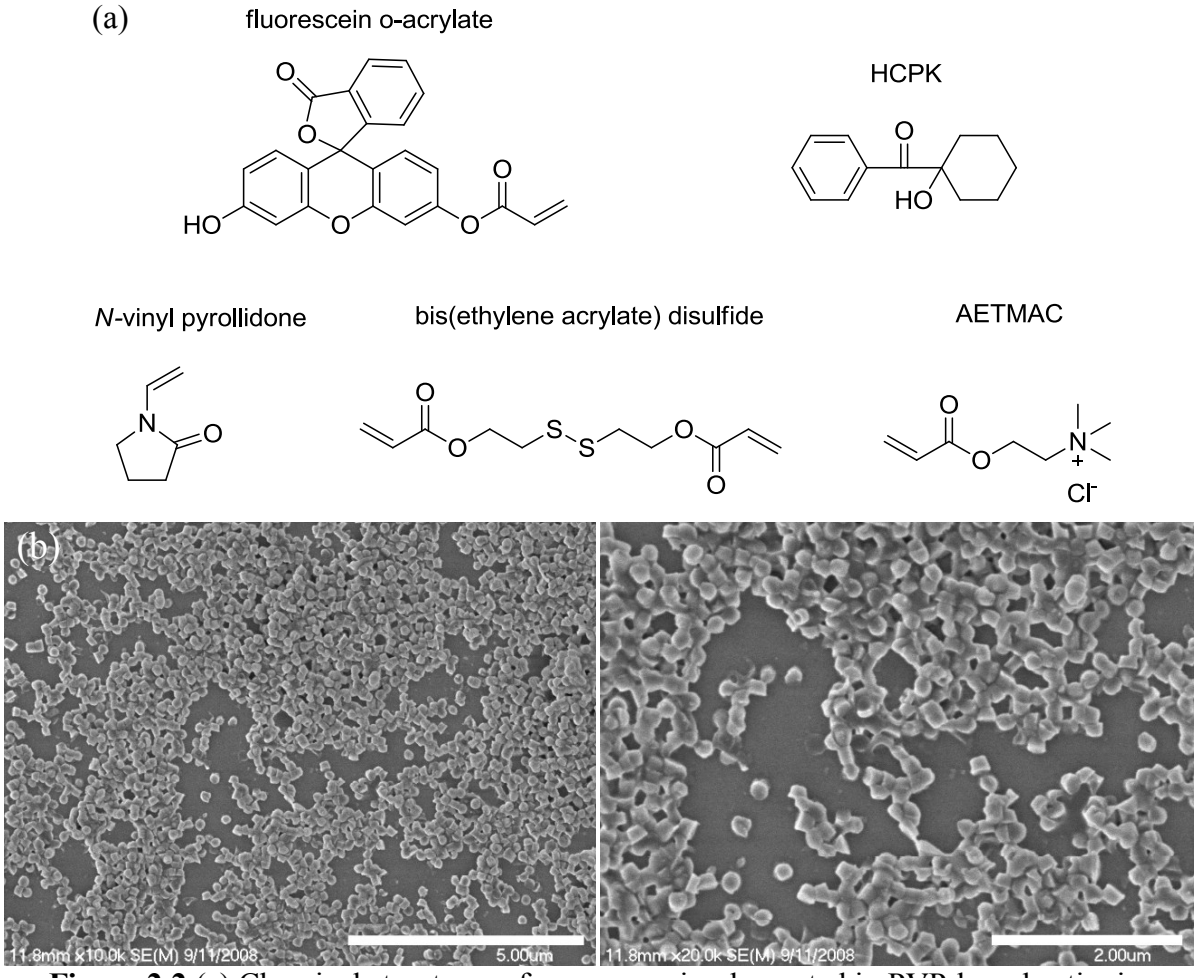

Figure 2.2 (a) Chemical structures of monomers implemented in PVP-based cationic hydrogel nanoparticles. (b) SEM micrographs of PVP-based particles containing siRNA illustrate cylindrical morphology and 200 x 200 nm dimensions.

2.2.4 Dosing PVP hydrogels on HeLa cells for cell uptake, cytocompatibility, and gene silencing

PVP particles containing luciferase siRNA were tested for their ability to silence expression of the firefly luciferase gene in human cervical carcinoma (HeLa) cells. Internalization of particles proceeded rapidly, reaching saturation at low dosing concentrations (Figure 2.3a). Cell viability was maintained above 75% up to 34 μg/mL particle dosing concentration (Figure 2.3b). Silencing of luciferase expression was observed at 34 μg/mL particle dose (25 nM siRNA for 1 wt% loading); however, at higher particle dosing concentrations, cell viability was completely compromised (Figure 2.3b). Although a window of gene silencing and tolerable cytotoxicity was observed, a particle composition that would be tolerated at high particle doses was desired to allow for complete biocompatibility.

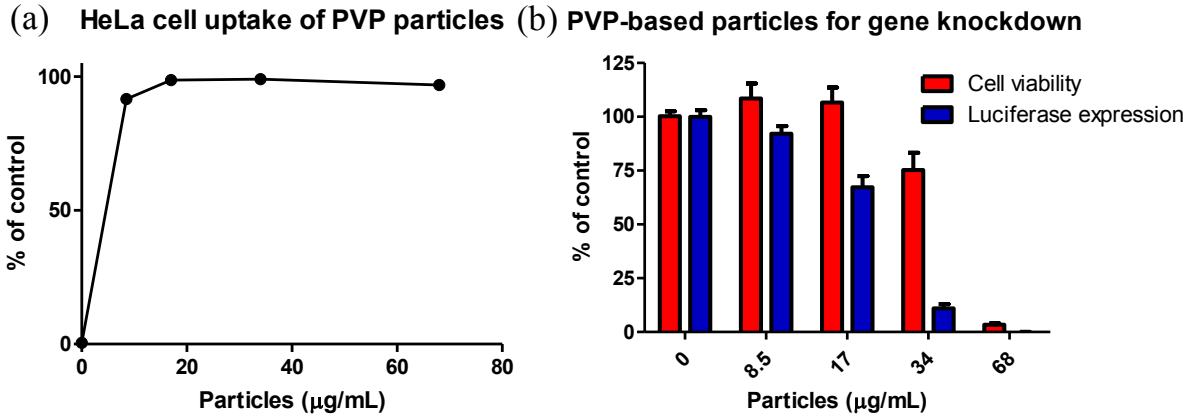

Figure 2.3 (a) Uptake of PVP-based particles by HeLa cells and (b) viability and luciferase expression of HeLa cells dosed with PVP particles for 4 h followed by 72 h incubation at 37 ºC.

In addition to a particle composition that would not elicit as much cytotoxicity, a particle matrix that would allow for robust covalent functionalization was required for targeting cell receptors and enabling systemic *in vivo* delivery. Furthermore, a different

approach to particle fabrication that would enable more flexible mold filling conditions (e.g. a composition that would not be sensitive to evaporation of volatile monomers) was pursued for faster particle production.

2.3 Poly(ethylene glycol)-based cationic hydrogel nanoparticles for delivery of siRNA

Seeking a more flexible particle fabrication procedure and biocompatible composition, PEG was investigated as a primary constituent of the particle matrix since evaporation should be negligible and the FDA has approved the use of PEG for several applications. PEG hydrogels offer attractive features for the encapsulation of biologics and therapeutics for biomedical applications.[22,23] Crosslinked PEG hydrogels offer robust mechanical properties while providing the ability to tune modulus and release rate (diffusion) of cargos through the crosslinking density. Plasmid DNA has been encapsulated in photocrosslinked PEG-based hydrogels with controlled degradation and release properties.[24,25] PEI-siRNA nano- and micro-particle polyplexes have been incorporated into photopolymerized PEG hydrogels for transfection of fibrosarcoma epithelial cells[26] and dendritic cells.[27]

In addition to serving as a hydrophilic, biocompatible network for encapsulation and release of biologics, PEG-grafted surfaces may enhance dispersibility (prevent aggregation) and cytocompatibility (minimize cellular toxicity) of nanoparticles while prolonging circulation time for delivery of siRNA.[28] For example, combinatorial synthesis of core-shell nanoparticles containing monomethoxy oligo(ethylene oxide), to provide a hydrophilic shell, enabled encapsulation of siRNA, cellular internalization, and gene silencing *in vitro* and *in vivo*.[29] PEG acts as a major component of self-assembled cyclodextrin-based polymer

nanoparticles (CALAA-01) containing siRNA in the first targeted delivery of siRNA to humans for therapeutic purposes.[30] Adamantane-PEG and transferrin-modified adamantane-PEG interact with hydrophobic domains of cyclodextrin through a strong non-covalent inclusion complex to provide ligand- and PEG-grafted nanoparticle surfaces for tumor delivery.

To obtain a PRINT hydrogel matrix that would also enable conjugation of ligands through efficient reactions, a primary amine-containing monomer (2-aminoethyl methacrylate hydrochloride, AEM) was included as a major component of the composition. AEM also provides a positive charge to promote electrostatic attraction of siRNA to the particle while enabling cell uptake and transfection. The approach to particle fabrication involves a film-split procedure where the pre-particle solution is cast onto a sheet of PET to produce a thin film of appropriate thickness to fill mold cavities. PEG_{1K} dimethacrylate was explored as the crosslinker while monomethoxy PEG_{5K} acrylate served as the hydrophile to yield a porous, crosslinked network through which siRNA may diffuse and exit the particle as well as creating PEG-grafted surfaces. To minimize cytotoxicity and further promote dispersion in aqueous media, particles were PEGylated and tested for their *in vitro* behavior toward cell uptake and tolerance as well as gene knockdown.

2.3.1 Experimental

2.3.1.1 Materials

N,N-dimethylformamide (DMF) (Acros Organics – DNase, RNase, and protease free, 99.8%), DEPC-treated water (Ambion, Inc.), and potassium chloride solution (0.0100N ±0.0001N, EMD Chemicals) were obtained from Fisher Scientific. PEG_{1K} dimethacrylate

was purchased from Polysciences, Inc. and monomethoxy PEG_{5K} acrylate was obtained from Creative PEGWorks. Anti-luciferase and control siRNA genome #3 were obtained from Dharmacon, Inc.: control siRNA sense: 5'-AUGUAUUGGCCUGUAUUAGUU-3'; anti-sense: 5'-P-CUAAUACAGGCCAAUACAUU-3'. 2 mil wire wound rod was purchased from R.D. Specialties. Remaining reagents were purchased from Sigma Aldrich or mentioned in 2.2.1.1.

2.3.1.2 Fabrication of PEG-based hydrogels containing siRNA

2-aminoethyl methacrylate hydrochloride (50 wt%), PEG_{1K} dimethacrylate (23 wt%), $mPEG_{5K}$ acrylate (20 wt%), 1-hydroxycyclohexyl phenyl ketone (1 wt%), and fluorescein *o*-acrylate (1 wt%) were dissolved in DMF to which a 50 mg/mL solution of siRNA (5 wt%) in DEPC-treated water was added to yield a 4.5 wt% solution of solids. With a RNaseZAP-treated 2 mil wire wound rod, 150 μL of solution was cast at 6 ft/min on a sheet of poly(ethylene terephthalate) (PET) while evaporating solvent with a heat gun to yield a transparent film. 200 x 200 nm cylindrical PFPE molds (4 x 12", Liquidia Technologies) were laminated against the film at 45 psi and 6 ft/min. The mold was delaminated from the film followed by lamination against a corona-treated PET sheet and curing for 5 min in a UV chamber (λ_{max} = 365 nm, 90 mW/cm^2). The mold was delaminated from the PET sheet, revealing an array of particles on the PET sheet that were collected mechanically with DEPC-treated water using a cell scraper (1 mL/48 in^2 of mold). The particle dispersion was centrifuged at 4 °C and 14 krpm for 15 min, followed by removal of the supernatant and re-suspension in an appropriate volume of water for thermogravimetric analysis to determine particle yield.

2.3.1.3 Functionalization of PEG particles

PEGylation through imine formation: particles were dispersed in pH 6.6 buffer at 1 mg/mL to which monomethoxy PEG_{5K} monoaldehyde (2 wt eq) was added and the reaction was allowed to proceed for 6 h followed by washing particles with buffer.

PEGylation through amide formation: particles were dispersed in DMF at 2 mg/mL to which monosuccinimidyl succinate monomethoxy PEG_{2K} (2 wt eq) and pyridine (4 wt eq) were added and reacted for 6 h followed by washing particles and re-suspending them in water.

2.3.1.4 Characterization of hydrogel nanoparticles

ζ-potential, diameters, yield, and morphology of particles was determined as previously described in 2.2.1.4. The release of siRNA from particles was evaluated by agarose gel electrophoresis: siRNA-loaded particles were incubated in PBS at 37°C for indicated times followed by centrifugation at 14 krpm for 15 min at 4°C. The supernatants were collected and saved at -80 °C. 12 μL of sample (supernatants from particle dispersions, siRNA solutions, or particle dispersions) was mixed with 3 μL of 6x loading buffer (60% glycerol, 0.12 M EDTA in DEPC-treated water) and loaded into the gel. 70 V/cm was applied for 25 min and the gel was then imaged with ImageQuant LAS 4000 (GE). Analysis of siRNA band intensity was conducted with Image J software for quantification. siRNA loading was calculated by comparing the maximum amount of siRNA released to the particle mass. Encapsulation efficiency of siRNA was calculated by comparing the wt% of final siRNA loading to the siRNA charged into the pre-particle composition (5 wt% of particle).

2.3.1.5 Cell culture and confocal laser scanning microscopy

Cell culture and assays were conducted in a similar manner as reported in 2.2.1.5. For confocal microscopy, HeLa/luc cells were plated in 8-well chamber slides (BD) at 10,000/well and incubated overnight at 37°C. Cells were dosed with green fluorescent particles (fluorescein or DyLight 488 labeled) in OPTI-MEM at 37 °C (5 % CO_2) for 4 h. Cells were then washed three times with PBS, fixed with 4% paraformaldehyde for 10 min, and permeabilized with 0.5% saponin for 30 min at room temperature. Cells were stained with 100 nM phalloidin-AlexaFluor 555 for actin for 1 h at room temperature, and then counterstained with 30 μM DAPI for 15 min. Images were collected with LSM710 confocal laser scanning microscope (Carl Zeiss).

2.3.2 Fabrication and characterization of PEG-based nanoparticles

The structures of new components in PRINT particles are illustrated in Figure 2.4a. As a preliminary evaluation of the behavior of PEG-based particles with cells, they were tested for cell internalization and toxicity. siRNA was not included in the composition; to compensate for its loss, the crosslinker content was increased to 23 wt% and the hydrophile to 25 wt%. Also, THF and DMF were both initially tested for preparing particles as the solvent of the pre-particle solution. To minimize toxicity from positively charged particles and to provide a stealth layer for future application, particles were PEGylated. Primary amines from AEM in the particle matrix were reacted with an aldehyde-terminated monomethoxy PEG_{5K} to yield imine-linked PEGs (Figure 2.4b). Before PEGylation, ζ-potential of particles was +33.9 ± 4.1 mV with *Z*-average diameter of 289.0 ± 23.1 nm. The ζ-potential of particles was reduced to +24.0 ± 1.0 mV after PEGylation. The morphology of particles appears cylindrical with correct dimensions, yielding a notably “soft” appearance,

most likely attributable to the rubbery, porous PEG matrix (Figure 2.4c). PEGylated particles prepared in THF or DMF were readily internalized by HeLa cells (Figure 2.5a) and did not elicit any cytotoxicity. Cell viability was maintained greater than 90% across all doses (Figure 2.5b).

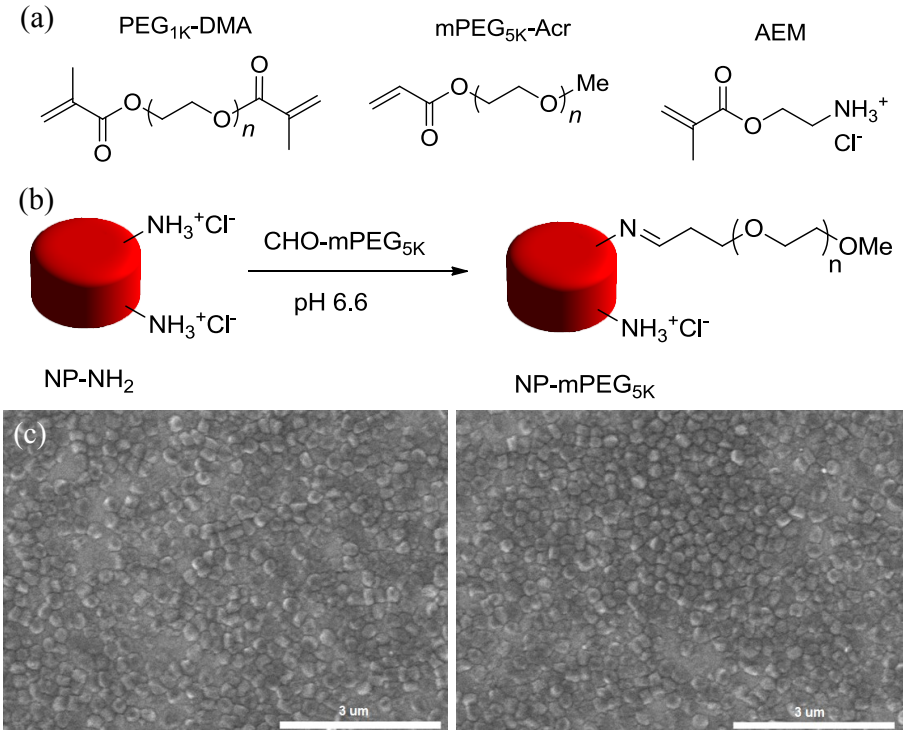

Figure 2.4 (a) Chemical structures of monomers and macromonomers implemented in cationic PRINT particles. (b) Reaction scheme for PEGylation of primary amine-containing hydrogels with aldehyde-terminated $mPEG_{5K}$ through imine formation. (c) SEM micrographs of cationic PEG-based hydrogels illustrate cylindrical dimensions and soft qualities.

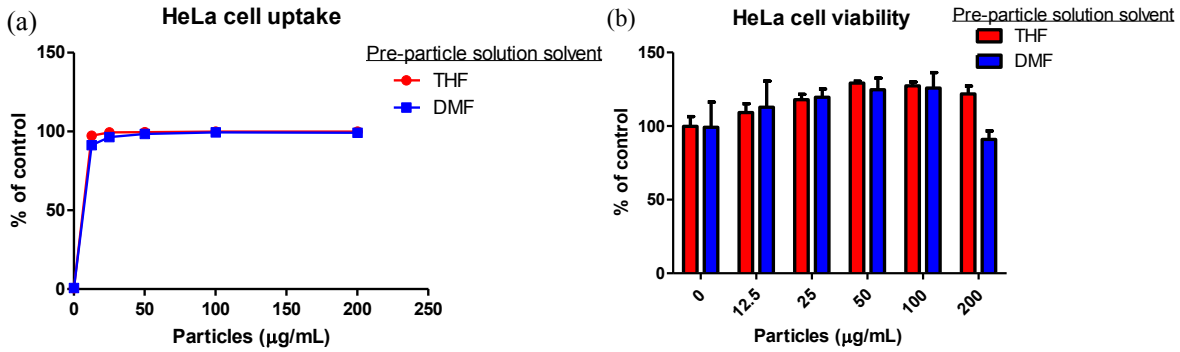

Figure 2.5 (a) HeLa cell uptake of PEG-based particles prepared from THF and DMF pre-particle solutions. (b) Viability of HeLa cells dosed with PEG-based particles prepared from THF and DMF pre-particle solutions.

2.3.3 Delivery of siRNA *via* hydrogels PEGylated with imines

DMF was chosen as the solvent for the pre-particle solution albeit a heat gun is required to produce a dry film quickly while THF is sufficiently volatile. Small precipitates were noticed when THF was used as the solvent after anti-luciferase or control siRNAs were added to the pre-particle solution. DMF has a higher dielectric constant than THF, minimizing potential interactions between siRNA and pre-particle solution components as well as allowing for dissolution of salts. PEG-based particles were prepared containing luciferase and control siRNA. SEM micrographs of particles reveal their cylindrical nature (Figure 2.6) while light scattering demonstrates their size is roughly 250 nm with a ζ-potential of ca. + 35 mV prior to PEGylation (Figure 2.6). ζ-potentials of particles decreased by approximately 10 mV after PEGylation (Table 1.1).

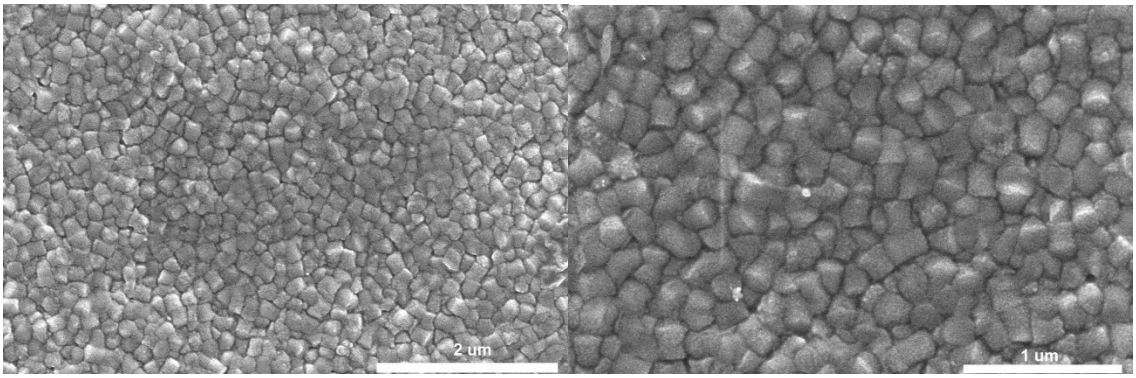

Figure 2.6 SEM micrographs of PEG-based hydrogel nanoparticles confirms cylindrical dimensions.

Table 2.1 ζ-potential and dynamic light scattering analysis of siRNA-charged, PEG-based particles before and after PEGylation.

	Luc siRNA		Control siRNA	
	Before PEGylation	After PEGylation	Before PEGylation	After PEGylation
ζ-potential (mV)	+36.5 ± 0.8	+24.0 ± 1.0	+32.2 ± 0.6	+22.4 ± 2.0
D_z (nm)	240.8 ± 6.1		277.7 ± 11.8	

Uptake of particles by HeLa cells occurred at low doses while cell viability was maintained across all dosing concentrations (Figure 2.7a). Luciferase expression persisted in HeLa cells dosed with particles containing control siRNA (2.7b). However, dose-dependent knockdown of luciferase gene was observed in HeLa cells dosed with particles containing luciferase siRNA. The half maximal effective concentration (EC_{50}) for reducing luciferase expression was 68 µg/mL particle dosing concentration (2.7c).

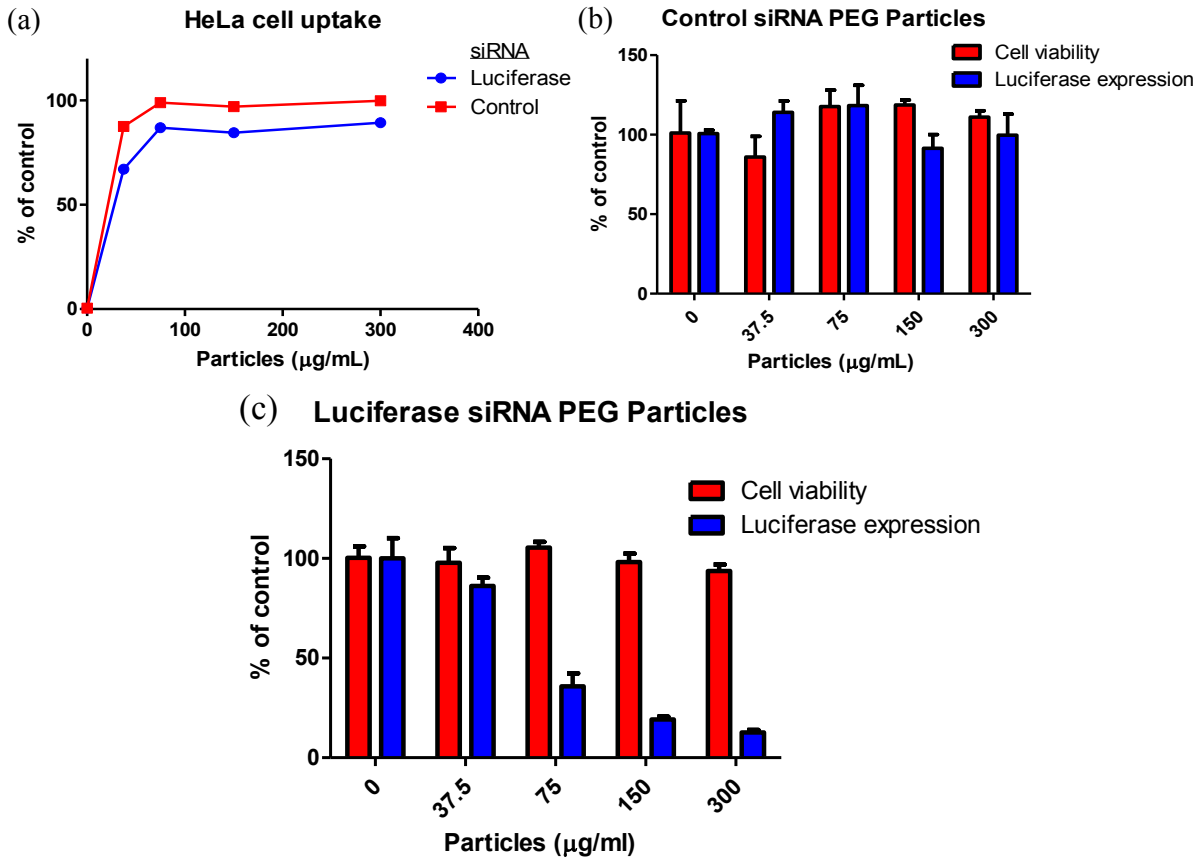

Figure 2.7 (a) HeLa cell uptake of PEG-based hydrogel nanoparticles after 4 h dosing time. Viability and luciferase expression of HeLa cells dosed with (b) control and (c) luciferase siRNA-containing nanoparticles for 4 h followed by 72 h incubation at 37 ºC.

2.3.4 Delivery of siRNA *via* hydrogels PEGylated through amide linkages

To see whether the reaction conditions had an effect on particle integrity and gene silencing activity, particles were PEGylated through amide bonds. Moreover, PEGylation of

hydrogels through amidation provides stable bonds that will persist in an aqueous environment, whether *in vivo* or when stored in buffer.

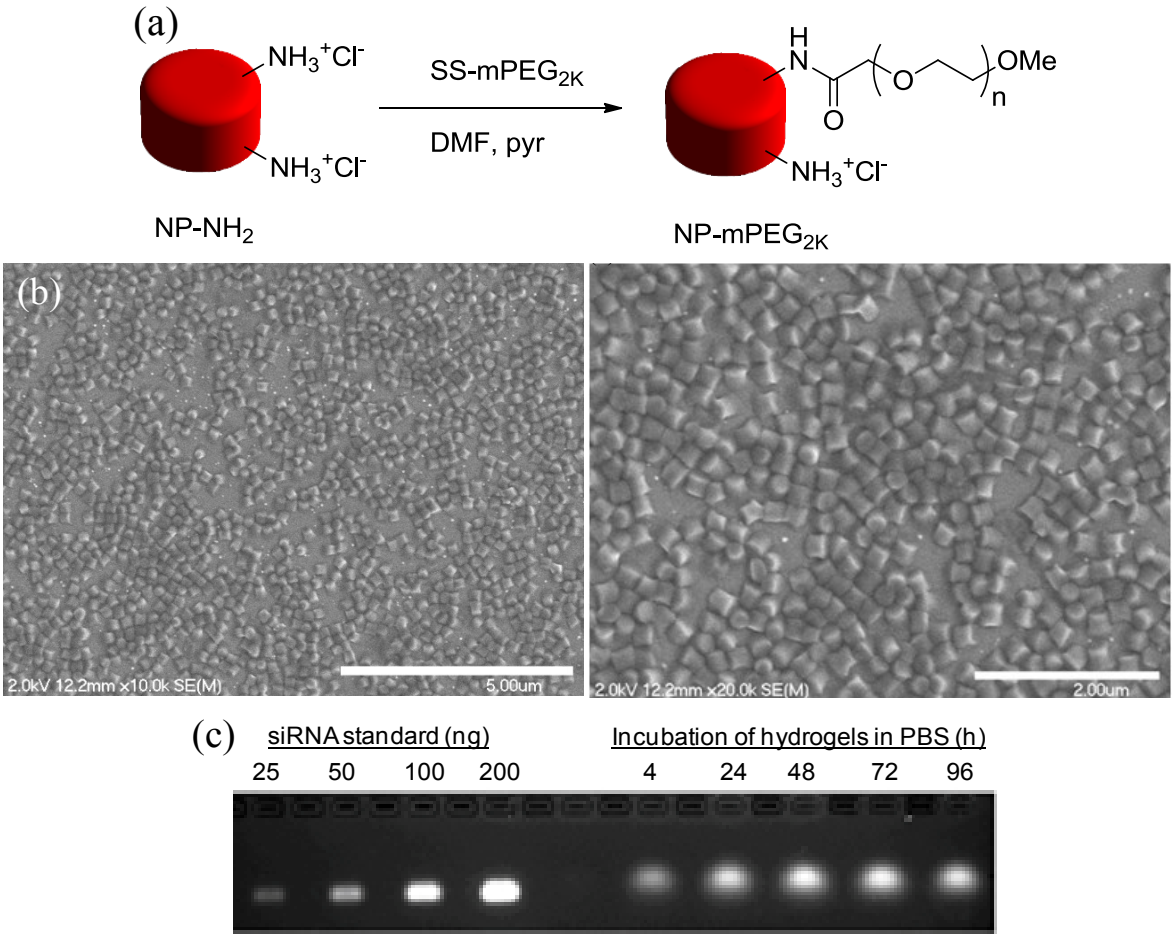

Figure 2.8 (a) Reaction scheme for the PEGylation of hydrogels with succinimidyl succinate monomethoxy PEG_{2K} through amidation. (b) SEM micrographs of PEG-based hydrogel nanoparticles demonstrates cylindrical features, monodispersity, and 200 x 200 nm dimensions. (c) Gel electrophoresis analysis of the time-dependent release of siRNA from hydrogels incubated in PBS at 2 mg/mL and 37 ºC.

Primary amines from AEM were reacted with a succinimidyl succinate ester-activated, monomethoxy PEG in organic solvent using the weak base catalyst pyridine (Figure 2.8a). Particle integrity was maintained as the morphology of the particles appeared appropriate: cylindrical in shape with height and diameter of 200 nm (Figure 2.8b). Time-dependent release of siRNA from particles was investigated by incubating particles in PBS at

37 ºC and taking aliquots over 96 h. Release of siRNA appeared to reach a maximum concentration around 48 h, indicating an ion-triggered diffusion of cargo through the crosslinked network (2.8c). Based on the siRNA standard and through semi-quantitative analysis using ImageJ, loading of siRNA was calculated to be 1.4 wt% (28% encapsulation efficiency).

Table 2.2 Zetasizer analysis of siRNA-charged hydrogels before and after PEGylation.

Particle (siRNA)	ζ-potential (mV)	D_z (nm)
NP-NH_2 (luciferase)	+16.6 ± 0.38	438.8 ± 8.9
NP-NH_2 (control)	+17.6 ± 0.55	445.0 ± 10.4
NP-$mPEG_{2K}$ (luciferase)	+10.2 ± 0.42	390.9 ± 5.0
NP-$mPEG_{2K}$ (control)	+9.72 ± 0.29	391.9 ± 8.5

Dynamic Light Scattering (DLS) showed that particles had diameters around 400 nm and ζ-potentials of ca. +17 mV prior to PEGylation (and after exposure to PBS) while ζ-potential decreased to +10 mV after PEGylation (Table 2.2). When PEGylated particles were dosed on HeLa cells, rapid and complete internalization occurred at low doses for samples containing luciferase and control siRNA (Figure 2.9a). Cytotoxicity was not elicited by PEGylated particles as seen by the high cell viability out to high dosing concentrations (Figure 2.9b). Luciferase expression was maintained in HeLa cells treated with particles containing control siRNA while dose-dependent knockdown of luciferase expression was noted for cells dosed with particles charged with luciferase siRNA (Figure 2.9c). The EC_{50} for reducing luciferase expression was determined to be 5.8 μg/mL particle concentration (6 nM siRNA). Confocal microscopy of HeLa cells dosed with PRINT particles (Figure 2.10) shows uptake of particles and their distribution throughout the cellular cytoplasm as well as the perinuclear region.

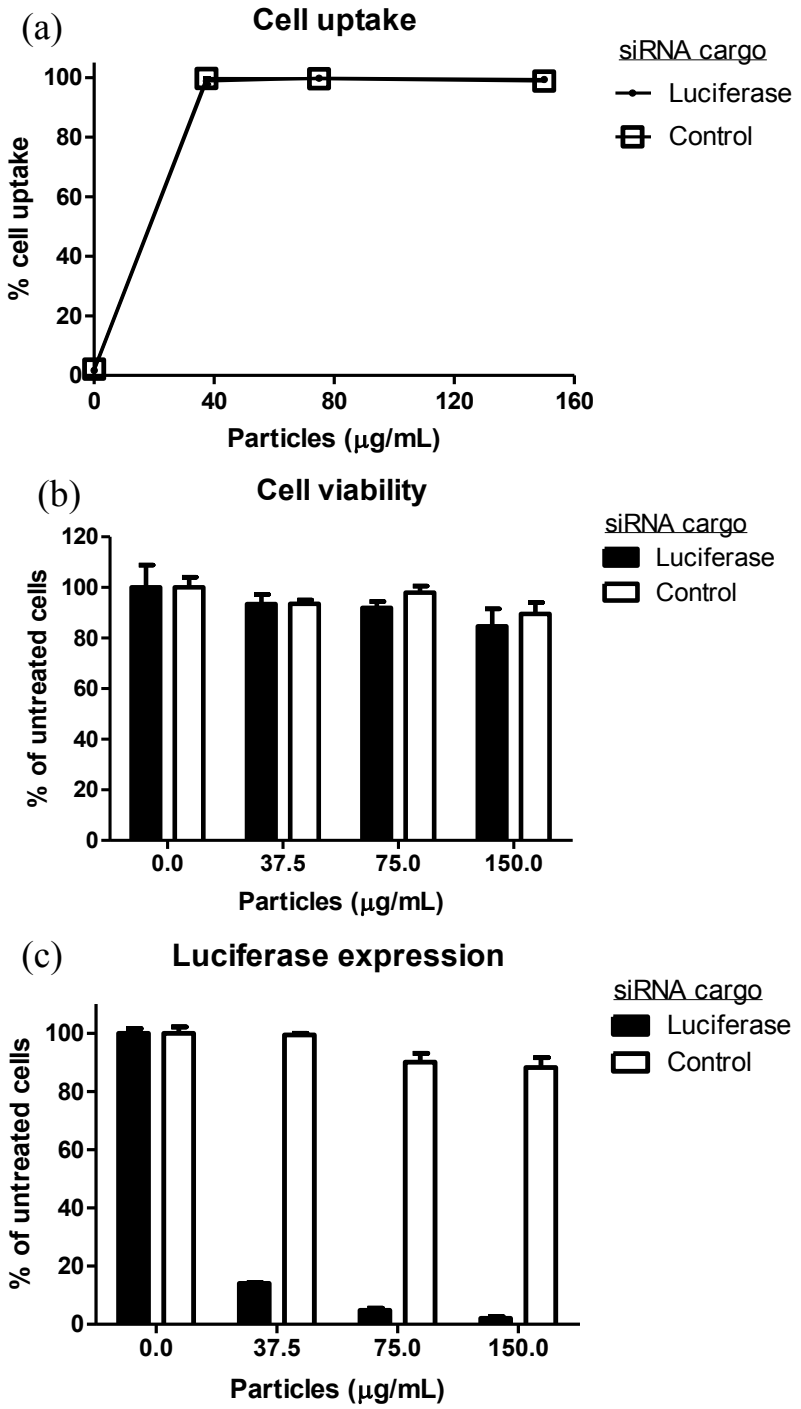

Figure 2.9 (a) HeLa cell uptake of PEGylated, siRNA-containing hydrogel nanoparticles after 4 h dosing at 37 ºC in cell media. (b) Luciferase expression of HeLa cells dosed with luciferase and control siRNA-containing particles for 4 h followed by 72 h incubation at 37 ºC. (c) Viability of HeLa cell dosed with PEGylated, siRNA-containing hydrogels. Cells were dosed with particles for 4 h and incubated for 72 h in media.

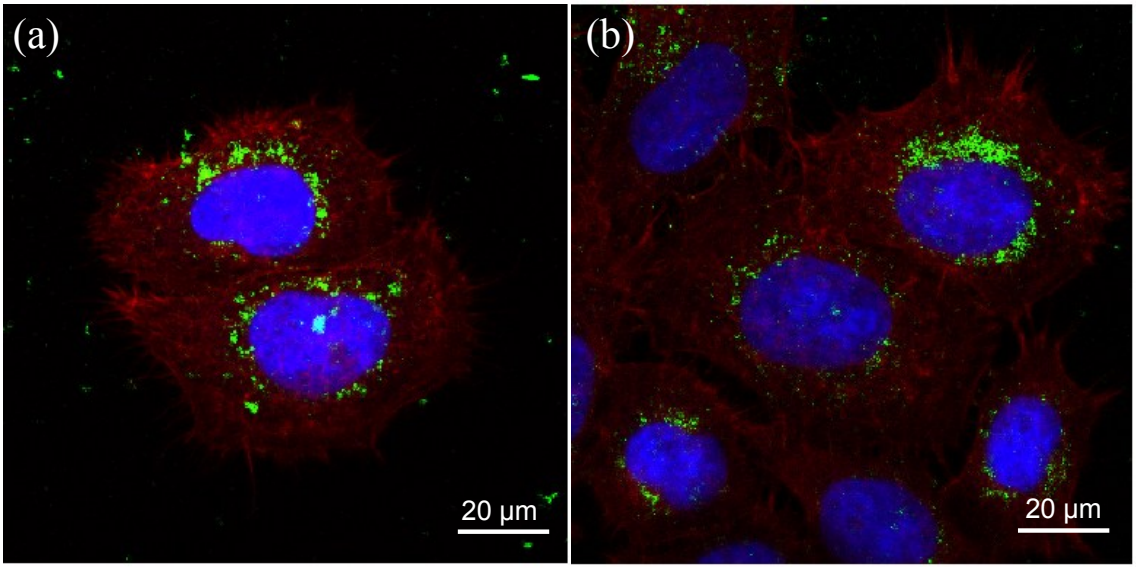

Figure 2.10. Confocal micrographs of HeLa/luc cells dosed with 50 μg/mL of particles containing (a) luciferase or (b) control siRNA cargos for 4 h. Cellular actin cytoskeleton was stained with phalloidin (red) and nuclei with DAPI (blue), while particles (green) were labeled with the fluorescent monomer fluorescein *o*-acrylate during particle fabrication.

2.3.5 Conclusions

siRNA was physically encapsulated in cationic hydrogels, which were subsequently PEGylated prior to dosing on HeLa cells. PEGylated particles slowly released siRNA in neutral buffer under physiological conditions. With rapid cell internalization, efficient gene knockdown was attained by PEGylated hydrogels where cell viability was maintained across all dosing concentrations. Subsequent efforts to silence gene expression in target cells *via* PRINT nanoparticles entail covalent functionalization of particles with targeting ligands such that cell-specific gene silencing may be realized.

2.4 Targeting cancer cells with ligand-conjugated hydrogels for gene silencing

Numerous receptors are over-expressed as markers of diseased cells and may be harnessed for internalization of nanoparticles through specific ligand-receptor associations. The transferrin receptor is highly expressed by several cancer cell lines due its involvement

in iron intake and cell proliferation. Ligands for the transferrin receptor used in tumor cells include anti-transferrin receptor antibodies (e.g. OKT9 for mice, human transferrin for human cell lines) with control proteins like Immunoglobulin G1 (IgG1) and holotransferrin. Reaction of amines from particles with activated, biotinylated PEG linkers allows for conjugation of antibodies through avidin-biotin strategies as has been previously demonstrated by Jin Wang *et al*.[31]. Furthermore, transferrin proteins were covalently reacted to maleimide-grafted PRINT nanoparticles to demonstrate the complex role of multivalency for nanoparticles targeting the transferrin receptor in cancer therapies. Specifically, drug-free targeted nanoparticles elicited death in Ramos cells through an apoptotic pathway as indicated by increased caspase 3/7 activity when presented with PRINT particles conjugated with human transferrin at high surface density.

Self-assembled polymer nanoparticles have been explored for targeted delivery of siRNA.[32,33] For example, after receptor-mediated endocytosis of cyclodextrin-based polymeric nanoparticles targeting the transferrin receptor, particles may become highly protonated and disrupted by harnessing the "proton sponge effect" to escape the endosome and deliver siRNA cargo effectively to the cytoplasm to knockdown gene expression.[34–36]

For particles covalently functionalized with stealthing and targeting ligands, inclusion of endosomal escape agents or reversibly masking lytic behavior of delivery vehicles has been pursued. GALA, a 30 amino acid pore-forming peptide that becomes membrane-lytic after exposure to an endosomal pH environment, was incorporated into small unilamellar vesicles targeting the transferrin receptor to enhance gene delivery.[37] To pursue effective delivery of siRNA from nanoparticles covalently functionalized with ligands, reversible functionalization of particle surfaces through labile bonds to ligands may enable escape from

the endosome after receptor-mediated endocytosis of targeted particles by cancer cells. Furthermore, masking the endosomolytic activity of carriers is required for targeting cells specifically and avoiding non-specific cell uptake. Functional maleic anhydride derivatives were pursued for masking primary amines on endosomolytic poly(vinyl ether)s, composed of alkyl and amino groups, to form stable maleamates under physiological conditions.[38] Maleamates exhibit sensitivity to slightly acidic conditions, hydrolyzing to yield the starting primary amine and maleic anhydride. Subsequent application of maleamate-masked, hepatocyte-targeted siRNA-conjugated poly(vinyl ether)s enabled effective *in vivo* gene silencing.[39] Functional maleic anhydride derivatives may be applied to cationic, amine-containing PRINT hydrogels to reversibly mask endosomolytic features while enabling stealthing and targeting properties.

2.4.1 Experimental

2.4.1.1 Materials

Monosuccinimidyl succinate ester (SCM)-PEG_{2K}-biotin, amine-PEG_{2K}-biotin, and monomethoxy PEG_{5K} monoacrylate was purchased from Creative PEGWorks. Anti-human CD71 (transferrin receptor) biotinylated OKT9 monoclonal antibody and biotinylated mouse IgG1 isotype control were purchased from eBioscience. UltraAvidin was obtained from Leinco Technologies. Remaining reagents were purchased from Sigma Aldrich.

2.4.1.2 Synthesis of carboxylic acid-functionalized 2,3-dimethyl maleic anhydride (CDM)

Triethyl-2-phosphonopropionate (5 g, 21 mmol) was added to a solution of sodium hydride (0.41 g, 18 mmol) in 36 mL anhydrous tetrahydrofuran (THF). After the bubbling

ceased, a solution of dimethyl-2-oxoglutarate (2.5 g, 14 mmol) in 7 mL anhydrous THF was added and stirred for an hour. Then 7 mL of water was added and the THF was removed by rotary evaporation. The resulting aqueous suspension was extracted with 3 × 50 mL ethyl ether. The ether extractions were combined, dried over sodium sulfate, filtered and concentrated to a dark orange oil. The oil was purified by silica gel chromatography using a 2:1 ether:hexane eluent to obtain 2.1 g of triesters (geometric isomers of *E*- and *Z*-olefins) as a yellow oil. The mixture of triesters was dissolved in a 35 mL solution of 3.2 g of potassium hydroxide in a 1:1 mixture of water and ethanol. The resulting solution of triesters was heated to reflux for 1.5 h. The ethanol was then removed by rotary evaporation and the resulting aqueous solution was acidified to pH 0 with 2 M hydrochloric acid (HCl) and stirred for 10 min. This aqueous solution was then extracted with 2 x 250 mL ethyl acetate. The ethyl acetate extractions were combined, dried over sodium sulfate, filtered, and concentrated *in vacuo* to provide a yellow oil. CDM was recrystallized from the oil by mixing in a minimal amount of diethyl ether and maintaining the oil:ether (1:2) mixture under an atmosphere saturated with pentane vapors overnight. The resulting, obese-looking crystals were filtered, washed with cold diethyl ether, and ground up using a mortar and pestle to afford 1.3 g of pure CDM as a fine, white powder (overall yield 50%). ^{1}H-NMR (400 MHz, $CDCl_3$) δ = 10.8 (br, 1H, O*H*), δ = 2.77 (t, *J* = 7.2 Hz, 2H), δ = 2.68 (t, *J* = 7.2 Hz, 2H), δ = 2.11 (s, 3H). Melting point: 97 – 98°C.

2.4.1.3 Synthesis of CDM-PEG-biotin

CDM (20 mg, 0.11 mmol) and EDC (21 mg, 0.11 mmol) were dissolved in 2.5 mL of dry dichloromethane (DCM). To this solution was added biotin-PEG_{45}-NH_2 (240 mg, 0.11 mmol) and then DMAP (16 mg, 0.13 mmol). The reaction was stirred for 8 hrs. Five drops of

TFA was added to the mixture and stirred for 5 min. The reaction mixture was washed with 1 M HCl and then a saturated solution of $NaHCO_3$, dried over sodium sulfate, filtered, and concentrated *in vacuo* to afford CDM-PEG-biotin as a viscous oil (200 mg, 72% yield). ^{1}H-NMR (400 MHz, $CDCl_3$) δ = 7.91 (br, 1H, N*H*), δ = 6.84 (br, 1H, N*H*), δ = 6.80 (br, 1H, N*H*), δ = 6.04 (br, 1H, N*H*), δ = 4.48 (s, 1H), δ = 4.30 (s, 1H), δ = 3.78 (t, *J* = 4 Hz, 2H), δ = 3.48-3.61 (m, 200H), δ = 3.36-3.44 (m, 6H), δ = 3.07-3.20 (m, 2H), δ = 2.66-2.90 (m, 9H), δ = 2.50-2.54 (m, 3H), δ = 2.15-2.23 (m, 2H), δ = 2.08 (s, 3H), δ = 1.55-1.79 (m, 4H), δ = 1.35-1.49 (m, 2H).

2.4.1.4 Synthesis of carboxylic acid-functionalized tetrahydrophthalic anhydride (CTA) precursor

Synthesis of methyl 2-tributylstannylacrylate. Methyl propiolate (10 g, 119 mmol) was added to 450 mL of dry THF and the solution was cooled to 0°C. Bis(triphenylphosphine)-palladium(II)chloride (417 mg, 0.76 mmol) was added to the cooled solution. After tributyltin hydride (38.1 g, 131 mmol) was added dropwise to the stirring solution at 0°C, the solution was stirred for an additional 10 min at room temperature. The solution was concentrated *in vacuo* and the resulting thick syrup was purified by silica gel chromatography using hexanes as the eluent to obtain a clear viscous oil (36 g, 81% yield). ^{1}H-NMR (400 MHz, $CDCl_3$) δ = 6.89 (d, *J* = 2 Hz, 1H), δ = 5.92 (d, *J* = 2 Hz, 1H), δ = 3.73 (s, 3H), δ = 1.49 (m, 6H), δ = 1.31 (m, 6H), δ = 0.97 (m, 6H), δ = 0.88 (t, *J* = 7.2 Hz, 9H).

Synthesis of 2,3-dicarbomethoxy-1,3-butadiene. A solution of $Cu(NO_3)_2 \cdot 3H_2O$ (5 g, 21 mmol) in 20 mL of THF was added to methyl 2-tributylstannylacrylate (8 g, 21 mmol). The reaction mixture was stirred for 10 min at room temperature until it turned brown. It was then

diluted with 300 mL of ethyl acetate and washed successively with 250 mL of 5% aqueous ammonia, 250 mL of water, and 250 mL of brine. The organic layer was dried over sodium sulfate, filtered and concentrated *in vacuo*. The resulting crude product was purified by silica chromatography using a EtOAc:hexanes (1:1) eluent to obtain a yellow liquid (2 g, 55% yield). Next, a solution containing 2,3-dicarbomethoxy-1,3-butadiene (1 g, 5.9 mmol) and methyl acrylate (4.0g, 47 mmol) in 210 mL dry toluene was heated to reflux at 115°C for 2 days. The solution was then concentrated *in vacuo* and the resulting crude mixture was purified by silica chromatography using a EtOAc: hexanes (1:1) eluent to obtain a viscous oil (470 mg, 31% yield). ^{1}H-NMR (400 MHz, $CDCl_3$) δ = 3.76 (s, 6H), δ = 3.71 (s, 3H), δ = 2.50-2.70 (m, 4H), δ = 2.32-2.41 (m, 1H), δ = 2.08-2.12 (m, 1H), δ = 1.66-1.76 (m, 1H).

2.4.1.5 Synthesis of carboxylated tetrahydrophthalic anhydride-derivatized $mPEG_{12}$

1,2,4-tricarbomethoxy-1-cyclohexene (0.5 g, 2 mmol) was dissolved in a 20 mL solution of 1.8 g of potassium hydroxide in a 1:1 mixture of water and ethanol. The resulting solution of triesters was heated to reflux for 1.5 h. The ethanol was then removed by rotary evaporation and the resulting aqueous solution was acidified to pH 0 with 2 M hydrochloric acid (HCl) and stirred for 10 min. This aqueous solution was then extracted with 2 x 250 mL ethyl acetate. The ethyl acetate extractions were combined, dried over sodium sulfate, filtered, and concentrated *in vacuo* to obtain CTA as a white solid. Without further purification, CTA (20 mg, 0.11 mmol) and EDC (42 mg, 0.22 mmol) were dissolved in 2.5 mL of dry dichloromethane (DCM). To this solution was added $mPEG_{12}$-NH_2 (123 mg, 0.22 mmol) and then DMAP (32 mg, 0.26 mmol). The reaction was stirred for 8 hrs. Five drops of TFA was added to the mixture and stirred for 5 min. The reaction mixture was washed with 1 M HCl and then a saturated solution of $NaHCO_3$, dried over sodium sulfate, filtered, and

concentrated *in vacuo* to afford the title compound as a viscous oil (17 mg, 21% yield). ^{1}H-NMR (400 MHz, $CDCl_3$) δ = 3.49-3.69 (m, 48H), δ = 3.38 (s, 3H), δ = 0.73-2.78 (m, 7H).

2.4.1.6 Fabrication and functionalization of hydrogel nanoparticles

PEG-based, cationic particles were prepared as previously described in 2.3.2. For biotinylation, particles were reacted with SCM- or CDM-PEG_{2K}-biotin in DMF at 2 mg/mL for 2 h using pyridine (4 wt eq). Non-biotinylated amines were quenched with various anhydrides (2 wt eq unless noted otherwise) in DMF at 2 mg/mL with pyridine (4 wt eq) for 30 min. Fluorescence of particles was compromised with most anhydrides due to acylation of fluorescein *o*-acrylate; therefore, particles quenched with small molecule anhydrides were treated with a 10% (v/v) of piperidine in DMF to restore fluorescence. Particles were washed with PBS and then incubated at 2 mg/mL with avidin (0.25 wt eq) for 30 min. Afterward, particles were isolated *via* centrifugation and washed with PBS to remove any free avidin. Biotinylated antibodies were then incubated with avidin-conjugated particles at 2 mg/mL for 20 min in PBS at various stoichiometric ratios followed by washing particles to remove unbound antibody.

2.4.1.7 Characterization of hydrogel nanoparticles

ζ-potential measurements were conducted on 20 μg/mL particle dispersions in 1 mM KCl using a Zetasizer Nano ZS Particle Analyzer (Malvern Instruments Inc.). Studying ζ-potential of functionalized particles as a function of pH was carried out using the MPT-2 Autotitrator. DLS measurements were conducted on particle dispersions using 90Plus Particle Size Analyzer (Brookhaven Instruments Inc.). Gel electrophoresis studies were carried out in a similar manner as covered in 2.3.1.4.

2.4.2 Functionalization of hydrogels for targeting the transferrin receptor

Biotinylated anti-transferrin CD71 receptor monoclonal antibody OKT9 and isotype control monoclonal antibody Immunoglobulin G1 (IgG1) were non-covalently conjugated to particles through avidin-biotin binding strategies. As an initial demonstration of the potential for the PEG-based, siRNA-containing particles to target the transferrin receptor, a protocol similar to that established by Wang *et al.*[31] was carried out (Figure 2.11). First, particles were biotinylated with SCM-PEG_{2K}-biotin followed by quenching unreacted amines with acetic anhydride. Particles were conjugated with avidin for subsequent addition of biotinylated antibodies. Resulting ζ-potentials of targeted particles were negative with diameters around 350 nm (Table 2.3). To determine the minimal amount of antibody required for receptor-mediated endocytosis, the concentration of biotinylated antibodies was screened in the conjugation reaction. A dose- and ligand density-dependent increase in cell uptake was observed for OKT9-conjugated particles (2.12a). Conversely, uptake of IgG1-conjugated particles was not observed across all dosing concentrations and antibody:particle ratios (2.12b). A minimal antibody:particle ratio of 10 was then established for subsequent efforts in the targeted delivery of siRNA.

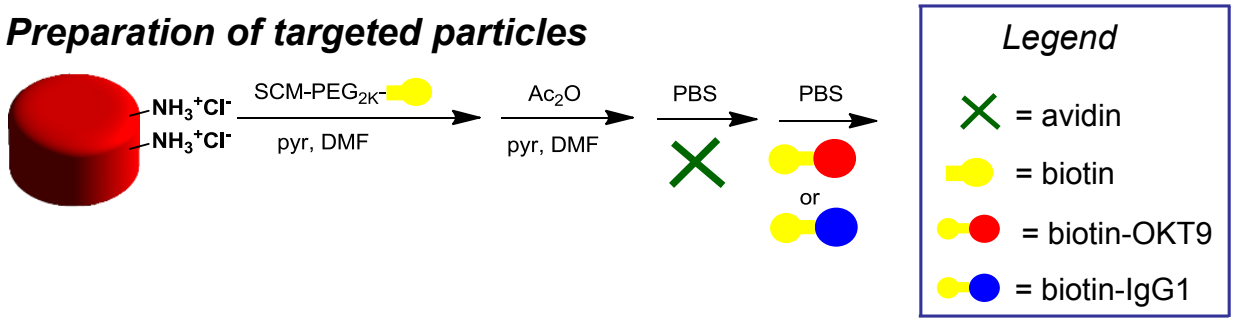

Figure 2.11 Reaction scheme for multi-step preparation of targeted particles through conjugation of biotinylated proteins to amine-quenched, avidinated particles.

Table 2.3 ζ-potential and DLS of protein-functionalized nanoparticles.

	Antibody-conjugated particles	
	OKT9	IgG1
ζ-potential (mV)	-15.0 ± 0.8	-9.7 ± 0.4
D_z (nm)	381.0 ± 14.0	334.0 ± 21.0

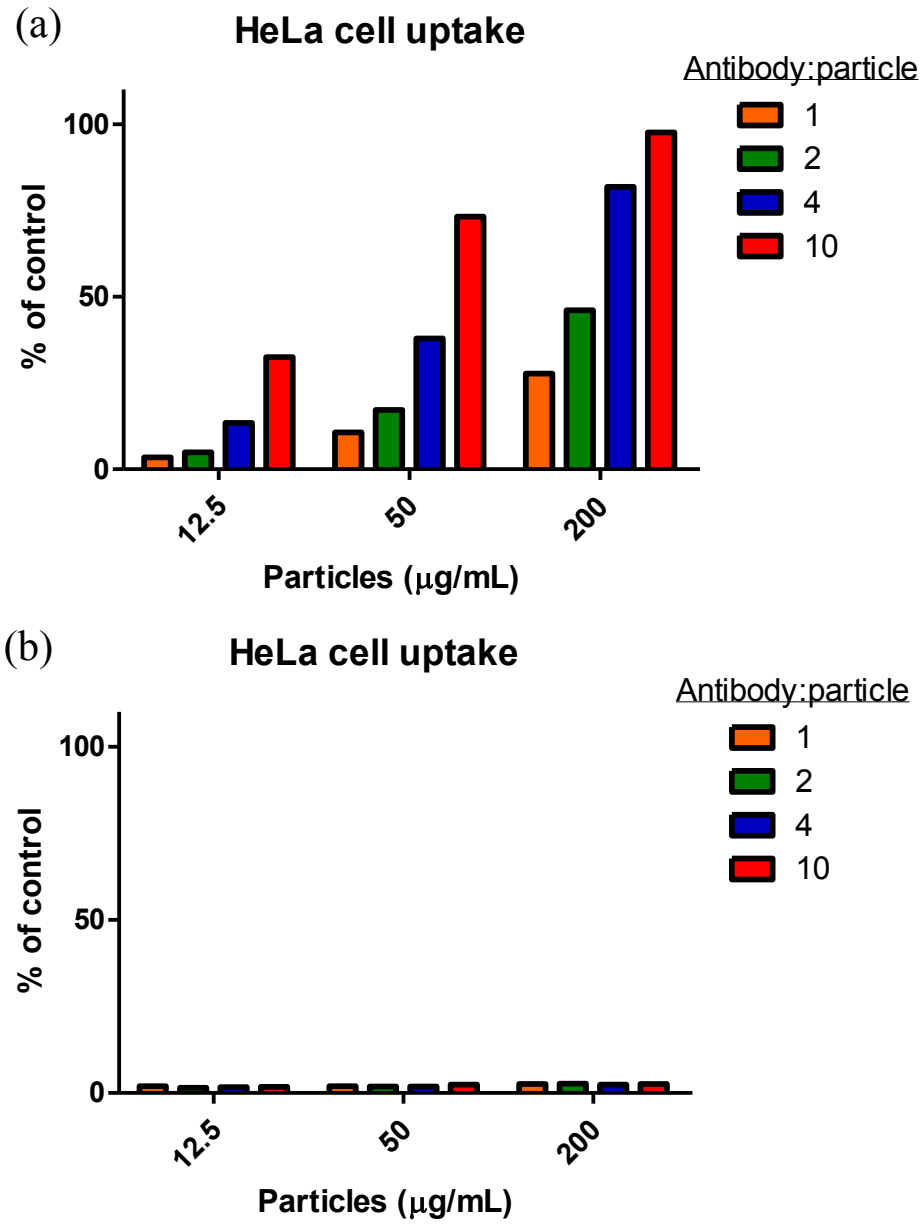

Figure 2.12 HeLa cell uptake of (a) OKT9- and (b) IgG-conjugated hydrogel nanoparticles at multiple antibody:particle ratios and particle dosing concentrations. HeLa cells were dosed with particles for 4 h at 37 ºC in media. Antibody:particle ratio symbolizes milliequivalents of protein per mg of particle (wt/wt).

2.4.3 Targeted delivery of siRNA to cancer cells *via* hydrogels conjugated with targeting and stealthing ligands through labile bonds

To ensure delivery of siRNA from the carrier to the cytoplasm of the target cell, endosomal escape is required after receptor-mediated endocytosis. Endosomolysis was enabled by the cationic amine-containing monomer; however, if all amines are irreversibly reacted, endosomal escape may be hindered. Therefore, reversible covalent modification of amines with maleic anhydride derivatives was pursued. Maleic anhydride derivatives (with substituents located at the 2 or 3 position) can react with amines to form acid-labile maleamates (Figure 2.13). The degree of acid lability for the maleamate depends on the steric constraints of the substituents. Generally, pH sensitivity increases with the number of substituents and resistance to ring opening. Maleic anhydride derivatives have been applied to polycations in gene therapy and drug delivery endeavors to reversibly mask their charge.[40,41]

To investigate the behavior of maleamates on PRINT particles, a series of maleic anhydride derivatives were evaluated for their ability to enable cell-specific uptake of antibody-conjugated particles. Select anhydrides were further tested for their ability to cleave under endosomal conditions and yield positively charged particles that should be able to achieve endosomal escape. A maleic anhydride-activated, biotin-terminated PEG was synthesized for reversible conjugation of ligands (Figure 2.13). Targeted particles were prepared in the manner previously described with a couple adjustments to the protocol: particles were biotinylated with CDM-PEG_{2K}-biotin and instead of quenching non-biotinylated amines with acetic anhydride, maleic anhydride derivatives were implemented.

ζ-potential of particles reacted with maleic anhydride indicated that they had been functionalized as denoted by their negative values (Table 2.4).

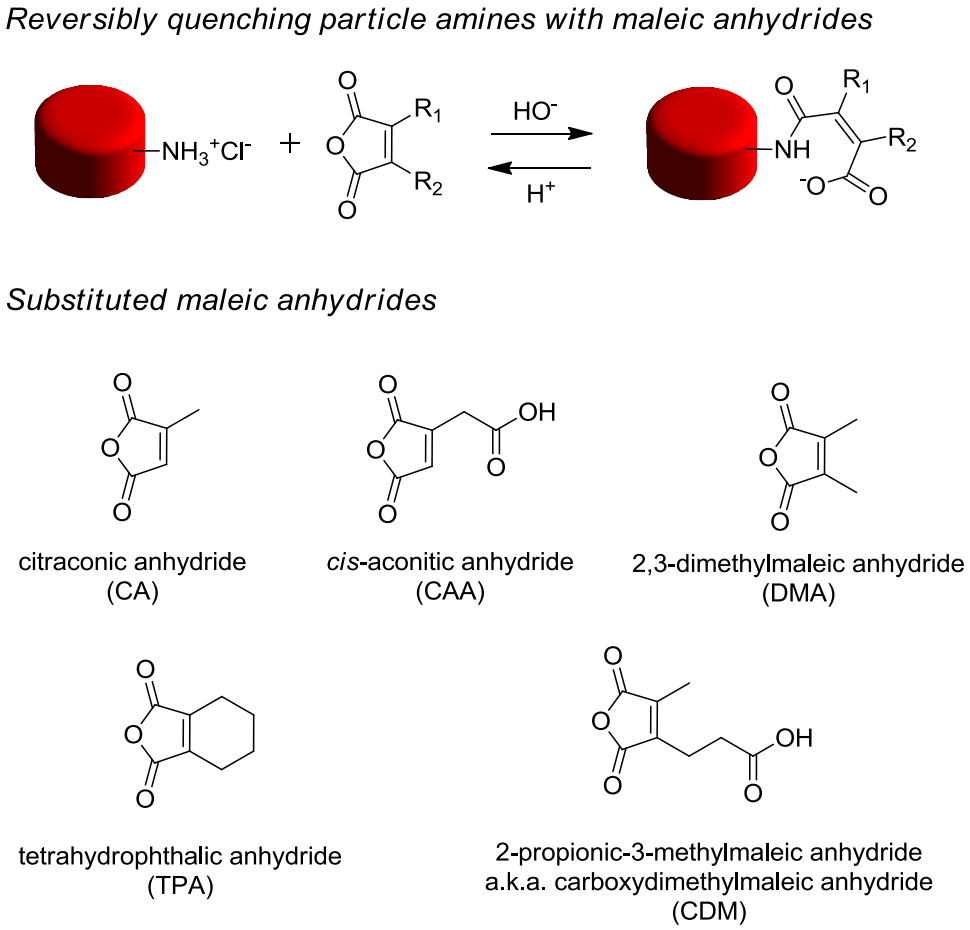

Figure 2.13 Reaction scheme for reversibly quenching amines with maleic anhydride derivatives, whose chemical structures are illustrated. Chemical structure of CDM-activated, biotin-terminated PEG_{2K} is shown for the preparation of particles functionalized with acid-labile ligands.

HeLa cell uptake of OKT9-conjugated particles quenched with all anhydrides reached saturation at relatively low doses while non-specific uptake of IgG1-conjugated particles increased with acid lability of the maleamate (Figure 2.14). Particularly, DMA-quenched

particles exhibited high background uptake (60% at 100 μg/mL) while the next most acid labile maleamate (CDM) reached greater than 15% uptake at 200 μg/mL. The remaining anhydride-quenched particles displayed markedly low background uptake of IgG1-conjugated particles.

Table 2.4 ζ-potential of antibody-conjugated particles quenched with different maleic anhydrides.

Anhydride	ζ-potential of targeted particles (mV)	
	OKT9	IgG1
DMA	-15.1	-16.3
CDM	-7.2	-7.7
TPA	-27.9	-28.4
CA	-24.7	-21.1
CAA	-30.3	-22.4
Ac_2O	-11.2	-11.3

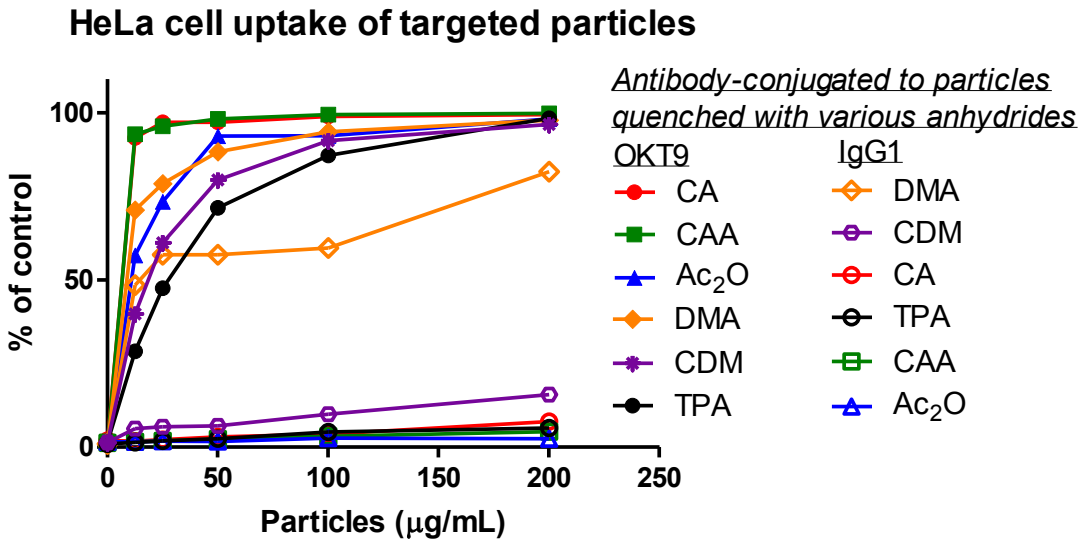

Figure 2.14 HeLa cell uptake of OKT9- and IgG1-conjugated particles quenched with different maleic anhydrides.

The ζ-potential behavior of particles quenched with anhydrides that demonstrated targeting selectivity and were known to cleave under mildly acidic conditions were evaluated after incubation in different buffers. Specifically, particles were incubated in PBS and pH 5.5 (citrate) buffer at 37 ºC for 25 min to observe maleamate lability under physiological and

endosomal conditions (lifetime of endosome), respectively. CDM-quenched particles became slightly positive after incubation in neutral buffer, most likely due to a burst hydrolysis, which may account for some non-specific uptake. When CDM-quenched particles were incubated in buffer of endosomal pH for 25 min, they became more highly charged with a ζ-potential around that of bare hydrogels (Table 2.5).

With pH sensitivity intermediate between CDM and mono-substituted maleic anhydrides, TPA was investigated for its ability to form maleamates that maintain a negative ζ-potential under physiological conditions and respond to an acidic environmental trigger for hydrolysis. Indeed, TPA-quenched particles resumed a negative ζ-potential after incubation in PBS while they become positively charged after incubation in acidic buffer. The mono-substituted maleic anhydride, *cis*-aconitic anhydride, was tested for ζ-potential behavior: a negative charge was maintained under physiological conditions and after exposure to an acidic environment. Therefore, CDM and TPA were selected for their ability to yield siRNA-containing, targeted particles.

Table 2.5 ζ-potential analysis of functionalized particles after exposure to physiological and endosomal conditions.

Quenching group	ζ-potential after 25 min in buffer at 37 ºC	
	pH 7.4 (mV)	pH 5.5 (mV)
CDM	+4.09 ± 3.51	+11.3 ± 3.36
TPA	-32.5 ± 4.68	+9.06 ± 3.23
CAA	-30.3 ± 5.71	-26.5 ± 3.64
None	+12.0 ± 4.56	+11.8 ± 3.48

Progression of the endosomal environment was mimicked to study the ζ-potential of CDM- and Ac_2O-quenched particles by incubating particles in buffer that decreased from pH

7.4 to 5.4 over 25 min (Figure 2.15). Acetic anhydride-quenched particles resumed a slightly negative ζ-potential while CDM-functionalized particles gradually became positively charged after exposure to endosomal conditions.

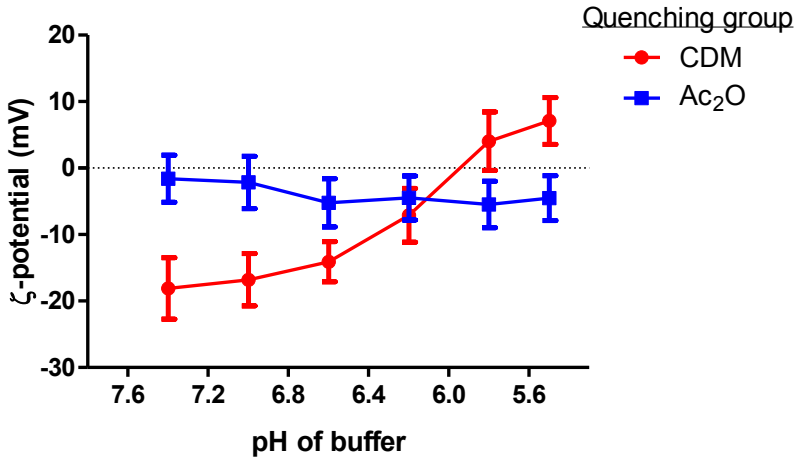

Figure 2.15 ζ-potential of CDM- and Ac_2O-quenched particles as a function of pH over 25 min.

When luciferase siRNA-charged, TPA- and CDM-quenched targeted particles were dosed on HeLa cells, gene knockdown was not observed (Figure 2.16a,b) although selective cell uptake of OKT9-conjugated particles was noted. To investigate the lack of gene silencing, the siRNA remaining in functionalized particles was evaluated through gel electrophoresis. Significant loss of siRNA was encountered in the reactions carried out on particles for functionalization with stealthing and targeting ligands (Figure 2.16c). The effect of each reaction condition in the multi-step preparation of targeted particles required analysis.

After establishing that siRNA was lost, the effect of acetylating particles on the integrity of siRNA was compared to PEGylated nanoparticles. siRNA was retained in particles exposed to conjugation conditions while five minutes of acetylation rendered particles essentially absent of siRNA (Figure 2.17a). Quenching particles with anhydrides

may damage siRNA through acylation and destroy the electrostatic attraction of siRNA to amines.

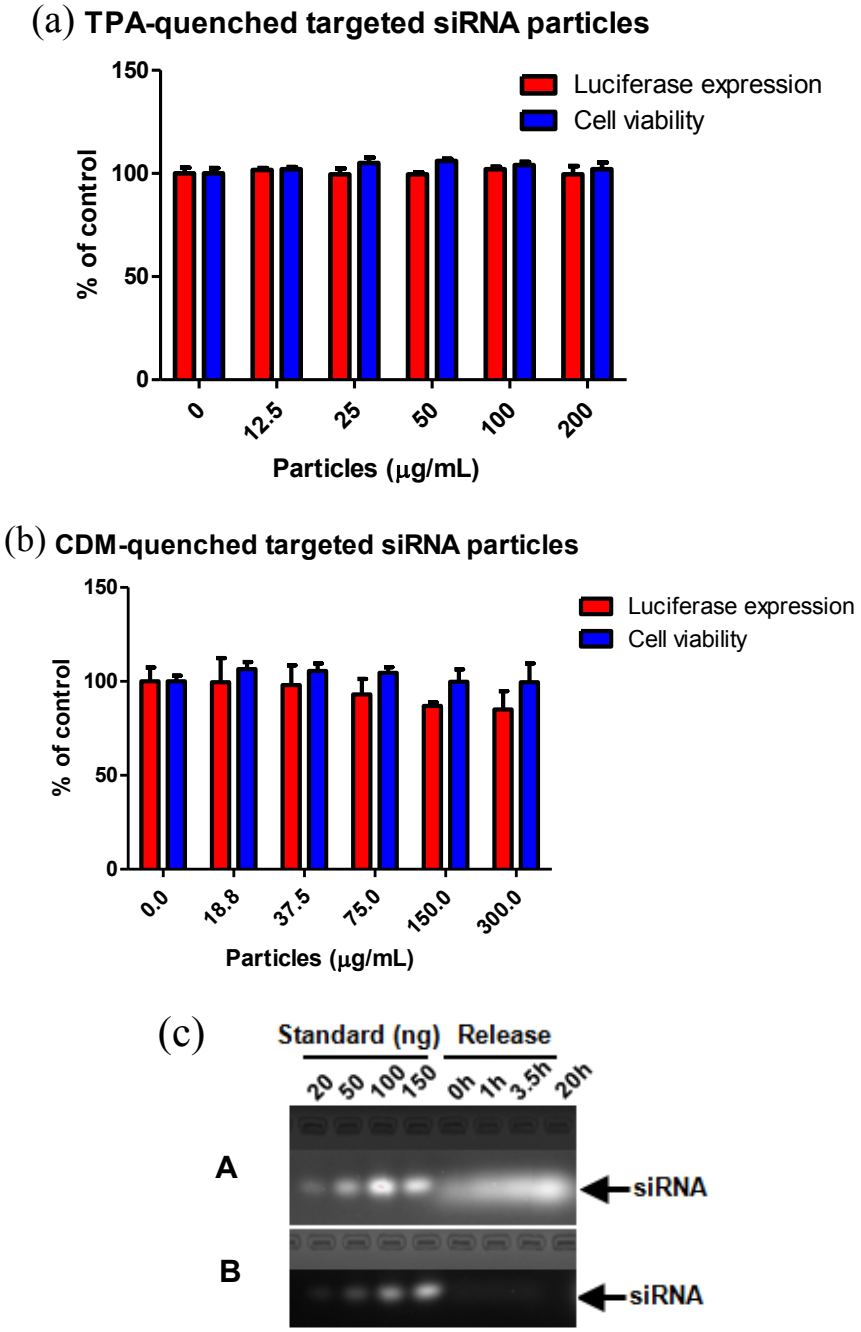

Figure 2.16 Viability and luciferase expression of HeLa cells dosed with (a) TPA- and (b) CDM-quenched, antibody-conjugated particles. (c) Gel electrophoresis of siRNA released from (A) PEGylated nanoparticles and (B) transferrin receptor-targeted nanoparticles.

The effect of salt concentration on extracting siRNA was also investigated by incubating particles in increasingly concentrated KCl salt solutions. After 17 h incubation in different buffers, the amount of siRNA remaining in the particle decreased with increasing salt concentration of the buffer (Figure 2.17b). Therefore, siRNA may diffuse from hydrogels under an ionic environment in a time- and salt concentration-dependent manner. To overcome the significant loss of siRNA with small molecule anhydrides, maleic anhydride derivatives of monomethoxy ethylene glycol oligomers were pursued such that penetration of quenching groups throughout the particle matrix and resulting loss of siRNA would be minimized, i.e. particle surfaces were targeted for PEGylation through use of larger anhydride derivatives.

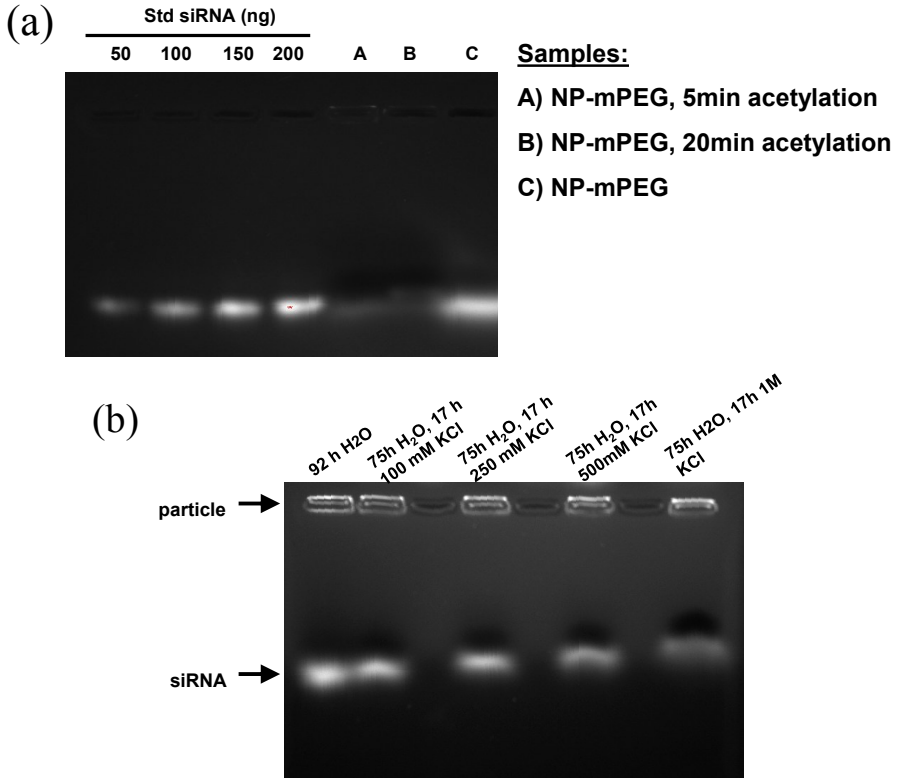

Figure 2.17 (a) Gel electrophoresis of siRNA released from particles exposed to different reaction conditions after incubation in PBS at 37 ºC for 22 h. (b) Gel electrophoresis of siRNA remaining from particles loaded into wells after incubation in water or KCl solutions of different ionic strength.

2.4.4 Conjugation of PEGylated ligands and stealthing groups to nanoparticles for targeted delivery of siRNA

CDM-activated ethylene glycol oligomers of eight and twelve repeat units were tested for their impact on the integrity of siRNA associated with particles. After incubating functionalized particles in buffer to release siRNA, loss of siRNA appeared minimal, especially with CDM-mPEG$_{12}$ (Figure 2.18). The ζ-potentials of CDM-mPEG$_{12}$-functionalized particles were found to be negative, indicating masking of cationic primary amines. Therefore, it seemed appropriate to test the cell uptake selectivity, cell viability, and gene silencing capability of CDM-masked, targeted particles containing luciferase siRNA.

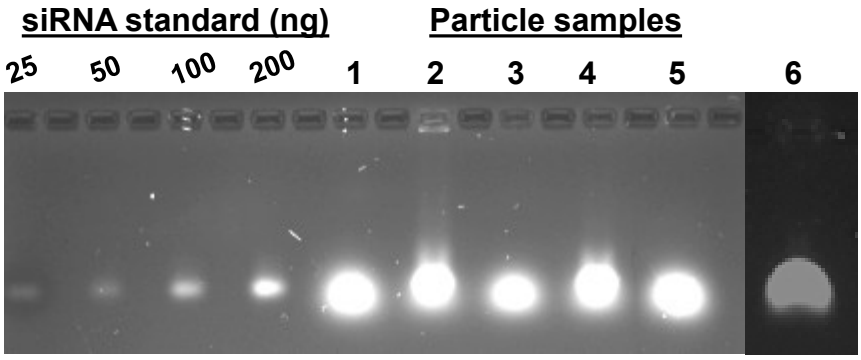

Figure 2.18 Gel electrophoresis of siRNA released from particles functionalized with different ligands after incubation in PBS at 2 mg/mL and 37 ºC.

Cell uptake of CDM-mPEG$_{12}$-masked particles differed from particles quenched with the small molecule CDM in that non-specific uptake of IgG1-conjugated particles was notably high (70 % at 200 μg/mL) (Figure 2.19a). The acid sensitivity of particles quenched with CDM-mPEG$_{12}$ most likely is higher than that of CDM-quenched particles due to a lower density of maleamates from steric crowding of mPEGs and limited diffusion into the interior

of particles. Acid lability of CDM-mPEG-masked particles was significantly high such that complete cell death was induced at the highest particle dosing concentration (200 μg/mL) (Figure 2.19b). Cell death may have been encountered potentially from excessive exposure of particle amines prior to endocytosis such that cell lysis occurred from the highly positively charged particle. Significant luciferase knockdown was not elicited by CDM-mPEG-masked, targeted particles. Due to the high toxicity encountered with targeted particles, a maleamate-derivatized $mPEG_{12}$ with moderate acid lability was desired.

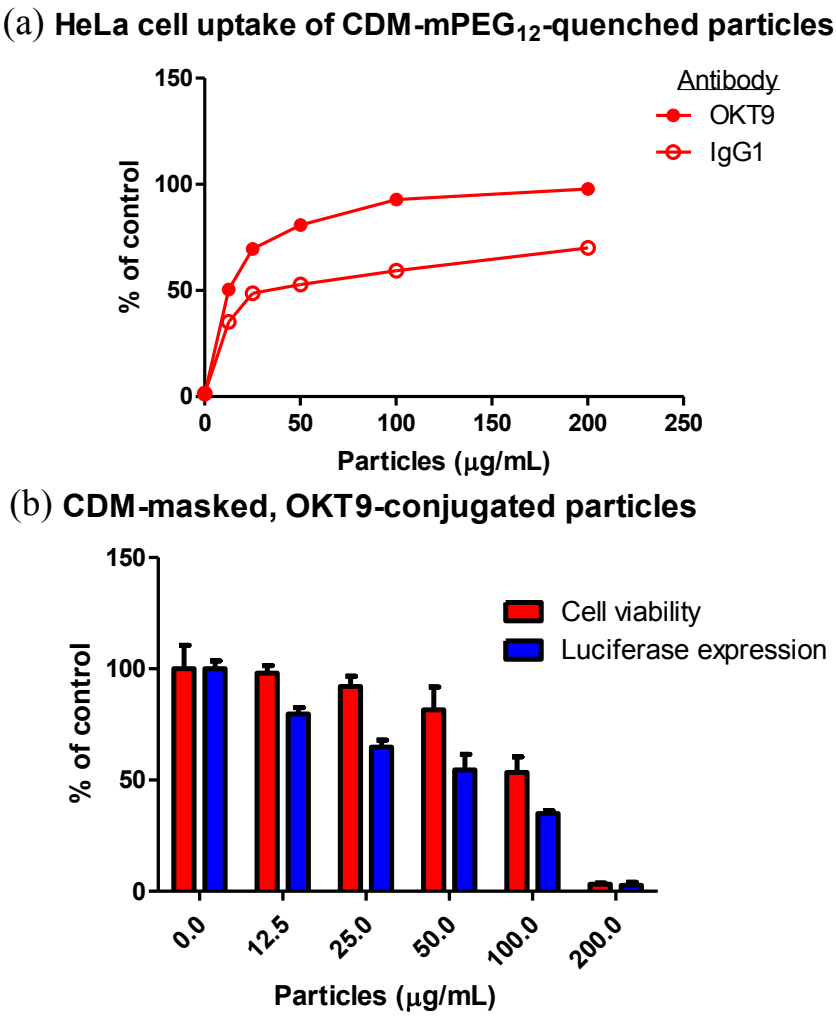

Figure 2.19 (a) HeLa cell uptake of OKT9- and IgG-conjugated particles quenched with CDM-$mPEG_{12}$ after 4 h dosing time. (b) Viability and luciferase expression of HeLa cells dosed with CDM-masked, OKT9-conjugated particles for 4 h followed by 48 h incubation in media at 37 ºC.

Carboxy-installed, tetrahydrophthalic anhydride (CTA)-derivatized $mPEG_{12}$ was synthesized and tested for its effect on siRNA integrity in particles. Roughly 75% of siRNA remained in particles functionalized with CTA-$mPEG_{12}$ relative to PEGylated nanoparticles while particles quenched with TPA do not reveal the presence of any remaining siRNA (Figure 2.20b). Next, siRNA-containing, CTA-$mPEG_{12}$-quenched targeted particles were prepared for luciferase knockdown studies using SCM-PEG_{2K}-biotin and SCM-$mPEG_{12}$ as the non-endosomolytic, control system. Functionalization of particles to create a wholly acid-labile, transferrin receptor-targeted particle system is illustrated in Figure 2.20a. Like TPA-masked particles, the ζ-potential of ligand-functionalized, CTA-$mPEG_{12}$-masked particles remained negative (-3.24 ± 3.23 mV) under cell dosing conditions (PBS, pH 7.4 at 37˚C) for at least 4 h while it turned positive (+4.53 ± 3.07 mV) under endosome-like conditions (pH 5.5 at 37˚C) in only 25 min. These ζ-potential values projected minimal non-specific cell uptake of targeted particles while providing endosomal escape of the cargo before lysosomal degradation of the siRNA cargo.

Transferrin receptor-targeted, CTA-$mPEG_{12}$-masked particles were tested for luciferase siRNA delivery on HeLa/luc cells. Three types of particles were fabricated: OKT9-labeled particles carrying 1) luciferase siRNA or 2) control siRNA, and IgG1-labeled particles carrying 3) luciferase siRNA. As a negative control for these acid-labile particles, another set of particles conjugated with NHS-PEG_{2K}-biotin and NHS-$mPEG_{12}$ were prepared, generating particles with non-labile amides on the surface. Zetasizer characterization of antibody-conjugated hydrogels with different cargos and ligands demonstrates similar diameters among particles and negative ζ-potentials (Table 2.6). When HeLa/luc cells were

treated with CDM-mPEG$_{12}$- and NHS-mPEG$_{12}$-quenched particles, higher uptake of OKT9-labeled particles compared to the IgG1-labeled analogs (Figure 2.21) was observed.

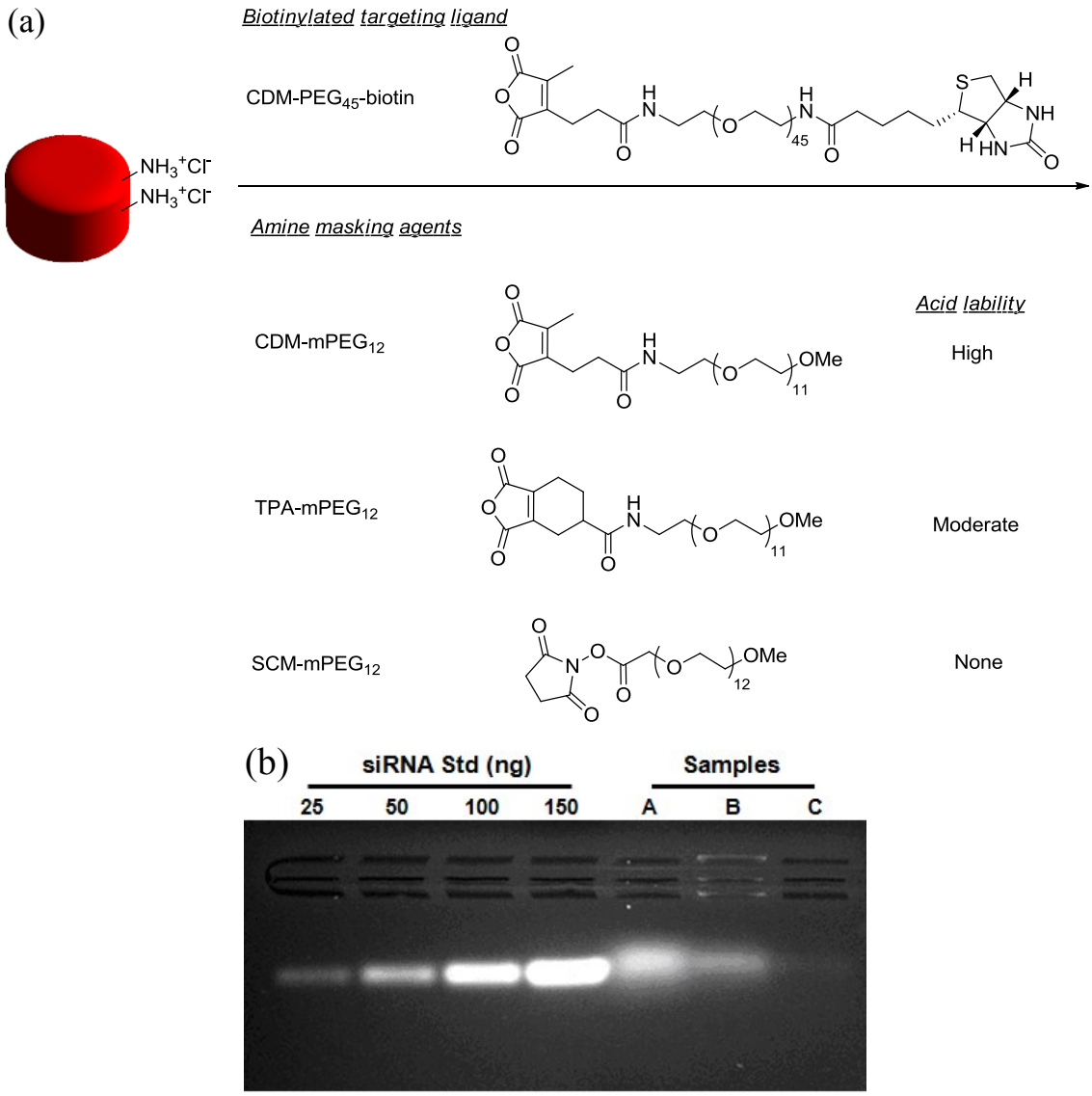

Figure 2.20 (a) Establishment of wholly acid-labile system: functionalization of hydrogel nanoparticles with a biotinylated targeting ligand and different amine masking agents. (b) Gel electrophoresis comparison of siRNA released after 48 h incubation from (A) cationic NP-mPEG$_{2K}$, (B) CTA-mPEG$_{12}$- and (C) TPA-quenched targeted particles confirm that siRNA damage or loss occurred during the acylation reaction with TPA while a reasonable amount of cargo still remained for the targeted, CTA-mPEG$_{12}$-quenched particles relative to that of cationic particles.

Table 2.6 Characterization of antibody-conjugated, CTA/NHS-mPEG$_{12}$-quenched hydrogels.

mPEG$_{12}$, antibody, siRNA	ζ-potential / mV	D_z / nm	PDI
CTA, OKT9, luc	-17.3 ± 0.40	414.4 ± 7.0	0.126
CTA, IgG, luc	-14.4 ± 0.29	420.7 ± 5.4	0.166
CTA, OKT9, crtl	-18.1 ± 0.68	404.4 ± 4.5	0.174
CTA, IgG, crtl	-18.3 ± 0.42	409.1 ± 13.5	0.124
NHS, OKT9, crtl	-6.29 ± 0.27	454.3 ± 6.2	0.142
NHS, OKT9, luc	-7.56 ± 0.31	426.1 ± 12.3	0.155
NHS, IgG1, luc	-5.72 ± 0.15	434.3 ± 11.7	0.124

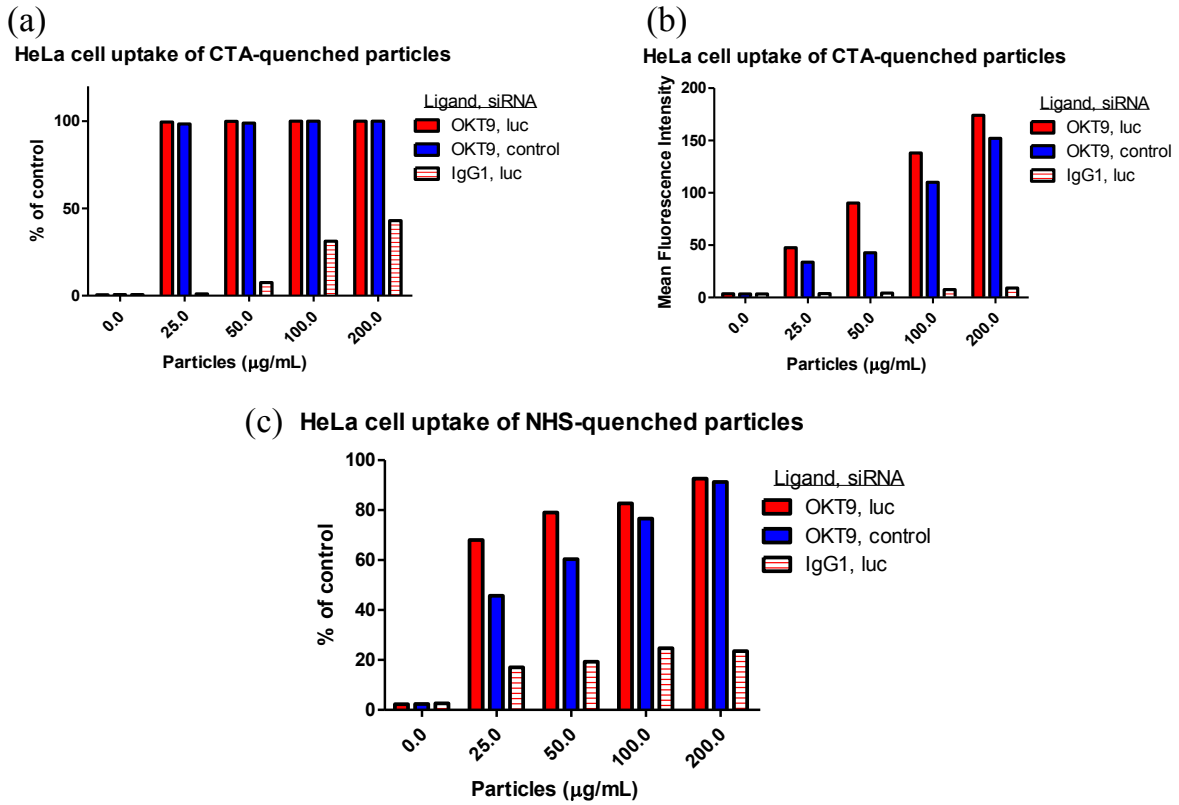

Figure 2.21 HeLa cell uptake of CTA-mPEG$_{12}$-quenched particles after 4 h dosing expressed as (a) % control and (b) mean fluorescence intensity. (c) HeLa cell uptake of NHS-mPEG$_{12}$-quenched particles after 4 h dosing.

50% reduction in luciferase expression was seen for HeLa cells dosed with CTA-mPEG$_{12}$-masked, luciferase siRNA-containing particles at 200 µg/mL (ca. 100 nM siRNA) in Figure 2.22c, whereas particles carrying control siRNA or IgG1-labeled particles carrying luciferase siRNA did not reduce luciferase expression (Figure 2.22a,b). Also, the CTA-

$mPEG_{12}$-masked particles did not display any detectable cytotoxicity by the MTS assay. Thus, enhanced uptake of negatively charged particles afforded by transferrin receptor-mediated endocytosis allowed enough particles to enter cells to cause observable knockdown of the target gene. Although non-acid labile groups (NHS-) provided targeting specificity (Figure 2.23), knockdown of luciferase expression was not achieved, which indicates that the unmasking of the surface amines is the underlying mechanism for endosomal escape. CTA-$mPEG_{12}$-masked targeted particles showed lower knockdown efficiency compared to the cationic NP-$mPEG_{2K}$, which may be attributed to the lower siRNA encapsulation level of targeted particles (0.7 wt%) which is about half that of cationic NP-$mPEG_{2K}$ (1.4 wt%) (Figure 2.24). Although gene silencing was achieved with targeted particles, a composition that transfects more efficiently while enabling access to other organs such as the liver was desired.

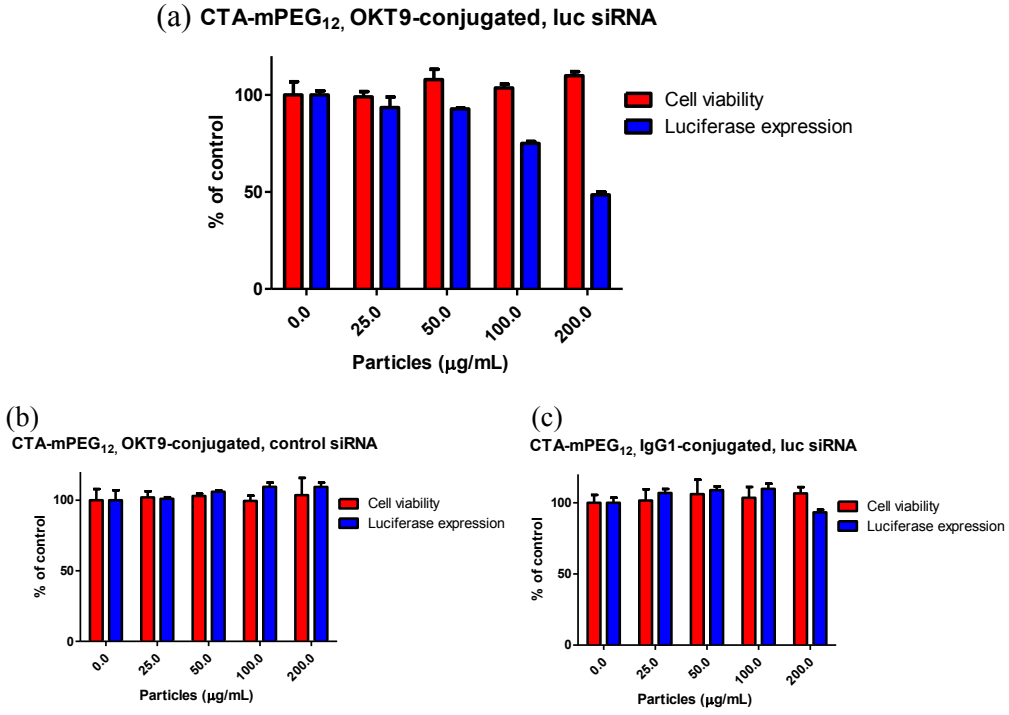

Figure 2.22 Viability and luciferase expression of HeLa cells dosed with CTA-$mPEG_{12}$-quenched particles containing control or luciferase siRNA conjugated with OKT9 or IgG antibodies for 4 h followed by 48 h incubation in media.

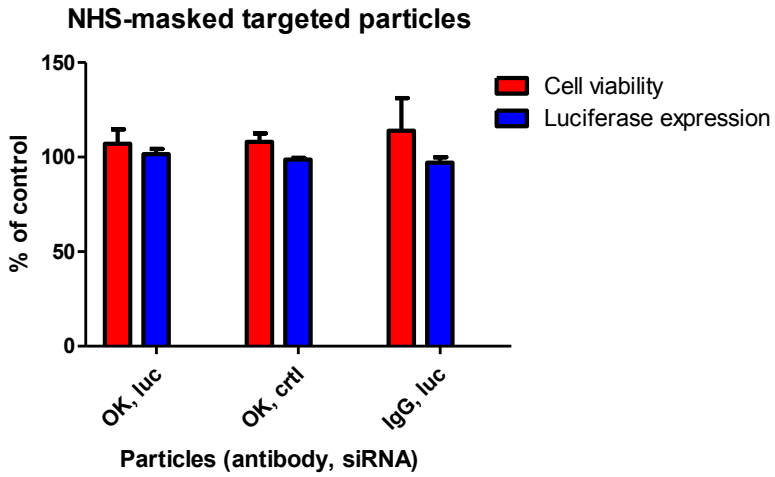

Figure 2.23 Viability and luciferase expression of HeLa cells dosed with NHS-mPEG$_{12}$-quenched particles containing luciferase or control siRNA conjugated with OKT9 or IgG1 antibodies when dosed at 200 µg/mL for 4 h followed by 48 h incubation in media.

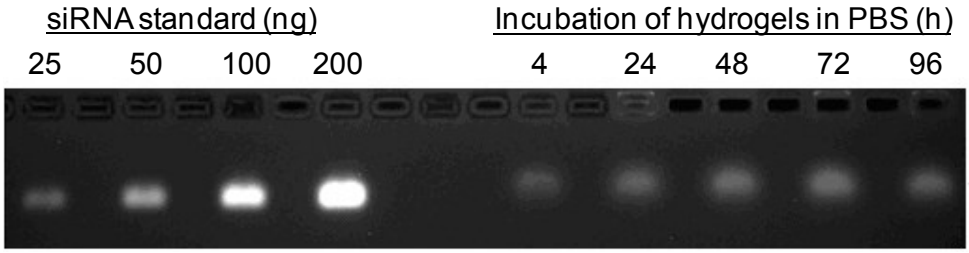

Figure 2.24 Time-dependent release of siRNA from hydrogels after post-fabrication functionalization with targeting ligands when incubated at 2 mg/mL and 37 °C in PBS demonstrates loss of physically entrapped cargo (0.7 wt% encapsulated compared to 1.4 wt% originally encapsulated). Post-fabrication functionalization involved step-wise biotinylation, PEGylation, avidination, and conjugation of biotinylated protein to particles accompanied by multiple washes of particles.

2.5 Optimization of rice-shaped hydrogel nanoparticle composition for gene silencing in hepatocytes

PEGylated nanoparticles can passively target liver cells, namely hepatocytes and Kupffer cells. Hepatic parenchyma composes the main connective tissue of the liver and serves important regulatory roles, which are also implicated in several diseases. Kupffer cells are the liver's immune cells (macrophages) located in sinusoidal walls as part of the mononuclear phagocytic system. Since the liver contributes to major vascular, metabolic, and

secretory functions, diseases developed in hepatocytes are of interest and may be addressed with RNAi. Infectious and metabolic disorders in hepatocytes may be treated with siRNA delivery vectors after systemic administration. Size, shape, and surface characteristics of nanoparticles influence their biodistribution; yet, common organs of nanoparticle accumulation are the spleen and liver due to diffusion, filtration, or clearance.

To prepare nanoparticles that would have potential for delivery to hepatocytes with ~150 nm fenestrations, a smaller particle dimension was adopted (80x320 nm) in which one dimension is less than the size of liver fenestrations. To optimize gene knockdown and maximize cytocompatibility, the structure of amine-containing monomers and their content were screened in addition to varying the siRNA loading. Amine monomers have been screened in the development of combinatorial libraries of poly(β-amino ester)s[42,43] and lipid-like materials[44,45] for transfection of cells with pDNA and siRNA. Monomers with pH-dependent degree of amine protonation and permanent charges potentially present different degrees of internalization, endosomolytic activity, and siRNA binding/release properties. Combinations of primary amine and quaternary ammonium-containing monomers with (meth)acrylamide and (meth)acrylate polymerizable groups were tested for their capacity to enable transfection *via* hydrogel nanoparticles. To provide a crosslinked, hydrophilic network, PEG_{700} diacrylate and tetraethylene glycol monoacrylate were implemented as the crosslinker and hydrophile.

2.5.1 Experimental

2.5.1.1 Materials

Poly(vinyl alcohol), 75% hydrolyzed with MW ≈ 2 kDa, was obtained from Acros Organics. PEG_{700} diacrylate, Irgacure 2959, 2-(acryloylamino)-*N,N,N*-trimethylethanaminium iodide, and tetraethylene glycol were purchased from Sigma. Tetraethylene glycol monoacrylate (HP_4A) was synthesized in-house and kindly provided by Dr. Matthew C. Parrott, Dr. Ashish Pandya, and Mathew Finniss. 2-aminoethyl methacrylate hydrochloride was purchased from Polysciences, Inc. 5 mil wire wound rod was purchased from R. D. Specialties. 80 x 320 nm PRINT molds were graciously supplied by Liquidia Technologies. Remaining reagents and materials were obtained as included in previous experimental sections.

2.5.1.2 Fabrication of cationic rice-shaped nanoparticles

Primary and quaternary amine-containing, (meth)acrylate- and (meth)acrylamide-based monomers were implemented in particle matrices (Figure 2.24a). The composition of the pre-particle solution for preparation of hydrogel nanoparticles is listed in Table 2.7 where the amine content was tested at 30 and 50 wt% while charging each with 5 or 10 wt% siRNA. The pre-particle solution was prepared at 2.5 wt% in DEPC-treated water. To enable wetting of pre-particle solution contents on PET from a water solution and to increase porosity, poly(vinyl alcohol) was implemented. Furthermore, a water-soluble photoinitiator (Irgacure 2959) was used in the pre-particle solution. With a #5 Mayer Rod, a film was cast on a sheet of PET, which was subsequently laminated to Liquidia molds (80x320 nm dimensions) at 40 psi. Next, the mold was delaminated from the PET sheet and laminated to

a sheet of corona-treated PET at 40 psi. The mold-PET sandwich was then cured for 5 min in a UV oven. Particles were collected mechanically using a cell scraper and water (ca. 1 mL per foot).

Table 2.7 Compositions of pre-particle solutions for screening siRNA delivery efficiency.

Component	wt %	
siRNA	5	10
Amine	30, 50	30, 50
HP_4A	49, 29	44, 24
Poly(vinyl alcohol)	10	10
Irgacure 2959	1	1
PEG_{16}-DA	5	5

2.5.1.3 Particle characterization, cell culture, and cell assay

Particles were characterized and cell culture/assays were conducted in a manner similar to those reported in previous experimental sections.

2.5.2 Characterization and *in vitro* behavior of cationic rice hydrogel nanoparticles

Rice-shaped hydrogel nanoparticles prepared with different amine-containing monomers (Figure 2.25a) demonstrated that ζ-potential increased with amine content (except for with AETMAC), exhibiting values from +28 to +40 mV (Table 2.8). In general, the ζ-potential of particles was higher for 50 wt% AEM relative to 30 wt% AEM. The chemical structures of new monomers implemented in the particle matrix illustrate the use of an oligomeric ethylene glycol acrylate, PEG diacrylate crosslinker, water-soluble benzoin photoinitiator, and poly(vinyl alcohol) as a porogen and PET-wetter (Figure 2.25b). SEM micrographs of select rice-shaped nanoparticles confirmed their 80x320 nm dimensions, monodispersity, and soft features (Figure 2.25c).

Luciferase siRNA-charged hydrogel nanoparticles fabricated from different amine monomers were screened for transfection efficiency on luciferase-expressing HeLa cells. For AEM-based hydrogels, luciferase expression and viability decreased with increasing amine content and particle dosing concentration (Figure 2.26). Gene silencing efficiency increased with siRNA loading for both amine contents. The EC_{50} for silencing luciferase expression was plotted for each particle composition using Lipofectamine^{TM} 2000 as the common transfection benchmark (Figure 2.27). Acrylamide monomers were found to be more potent materials for gene silencing than their acrylate analogs. Combining primary and quaternary amine functionalities did not enhance transfection relative to primary amines. Higher amine contents elicited luciferase knockdown more effectively. In general, cell viability decreased at higher particle dosing concentrations and amine contents. The most effective composition for silencing luciferase expression was based on 50 wt% AEMAm and 10 wt% siRNA charged into the pre-particle solution.

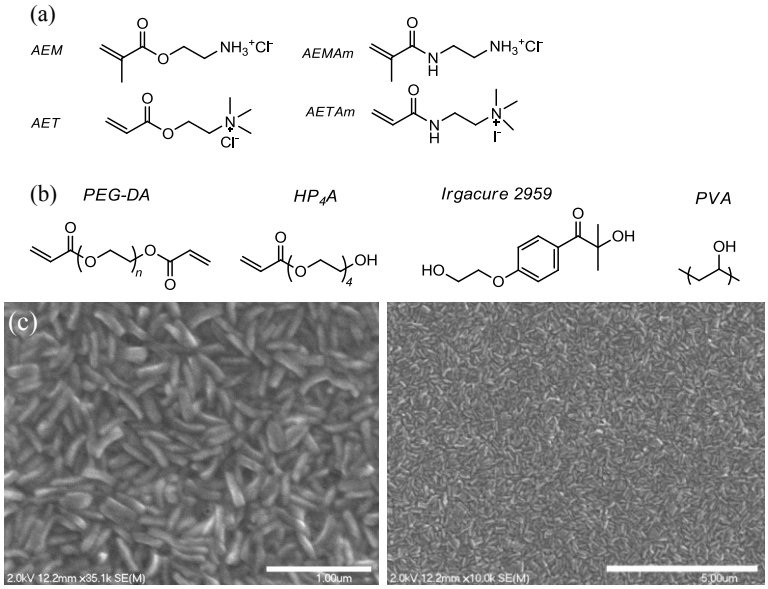

Figure 2.25 Chemical structures of (a) primary amine and quaternary ammonium (meth)acrylate and (meth)acrylamide monomers and (b) new monomers implemented in cationic hydrogel matrices. (c) SEM micrographs of select rice-shaped hydrogel nanoparticles (30% AEM, 5 wt% siRNA).

Table 2.8 ζ-potentials of cationic hydrogel nanoparticles prepared with different amine-containing monomers.

Amine Monomer	ζ-potential (mV) Amine, siRNA (wt%)			
	50,5	50,10	30,10	30,5
AEMAm	+35.9 ± 1.3	+35.4 ± 0.6	+31.8 ± 0.7	+31.1 ± 1.1
AEM	+39.8 ± 0.6	+38.8 ± 1.1	+34.6 ± 0.6	+34.8 ± 0.6
AETAm	+30.3 ± 1.1	+31.1 ± 0.5	+26.3 ± 0.1	+26.0 ± 1.1
AET	+27.7 ± 2.4	+37.6 ± 0.4	+31.1 ± 0.4	+33.5 ± 0.8
AEM-AET (50-50)	+37.1 ± 4.9	+34.2 ± 4.9	+30.4 ± 0.7	+31.7 ± 1.7

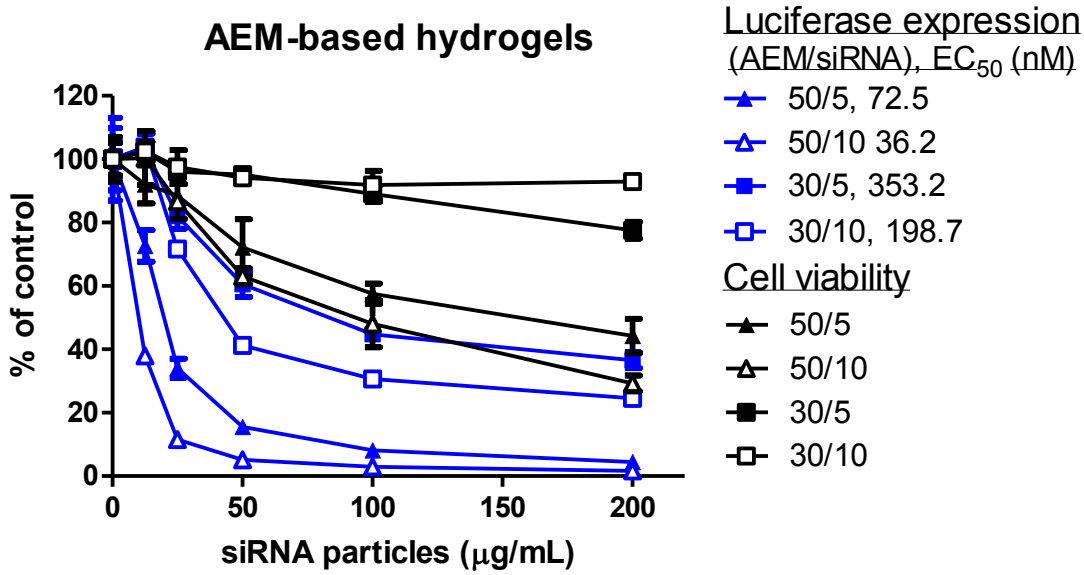

Figure 2.26 Viability and luciferase expression of HeLa cells dosed with AEM-based cationic hydrogel nanoparticles containing siRNA. Half-maximal effective concentration (EC_{50}) of siRNA (nM) required for gene knockdown is based on 5 wt% siRNA charged into the pre-particle solution.

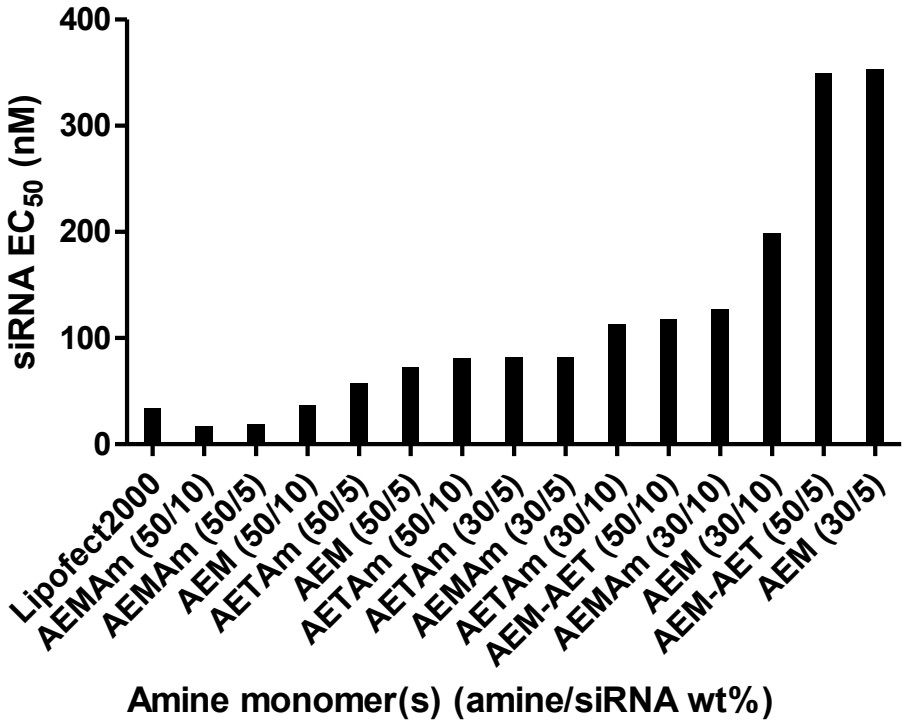

Figure 2.27 Half maximal effective concentration (EC_{50}) of siRNA (nM) required to reduce gene expression by 50%. For each particle sample, EC_{50}s were based on 5 or 10 wt% siRNA loading into hydrogel nanoparticles.

2.6 Reversibly coating rice-shaped particles with terpolymer ligands through polyelectrolyte attraction for targeting hepatocytes

Hepatocytes express asialoglycoprotein receptors, which recognize and internalize galactose, lactose, and *N*-acetylgalactosamine ligands. Nanoparticles and gene delivery vectors have been functionalized with these sugar ligands for targeted gene therapy. For example, a lactosylated PEG-siRNA conjugate was linked *via* an acid-labile β-thiopropionate to poly(L-lysine) to form polyion complex micelles that demonstrated *in vitro* gene knockdown.[46] Additionally, galactose-terminated PEG-functionalized PEI was pursued for delivery of DNA to human hepatocarcinoma (HepG2) cells, which enhanced transfection efficiency relative to PEI.[47] *N*-acetylgalactosamine-grafted dynamic polyconjugates demonstrated effective *in vivo* delivery of siRNA to hepatocytes.[39] siRNA has been

conjugated to galactose- and mannose-terminated PEGs *via* a disulfide linkage for *in vitro* gene silencing.[48] The delivery of pDNA-galactosylated poly(L-lysine) complexes was investigated for targeted delivery to HepG2 cells while exploring the influence of fusogenic peptides.[49] HepG2 cell internalization of magnetic nanoparticles surface-modified with galactose, glucose, and sialic acid was studied, focusing on spatial orientation of ligands.[50] The attachment of hepatocytes was enhanced by poly(acrylic acid)-grafted PET films functionalized with galactose.[51]

Recently, cationic nanoparticles have been coated electrostatically with polyanion-based ligands to alter surface properties and enable targeting capabilities. Coating nanoparticles electrostatically avoids modification of the biophysical properties of nanoparticles encountered through covalent functionalization. Increasing covalent ligand substitution of cationic polymers can decrease gene delivery efficiency (condensation and endosomal escape) by modifying the polymer's original functionality.[52,53] Poly(glutamic acid)-based RGD ligands (which target integrin receptors on endothelial cells) were coated on cationic poly(β-amino ester) nanoparticles to enable ligand-specific gene delivery to human primary cells[54] while also demonstrating serum stability. Peptide ligands without receptor specificity but rather varying in charge density were tethered to poly(glutamic acid) to observe the effect on biodistribution and gene delivery when coated on cationic poly(β-amino ester) nanoparticles.[55] A low coating density of PGA ligands without a cationic insert promoted accumulation in liver and gene delivery.

After screening PRINT particle compositions to establish effective transfection, the ideal composition was tested in nanoparticles for targeting hepatocytes with electrostatic coatings. Poly(acrylic acid)-based terpolymers were synthesized with galactose and glucose

(control) ligands, PEG spacers, and mPEG stealth layers. Ligand density was tested for selective receptor-mediated endocytosis in mouse-derived hepatocytes *in vitro*. Gene silencing properties and *in vivo* biodistribution of coated nanoparticles was also evaluated.

2.6.1 Experimental

2.6.1.1 Materials

DyLight 488 maleimide, Float-a-lyzer dialysis units, methanol, dichloromethane, and silica gel were purchased from Fisher Scientific. Poly(ethylene glycol) derivatives were obtained from Laysan Bio, Inc. (SCM-PEG_{2K}-NHBoc) and Creative PEGWorks ($mPEG_{5K}$-NH_2). AlexaFluor 555 maleimide was purchased from Invitrogen. Polyacrylic acid (molecular weight ≈ 1,800 g/mol), 4-aminophenyl galactopyranoside, 4-aminophenyl glucopyranoside, and remaining chemicals were purchased from Sigma Aldrich or obtained elsewhere as previously reported. FVII siRNA was purchased from Dharmacon, Inc. with sense sequence 5'-GGAucAucucAAGucuuAcT*T-3' and antisense sequence 5'-GuAAGAcuuGAGAuGAuccT*T-3' where 2'-OMe modified nucleotides are in lower case and phosphorothioate linkages are represented by asterisks. Amine-modified ELAV1 and FVII siRNAs were provided by Novartis.

2.6.1.2 Synthesis of ligands for stealthing particles and targeting hepatocytes

Synthesis of PAA-$mPEG_{5K}$. PAA (MW ≈ 1,800 g/mol, 180 mg, 2.5 mmol) was reacted with mPEG-NH_2 (4.5 g, MW ≈ 4,500 g/mol, 0.4 eq) in a 250-mL round-bottomed flask containing 0.1 M MES buffer (170 mL, pH 5) along with EDC (1.16 g, 3 eq) and sulfo-NHS (0.54 g, 1 eq) for 4 h followed by raising the pH to 7.4 and allowing the reaction to proceed for 96 h. Crude product was concentrated by lyophilization and subsequently dialyzed (Slide-a-lyzer)

repeatedly with a 20 kDa MWCO membrane in DI water for 48 h followed by freeze-drying to yield PAA-mPEG. The yield of product was 3.30 g (64% yield). Degree of mPEG substitution on PAA was determined to be 25 mol% *via* ^{1}H NMR.

Synthesis of galactose/glucose-PEG-NHBoc and -NH_2. SCM-PEG-NHBoc (MW ≈ 2,000 g/mol, 0.6 g, 0.3 mmol) was dissolved in anhydrous DMF (10 mL). Separately, 4-aminophenyl galacto/glucopyranoside (1.0 g, 10 eq) was dissolved in anhydrous DMF (15 mL) and combined with the PEG solution in an oven-dried, N_2-purged 50 mL round-bottomed flask. The reaction was left to proceed for 16 h at room temperature. Solvent was removed *via* rotary evaporation followed by purification *via* silica gel column chromatography (85:15 DCM:MeOH) to provide 0.43 g of galactose/glucose-PEG-NHBoc (72%). Subsequently, ^{t}Boc groups were removed by dissolving the product in 50:50 DCM:TFA (12 mL) and stirring for 1 h. Solvents were removed *via* rotary evaporation and the product was dissolved in minimal volume of PBS and dialyzed (Slide-a-lyzer) with a 2 kDa MWCO membrane against PBS and then DI water repeatedly followed by lyophilization and filtration to yield galactose/glucose-PEG-NH_2. Sugar-functionalized PEGs were analyzed by ^{1}H NMR and MALDI-MS.

The observed molecular weight distribution of Boc-deprotected, sugar-functionalized PEG (Figure 2.28a) matched the predicted molecular weight, differing less than 0.5 mass/charge ratio over relevant molecular masses as noted in the MALDI-MS spectrum (Figure 2.28b) and Table 2.9.

Synthesis of PAA-gal/glu. PAA-mPEG (60 mg, 2 umol) and galactose (gal)/glucose (glu)-PEG-NH_2 (0.5, 2, or 8 eq) were reacted in PBS (12 mL) along with EDC (6 eq) and sulfo-NHS (6 eq) after first activating in 0.1 M MES buffer. The reaction was allowed to proceed

for 48 h after which the crude product was purified *via* repeated dialysis (20 kDa MWCO) over 48 h, followed by lyophilization, providing PAA-gal/glu terpolymers with ca. 10, 20, and 30 mol% substitution of sugars when 0.5, 2, and 8 eq were implemented in reactions.

2.6.1.3 Characterization of ligands, cell assays, and coating cationic hydrogels with poly(acrylic acid)-based ligands

Characterization of polymers was carried out by ^{1}H NMR (400 MHz) and MALDI-MS (IonSpec-FTMS, 9.4T). Cell culture, assays, and microscopy were conducted as previously described using human hepatocarcinoma (HepG2) and mouse-derived hepatocyte (AML12) cell lines.

PAA-mPEG: ^{1}H NMR (400 MHz, D_2O) δ = 3.49-3.69 (m, 100H), δ = 2.40-1.01 (m, 3H). Galactose-PEG-NHBoc: ^{1}H NMR (400 MHz, $CDCl_3$) δ = 2.85 (s, 9H), 7.05 (d, 2H), 7.55 (d, 2H). PAA-gal10: ^{1}H NMR (400 MHz, D_2O) δ = 3.49-3.69 (m, 4755H), 7.05 (d, 2H), 7.55 (d, 2H). PAA-gal20: ^{1}H NMR (400 MHz, D_2O) δ = 3.49-3.69 (m, 3433H), 7.05 (d, 2H), 7.55 (d, 2H). PAA-gal30: ^{1}H NMR (400 MHz, D_2O) δ = 3.49-3.69 (m, 2699H), 7.05 (d, 2H), 7.55 (d, 2H). ^{1}H NMR and mass spectra analysis was similar for glucose-derived ligands.

For screening the effect of ligand density on ζ-potential, particles were incubated with various weight ratios of ligands in PBS for at least 30 min prior to analysis. Coated hydrogels were prepared by mixing a 2 mg/mL dispersion of hydrogels in water with an equal volume of ligand solutions (at different concentrations) in 2x PBS. A 30 μL aliquot was then taken for dilution into 1 mL of 1 mM KCl to obtain ζ-potential measurements. The optimal ligand density was then implemented in subsequent studies directly when harvesting particles or after fabrication. To study the pH-responsiveness of coated hydrogels, which had been

washed with buffer, they were re-suspended in buffers of different pH; afterward, a 30 µL aliquot was taken for dilution in 1 mM KCl and ζ-potential analysis.

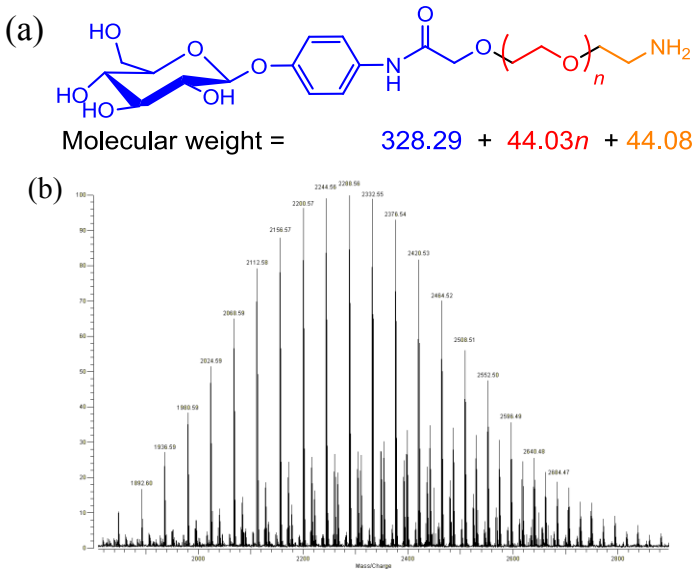

Figure 2.28 (a) Structural breakdown of galactose-PEG-NH_2 for predicting molecular weight as would be observed by MALDI-MS in Table 2.9. (b) MALDI-MS spectrum of galactose-PEG-NH_2.

Table 2.9 Molecular weight (MW) analysis by MALDI-MS of galactose-PEG-NH_2 with predicted and observed mass based on repeat units (*n*) of PEG.

n	Predicted MW + Na^+	Observed MW + Na^+
34	1892.38	1892.60
35	1936.41	1936.59
36	1980.44	1980.59
37	2024.47	2024.59
38	2068.50	2068.59
39	2112.53	2112.58
40	2156.56	2156.57
41	2200.59	2200.57
42	2244.62	2244.56
43	2288.65	2288.56
44	2332.68	2332.55
45	2376.71	2376.54
46	2420.74	2420.53
47	2464.77	2464.52
48	2508.80	2508.51
49	2552.83	2552.50
50	2596.86	2596.49
51	2640.89	2640.48
52	2684.92	2684.47

2.6.1.4 Intravenous injection of nanoparticles and analysis of tissues

Particles were administered intravenously into C57BL/6 mice (6-10 weeks old) at 0.5 mg/mouse in 150 μL water or PBS. 48 h after dosing, mice were bled submandibularly for blood samples, then euthanized with CO_2 followed by cervical dislocation, and major organs were collected for further analysis, including liver, lung, spleen, kidney, and heart.

To track particle distribution *in vivo*, the isolated organs were imaged with IVIS Luminar (Calipar Life Sciences) for particle-associated fluorescence (DyLight 680 or DyLight 488 maleimide) and analyzed with Living Image software.

For histology analysis, liver tissues were frozen in O.C.T. compound, and 5 μm sections were made with Cryostat (Leica). Sections were fixed in acetone for 5 min at 4°C, rehydrated in PBS, and blocked with 10% BSA for 30 min at room temperature. Sections were then stained with rat anti-mouse MARCO (Santa Cruz Biotechnology) for 1 h at room temperature, followed by AlexaFluor 647-labeled goat anti-rat antibody (Invitrogen) plus 100 nM phalloidin AlexaFluor 555 (Invitrogen) and 30 μM DAPI (Fisher Scientific) for 30 min at room temperature. After washes, sections were mounted in FluorSave reagent (CalBiochem) and observed with Zeiss 710 confocal scanning microscope.

For quantitative RT-PCR analysis of target gene expression, small pieces of liver tissues were preserved in 1 mL RNALater (Qiagen) at room temperature overnight. RT-PCR amplification and quantification of gene expression were conducted as previously reported[56].

Primers and probes: Human β-actin, Forward: GGT CAT CAC CAT TGG CAA TG; Reverse: TAG TTT CGT GGA TGC CAC AG; Probe: FCA GCC TTC CTT CCT GGG CAT GGA Q; Mouse Factor VII, Forward: ACA AGT CTT ACG TCT GCT TCT; Reverse:

CAC AGA TCA GCT GCT CAT TCT; Probe: FTC TCA CAG TTC CGA CCC TCA AAG TCQ. Mouse β-Actin, Forward: CTG CCT GAC GGC CAG GTC; Reverse: CAA GAA GGA AGG CTG GAA AAG A, Probe: FCA CTA TTG GCA ACG AGC GGT TCC GQ. F represents 5'-Fluorescein (FAM) and Q represents Quencher (TAMRA).

2.6.2 Behavior of cationic nanoparticles coated with terpolymer ligands

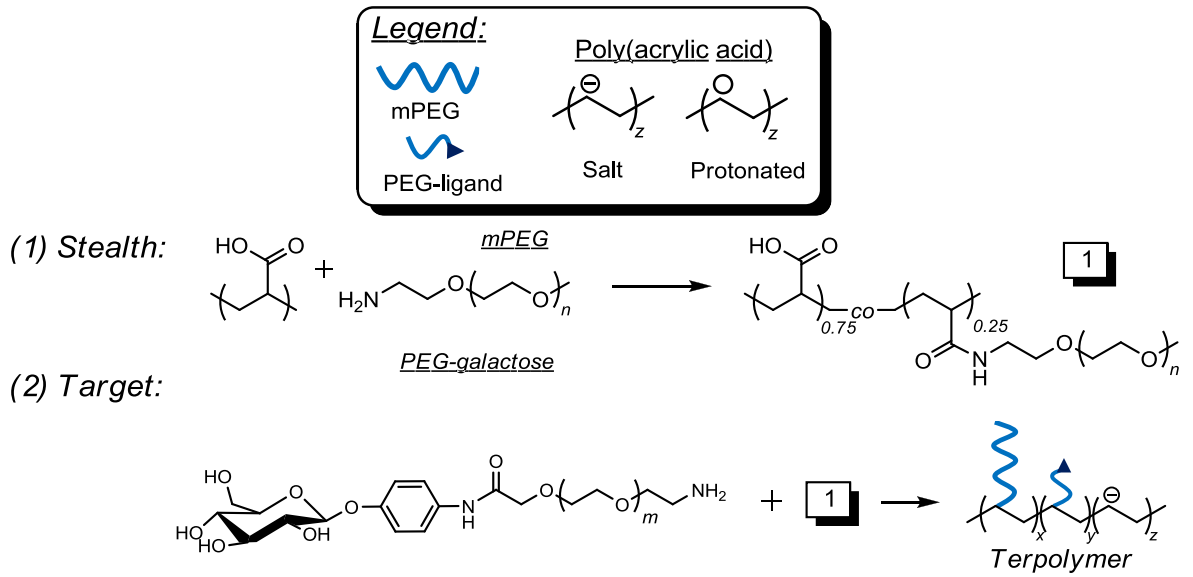

Figure 2.29 Two-step reaction scheme for preparation of PAA-based terpolymers with graphical illustrations.

PAA-based ligands were synthesized according to the reaction scheme illustrated in Figure 2.29. Cationic rice-shaped hydrogel nanoparticles were coated with PAA-based terpolymer ligands to negate the positive surface charge, provide a stealth PEG layer, and present saccharide ligands to target hepatocytes. After internalization by cells, the carboxylates from PAA should protonate in the endosome since the pH of the endosome approaches the pK_a of PAA (pK_a ~ 5). Protonation of carboxylates should result in dissociation of the ligand coating from particles due to loss of electrostatic attraction, revealing endosomolytic particles capable of siRNA delivery (Figure 2.30).

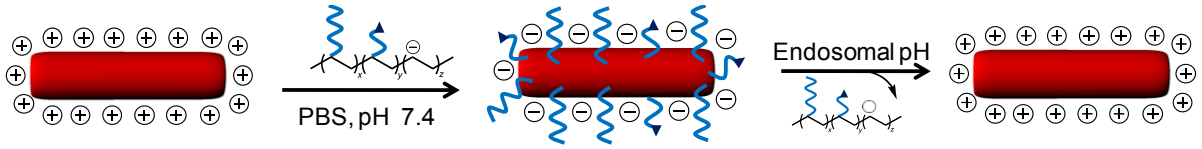

Figure 2.30 Illustration of coating cationic nanoparticles with PAA-based terpolymer ligands under physiological conditions followed by dissociation of the coating under endosomal conditions.

ζ-potential of bare cationic hydrogels decreased as a function of ligand concentration (Figure 2.31a) until a maximum around 30 wt eq of ligand to particle. At higher ligand ratios, charge screening most likely neutralizes the ζ-potential, approaching neutrality. Flocculation (aggregation or settling) of coated particles was not observed over 5 days when incubated in PBS at 4 ºC. The response of ligand coating stability on cationic hydrogels was assessed in a pH-dependent fashion (Figure 2.31b). Buffers (100 mM) with pH values ranging from 5.0 to 7.0 were prepared with citric acid and dibasic sodium phosphate. ζ-potential was determined as a function of pH for hydrogels coated with 20 wt eq ligand. From physiological pH (7.4) to endosomal conditions (pH 5.5), ζ-potential increases linearly (r^2 = 0.98), proceeding from negative values to positive ones due to protonation of carboxylates and dissociation of the coating. It is notable that ζ-potential magnitudes are not as great in these studies as compared to previous ones, probably because these hydrogels were not incubated in buffer, isolated, and re-suspended in 1 mM KCl.

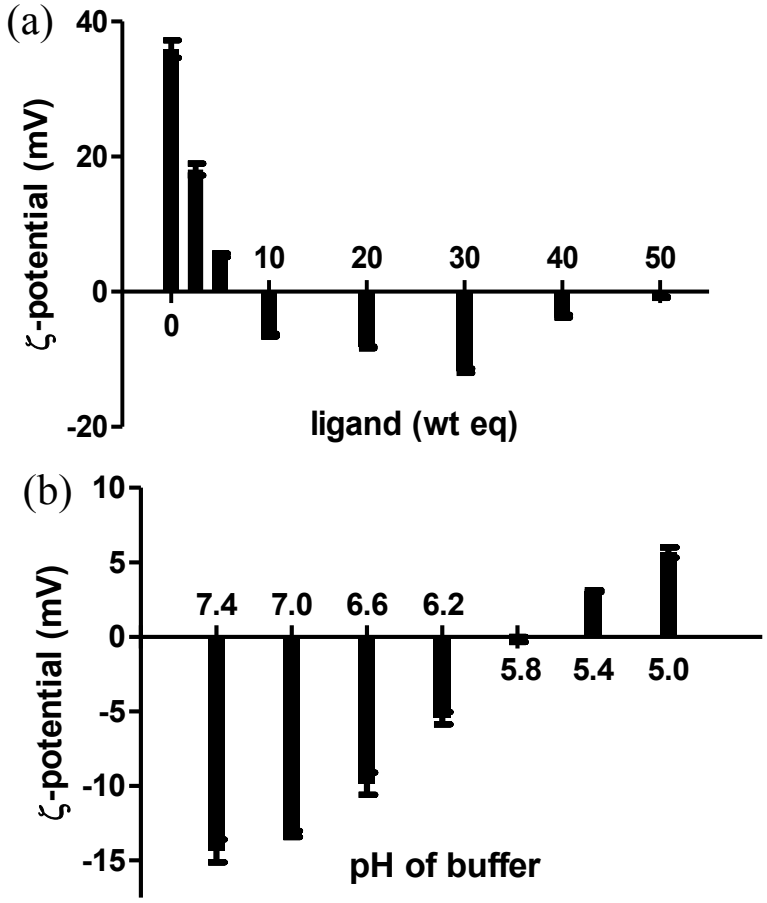

Figure 2.31 (a) ζ-potential of cationic nanoparticles as a function of ligand concentration, demonstrating ligand density-dependent surface properties. (b) ζ-potential of coated nanoparticles subjected to buffers of decreasing pH, mimicking the progression of the endosome.

2.6.3 Evaluation of *in vitro* targeting hepatocytes with coated nanoparticles

The most effective gene silencing composition (50% AEMAm cationic monomer) was implemented in targeting experiments. Coated hydrogels were prepared for *in vitro* dosing on mouse-derived hepatocyte cell line AML12 with 10 wt eq mPEG-PAA as well as mPEG-PAA functionalized with PEG-galactose and -glucose (Table 2.10) for evaluating time-dependent internalization (Figure 2.32a). The coating apparently minimized aggregation of hydrogels (smaller D_z with lower standard deviations) where coated hydrogels exhibited negative ζ-potentials. Minimal ligand was implemented such that asialoglycoprotein

receptors (ASGPRs) would not be overloaded or blocked by free galactose ligands that may potentially dissociate from particles during incubation. Cell uptake was pretty similar among the coated hydrogels. Specifically, time-dependent AML12 cell uptake studies demonstrated that coatings slowed the rate of internalization; yet, coatings did not provide receptor-mediated endocytosis. Nonetheless, AML12 cells tolerated coated hydrogels as noted by maintenance of cell viability out to high dosing concentrations while a slight decrease in viability was noted for cells dosed with cationic particles (Figure 2.32b).

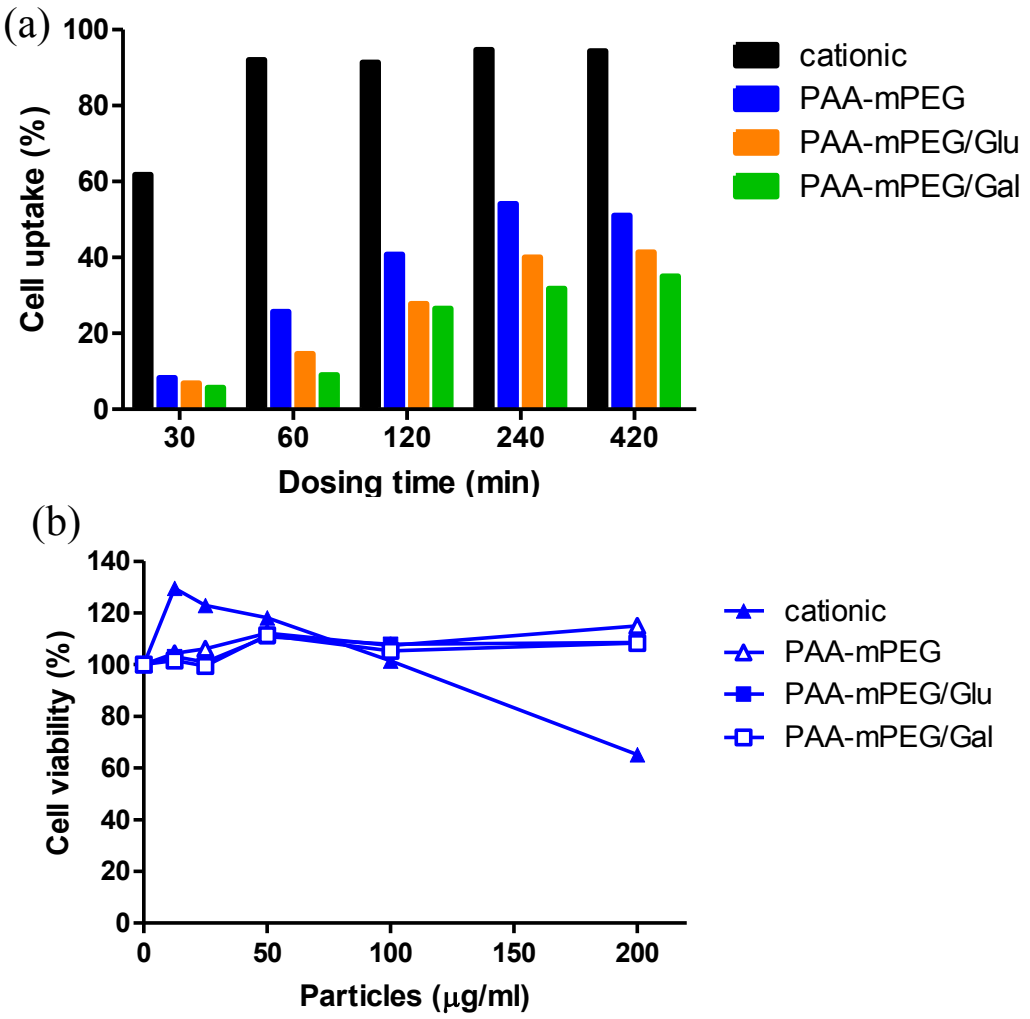

Figure 2.32 (a) Time-dependent AML12 cell uptake of bare 80x320 nm particles and ligand-coated particles at 100 μg/mL dosing concentration. (b) Viability of AML12 cells dosed with cationic and ligand-coated particles after 48 h incubation at 37 ºC.

Table 2.10 Zetasizer analysis of hydrogels dosed on hepatocytes.

Coating	ζ-potential / mV	D_z / nm
None	+37.6 ± 1.4	448.6 ± 18.7
mPEG	-8.3 ± 0.5	339.9 ± 2.4
Galactose	-9.9 ± 0.3	340.5 ± 6.0
Glucose	-11.2 ± 0.4	380.7 ± 8.9

The mol% substitution of sugar moieties on terpolymers was then screened at 10, 20, and 30 % to observe the effect on cell uptake specificity since ligand density has been demonstrated to influence receptor-mediated endocytosis. Zetasizer analysis of particles demonstrated that cationic particles exhibited positive ζ-potentials while coated particles exhibited negative values (Table 2.11). Cationic hydrogels were readily internalized by AML12 cells, reaching 100% cell uptake after 30 min of dosing cells with particles (Figure 2.33). As previously noted, the rate of internalization was slower for coated nanoparticles although differential uptake was not observed between galactose- and glucose-functionalized terpolymers.

Internalization of coated particles was then evaluated on human hepatocarcinoma (HepG2) cells to observe whether uptake behavior would be different in another liver cell line. After 1 h dosing of particles on HepG2 cells, cationic particles were mostly internalized and notable uptake of coated particles occurred at moderate particle doses (Figure 2.34a). Coated particles exhibited reduced uptake relative to cationic particles at short time points. Selective uptake of galactose-coated particles was not signficantly apparent after 1 h relative to glucose-coated particles. After 24 h, complete uptake of all particles was observed across all particle dosing concentrations (Figure 2.34b). Therefore, the electrostatic coatings appear to stealth particles, minimize the rate of internalization, and decrease toxicity; however, selective targeting of hepatocytes was not observed for galactose-coated particles relative to glucose-coated particles by human and mouse hepatocytes *in vitro*.

Table 2.11 ζ-potential of bare and ligand-coated cationic hydrogels.

Ligand (mol%)	ζ-potential (mV)
None (cationic)	+9.9 ± 0.7
PAA-gal 10	-4.6 ± 0.3
PAA-gal 20	-6.0 ± 0.5
PAA-gal 30	-5.0 ± 0.3
PAA-glu 10	-6.9 ± 0.0
PAA-glu 20	-4.8 ± 0.6
PAA-glu 30	-8.5 ± 1.8

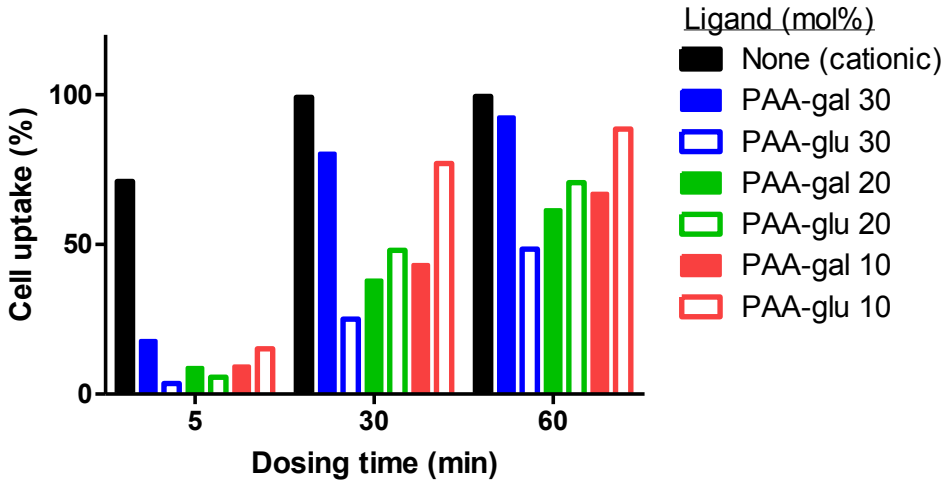

Figure 2.33 Time-dependent AML12 cell uptake of cationic particles coated with terpolymer ligands bearing different degrees of ligand substitution when dosed at 100 µg/mL.

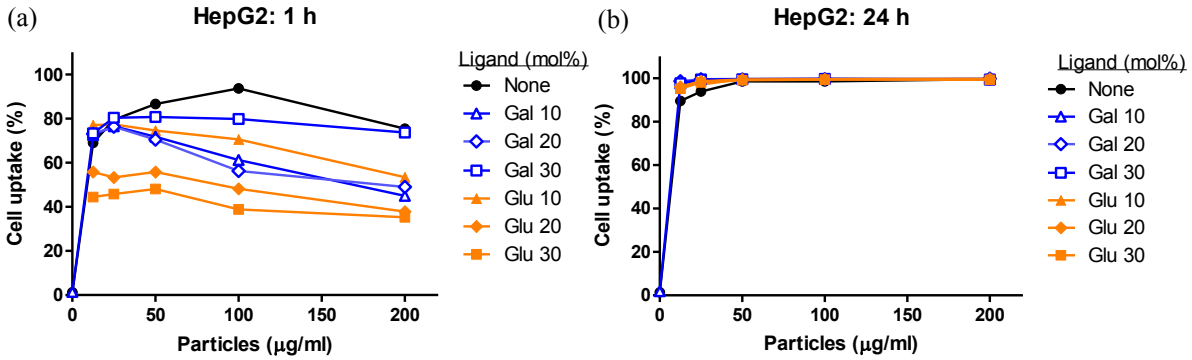

Figure 2.34 HepG2 cell uptake of bare 80x320 nm hydrogel nanoparticles and ligand-coated hydrogels bearing different mol% of ligand after (a) 1 h and (b) 24 h dosing times.

The absence of selective uptake for galactose- and glucose-coated nanoparticles may be attributed to size restrictions and strict spacing requirements among sugar moieties imposed by asialoglycoprotein receptors. Glycolipid-laden liposomes were prepared with sizes ranging from 30 to 90 nm in diameter and evaluated for specific uptake by

asialoglycoprotein receptors.[57] Particles with a diameter greater than 70 nm could not be recognized and processed by asialoglycoprotein receptors. Galactosylated poly(β-amino ester)s did not enhance delivery to hepatocytes or increase specificity.[58] The spatial orientation of ligands was seen to influence the receptor-mediated uptake of magnetic nanoparticles where tri-antennary ligands provided effective internalization.[50] The mol% incorporation of a tri-antennary *N*-acetylgalactosamine PEG-lipid conjugate was incorporated into ionizable lipid nanoparticles with diameters ranging from 40-70 nm.[59] Clearly many factors influence the uptake specificity of galactose ligand-coated nanoparticles. Therefore, future endeavors to obtain asialoglycoprotein receptor-mediated endocytosis of galactose-decorated PRINT nanoparticles may require diameters less than 70 nm with a high density of ligands presented in a triantennary fashion.

2.6.4 Factor VII gene knockdown *in vitro* by rice-shaped hydrogel nanoparticles

Although selective uptake of nanoparticles was not observed, evaluation of gene silencing properties and *in vivo* behavior was pursued since the coatings enabled attractive features such as stealth-like properties, minimization of toxicity, and maintenance of particle dispersion stability. Circulating in serum as an inactive precursor protease, Factor VII (FVII) allows for quick determination of potential for efficacy in delivering siRNA *via* hydrogels to liver hepatocytes by measuring serum protein levels through robust chromogenic assays. The composition of hydrogels (Table 2.12) selected for delivery of Factor VII was based on the experiments screening amine-containing monomers as well as siRNA and amine content for the lowest EC_{50}. Zetasizer analysis (Table 2.13) of all hydrogels dosed on cells illustrates that coated hydrogels had negative ζ-potentials where the magnitude was greater for washed

particles than unwashed ones. siRNA was released from hydrogels by washing with 10x PBS and the encapsulation efficiency was determined to be 79.8 ± 4.2 % (Figure 2.35).

Table 2.12 Composition of cationic hydrogels for delivery of Factor VII.

Component	wt%
AEMAm	50
HP_4A	23
Poly(vinyl alcohol)	10
Irgacure 2959	1
DyLight 488 maleimide	1
PEG_{16}-DA	5
Factor VII siRNA	10

Table 2.13. Zetasizer analysis of hydrogels dosed on AML12 cells.

Coating	ζ-potential / mV	D_z / nm
None (cationic)	+27.9 ± 0.8	299.8 ± 5.9
PAA-mPEG*	-16.7 ± 0.3	307.5 ± 5.7
PAA-mPEG	-8.5 ± 0.3	323.6 ± 5.7
PAA-gal*	-18.9 ± 1.0	335.7 ± 0.5
PAA-gal	-11.7 ± 0.4	354.2 ± 5.2

*Denotes that particles had been washed in buffer prior to dosing cells.

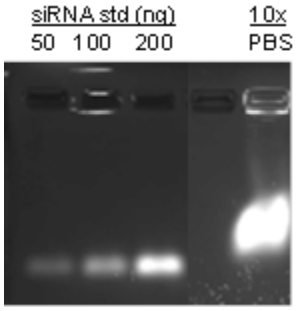

Figure 2.35 Gel electrophoresis analysis of siRNA released from particles incubated in 10x PBS.

All particles were tolerated pretty well by AML12 cells: no change in cell viability was noted for coated hydrogels while cationic ones elicited a slight decrease at the highest dosing concentration. Cationic hydrogels were internalized to a greater degree than all coated rice particles; yet, AML12 cells internalized all particles (cell uptake ~ 100%) after 48 h dosing and incubation time even at low particle concentrations (Figure 2.36a). Based on

confocal microscopy images (Figure 2.37), a significant number of all rice hydrogels were internalized by AML12 cells, distributing throughout the cytoplasm and perinuclear region.

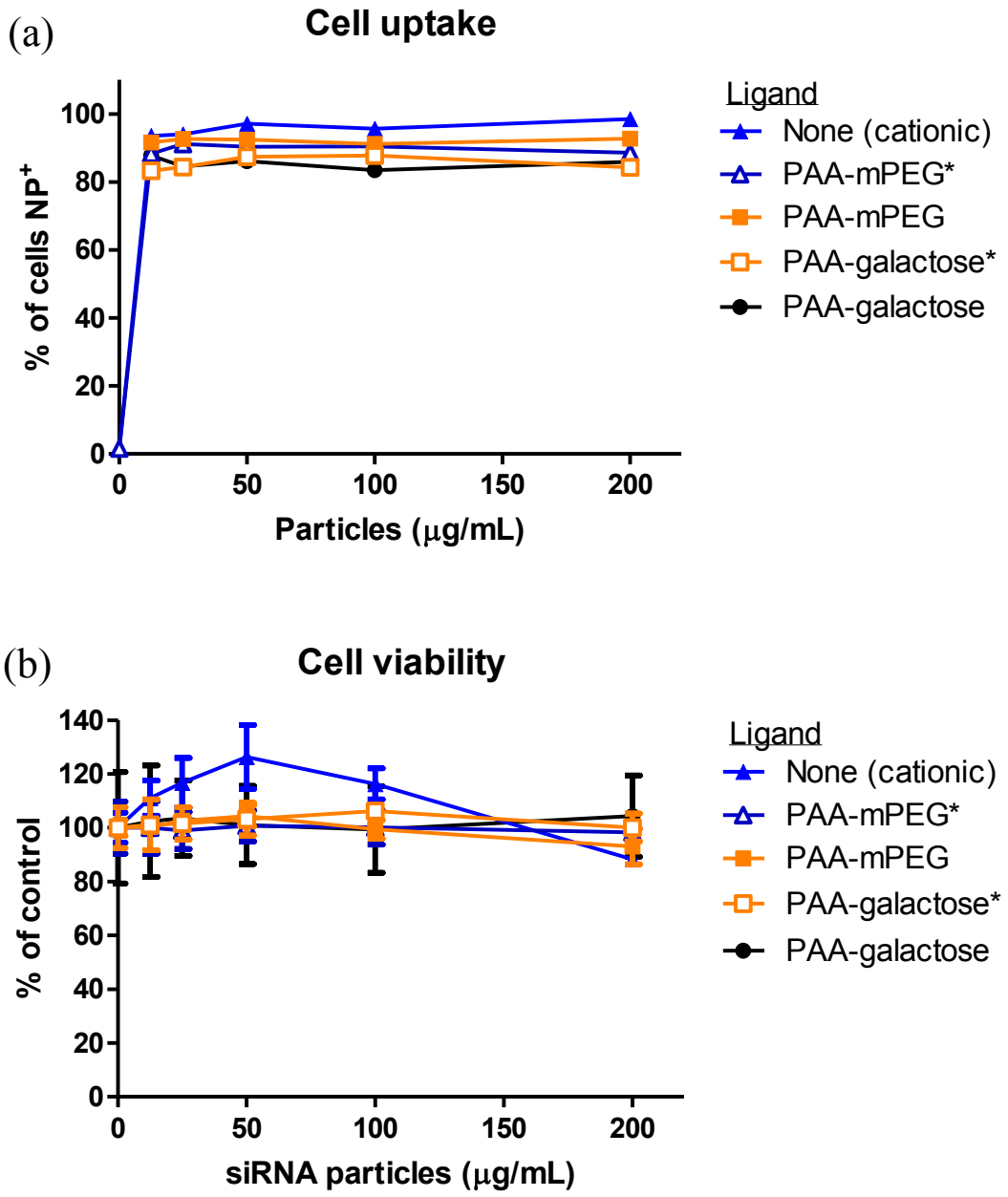

Figure 2.36 (a) AML12 cell uptake of bare and ligand-coated hydrogel nanoparticles. (b) Viability of AML12 cells dosed with bare and ligand-coated, siRNA-containing nanoparticles. *Denotes that particles were washed in buffer prior to dosing on cells.

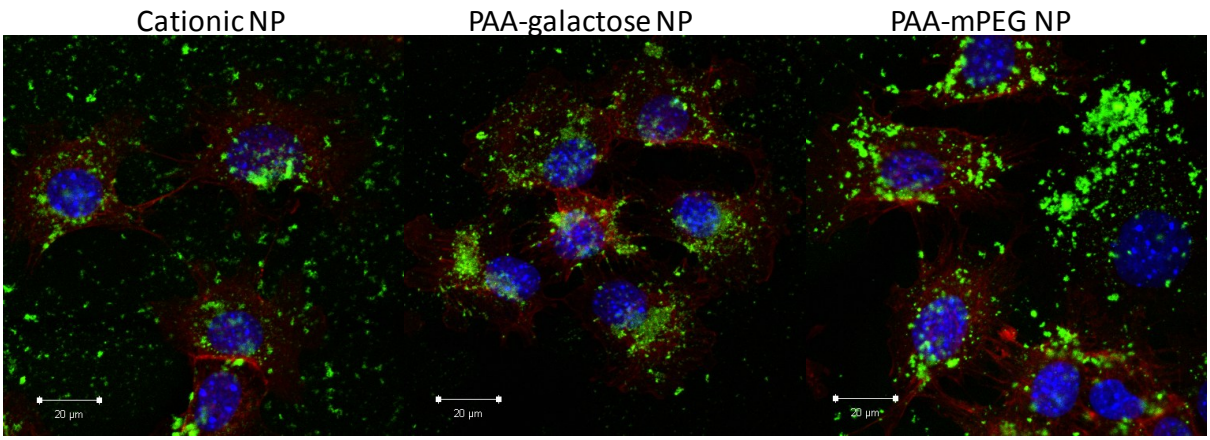

Figure 2.37 Confocal microscopy overlay images of AML12 cells incubated with cationic and coated hydrogels (tagged green with DyLight 488 maleimide). Nucleus was stained with DAPI (blue) and actin was stained with Phalloidin (red).

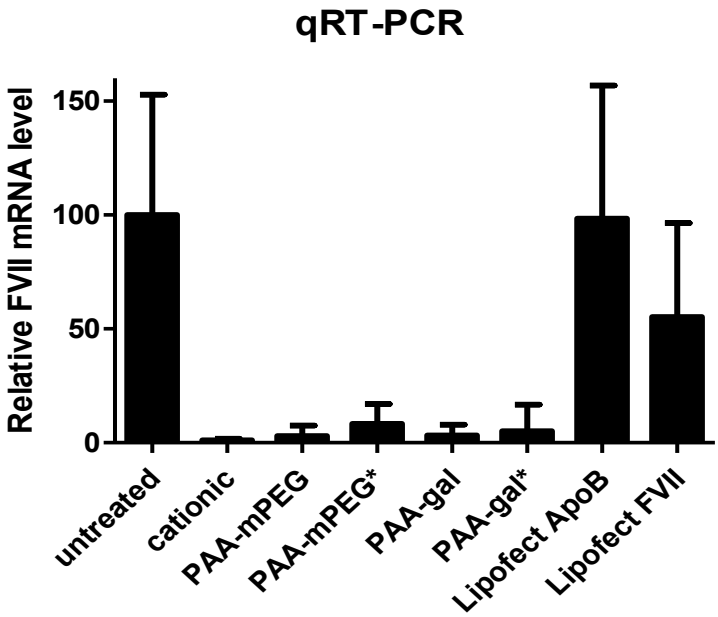

Figure 2.38 qRT-PCR for relative FVII mRNA level in AML12 cells dosed with hydrogels containing FVII siRNA and Lipofectamine™ 2000 mixed with either ApoB or FVII siRNA. Cationic rice particles or hydrogels coated with PAA-mPEG or -gal were dosed on cells and incubated for 48 h. *Denotes that particles were washed in buffer prior to dosing on cells.

qRT-PCR was conducted for analysis of relative FVII levels in AML 12 cells dosed with hydrogels and Lipofectamine-siRNA complexes (Figure 2.38). Significant suppression of FVII mRNA levels was observed for cells dosed with hydrogels containing FVII siRNA while Lipofectamine™ 2000 did not elicit as efficient gene knockdown. Control siRNA (Apo

B) mixed with Lipofectamine™ 2000 did not decrease FVII mRNA levels. Selective mRNA knockdown by targeted hydrogels was not observed since AML12 cells internalize PAA-mPEG-coated particles after ca. 48 h dosing and incubation time. Furthermore, coated particles that were dosed on cells directly or washed with PBS both provided efficient gene knockdown.

2.6.5 Injection of rice-shaped hydrogel nanoparticles into mice

80x320 nm cationic, PAA-gal-, and PAA-glu-coated hydrogel nanoparticles were injected into the tail vain of B6 mice (n=3, 150 μL of 2 mg/mL dispersion). Livers were harvested 48 h post-injection and 5 μm cryosections were stained. Actin was stained red with Phalloidin and macrophages were tagged magenta with anti-macrophage antibody (MAC387). Particles were tagged green through incorporation of DyLight 488 maleimide. Rice hydrogels were shown to be partially localized with Kupffer cells. Cationic particles were found lining hepatocytes while hydrogel nanoparticles coated with PAA-based ligands were notably internalized by hepatocytes and distributed throughout the cell (Figure 2.39). Gene silencing was not observed by RT-PCR, most likely due to inefficient delivery of siRNA to hepatocytes. To enable systemic delivery of siRNA entrapped in rice-shaped hydrogels, a covalent incorporation approach with triggered cargo release was desired to maximize delivery of siRNA to hepatocytes *in vivo*.

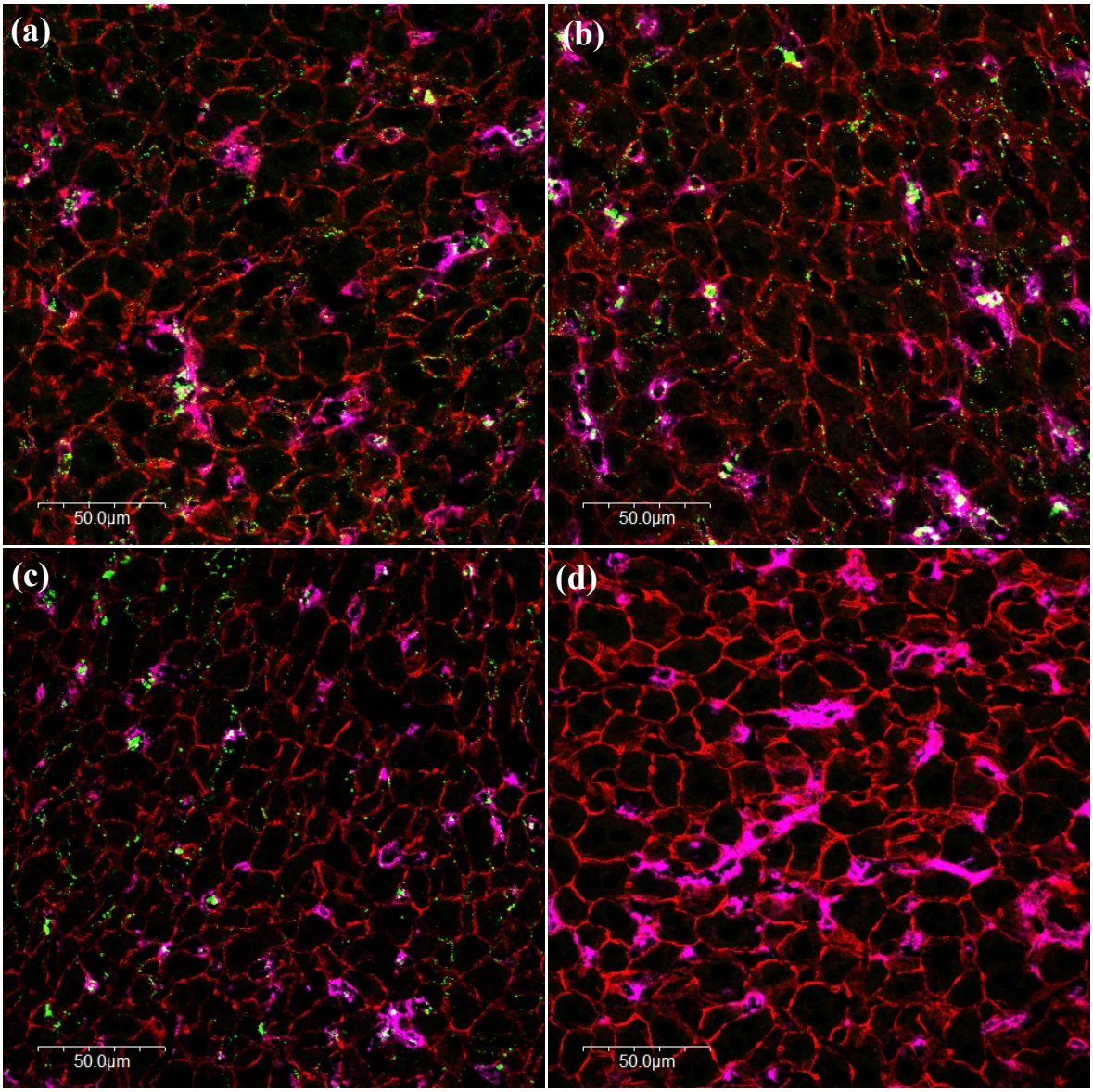

Figure 2.39 Confocal microscopy of tissues from mice injected with different nanoparticles: (a) PAA-glu and (b) PAA-gal with 30 mol% substitution of saccharides, (c) cationic nanoparticles, and (d) no nanoparticles (PBS).

2.7 Future directions for delivery of physically-entrapped siRNA in PRINT particles

Given the potential for plug-and-play approaches to the fabrication of PRINT particles, a wide range of chemical compositions and functionalities may be accessed for delivery of siRNA. Chemical compositions may include use of degradable matrices,

endosomolytic moieties, and reactive handles for controlled release of siRNA, high transfection efficiency, and functionalization with ligands.

2.7.1 Range of particle matrices for encapsulation of siRNA and delivery to cells

Polysaccharides, biopolymers, and polyesters are attractive matrices for PRINT particles to carry siRNA since they are biodegradable and should not pose toxic or immunogenic responses. Alginate, a carboxylic acid-containing polysaccharide, may be mixed with siRNA followed by the addition of calcium for ionic crosslinking toward the transfection of cells. Use of calcium phosphate in particular could enhance endosomal escape as demonstrated by efficient systemic siRNA transfection using biodegradable calcium phosphate nanoparticles with lipid coatings.[60] Collagen, atelocollagen, and agar may serve as gel-like networks for encapsulation and transfection with siRNA. Solution or thermal processing could be conducted to produce PRINT particles.[61]

Atelocollagen consists of three polypeptide chains (mainly GXY) in a helical structure and acts as a rod-like polymer (MW ~ 300 kDa, length ~ 300 nm, diameter 1.5 nm). With low antigenicity (due to removal of telopeptides from collagen), atelocollagen is biocompatible and biodegradable. Exhibiting water solubility at lower temperatures and solidifying to refibrillation over 30 ºC, the sol-gel transition of atelocollagen may be controlled with pH, salt concentration, temperature, and chemical modifications. Atelocollagen has been demonstrated to enhance accumulation of particles in tumor sites and enable effective *in vitro* and systemic *in vivo* delivery of siRNA.[62–67] Protein matrices that are rendered transiently insoluble may be used for delivery of siRNA as has been demonstrated

by Jing Xu *et al*.[68] Avidin could be an interesting matrix to which biotinylated targeting ligands (e.g. proteins) and/or PEG linkers could be non-covalently conjugated.

Water-soluble polysaccharides like dextran, sugars like galactose, and polyols like poly(vinyl alcohol) could be mixed with siRNA to produce PRINT particles through solution of thermal filling techniques. Chlorosilanes may be harnessed to crosslink particles and produce a degradable matrix.[69] Alternatively, particles may be lipidized with lipid-chlorosilanes to produce hydrophobic surfaces onto which functional lipids may be physisorbed (Figure 2.40). For example, as has been demonstrated by W. Hasan *et al.*, hydrophobic PRINT particles may be coated with transfecting lipids (DOTAP and DOPE) for effective delivery of siRNA. Additionally, PEG-lipids could be adsorbed to particles to provide a stealth layer in addition to ligands for targeting cell receptors. Distearoylphosphoethanolamine (DSPE)-PEG-maleimide could be functionalized with proteins, peptides, or small molecules to serve as a targeting ligand.

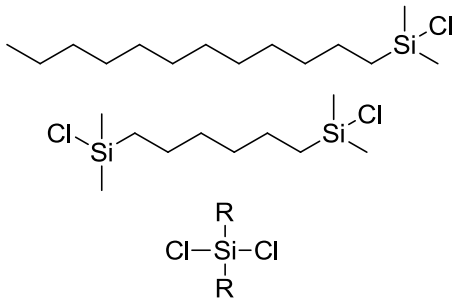

Figure 2.40 Structures of lipidated chlorosilanes, hydrophobic bischlorosilanes, and dichlorosilanes where R may consist of different alkyl substituents.

Degradable hydrogel matrices may be implemented for the delivery of siRNA using crosslinkers with degradable linkages. Acid-sensitive linkages include hydrazones, acetals, ketals, and silyl ethers for which photopolymerizable crosslinkers may be synthesized (Figure 2.41) to produce degradable PRINT particles as has been previously demonstrated

with the controlled degradation rate of a family of alkyl-substituted bifunctional silyl ether crosslinkers.[70] Enzymatically degradable crosslinkers with peptide sequences that may be cleaved by endosomal and lysosomal proteinases such as Cathepsin B, which plays a role in cancer progression, could be useful for controlled intracellular delivery of cargos.[71,72]

A disulfide-containing crosslinker with greater water solubility (Figure 2.41) may be synthesized through step-growth polymerization of triethylene glycol diamine with bis(ethylene acrylate) disulfide. Acid- and reductively-labile crosslinkers could be synthesized to provide two mechanisms for degradation by reacting dichlorosilanes with 2,2'-dithiodiethanol.

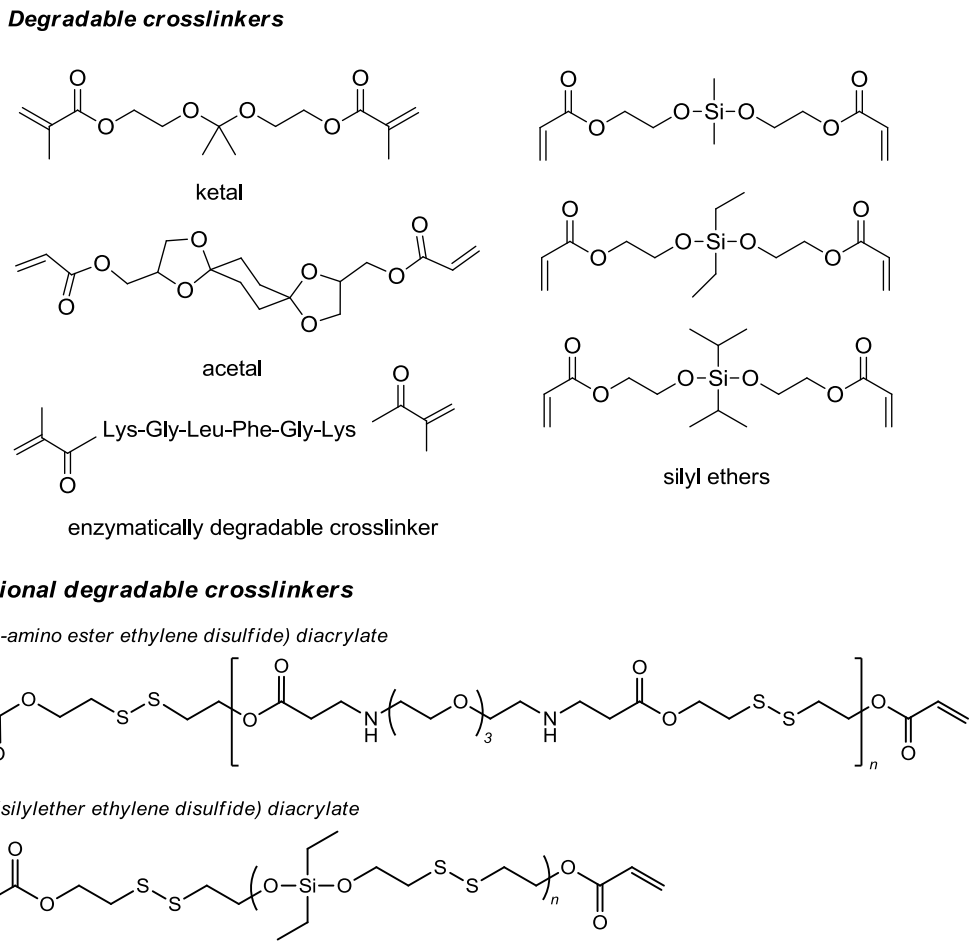

Figure 2.41 Structures of degradable crosslinkers for hydrogel particles.

2.7.2 Cationic hydrogels

Amine monomers such as amine-containing acrylates and thiols may be pursued for incorporation into cationic hydrogel particles to modulate the charge density, electrostatic attraction with siRNA, availability of functional handles, cell internalization profiles, endosomal escape, and toxicity of the delivery vector (Figure 2.42). Amines with different degrees of substitution may be pursued to further harness the proton-sponge effect. (Meth) acrylate and (meth) acrylamide, amine-containing monomers could provide different degrees of hydrogen bonding with siRNA to influence release properties. Amine-containing monomers that are not commercially available may be synthesized according to Fig 2.43 by reacting primary amine-terminated, amine-containing molecules with acid chloride- or *N*-hydroxysuccinimide-activated acrylates.

A library of amine-containing acrylates may be synthesized by reacting amine-containing small molecules (Figure 2.44) with the appropriate activated acrylate. Additionally, amines may be reacted with thiirane (ethylene sulfide) to yield free thiols that may polymerize into the particle matrix through photoinitiated thiol-ene addition. Cysteine-containing endosomolytic peptides may also be used for covalent incorporation into particles where thiol groups may serve as chain transfer agents. The cysteine-containing peptides may be endosomolytic peptide derivatives like KALA and GALA. Additionally, peptides full of arginine, histidine, and lysine residues may be designed to harness guanidino, imidazole, and primary amine functional groups for enhanced endosomolysis.

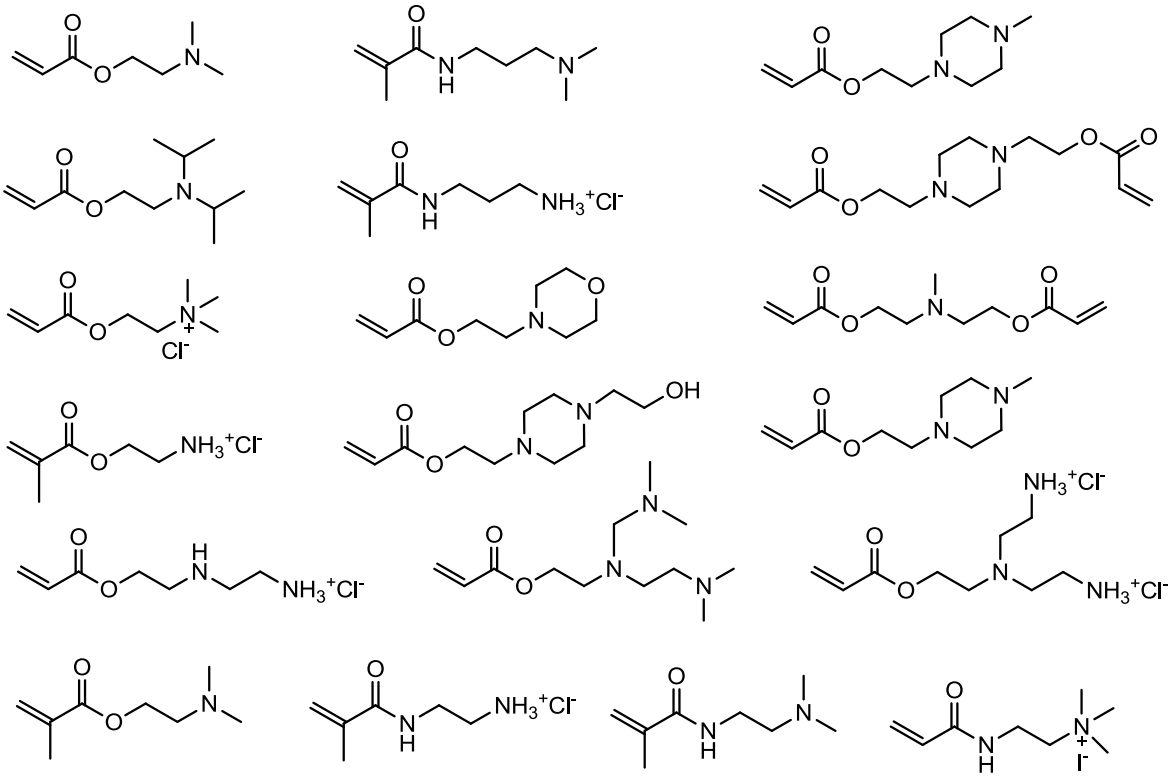

Figure 2.42 Structures of amine-containing acrylic monomers that may be purchased commercially or specially synthesized.

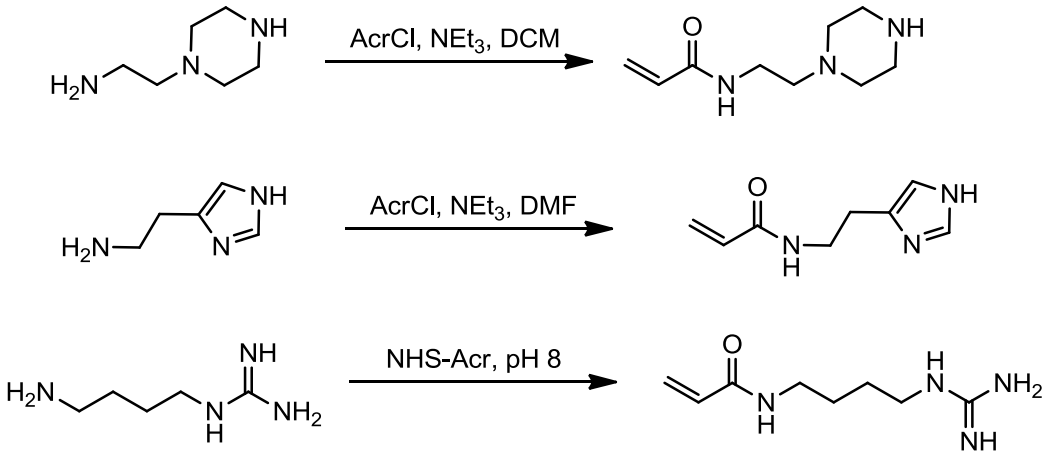

Figure 2.43 Reaction schemes for the synthesis of amine-containing monomers.

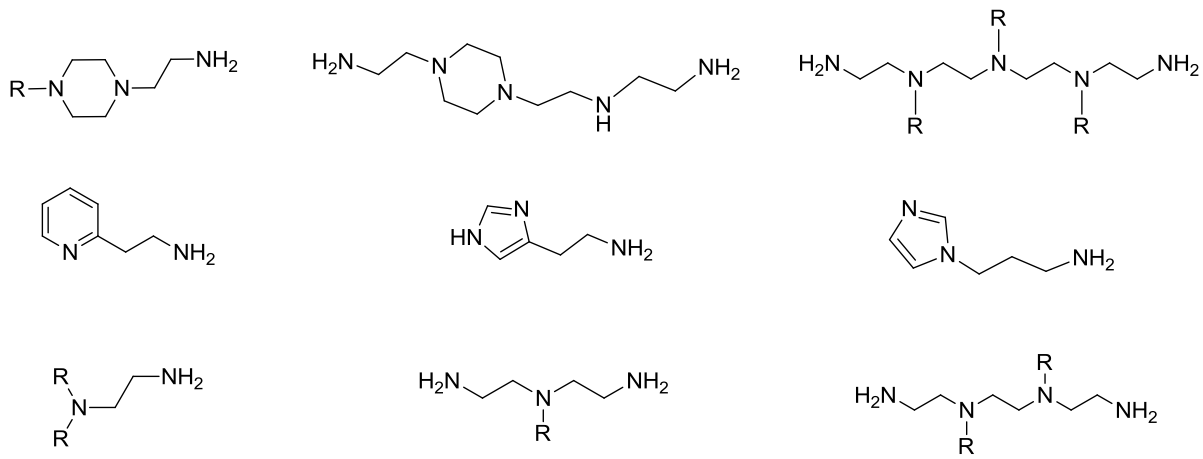

Figure 2.44 Structures of amine-containing small molecules that may be used to synthesize acrylamide-based or thiol-presenting cationic monomers using acryloyl chloride or thiirane. R = H or CH_3.

2.7.3 Ligands for reversible covalent conjugation

To create a wholly acid-labile, ligand-decorated particle surface, CDM-activated, maleimide-terminated PEG may be synthesized by reacting amine-PEG-maleimide with CDM. Subsequently, non-PEGylated amines may be quenched using CTA-mPEG as previously demonstrated. Amine- and thiol-containing peptides, proteins, or small molecules may be conjugated to the maleimide group through Michael addition. Unreacted maleimide groups may be quenched with small molecules like ethanolamine or oligomers like monomethoxy-PEG-amine. For targeting tumor endothelial cells, thiol-containing RGD (RAD control) peptides may be conjugated to the maleimide group. To reach liver hepatocytes, *N*-acetyl-D-galactosamine (glucosamine control) could be conjugated as well. A wide range of protein and antibody ligands should be accessible to target nanoparticles to cell receptors since the proteins have a reasonable number of lysine and cysteine residues that may be harnessed for nucleophilic addition to maleimide groups.

2.7.4 Ligands for electrostatic complexation to nanoparticles

Polyelectrolyte attraction of polyanionic ligands to cationic nanoparticles was previously covered in section 2.6. Further development of coated PRINT particles with polyacid-based ligands could potentially enable stealthing and selective uptake if designed appropriately. Instead of randomly grafting mPEG and PEG-ligand chains from the polyacid backbone with few repeat units, polyacid tethers may be more effective to instill polyelectrolyte attraction between particles and ligands. For example, similar to previously reported studies,[54,55] poly(glutamic acid)- or poly(aspartic acid)-tethered peptide or small molecule ligands may enable stealthing properties, alter biodistribution, and yield receptor-mediated endocytosis for gene delivery. Polyacids are particularly attractive for coating cationic nanoparticles since they should disassociate in the endosomal environment due to the pH sensitivity of ionizable carboxylic acid groups. Other polyanions including groups like phosphates and sulfates may enable electrostatic attraction to cationic nanoparticles; however, the interaction may be substantial such that disassembly and shedding of the coating does not readily occur under intracellular conditions when also considering that the phosphate and sulfate groups may not protonate under endosomal conditions. Another approach to polyanion-tethered ligands may entail controlled radical polymerization of an anionic monomer (e.g. acrylic acid) followed by end functionalization for conjugation of PEG or PEG-ligands. Side-by-side comparison of polyanion-tethered ligands compared to polyanions with randomly distributed ligands would uncover the effect of substituent placement on the stability of the coating and ability to target cells for receptor-mediated endocytosis.

References

(1) Naeye, B.; Raemdonck, K.; Remaut, K.; Sproat, B.; Demeester, J.; DeSmedt, S. C. *European Journal of Pharmaceutical Sciences* **2010**, *40*, 342-351.

(2) Raemdonck, K.; Van Thienen, T. G.; Vandenbroucke, R. E.; Sanders, N. N.; Demeester, J.; De Smedt, S. C. *Advanced Functional Materials* **2008**, *18*, 993-1001.

(3) Blackburn, W. H.; Dickerson, E. B.; Smith, M. H.; McDonald, J. F.; Lyon, L. A. *Bioconjugate Chemistry* **2009**, *20*, 960-968.

(4) Hu, Y.; Atukorale, P. U.; Lu, J. J.; Moon, J. J.; Um, S. H.; Cho, E. C.; Wang, Y.; Chen, J.; Irvine, D. J. *Biomacromolecules* **2009**, *10*, 756-765.

(5) Krebs, M. D.; Jeon, O.; Alsberg, E. *Journal of the American Chemical Society* **2009**, *131*, 9204-9206.

(6) Mumper, R. J.; Duguid, J. G.; Anwer, K.; Barron, M. K.; Nitta, H.; Rolland, A. P. *Pharmaceutical Research* **1996**, *13*, 701-709.

(7) Mumper, R. J.; Wang, J.; Klakamp, S. L.; Nitta, H.; Anwer, K.; Tagliaferri, F.; Rolland, a P. *Journal of Controlled Release* **1998**, *52*, 191-203.

(8) Park, I.-K.; Jiang, H.-L.; Cook, S.-E.; Cho, M.-H.; Kim, S.-I.; Jeong, H.-J.; Akaike, T.; Cho, C.-S. *Archives of Pharmacal Research* **2004**, *27*, 1284-1289.

(9) Bauhuber, S.; Hozsa, C.; Breunig, M.; Göpferich, A. *Advanced Materials* **2009**, *21*, 3286-3306.

(10) Cerritelli, S.; Velluto, D.; Hubbell, J. A. *Biomacromolecules* **2007**, *8*, 1966-1972.

(11) Oh, J. K.; Siegwart, D. J.; Lee, H.-il; Sherwood, G.; Peteanu, L.; Hollinger, J. O.; Kataoka, K.; Matyjaszewski, K. *Journal of the American Chemical Society* **2007**, *129*, 5939-5945.

(12) Petros, R. A.; Ropp, P. A.; DeSimone, J. M. *Journal of the American Chemical Society* **2008**, *130*, 5008-5009.

(13) Piest, M.; Lin, C.; Mateos-Timoneda, M. A.; Lok, M. C.; Hennink, W. E.; Feijen, J.; Engbersen, J. F. J. *Journal of Controlled Release* **2008**, *130*, 38-45.

(14) Miyata, K.; Kakizawa, Y.; Nishiyama, N.; Yamasaki, Y.; Watanabe, T.; Kohara, M.; Kataoka, K. *Journal of Controlled Release* **2005**, *109*, 15-23.

(15) McAllister, K.; Sazani, P.; Adam, M.; Cho, M. J.; Rubinstein, M.; Samulski, R. J.; DeSimone, J. M. *Journal of the American Chemical Society* **2002**, *124*, 15198-15207.

(16) Feener, E. P.; Shen, W. C.; Ryser, H. *Journal of Clinical Investigation* **1986**, *77*, 977-984.

(17) Schafer, F. Q.; Buettner, G. R. *Free Radical Biology & Medicine* **2001**, *30*, 1191-1212.

(18) Wurtmann, E. J.; Wolin, S. L. *Critical Reviews in Biochemistry and Molecular Biology* **2009**, *44*, 34-49.

(19) Herndon, J. H.; Freeman, R. G. *Annual Review of Medicine* **1976**, *27*, 77-87.

(20) Kielbassa, C.; Roza, L.; Epe, B. *Carcinogenesis* **1997**, *18*, 811-816.

(21) Sinha, R. P.; Häder, D.-P. *Photochemical & Photobiological Sciences* **2002**, *1*, 225-236.

(22) Lin, C.-C.; Anseth, K. S. *Pharmaceutical Research* **2009**, *26*, 631-43.

(23) Peppas, N. A.; Hilt, J. Z.; Khademhosseini, A.; Langer, R. *Advanced Materials* **2006**, *18*, 1345-1360.

(24) Lee, J. I.; Kim, H. S.; Yoo, H. S. *International Journal of Pharmaceutics* **2009**, *373*, 93-99.

(25) Chun, K. W.; Lee, J. B.; Kim, S. H.; Park, T. G. *Biomaterials* **2005**, *26*, 3319-3326.

(26) Tseng, S.-J.; Chien, C.-C.; Liao, Z.-X.; Chen, H.-H.; Kang, Y.-D.; Wang, C.-L.; Hwu, Y.; Margaritondo, G. *Soft Matter* **2012**, *8*, 1420-1427.

(27) Singh, A.; Suri, S.; Roy, K. *Biomaterials* **2009**, *30*, 5187-5200.

(28) Klibanov, A. L.; Maruyama, K.; Torchilin, V. P.; Huang, L. *FEBS letters* **1990**, *268*, 235-237.

(29) Siegwart, D. J.; Whitehead, K. A.; Nuhn, L.; Sahay, G.; Cheng, H.; Jiang, S.; Ma, M.; Lytton-Jean, A.; Vegas, A.; Fenton, P.; Levins, C. G.; Love, K. T.; Lee, H.; Cortez, C.; Collins, S. P.; Li, Y. F.; Jang, J.; Querbes, W.; Zurenko, C.; Novobrantseva, T.; Langer, R.; Anderson, D. G. *Proceedings of the National Academy of Sciences of the United States of America* **2007**, *104*, 12982-12987.

(30) Davis, M. E. *Molecular Pharmaceutics* **2009**, *6*, 659-668.

(31) Wang, J.; Tian, S.; Petros, R. A.; Napier, M. E.; DeSimone, J. M. *Journal of the American Chemical Society* **2010**, *132*, 11306-11313.

(32) Shi, J.; Xiao, Z.; Kamaly, N.; Farokhzad, O. C. *Accounts of Chemical Research* **2011**, *44*, 1123-1134.

(33) Davis, M. E.; Chen, Z. G.; Shin, D. M. *Nature Reviews Drug Discovery* **2008**, *7*, 771-782.

(34) Bartlett, D. W.; Su, H.; Hildebrandt, I. J.; Weber, W. A.; Davis, M. E. *Proceedings of the National Academy of Sciences of the United States of America* **2007**, *104*, 15549-15554.

(35) Heidel, J. D.; Yu, Z.; Liu, J. Y.-C.; Rele, S. M.; Liang, Y.; Zeidan, R. K.; Kornbrust, D. J.; Davis, M. E. *Proceedings of the National Academy of Sciences of the United States of America* **2007**, *104*, 5715-5721.

(36) Davis, M. E.; Zuckerman, J. E.; Choi, C. H. J.; Seligson, D.; Tolcher, A.; Alabi, C. A.; Yen, Y.; Heidel, J. D.; Ribas, A. *Nature* **2010**, *464*, 1067-1070.

(37) Li, W.; Nicol, F.; Szoka, F. C. *Advanced Drug Delivery Reviews* **2004**, *56*, 967-985.

(38) Rozema, D. B.; Ekena, K.; Lewis, D. L.; Loomis, A. G.; Wolff, J. A. *Bioconjugate Chemistry* **2003**, *14*, 51-57.

(39) Rozema, D. B.; Lewis, D. L.; Wakefield, D. H.; Wong, S. C.; Klein, J. J.; Roesch, P. L.; Bertin, S. L.; Reppen, T. W.; Chu, Q.; Blokhin, A. V.; Hagstrom, J. E.; Wolff, J. A. *Proceedings of the National Academy of Sciences of the United States of America* **2007**, *104*, 12982-12987.

(40) Du, J.-Z.; Du, X.-J.; Mao, C.-Q.; Wang, J. *Journal of the American Chemical Society* **2011**, *133*, 17560-17563.

(41) Meyer, M.; Philipp, A.; Oskuee, R.; Schmidt, C.; Wagner, E. *Journal of the American Chemical Society* **2008**, *130*, 3272-3273.

(42) Anderson, D. G.; Akinc, A.; Hossain, N.; Langer, R. *Molecular Therapy* **2005**, *11*, 426-434.

(43) Green, J. J.; Langer, R.; Anderson, D. G. *Accounts of Chemical Research* **2008**, *41*, 749-759.

(44) Akinc, A.; Goldberg, M.; Qin, J.; Dorkin, J. R.; Gamba-Vitalo, C.; Maier, M.; Jayaprakash, K. N.; Jayaraman, M.; Rajeev, K. G.; Manoharan, M.; Koteliansky, V.; Röhl, I.; Leshchiner, E. S.; Langer, R.; Anderson, D. G. *Molecular Therapy* **2009**, *17*, 872-879.

(45) Love, K. T.; Mahon, K. P.; Levins, C. G.; Whitehead, K. a; Querbes, W.; Dorkin, J. R.; Qin, J.; Cantley, W.; Qin, L. L.; Racie, T.; Frank-Kamenetsky, M.; Yip, K. N.;

Alvarez, R.; Sah, D. W. Y.; de Fougerolles, A.; Fitzgerald, K.; Koteliansky, V.; Akinc, A.; Langer, R.; Anderson, D. G. *Proceedings of the National Academy of Sciences of the United States of America* **2010**, *107*, 1864-1869.

(46) Oishi, M.; Nagasaki, Y.; Itaka, K.; Nishiyama, N.; Kataoka, K. *Journal of the American Chemical Society* **2005**, *127*, 1624-1625.

(47) Sagara, K.; Kim, S. W. *Journal of Controlled Release* **2002**, *79*, 271-281.

(48) Zhu, L.; Mahato, R. I. *Bioconjugate Chemistry* **2010**, *21*, 2119-2127.

(49) Han, J.; Yeom, Y. I. *International Journal of Pharmaceutics* **2000**, *202*, 151-160.

(50) Lai, C.-H.; Lin, C.-Y.; Wu, H.-T.; Chan, H.-S.; Chuang, Y.-J.; Chen, C.-T.; Lin, C.-C. *Advanced Functional Materials* **2010**, *20*, 3948-3958.

(51) Yin, C.; Ying, L.; Zhang, P.-C.; Zhuo, R.-X.; Kang, E.-T.; Leong, K. W.; Mao, H.-Q. *Journal of Biomedical Materials Research. Part A* **2003**, *67*, 1093-1104.

(52) Kursa, M.; Walker, G. F.; Roessler, V.; Ogris, M.; Roedl, W.; Kircheis, R.; Wagner, E. *Bioconjugate Chemistry* **2003**, *14*, 222-231.

(53) Suh, W.; Han, S.-O.; Yu, L.; Kim, S. W. *Molecular Therapy* **2002**, *6*, 664-672.

(54) Green, J. J.; Chiu, E.; Leshchiner, E. S.; Shi, J.; Langer, R.; Anderson, D. G. *Nano Letters* **2007**, *7*, 874-879.

(55) Harris, T. J.; Green, J. J.; Fung, P. W.; Langer, R.; Anderson, D. G.; Bhatia, S. N. *Biomaterials* **2010**, *31*, 998-1006.

(56) Kim, H.-suk; Lee, G.; John, S. W. M.; Maeda, N.; Smithies, O. *Proceedings of the National Academy of Sciences of the United States of America* **2002**, *99*, 4602-4607.

(57) Rensen, P. C.; Sliedregt, L. A.; Ferns, M.; Kieviet, E.; van Rossenberg, S. M.; van Leeuwen, S. H.; van Berkel, T. J.; Biessen, E. A. *Journal of Biological Chemistry* **2001**, *276*, 37577-37584.

(58) Zugates, G. T. Synthesis and chemical modification of degradable polymers to enhance gene delivery. Ph.D. Dissertation, Massachusetts Institute of Technology, Cambridge, MA, 2007.

(59) Akinc, A.; Querbes, W.; De, S.; Qin, J.; Frank-Kamenetsky, M.; Jayaprakash, K. N.; Jayaraman, M.; Rajeev, K. G.; Cantley, W. L.; Dorkin, J. R.; Butler, J. S.; Qin, L.; Racie, T.; Sprague, A.; Fava, E.; Zeigerer, A.; Hope, M. J.; Zerial, M.; Sah, D. W. Y.; Fitzgerald, K.; Tracy, M. A.; Manoharan, M.; Koteliansky, V.; Fougerolles, A. D.; Maier, M. A. *Molecular Therapy* **2010**, *18*, 1357-1364.

(60) Li, J.; Chen, Y.-C.; Tseng, Y.-C.; Mozumdar, S.; Huang, L. *Journal of Controlled Release* **2010**, *142*, 416-421.

(61) Kelly, J. Y.; DeSimone, J. M. *Journal of the American Chemical Society* **2008**, *130*, 5438-5439.

(62) Hanai, K.; Takeshita, F.; Honma, K.; Nagahara, S.; Maeda, M.; Minakuchi, Y.; Sano, A.; Ochiya, T. *Annals of the New York Academy of Sciences* **2006**, *1082*, 9-17.

(63) Kinouchi, N.; Ohsawa, Y.; Ishimaru, N.; Ohuchi, H.; Sunada, Y.; Hayashi, Y.; Tanimoto, Y.; Moriyama, K.; Noji, S. *Gene Therapy* **2008**, *15*, 1126-1130.

(64) Minakuchi, Y.; Takeshita, F.; Kosaka, N.; Sasaki, H.; Yamamoto, Y.; Kouno, M.; Honma, K.; Nagahara, S.; Hanai, K.; Sano, A.; Kato, T.; Terada, M.; Ochiya, T. *Nucleic Acids Research* **2004**, *32*, e109.

(65) Mu, P.; Nagahara, S.; Makita, N.; Tarumi, Y.; Kadomatsu, K.; Takei, Y. *International Journal of Cancer* **2009**, *125*, 2978-2990.

(66) Takei, Y.; Kadomatsu, K.; Yuzawa, Y.; Matsuo, S.; Muramatsu, T. *Cancer Research* **2004**, 3365-3370.

(67) Takeshita, F.; Minakuchi, Y.; Nagahara, S.; Honma, K.; Sasaki, H.; Hirai, K.; Teratani, T.; Namatame, N.; Yamamoto, Y.; Hanai, K.; Kato, T.; Sano, A.; Ochiya, T. *Proceedings of the National Academy of Sciences of the United States of America* **2005**, *102*, 12177-12182.

(68) Xu, J.; Wang, J.; Luft, J. C.; Tian, S.; Owens, G.; Pandya, A. a; Berglund, P.; Pohlhaus, P.; Maynor, B. W.; Smith, J.; Hubby, B.; Napier, M. E.; Desimone, J. M. *Journal of the American Chemical Society* **2012**, *134*, 8774-8777.

(69) Parrott, M. C.; Pandya, A.; Napier, M. E.; Finniss, M.; DeSimone, J. M. ASYMMETRIC BIFUNCTIONAL SILYL MONOMERS AND PARTICLES THEREOF AS PRODRUGS AND DELIVERY VEHICLES FOR PHARMACEUTICAL, CHEMICAL AND BIOLOGICAL AGENTS. International Patent WO/2012/037358, March 22, 2012.

(70) Parrott, M. C.; Luft, J. C.; Byrne, J. D.; Fain, J. H.; Napier, M. E.; Desimone, J. M. *Journal of the American Chemical Society* **2010**, *132*, 17928-17932.

(71) Soyez, H.; Schacht, E.; Vanderkerken, S. *Advanced Drug Delivery Reviews* **1996**, *21*, 81-106.

(72) Podgorski, I.; Sloane, B. F. *Biochemical Society Symposia* **2003**, *276*, 263-276.

CHAPTER 3

REDUCTIVELY-RESPONSIVE SIRNA-CONJUGATED HYDROGEL NANOPARTICLES FOR GENE SILENCING IN LIVER HEPATOCYTES

3.1 Introduction to siRNA conjugates for gene silencing

Systemic administration of siRNA to target tissues and cells requires particular design features to overcome *in vivo* barriers such as degradation by nucleases in serum, clearance by the reticuloendothelial system, and filtration by major organs. To overcome *in vivo* challenges, siRNA conjugates offer beneficial characteristics such as enhanced serum stability, modification of biodistribution profiles, improved transfection efficiency, and avoidance of macrophage uptake. Lipid, peptide, antibody, and polymer siRNA conjugates have been explored for systemic delivery alone or when formulated as nanoparticles.[1] Lipids such as cholesterol have been conjugated to siRNA, e.g. *via* a pyrrolidone linkage, for enhanced transfection efficiency *in vitro* and silencing of apoB in mice after intravenous administration.[2] Cholesterol-conjugated siRNA has also been incorporated into core-shell nanoparticles to improve FVII gene silencing in mice.[3] Lipidated siRNA has been synthesized by attaching siRNA to dipalmitoyl phosphothioethanol *via* a disulfide linkage for enhanced nuclease stability, reductively-triggered release, and increased gene delivery efficiency *in vitro* when formulated as nanosized mixed polymeric micelles.[4]

Gene silencing in a rat model bearing an intracranially-transplanted brain tumor was elicited by siRNA-antibody conjugates. Specifically, biotinylated siRNA was conjugated to

blood brain barrier-targeted immunoliposomes through a streptavidin-functionalized antibody targeting the transferrin receptor.[5] Polyvalent nucleic acid nanostructures have been developed as a platform for oligonucleotide delivery[6] that does not require use of polymers, lipids, or ions for transfection. Propargyl ether-modified oligonucleotides can be absorbed to gold nanoparticle surfaces and crosslinked followed by dissolving away the gold core. High density of oligonucleotides in the correct orientation minimized nuclease degradation and afforded cell uptake for gene silencing. Quantum dots have been conjugated with siRNA *via* reductively-labile disulfide bonds to enable gene knockdown *in vitro* while control siRNA-conjugated quantum dots (with a non-degradable linkage) did not induce gene knockdown.[7]

Phage display allowed for the identification of a skin penetrating and cell entering (SPACE) peptide, which was conjugated to siRNA for skin delivery to knockdown target proteins (interleukin-10 and GADPH).[8] siRNA has been conjugated to polymers for enhanced transfection and delivery, e.g. to lactosylated PEG through an acid-labile linkage in the formulation of polyion complex micelles for enhanced intracellular delivery.[9] Additionally, siRNA has been covalently conjugated through disulfide linkages to hepatocyte-targeted poly(vinyl ether)s to elicit *in vivo* gene knockdown in mice livers after systemic administration.[10]

3.2 Preparation of polymerizable siRNA macromers for covalent incorporation into hydrogel nanoparticles

Acrydite DNA oligonucleotides have been incorporated into hydrogels for nucleic acid hybridization assays[11,12] while a CpG oligonucleotide methacrylamide has been copolymerized into acid-degradable microparticles to invoke immune responses.[13,14] For the triggered release of therapeutic conjugates from particles or delivery vectors under biologically relevant conditions, acid-labile,[15–17] enzymatically degradable,[18,19] and redox-sensitive linkages[20] have been examined. Glutathione and reducing enzymes are present at high concentrations inside cells relative to the extracellular space in normal and cancer cell lines.[21] Considering the serum stability of disulfide conjugates,[20,22] cleavage of disulfide linkages in therapeutic conjugates may selectively occur in the intracellular reducing environment. Disulfide-siRNA conjugates to polymers and lipids have been previously reported[4,10,23–25] as reductively-labile systems. In this work, siRNA was derivatized with a photopolymerizable acrylate bearing a degradable disulfide linkage for reversible covalent incorporation into the PRINT hydrogel nanoparticles.

3.2.1 Experimental

3.2.1.1 Materials

2,2'-dithiodiethanol, acryloyl chloride, PEG_{700} diacrylate, disuccinimidyl carbonate (DSC), 2-aminoethyl methacrylate hydrochloride (AEM), 1-hydroxycyclohexyl phenyl ketone (HCPK), fluorescein *O*-acrylate, tetraethylene glycol, and Irgacure 2959 were purchased from Sigma Aldrich. Poly(vinyl alcohol), 75% hydrolyzed with MW ≈ 2 kDa, was obtained from Acros Organics. Tetraethylene glycol monoacrylate (HP_4A) was synthesized in-house and kindly provided by Dr. Matthew C. Parrott, Dr. Ashish Pandya, and Mathew Finniss. PRINT molds were graciously supplied by Liquidia Technologies. siRNAs were purchased as duplexes from Dharmacon, Inc. Sense sequence of amine-modified and native

anti-luciferase siRNA: 5'-N6-GAUUAUGUCCGGUUAUGUAUU-3'; anti-sense: 5'-P-UACAUAACCGGACAUAAUCUU-3'. Sense sequence of amine-modified and native control siRNA: 5'-N6-AUGUAUUGGCCUGUAUUAGUU-3'; anti-sense: 5'-P-CUAAUACAGGCCAAUACAUU-3'. All other reagents were obtained from Thermo Fisher Scientific, Inc. in molecular biology grade or RNase-free when available.

3.2.1.2 Synthesis of siRNA macromers

Degradable disulfide macromer precursor: 2,2'-dithiodiethanol (15 mL, 0.12 mol) was dissolved in anhydrous DMF (250 mL) in a 500-mL round-bottomed flask containing NEt_3 (20.5 mL, 1.2 eq) under a N_2 blanket to which acryloyl chloride (11.0 mL, 1.1 eq) was added dropwise and allowed to react for 8 h. Crude product was extracted into dichloromethane against 5% LiCl and purified *via* silica gel chromatography (EtOAc:hexanes) to provide monoacrylate-substituted 2,2'-dithiodiethanol (63% yield). 2-((2-hydroxyethyl)disulfanyl)ethyl acrylate (10 g, 48 mmol) was dissolved in anhydrous acetonitrile (100 mL) in a N_2-purged 250-mL round-bottomed flask, followed by addition of disuccinimidyl carbonate (14.8 g, 1.2 eq). The reaction proceeded for 8 h and the product was purified by silica gel chromatography (EtOAc:hexanes 4:1) to afford 2-*N*-hydroxysuccinimide, 2'-acryloyl-dithiodiethanol as a clear, viscous liquid (82% yield). ^{1}H NMR (600 MHz, $CDCl_3$) δ = 6.46 (dd, J = 17.4 Hz, 1H), δ = 6.2 (dd, J = 10.7 Hz, 6.8 Hz, 1H), δ = 5.90 (dd, J = 10.7 Hz, 1H), δ = 4.59 (t, J = 6.5 Hz, 2H), δ = 4.45 (t, J = 6.5 Hz, 2H), δ = 3.05–3.00 (m, J = 6.8 Hz, 4H), δ = 2.87 (s, 4H).

Non-degradable siRNA conjugate precursor: N-hydroxyethyl acrylamide (15 mL, 0.14 mol) was dissolved with DSC (51.9 g, 1.4 eq) in ACN:DMF 4:1 (250 mL) and reacted for 16 h. Afterward, ACN was removed *via* rotary evaporation and product was extracted into EtOAc

against 5% LiCl. Product was concentrated and purified by silica gel column chromatography (EtOAc:hexanes 4:1) to provide 2-(succinimidyl carbonate)ethyl acrylamide (80% yield) as a fine white solid. ^{1}H NMR (600 MHz, $CDCl_3$) δ = 6.50 (br, 1H, *N*H), δ = 6.34 (dd, *J* = 17.1 Hz, 1H), δ = 6.19 (dd, *J* = 10.3 Hz, 6.4 Hz, 1H), δ = 5.71 (dd, *J* = 10.3 Hz, 1H), δ = 4.46 (t, *J* = 5.0, 2H), δ = 3.71 (m, *J* = 5.5 Hz, 2H), δ = 2.87 (s, 4H).

siRNA macromers: siRNA-NH_2 (2 mg, 148 nmol, anti-luciferase siRNA or control sequence) was dissolved in DEPC-treated PBS (200 μL) in a 1.5-mL RNase-free Eppendorf tube. Separately, 2-*N*-hydroxysuccinimide, 2'-acryloyl-dithiodiethanol (5.2 mg, 100 eq) or 2-(succinimidyl carbonate)ethyl acrylamide (3.8 mg, 100 eq) was dissolved in RNase-free DMF (150 μL) and added to the solution of siRNA. The reaction was allowed to proceed for 36 h where additional 100 eq of the acrylate or acrylamide were added to the reaction mixture every 12 h. 5 M NH_4OAc (50 μL) and EtOH (1.1 mL) were added to the reaction mixture, which was vortexed for 15 s. The sample was incubated in a -80 °C freezer for 4 h followed by centrifugation (14 krpm, 4 °C, 20 min) to pellet the siRNA. The supernatant was decanted and the pellet was washed twice with 70% EtOH (ice-cold) to provide siRNA prodrug (79% yield). HR-ESI-MS: *m/z* found for siRNA sense strand $[M-H]^-$ = 6832.366; *m/z* calc. for disulfide macromer $[M-H]^-$ = 7067.676; found $[M-H]^-$ = 7067.855; *m/z* calc. for siRNA acrylamide macromer $[M-H]^-$ = 6974.506; found $[M-H]^-$ = 6974.871.

3.2.1.3 Characterization of siRNA macromers and analysis of bioactivity

Characterization of siRNA prodrug precursors was carried out on a 600 MHz Bruker NMR Spectrometer equipped with a Cryoprobe and siRNA macromonomers were analyzed by an IonSpec Fourier Transform Mass Spectrometer FTMS (20503 Crescent Bay Drive, Lake Forest, CA 92630) with a nano electrospray ionization source in combination with a

NanoMate (Advion 19 Brown Road, Ithaca, NY 14850) chip based electrospray sample introduction system and nozzle operated in the negative ion mode as well as reversed phase high-performance liquid chromatography.

Analysis of siRNA macromonomers by reversed phase HPLC demonstrates that modifications of siRNA-NH_2 with acrylamide and disulfide precursors yield a single peak and increase retention time relative to unmodified siRNA-NH_2 (Figure 3.1). Oligonucleotides were analyzed using 0.1 M triethylammonium acetate buffer (pH 7.0) and a gradient of 0 to 35% acetonitrile over 20 min followed by a gradient to 100% acetonitrile over the next 15 min. HPLC runs were conducted at a flow rate of 0.2 mL/min using Zorbax Eclipse XDB-C18 column (4.6 x 150 mm, 5 µm, Agilent) and Agilent 1200 Series Multiple Wavelength Detector SL.

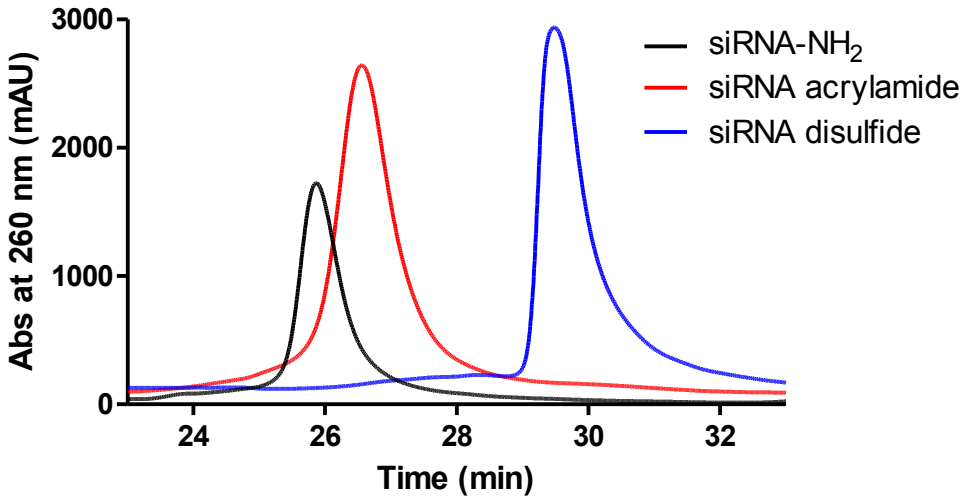

Figure 3.1 Analysis of native siRNA and siRNA macromers by reversed phase HPLC.

The activity of luciferase and control siRNA before and after derivatization with the disulfide precursor was tested *in vitro* using a HeLa cell line stably transfected with firefly luciferase reporter gene. The amine-terminated (native) and pro-drug siRNA were dosed on HeLa cells after complexation with Lipofectamine^{TM} 2000 transfection reagent. The siRNA

complexes were allowed to remain on the cells for 4 h followed by further incubation for 2 days at 37 ºC in cell media. Knockdown of luciferase expression was evaluated by measuring bioluminescence. Native and pro-drug siRNA elicited comparable knockdown (Figure 3.2) while gene silencing was absent when dosing control (inactive) siRNA. Maintenance of siRNA activity after modification indicates compatibility of the oligonucleotide with reaction and purification conditions involved in pro-drug synthesis.

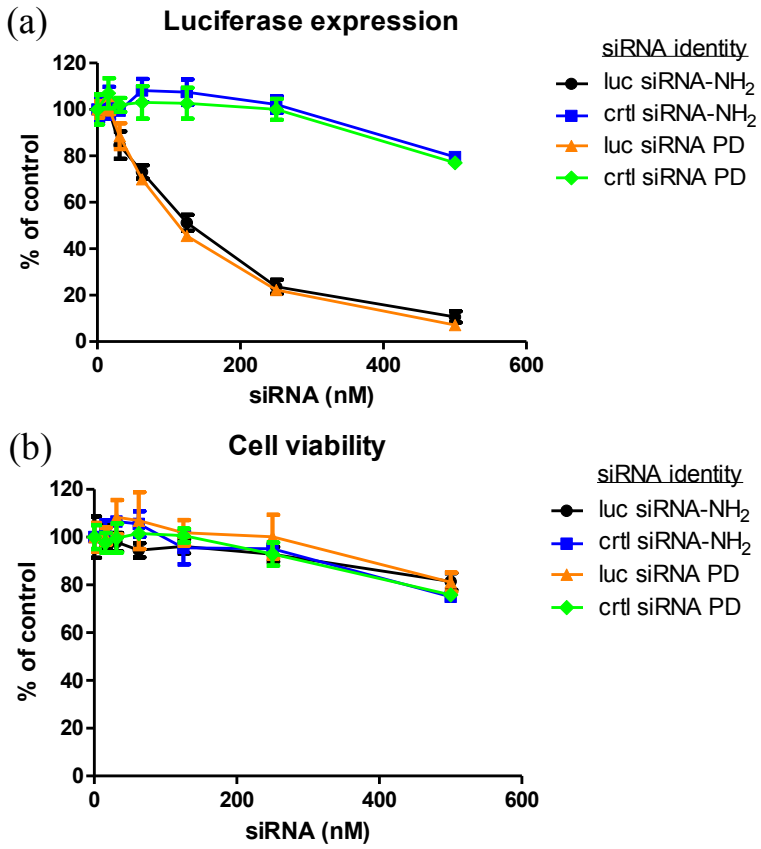

Figure 3.2 (a) Luciferase expression and (b) viability of HeLa/luc cells dosed with luciferase and control sequences of native (siRNA-NH_2) and degradable siRNA prodrug (PD) complexed to Lipofectamine 2000™ and incubated for 48 h. Retention of siRNA activity after macromonomer synthesis was confirmed by evaluating transfection efficiency before and after siRNA derivatization.

3.2.1.4 Particle characterization, analysis of siRNA by gel electrophoresis, and cell studies

Particle characterization and cell studies were conducted in a similar manner as reported in 2.3.1.

3.2.2 Fabrication of hydrogels *via* PRINT process for covalent incorporation of siRNA

For reversible covalent incorporation of siRNA into hydrogel nanoparticles, native siRNA-NH_2 was modified with a disulfide-containing acrylate precursor while implementing a non-degradable control acrylamide (Figure 3.3a). In the designed 'pro-siRNA hydrogels', it was envisioned that the siRNA cargo would be retained in the particle until entry of the particle into the cytoplasm of a cell, where the disulfide linkage would be cleaved in the reducing environment, allowing for release and delivery of the siRNA (Figure 3.3b). A water-based pre-particle composition containing the disulfide siRNA pro-drug and hygroscopic, liquid monomers was applied to fabricate cylindrical (d = 200 nm; h = 200 nm) loosely-crosslinked cationic PRINT hydrogel particles using a film-split technique. SEM micrographs confirmed the dimensions and shape of cylindrical siRNA-containing particles (Figure 3.3c).

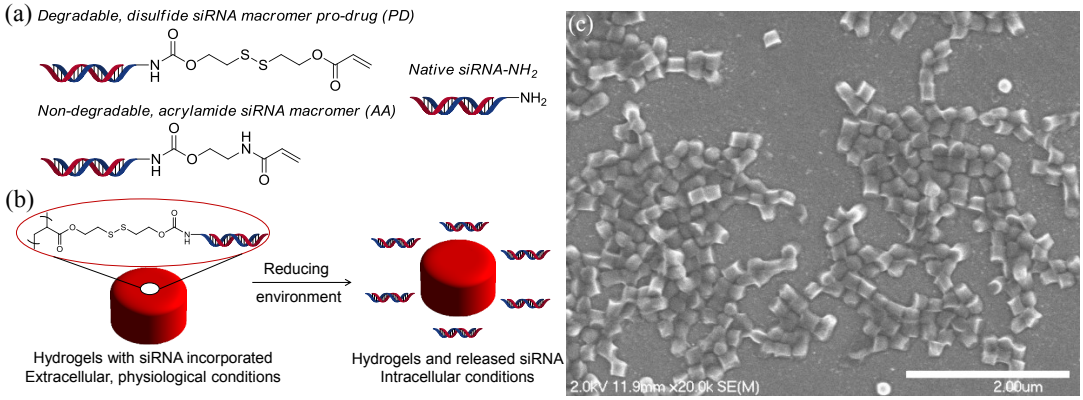

Figure 3.3 (a) Structures of degradable and non-degradable siRNA macromers as well as native siRNA, (b) Illustration of pro-siRNA hydrogel behavior under physiological and intracellular conditions, and (c) SEM micrograph of pro-siRNA, 200 x 200 nm cylindrical nanoparticles (scale bar = 2 μm).

The time-dependent release of the siRNA from the pro-drug PRINT hydrogel particles was evaluated under physiological and reducing conditions (Figure 3.4). The siRNA was retained in the hydrogel particles over 48 h at 37 °C in PBS while the siRNA was quickly released from hydrogels when incubated in a reducing environment (5 mM glutathione), reaching maximum concentration around 4 h (Figure 3.4a).

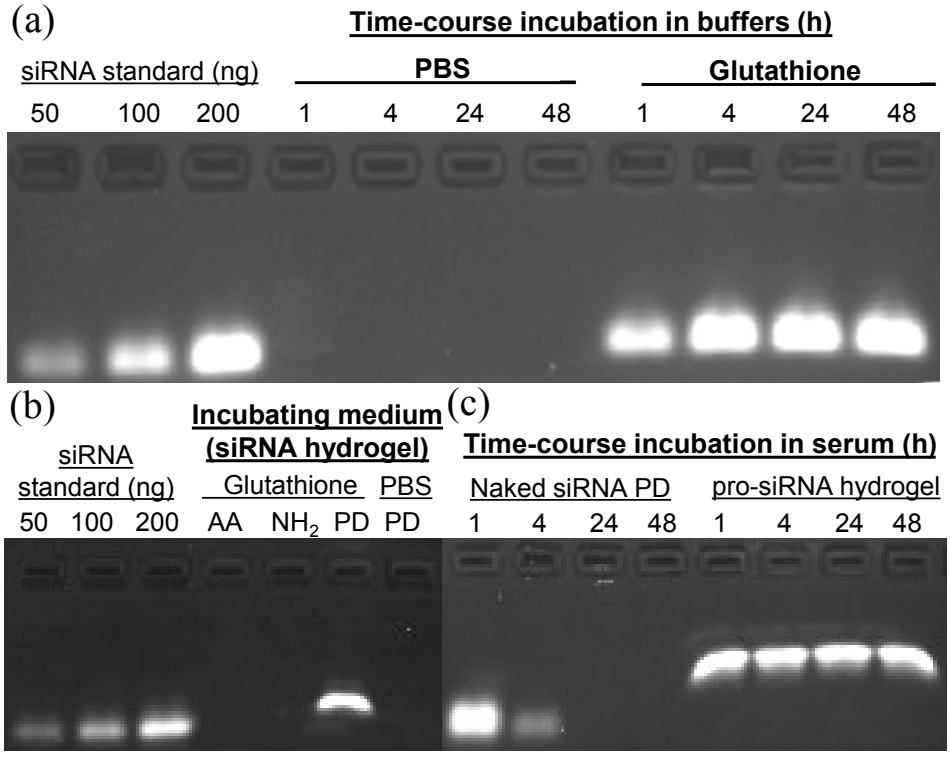

Figure 3.4 Release profiles and stability of siRNA in 30% AEM-based hydrogels. All hydrogels were washed with 10x PBS buffer to remove the sol fraction containing unconjugated siRNA before release studies were performed. (a) Time-dependent incubation of pro-siRNA hydrogels (1 mg/mL) in PBS and under reducing conditions (glutathione, 5 mM) at 37 °C. (b) Selective release of the disulfide-coupled siRNA prodrug (PD) from hydrogels under reducing conditions compared to the acrylamide (AA) macromer and native siRNA (NH_2). Hydrogels were incubated in 10x PBS with or without 5 mM glutathione for 4 h at 1 mg/mL and 37 °C. (c) Retention of siRNA integrity when conjugated to hydrogels after exposure to 10% fetal bovine serum (FBS) over time. Naked siRNA PD macromer was incubated at 36 μg/mL in 10% FBS for given times, proceeded by storage of solution. pro-siRNA hydrogels were incubated at 1.2 mg/mL in 10% FBS at 37 °C for given times followed by incubation in 10x PBS (5 mM glutathione) for 4 h at 1.2 mg/mL and 37 °C to release siRNA. Differences in siRNA migration observed in gels among the standards and samples which were released from hydrogels incubated in PBS and 10x PBS may arise from the differences in salt concentrations of sample solutions.

3.2.3 pro-siRNA hydrogels for gene silencing

3.2.3.1 Screening the amine content of hydrogel nanoparticles

The PRINT particles were designed to have a positive zeta potential to facilitate cell internalization and endosomal escape by including an amine monomer (AEM, 2-aminoethylmethacrylate hydrochloride). It is known that excessive amine content in hydrogels may disrupt and destroy the plasma membrane, eliciting cell death. Conversely, an insufficient amine content may not enable efficient cell uptake and endosomal escape for transfection. To optimize cytocompatibility and gene silencing efficiency of pro-siRNA hydrogels, the AEM content was varied from 5 to 50 wt% (Table 3.1). Pro-siRNA hydrogels were not PEGylated as were siRNA-complexed hydrogels whereby the cytocompatibility of bare particles would be determined. For systemic delivery of particles *in vivo*, sheddable coatings that reveal bare particles are attractive to enable targeting and endosomal escape for effective gene delivery.[26,27]

ζ-potentials of cationic hydrogels increased with amine content and the *Z*-average diameters (D_z) of the resultant particles ranged from 250 to 350 nm (Table 3.2). Encapsulation of the siRNA in the hydrogel PRINT particles reached a roughly constant value once the amine content was greater than or equal to 20 wt% (Figure 3.5). The encapsulation efficiency was determined to be ca. 35% for AEM contents ≥ 20 wt% while when only using 5% AEM, the encapsulation was lower (ca. 15%). When the pro-drug, disulfide-containing siRNA hydrogel PRINT particles were dosed onto luciferase-transfected cells (HeLa/luc) for 5 h followed by 48 h incubation at 37 °C, dose-dependent knockdown of the luciferase expression was observed (Figure 3.6a) for hydrogels with amine contents greater than 5 wt% AEM. Cytocompatibility was maintained at the lower amine contents and

dosing concentrations (Figure 3.6b). It appeared that the 30% AEM-containing PRINT hydrogel particles provided the ideal combination of gene silencing efficiency (EC_{50} ~ 20 nM siRNA) and cytocompatibility (even at high dosing concentrations).

Table 3.1 Composition of pre-particle solution for fabrication of pro-siRNA hydrogels.

Component	Function	wt %
PEG_{700} diacrylate	crosslinker	5
Tetraethyleneglycol monoacrylate	hydrophile	73–28
2-aminoethyl methacrylate HCl	cationic handle	5–50
Poly(vinyl alcohol) 2 kDa	porogen and PET-wetter	10
Irgacure 2959	photoinitiator	1
DyLight 488 maleimide	fluorescent dye	1
siRNA	cargo	5

Table 3.2 Zetasizer analysis of pro-siRNA hydrogels with variable amine content.

Amine content (wt%)	ζ-potential (mV)	D_z (nm)
5% AEM	+18.2 ± 0.5	350.2 ± 5.4
20% AEM	+22.6 ± 0.1	281.6 ± 1.9
25% AEM	+27.1 ± 0.3	307.4 ± 6.6
30% AEM	+27.9 ± 1.5	324.3 ± 5.6
40% AEM	+30.6 ± 1.0	281.3 ± 6.0
50% AEM	+34.1 ± 0.4	253.7 ± 3.4

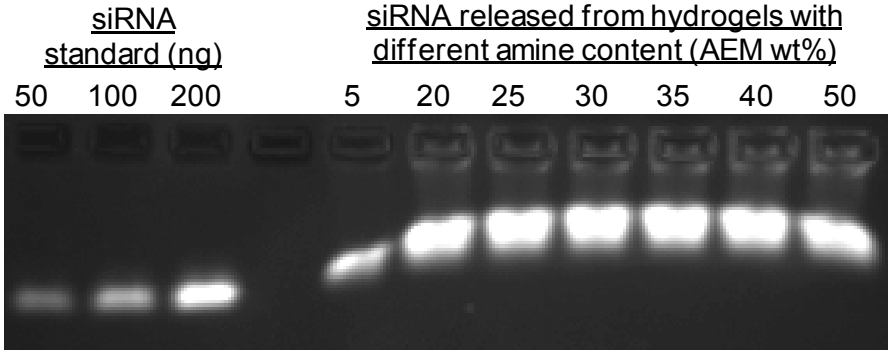

Figure 3.5 Gel electrophoresis of siRNA released from hydrogels prepared with different amine monomer contents. Hydrogels were incubated in 10x PBS containing 5 mM glutathione at 1.7 mg/mL for 4 h at 37 °C.

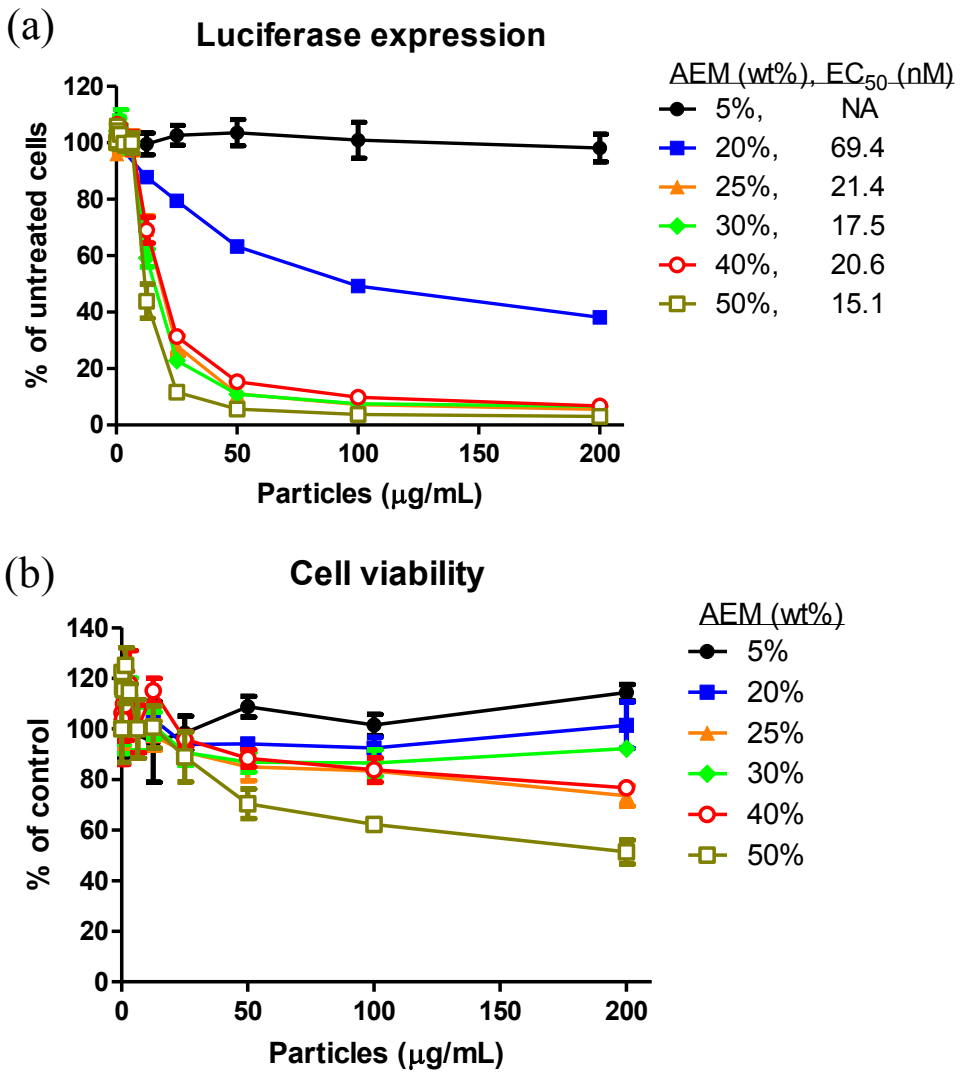

Figure 3.6 (a) Luciferase expression and (b) viability of HeLa/luc cells dosed with cationic pro-siRNA hydrogels fabricated with different amine (AEM) contents. Cells were dosed with particles for 5 h followed by removal of particles and 48 h incubation in media. Data are representative of two independent experiments. The error bars represent standard deviation from triplicate wells in the same experiment. Half maximal effective concentrations (EC_{50}s) of siRNA (nM) for luciferase gene knockdown are listed in the legend. EC_{50} was not available (NA) for hydrogels prepared with 5 wt% AEM due to the absence of dose-dependent luciferase knockdown.

3.2.3.2 Implementing additional siRNA cargos into hydrogel nanoparticles to investigate gene silencing specificity

To study the response of pro-siRNA hydrogels to a reducing environment, non-disulfide acrylamide siRNA-based hydrogel particles and native siRNA-complexed particles

were prepared as controls. Release of native siRNA-NH_2 occurred rapidly from these porous, loosely-crosslinked hydrogels (Figure 3.7). Figure 3.8 showed that different siRNAs were loaded into hydrogel particles and remained associated with particles directly after harvesting. Unconjugated siRNA was found in hydrogels charged with native siRNA or siRNA macromers due to incomplete conversion; therefore, in the following experiments all particles were extensively washed with 10x PBS to remove the sol fraction containing free siRNA.

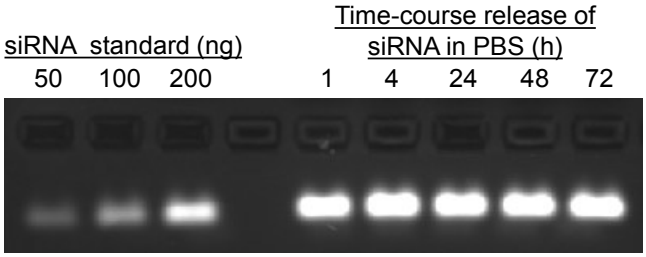

Figure 3.7 Gel electrophoresis of native siRNA-NH_2 released from 30 wt% AEM-based hydrogels over time in PBS at 1 mg/mL and 37 ºC shows rapid release of cargo.

To further investigate the *in vitro* gene knockdown efficacy of the PRINT hydrogel particles, the 30% AEM-based hydrogel composition was utilized with four different cargos: (1) native luc siRNA, (2) degradable disulfide luc siRNA, (3) non-degradable, acrylamide luc siRNA, and (4) degradable disulfide control siRNA. Zetasizer analysis of the hydrogel PRINT particles indicated that their size and charge were similar (Table 3.3) and gel electrophoresis (Figs. 3.9) allowed for confirmation of the release of the various cargos. After dosing the particles on cells and incubating for 48 h, cell viability was maintained above 80% for all of the samples across all dosing concentrations, except for the particles charged with the free siRNA (Figure 3.10). Uptake of all of the hydrogel particles approached saturation at around 50 μg/mL particle concentration (Figure 3.11a). Dose-dependent silencing of luciferase expression was elicited notably for the pro-drug, disulfide-based siRNA-containing

hydrogel particles while the control particles did not elicit significant gene knockdown (Figure 3.11b).

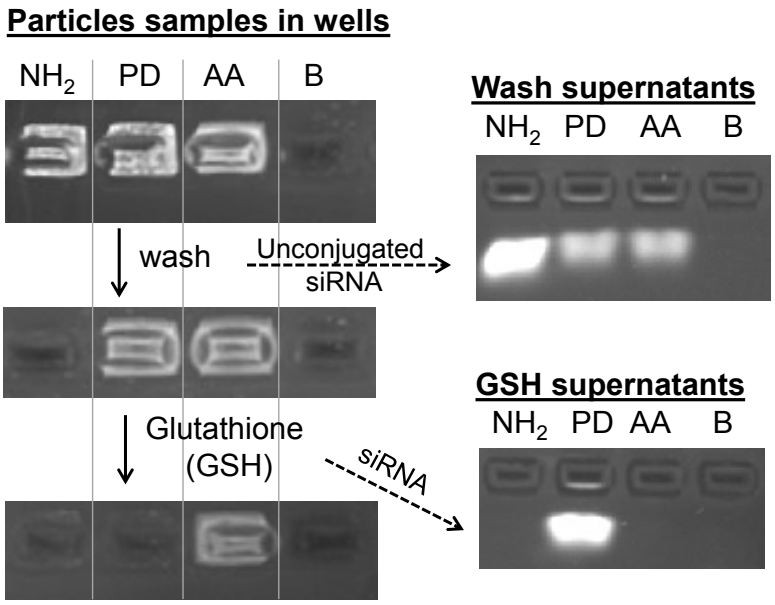

Figure 3.8 Characterization of particle work-up and behavior after harvesting by gel electrophoresis. Particles prepared from 30 wt% AEM-based composition without dye were charged with native siRNA (NH_2), disulfide pro-drug macromer (PD), and acrylamide macromer (AA) in addition to blank particles without siRNA (B). Particles were loaded into the wells of the gel (left) at 1 mg/mL to observe the presence of siRNA in hydrogels directly after harvesting particles, after washing unconjugated siRNA, and after incubation in glutathione-containing buffer. Corresponding unconjugated siRNA was washed from hydrogels with 10x PBS, isolated from the supernatant of particle dispersions, and run on the gel (right) as well as supernatants from particles incubated in 5 mM glutathione-containing buffer (10x PBS) for 4 h at 37 ºC to illustrate the removal of unconjugated siRNA and triggered release of the disulfide-conjugated siRNA.

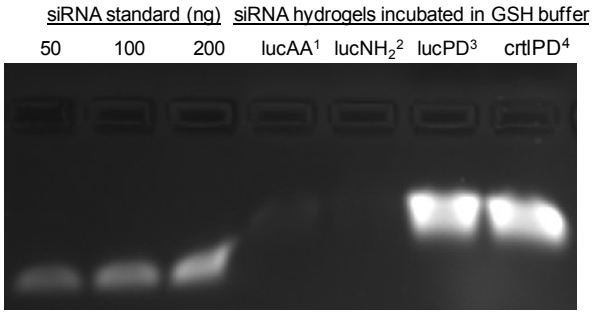

Figure 3.9 Gel electrophoresis analysis of siRNAs (abbreviation below) released from hydrogels incubated at 2.5 mg/mL for control knockdown studies under reducing conditions (5 mM glutathione, GSH) in 10x PBS for 4 h at 37 °C. $lucAA^1$: acrylamide non-degradable luciferase siRNA; NH_2^2: native amine luciferase siRNA; $lucPD^3$: degradable luciferase siRNA prodrug; $crtlPD^4$: degradable control siRNA prodrug.

Table 3.3 Zetasizer analysis of cationic hydrogels charged with different siRNAs.

siRNA cargo	ζ-potential (mV)	D_z (nm)
Luc prodrug	+17.3 ± 0.2	340.0 ± 7.0
Luc AA prodrug	+16.7 ± 0.2	292.6 ± 6.4
Luc NH_2	+20.8 ± 0.8	304.2 ± 6.7
Crtl prodrug	+17.4 ± 1.0	325.6 ± 1.2

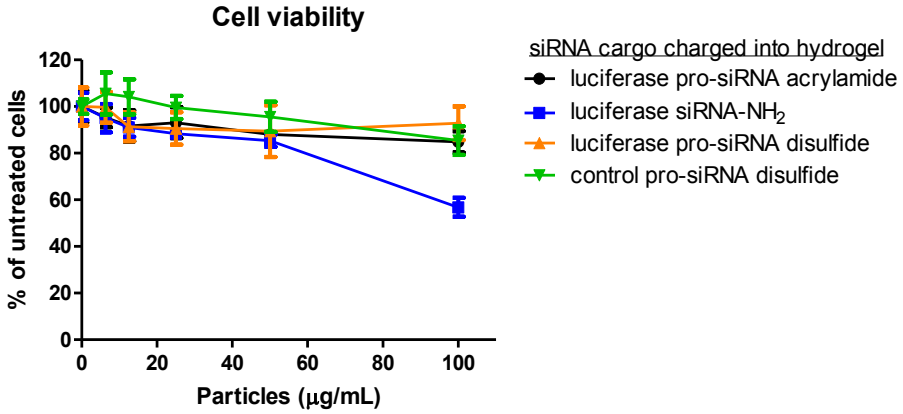

Figure 3.10 Viability of HeLa/luc cells dosed with cationic hydrogels charged with different siRNA cargos. Cells were dosed with particles for 4 h followed by removal of particles and 48 h incubation in media.

The transfection efficiency between siRNA-complexed, PEGylated particles and pro-siRNA hydrogels is comparable, which can be explained by differences in release characteristics. PEGylated particles release siRNA slowly in PBS while pro-siRNA hydrogels rapidly release siRNA under intracellular conditions. Confocal microscopy images of HeLa cells dosed with particles (Figs. 3.11c-f) illustrates uptake of the particles, which accumulated largely in the cytoplasm and perinuclear region. Given the internalization of cationic particles by HeLa cells and distribution throughout the cytoplasm and perinuclear area, potential exists for the encapsulation of other therapeutic nucleic acids in hydrogel nanoparticles to transfect diseased cells.

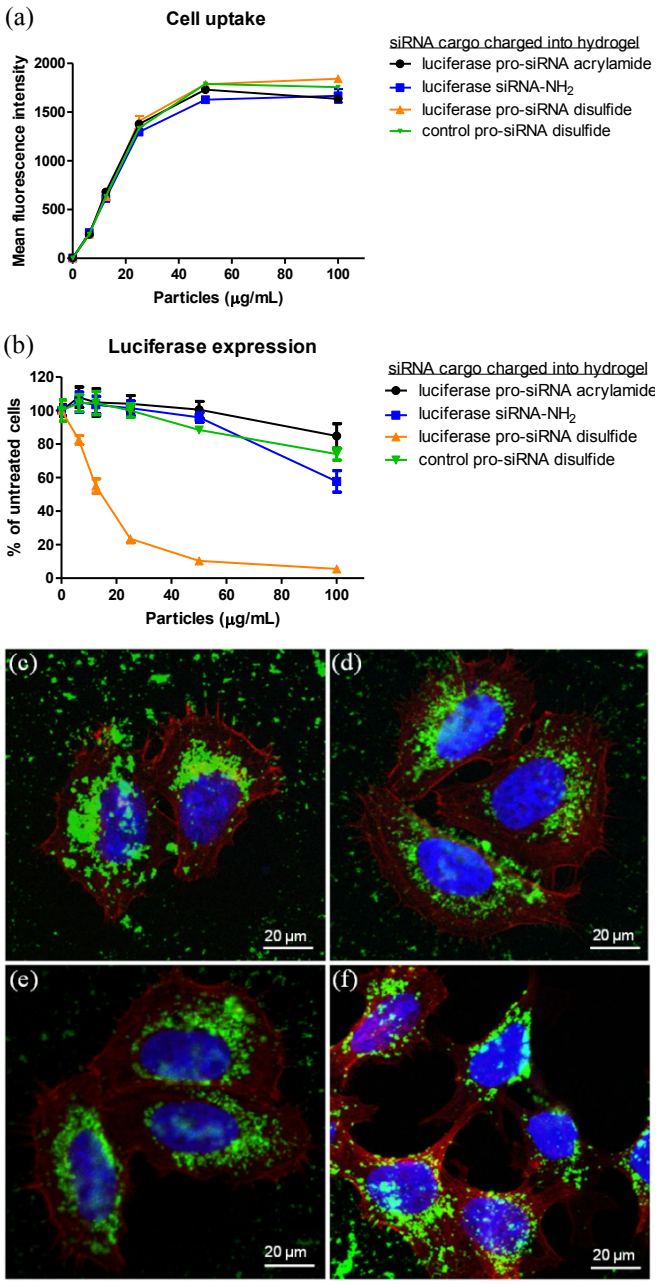

Figure 3.11 30% AEM-based hydrogel particles charged with different siRNA cargos for transfection of HeLa cells. (a) Cellular uptake. HeLa/luc cells were dosed with particles for 4 h followed by trypan blue treatment and flow cytometry analysis. (b) Luciferase expression. HeLa/luc cells were dosed with particles for 4 h followed by removal of particles and 48 h incubation in media. Data in (a) and (b) represent one of two independent experiments. The error bars represent standard deviation from triplicate wells in the same experiment. Note that all hydrogels were thoroughly washed after fabrication to remove non-conjugated siRNA in the sol fraction. (c)-(f) Confocal micrographs. HeLa/luc cells were dosed with 50 µg/mL hydrogels containing (c) luc PD (d) luc siRNA-NH_2, (e) luc acrylamide, and (f) control PD siRNA cargos for 4 h. Cellular actin cytoskeleton was stained with phalloidin (red) and nuclei with DAPI (blue) while particles (green) were labeled with the fluorescent monomer, DyLight 488 maleimide.

3.3 Targeting hepatocytes with PRINT particles

Since selective uptake of galactose-functionalized terpolymer ligand-coated PRINT hydrogel nanoparticles was not observed by hepatocytes *in vitro* and asialoglycoprotein receptors have requirements for uptake, e.g. specific restrictions on upper particle size limit (70 nm) for endocytosis and distinct spatial orientation of ligands presented at specific densities on nanoparticle surfaces, alterative receptors were sought. Hepatic receptors with additional flexibility in nanoparticle size and presentation of ligands may involve low density lipoprotein (LDL) receptors. LDL receptor-related protein 1 (LRP1), a transmembrane glycoprotein, plays many biological roles from endocytosis of numerous ligands to modulation of blood brain barrier function.[28,29] Hepatic functions of LRP1 involve clearance of plasma proteins like FVII. Most importantly, LRP1 and LRP2 can be targeted for endocytosis by lactoferrin-conjugated nanoparticles. Lactoferrin, a large, multifunctional glycoprotein related to transferrin, was conjugated to nanoparticles for systemic administration to enhance delivery to hepatocytes.[30]

LRP was identified to play a crucial role in the uptake of a peptide sequence from the tail fiber protein (p17) of a T7 phage in liver parenchymal cells *in vitro* and *in vivo*.[31] The p17-derived peptide was functionalized with streptavidin for conjugation to biotinylated liposomes. Targeted delivery of p17-conjugated liposomes to hepatocytes was demonstrated after tail vein injection into mice relative to control peptide-conjugated liposomes.[32] Adapting the lactoferrin protein and p17-derived peptides to PRINT particles, targeted delivery of particles to hepatocytes was investigated *in vitro* and *in vivo*.

3.3.1 Experimental

3.3.1.1 Materials

Previously obtained materials listed in 3.3 were used for these studies. SCM-PEG_{5K}-maleimide was from Laysan Bio, Inc. Succinic anhydride and lactoferrins (human and bovine) were purchased from Sigma Aldrich. The T7 phage p17 peptide was obtained from Genscript with a cysteine residue added to the N-terminus. BCA Protein Assay Kit was obtained from Pierce, Thermo Fisher Scientific.

3.3.1.2 Particle fabrication and characterization as well as cell studies

Particle fabrication was carried out in a similar manner as for 30 wt% AEM pro-siRNA hydrogels: for compositions without siRNA, the wt% of HP_4A was correspondingly increased. 80x180, 80x320, and 200x200 nm PRINT molds were graciously provided by Liquidia Technologies. Cell culture and analysis was conducted as described previously, using AML12, HepG2, and RAW cells in these experiments. Particle characterization by SEM, TGA, and Zetasizer analysis was conducted as previously described.

The bicinchoninic acid assay (BCA) was used to quantify protein or peptide conjugated to nanoparticles. Instructions were followed from the manufacturer for protein quantification in creating standards of protein using serial dilutions and particles were directly analyzed. 200 μL of reagent mixture was added to each well in 96-well plates to which 20 μL of sample (protein standard or particle dispersion) was added for absorbance reading on a Spectrophotometer at 562 nm.

3.3.1.3 Functionalization of particles with lactoferrin and p17-derived peptide

Particles were functionalized with biological ligands by first PEGylating particles at 0.5 mg/mL in anhydrous DMF for 6 h using pyridine base and SCM-PEG_{5K}-maleimide at

given weight equivalents. Optionally, non-PEGylated amines were quenched with succinic anhydride (2 wt eq) in anhydrous DMF at 1 mg/mL particle concentration for 2 h. Particles were washed with PBS and re-suspended in sodium borate buffer (pH 9.5) or other buffers at 0.5 mg/mL for conjugation of lactoferrin (or ethanolamine control ligand at given wt eq) for 4 h at given wt ratios, followed by washing with PBS. For conjugation of p17 peptide, particles were incubated with the peptide overnight in PBS at listed stoichiometric ratios. Lastly, particles were washed to remove any free ligand.

3.3.2 Lactoferrin conjugation strategies for enabling receptor-mediated endocytosis of 200 nm cylindrical hydrogels

Bovine lactoferrin was first pursued for conjugation to nanoparticles to enable receptor mediated endocytosis. The reaction scheme for preparing 200 nm targeted particles is outline in Figure 3.12. Particles were PEGylated with SCM-PEG_{5K}-maleimide followed by quenching half of the particles with succinic anhydride. Subsequently, particles were reacted with either lactoferrin or ethanolamine ($EtOHNH_2$, control ligand, 2 wt eq) in basic buffer. Zetasizer analysis of particles (Table 3.4) indicated that they all exhibited negative ζ-potentials. Unquenched particles embraced negative ζ-potentials most likely due to the intramolecular rearrangement that polymerized AEM readily undergoes to form an alcohol. Quenched particles showed ζ-potentials of greater magnitude, most likely due to the carboxylates contributing more anionic character.

Internalization of lactoferrin- and ethanolamine (control)-conjugated particles (Figure 3.13), which were not quenched with succinic anhydride, by AML12 cells reached ca. 100% at low dosing concentration. Mean fluorescence intensity (MFI) of AML12 cells dosed with unquenched particles shows high values, increasing with concentration. For quenched

particles, differential uptake was observed between lactoferrin- and ethanolamine-conjugated particles: lactoferrin reached maximum cell uptake around 50 μg/mL while control particles demonstrated low background uptake (ca. 20%) at this dose. MFI of AML12 cells illustrates a large difference in uptake between lactoferrin-conjugated particles and ethanolamine-quenched particles.

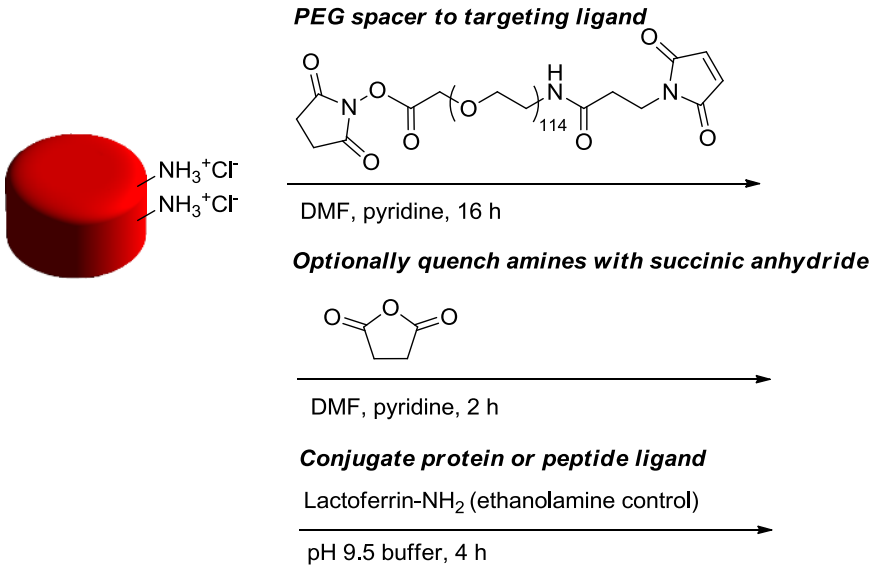

Figure 3.12 Reaction scheme for preparation of ligand-conjugated hydrogels.

Table 3.4 Zetasizer analysis of ligand-conjugated nanoparticles.

Particle (ligand)	ζ-potential (mV)	D_z (nm)
Lactoferrin, no quench	-2.5 ± 0.4	365.1 ± 2.4
Lactoferrin, quench	-6.5 ± 0.1	386.0 ± 4.4
$EtOHNH_2$, no quench	-2.2 ± 0.2	379.5 ± 23.7
$EtOHNH_2$, quench	-9.6 ± 0.1	384.9 ± 4.8

The effect of media (complete medium or OPTI-MEM) was explored on cell uptake selectivity of nanoparticles *in vitro*. Uptake of targeted, quenched 200 nm particles by AML12 cells was similar to previous studies where high internalization occurred at low doses for LTF-conjugated particles while uptake of LTF-free (ethanolamine-reacted, control) particles was notably lower when incubated in complete medium or OPTI-MEM (Figure

3.14a). MFI of AML12 cells incubated with particles illustrates a significant difference in uptake between LTF- and ethanolamine-conjugated particles (Figure 3.14b).

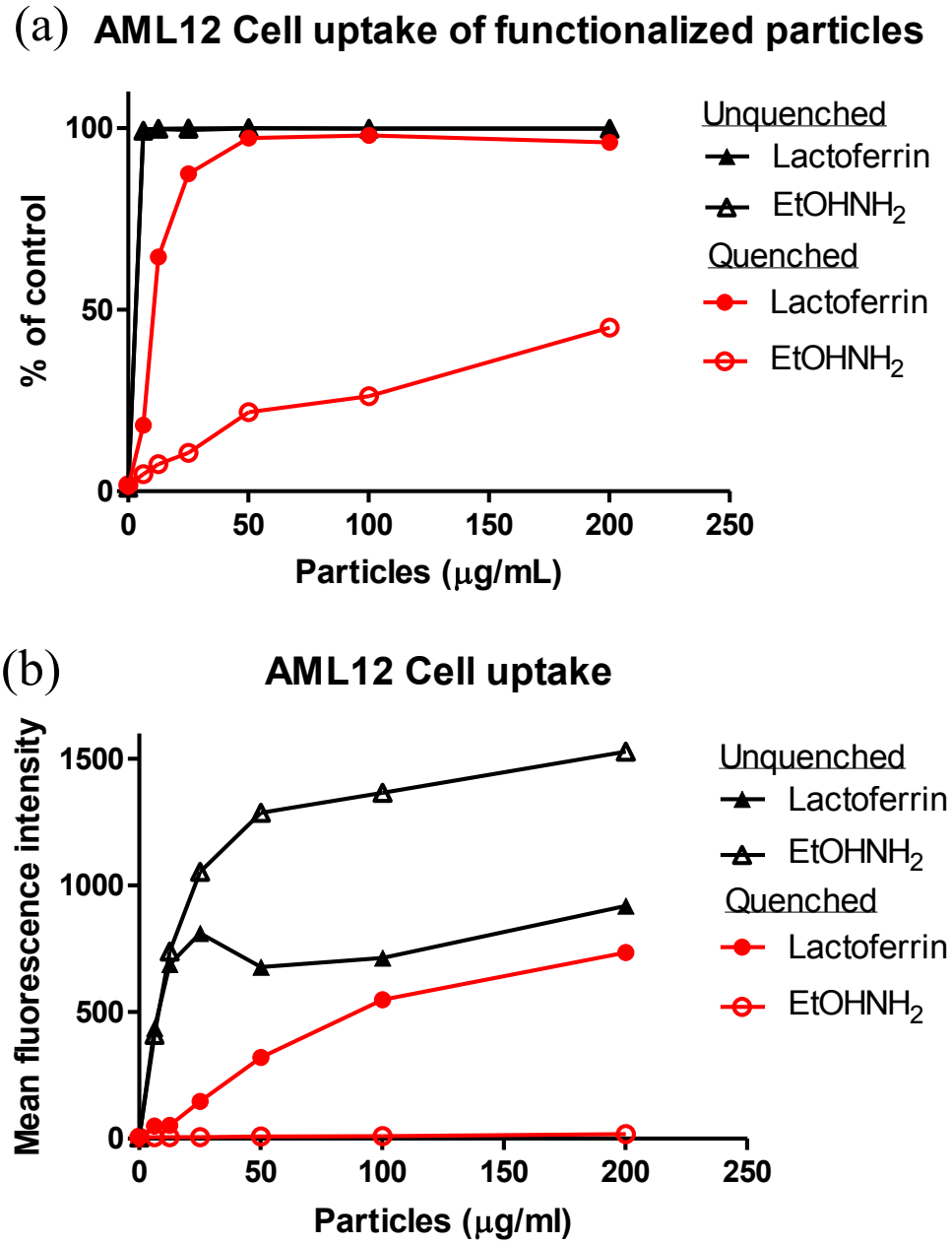

Figure 3.13 AML12 cell uptake of ligand-conjugated particles expressed as (a) % of control cells and (b) mean fluorescence intensity.

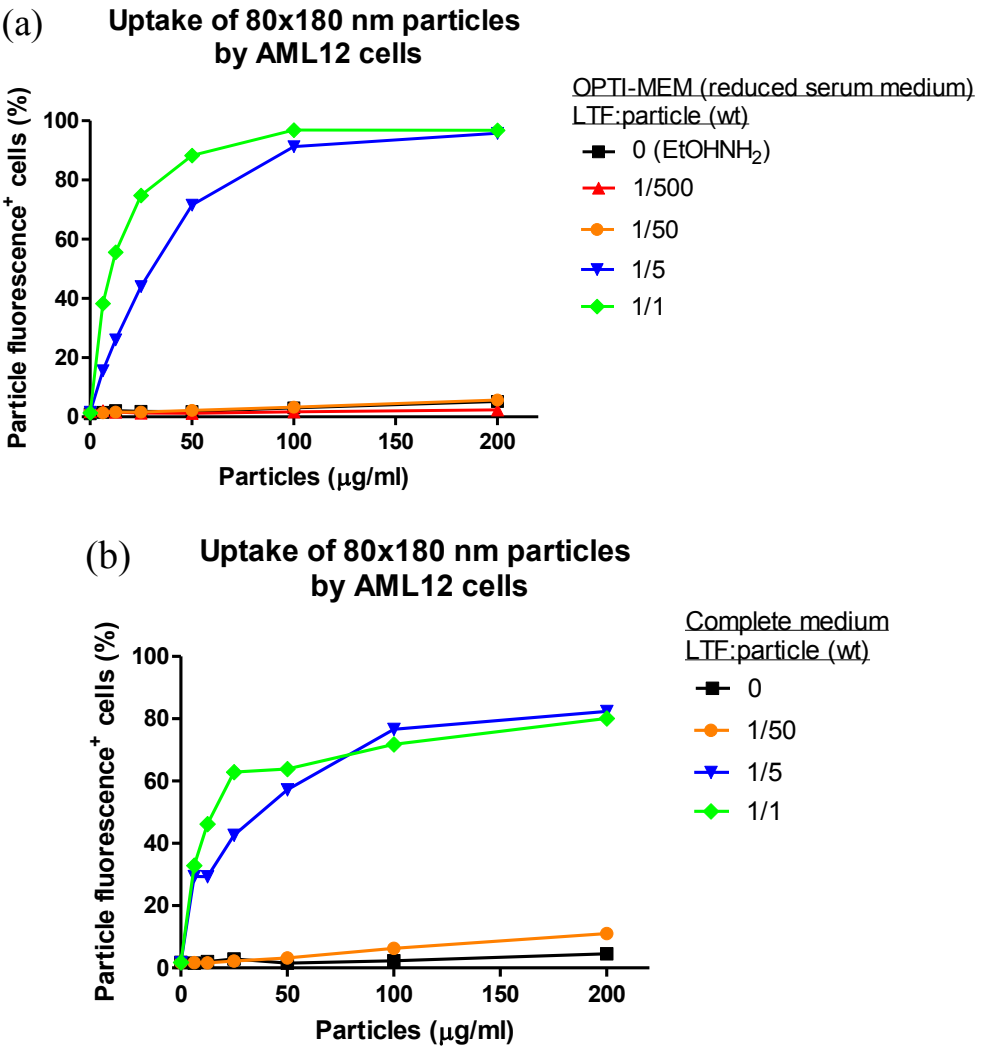

Figure 3.14. AML12 cell uptake after dosing with 200 nm ligand-conjugated particles expressed as (a) % of control cells and (b) mean fluorescence intensity.

3.3.3 Screening lactoferrin density on 80x180 nm hydrogels for targeting hepatocytes

To test the targeting capabilities of another particle dimension and to screen bovine lactoferrin ligand density, 80x180 nm hydrogel nanoparticles were prepared for functionalization with ligands at different reaction stoichiometries. Previously, 200 nm particles were prepared with 1 wt eq lactoferrin; for 80x180 nm particles, the stoichiometry was titrated to low concentrations and amines were quenched with succinic anhydride post-PEGylation. Zetaszier analysis (Table 3.5) illustrates that all functionalized particles

exhibited negative ζ-potentials around -10 to -15 mV with diameters of ca. 250 nm. These particles were dosed on AML12 cells along with previously-prepared 200 nm ligand-conjugated, quenched particles.

Uptake of targeted, quenched 200 nm particles by AML12 cells was similar to previous studies where high internalization occurred at low doses for LTF-conjugated particles while uptake of LTF-free (ethanolamine-reacted, control) particles was notably lower when incubated in complete medium or OPTI-MEM (Figure 3.15). MFI of AML12 cells incubated with particles illustrates a significant difference in uptake between LTF- and ethanolamine-conjugated particles (Figure 3.15b).

Table 3.5 Zetasizer analysis of functionalized 80x180 nm hydrogel nanoparticles.

Particle (ligand, wt eq)	ζ-potential (mV)	D_z (nm)
$EtOHNH_2$, 4	-14.5 ± 3.2	252.7 ± 15.4
Lactoferrin, 1	-9.8 ± 0.3	246.5 ± 4.7
Lactoferrin, 1/5	-10.0 ± 0.8	237.2 ± 3.5
Lactoferrin, 1/50	-11.7 ± 0.4	261.8 ± 3.0
Lactoferrin, 1/500	-12.5 ± 0.6	260.1 ± 11.6

Internalization of ligand-conjugated 80x180 nm hydrogel nanoparticles by AML12 cells shows similar trends to the 200 nm particles. Uptake of ligand-conjugated particles (at higher ligand density) reached saturation in a dose-dependent manner while the control (ethanolamine)-conjugated particles and low density LTF-conjugated particles were not readily internalized (Figure 3.15). Incubation of targeted particles in OPTI-MEM or complete medium (Figure 3.16) resulted in the same differential uptake between particles conjugated with sufficient protein and control particles.

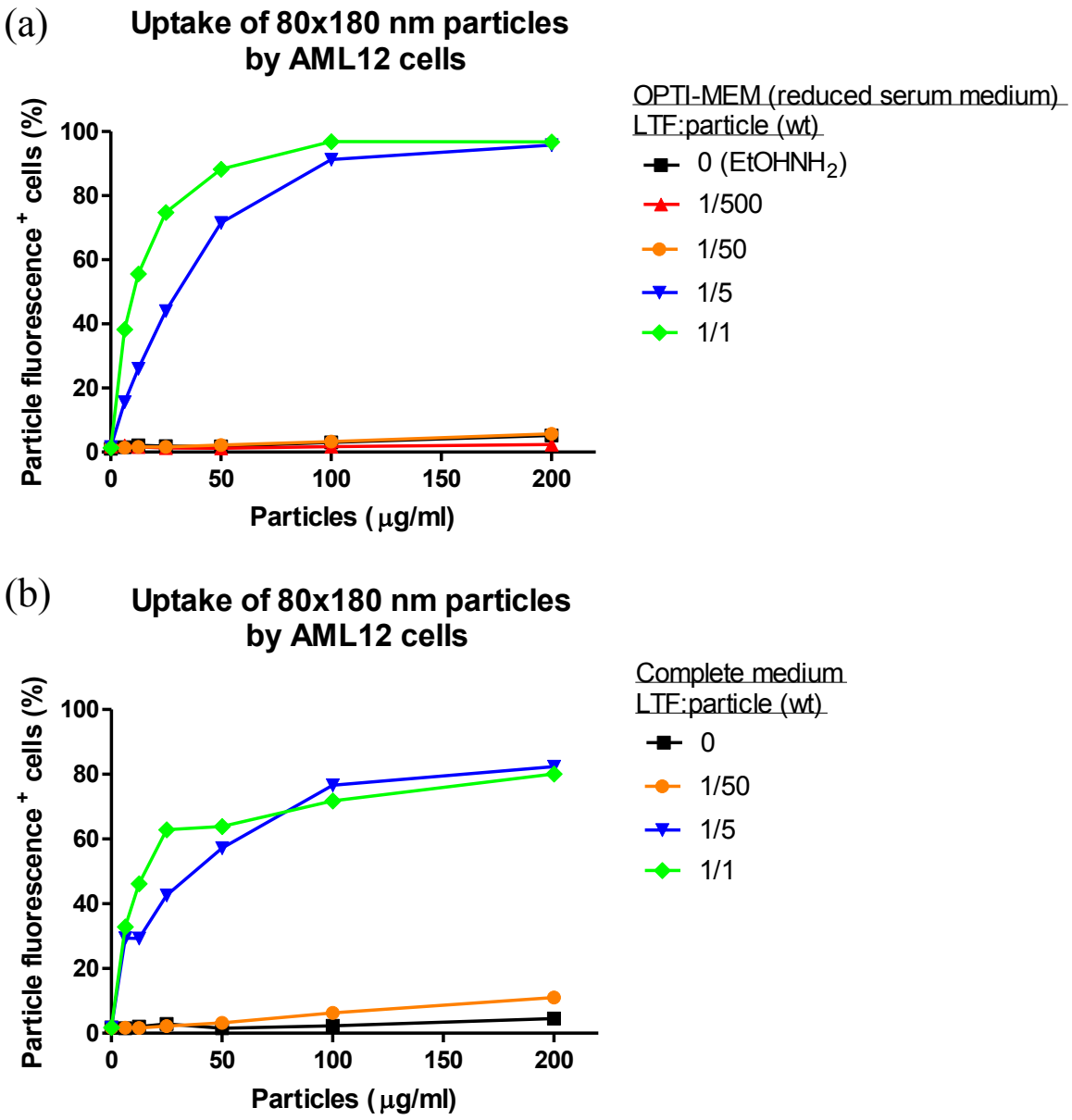

Figure 3.15 AML12 cell uptake of targeted particles incubated in (a) OPTI-MEM or (b) complete medium.

3.3.4 Evaluating human lactoferrin-conjugated nanoparticles targeted to mouse hepatocytes *in vitro*

80x180 nm hydrogel nanoparticles conjugated with human lactoferrin (LTF) were selectively internalized by AML12 mouse hepatocytes relative to control particles. Bovine lactoferrin was previously tested and demonstrated the same selective internalization,

suggesting that ligand recognition is conserved among species. 80x180 nm hydrogels were reacted with SCM-PEG_{5K}-maleimide followed by quenching non-PEGylated amines with succinic anhydride. PEGylated particles were then either reacted with human lactoferrin (hLTF) or ethanolamine (no LTF). Selective uptake of hLTF-conjugated hydrogels occurred across all dosing concentrations (Figure 3.16). Zetasizer analysis of particles (Table 3.6) showed that ζ-potentials were negative with diameters around 250 nm.

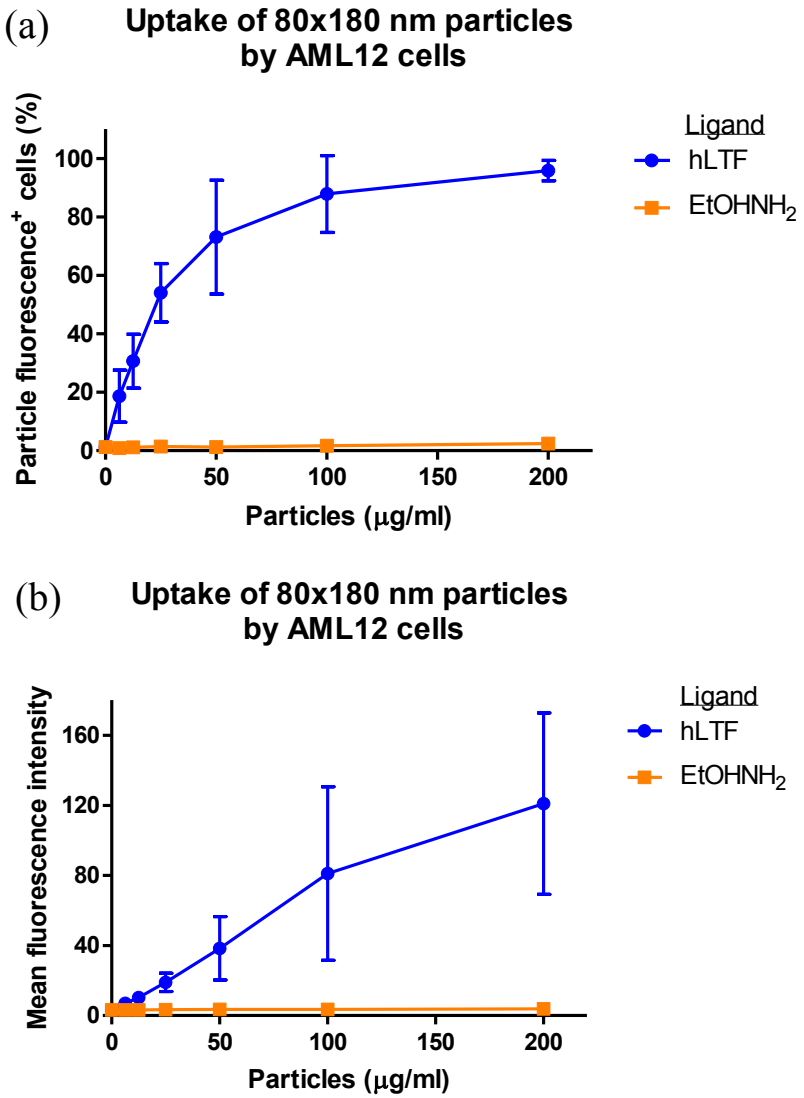

Figure 3.16 (a) AML12 cell uptake (%) of hydrogel nanoparticles functionalized with hLTF or $EtOHNH_2$. (b) Mean fluorescence intensity of AML12 cells dosed with functionalized particles.

Table 3.6 Zetasizer analysis of functionalized hydrogels.

Sample	ζ-potential (mV)	D_z (nm)
$EtOHNH_2$	-12.9 ± 1.1	270.0 ± 10.8
hLTF	-12.2 ± 1.1	231.4 ± 1.0

3.3.5 Targeting human and mouse hepatocytes with lactoferrin- and peptide-conjugated nanoparticles

Human lactoferrin- and T7 phage peptide-conjugated 80x180 nm hydrogel nanoparticles were tested for their selective uptake by HepG2 (human) and AML12 (mouse) hepatocytes relative to control particles and macrophages. Selective uptake of lactoferrin-conjugated particles was observed in HepG2 and AML12 hepatocytes while all particles were equally internalized by macrophages.

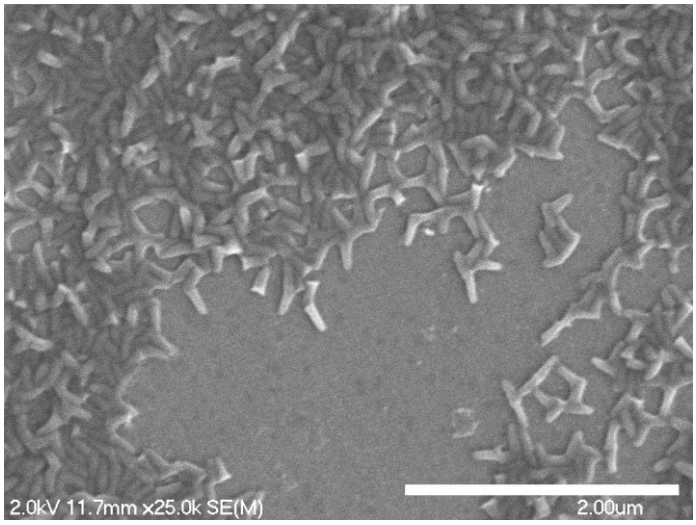

Figure 3.17 SEM micrograph of 80x180 nm hydrogel nanoparticles.

The morphology and dimensions of 80x180 nm hydrogel nanoparticles were assessed *via* SEM to provide visualization of the rod-shaped nanoparticles (Figure 3.17). Ligand-conjugated particles were prepared by reacting 80x180 nm particles with SCM-PEG_{5K}-maleimide followed by quenching non-PEGylated amines with succinic anhydride. Control particles were prepared by reacting maleimide-grafted particles with ethanolamine ($EtOHNH_2$) in basic buffer, peptide-conjugated particles were prepared by reacting a thiol-

terminated peptide with a maleimide-grafted particle in PBS, and lactoferrin-conjugated particles were obtained by incubating lactoferrin with particles in basic buffer.

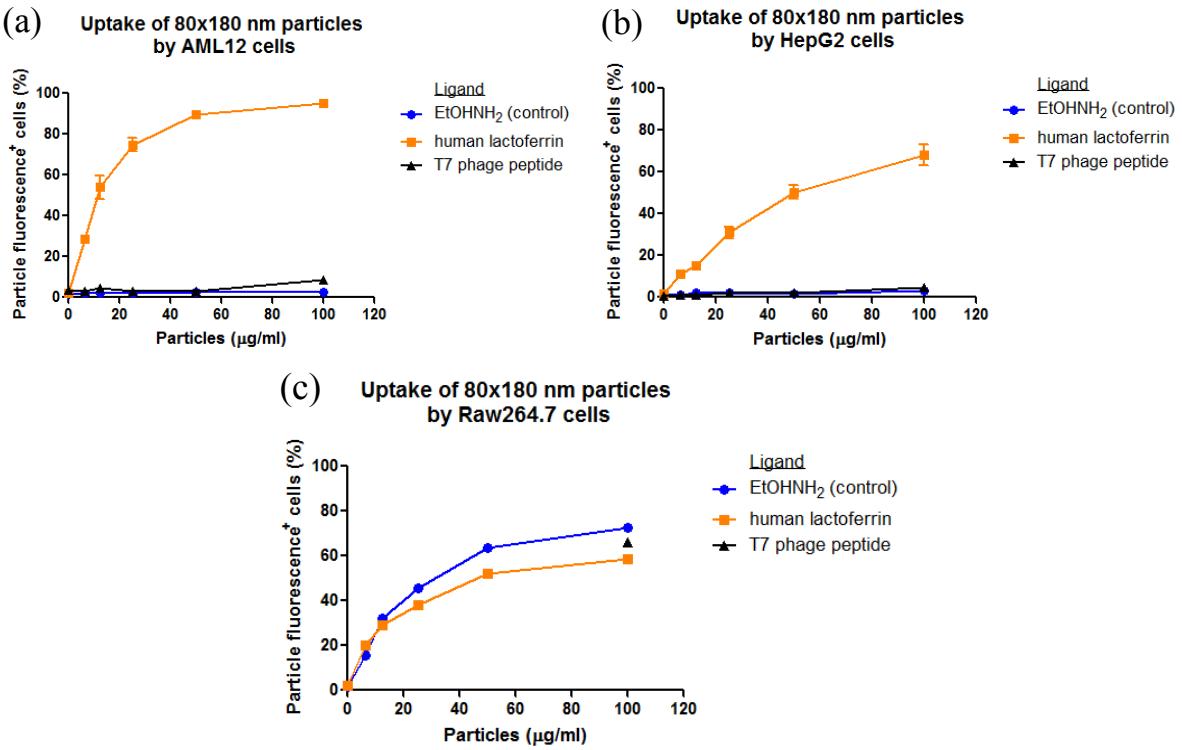

Figure 3.18 Cell uptake of ligand-conjugated particles. (a) AML12, (b) HepG2, and (c) RAW 264.7 cells were dosed with particles to investigate internalization of particles conjugated with different ligands.

Selective uptake of lactoferrin-conjugated particles by HepG2 and AML12 hepatocytes was observed (Figure 3.18a,b) relative to control particles. Peptide-conjugated particles were not readily internalized by hepatocytes, potentially due to insufficient ligand density. RAW macrophages internalized lactoferrin- and peptide-conjugated particles similarly at the highest particle dosing concentration. Confocal microscopy was conducted on AML12 and RAW cells dosed with all three types of particles (Figure 3.19 and 3.20). A confocal microscopy image was also obtained for HepG2 cells dosed with lactoferrin-conjugated particles (Figure 3.20d). Notable uptake of particles by AML12 cells was only observed for cells dosed with ligand-conjugated particles (Figure 3.19c) relative to control

(Figure 3.19b) and peptide-conjugated (Figure 3.19d) particles. Internalization of all three particle samples by RAW cells can be noted in the confocal micrographs shown in Figure 3.20a-c. Uptake of lactoferrin-conjugated particles by HepG2 cells can be inferred from the confocal micrograph of Figure 3.20d although actin is not apparent.

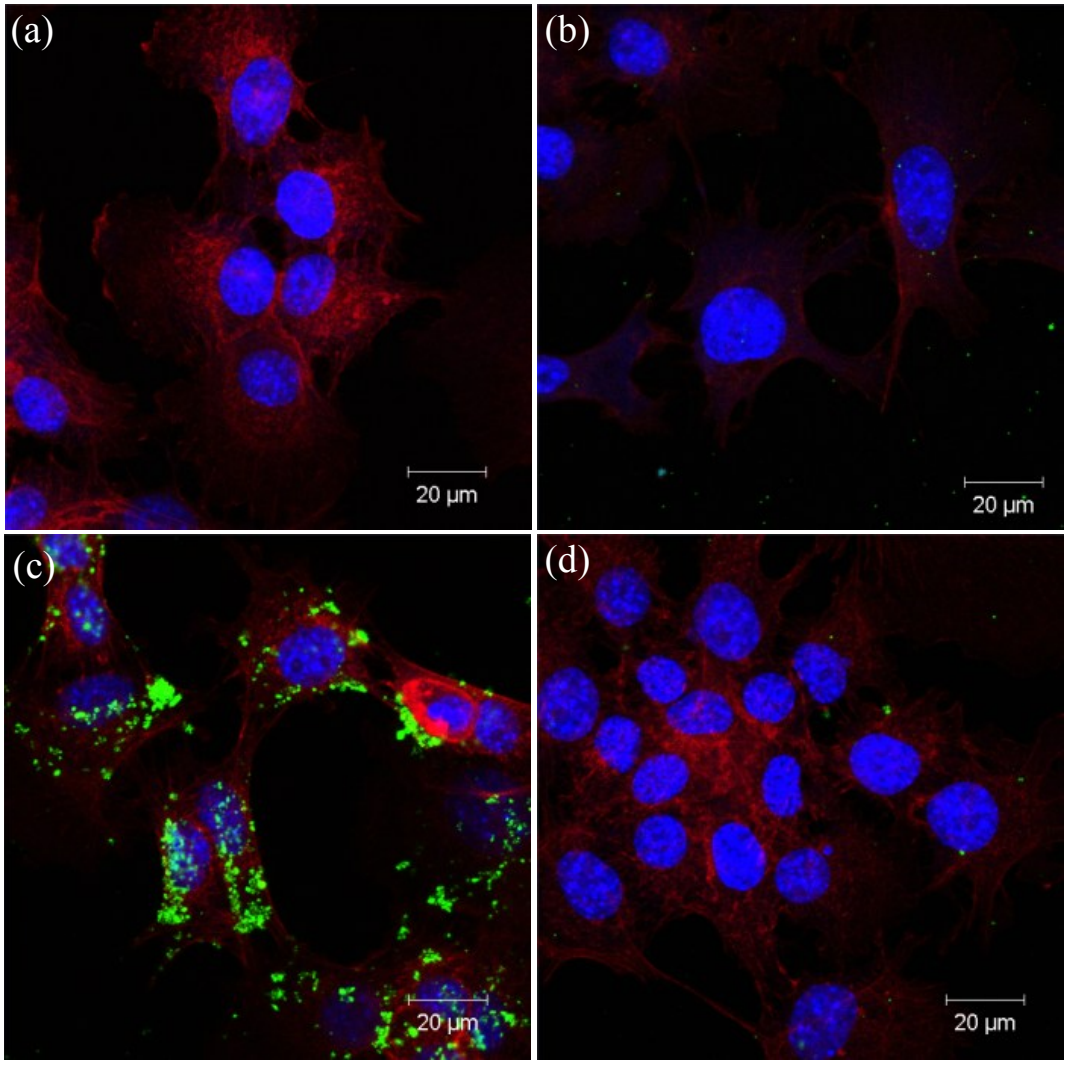

Figure 3.19 (a)-(d) Confocal micrographs of AML12 cells dosed with ligand-conjugated particles. (a) Cells were not dosed with particles. (b)-(d) AML12 cells were dosed with (b) control particles, (c) human lactoferrin-conjugated particles, (d) peptide-conjugated particles. Actin was stained with Phalloidin (Alexa Fluor 555, red), nuclei were stained with DAPI (blue), and particles were labeled green with DyLight 488 maleimide.

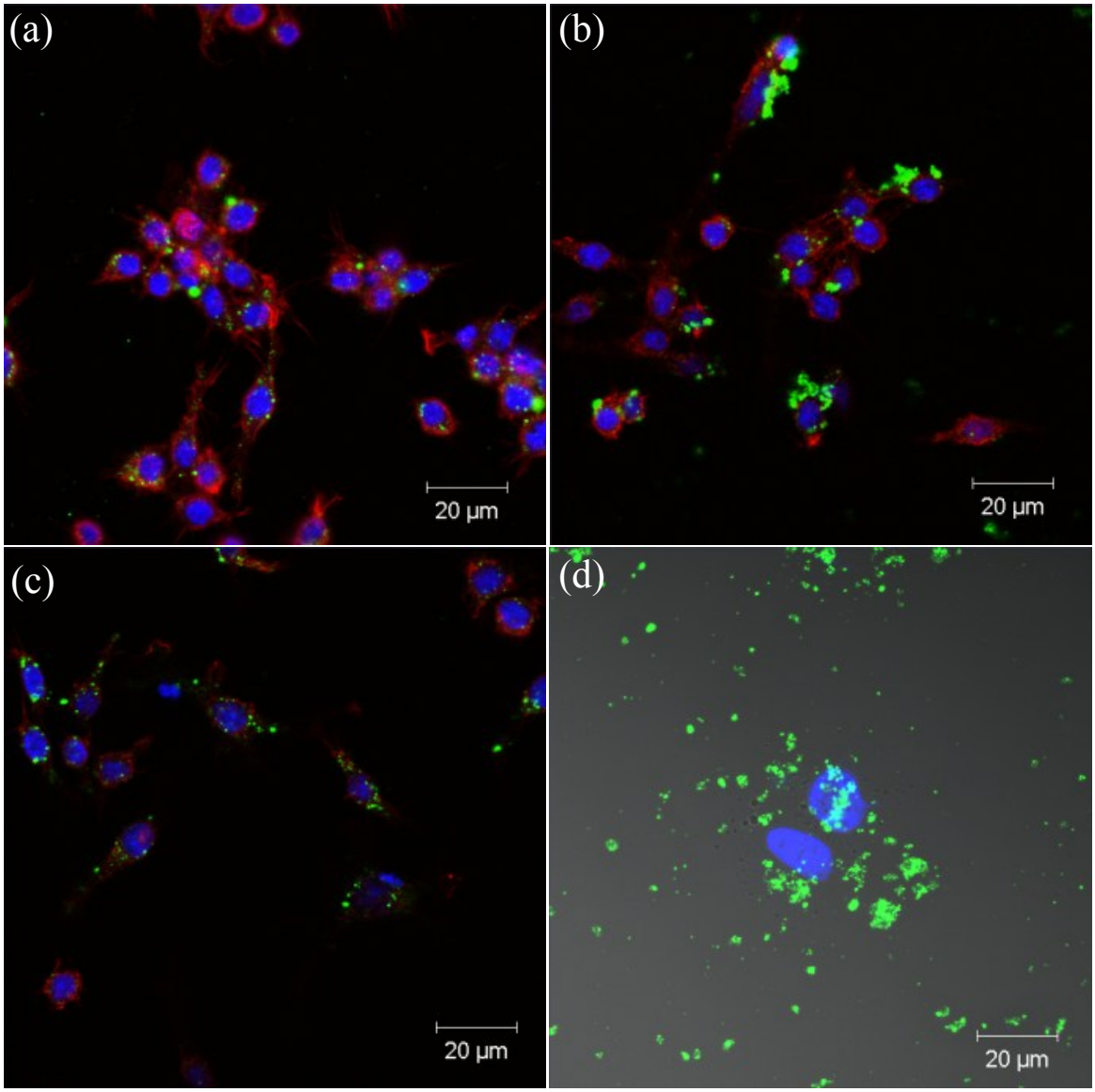

Figure 3.20 Confocal micrographs of (a)-(c) RAW cells and (d) HepG2 cells dosed with ligand-conjugated particles. (a)-(c) RAW cells were dosed with (a) control particles, (b) human lactoferrin-conjugated particles, and (c) peptide-conjugated particles. (d) HepG2 cells were dosed with lactoferrin-conjugated particles. Actin was stained with Phalloidin (Alexa Fluor 555, red), nuclei were stained with DAPI (blue), and particles were labeled green with DyLight 488 maleimide.

3.3.6 Screening peptide density on hydrogel nanoparticles for targeting hepatocytes *in vitro*

A cysteine-terminated T7 phage p17 peptide was tested as a ligand on nanoparticles to target hepatocytes. 200 nm cylindrical particles were functionalized with the peptide at

various ratios and a control ligand (ethanolamine). Particles functionalized with the peptide at the highest stoichiometric ratio enabled selective uptake.

200 x 200 nm cylindrical cationic hydrogel nanoparticles were prepared using the 30 wt% AEM-based composition. Particles were reacted with SCM-PEG_{5K}-maleimide followed by quenching non-PEGylated amines with succinic anhydride. The cysteine-terminated peptide was conjugated to particles through thiol-maleimide addition at 0.25, 0.5, and 1.0 wt equivalent. The BCA assay was utilized for quantifying the number of peptides conjugated to nanoparticles (Table 3.7). The amount of peptide conjugated to particles was detectable at the highest peptide:particle stoichiometric ratio. Zetasizer analysis of targeted particles demonstrated that their diameters were around 300 nm while ζ-potential values were around -10 mV (Table 3.7). Particles were dosed on hepatocytes for *in vitro* analysis of targeting capabilities of the peptide.

Table 3.7 Zetasizer analysis of peptide- and control ligand-conjugated particles.

Ligand, equiv	D_z (nm)	ζ-potential (mV)	Peptides/particle
$EtOHNH_2$, 1.0	307.7 ± 2.8	-15.0 ± 3.2	NA
Peptide, 0.25	304.4 ± 3.9	-8.9 ± 0.2	NA
Peptide, 0.5	306.3 ± 3.7	-8.0 ± 0.1	NA
Peptide, 1.0	325.6 ± 3.4	-8.1 ± 0.3	8.31×10^4

NA denotes that the signal was below the lower limit of detection.

AML12 cell uptake of functionalized particles occurred most notably for particles reacted with the phage peptide at the highest stoichiometric ratio (Figs. 3.21a,b) while remaining particle samples were not readily internalized. Lower peptide ratios during the conjugation reaction may not have enabled sufficient functionalization of particles to be recognized by hepatocyte receptors.

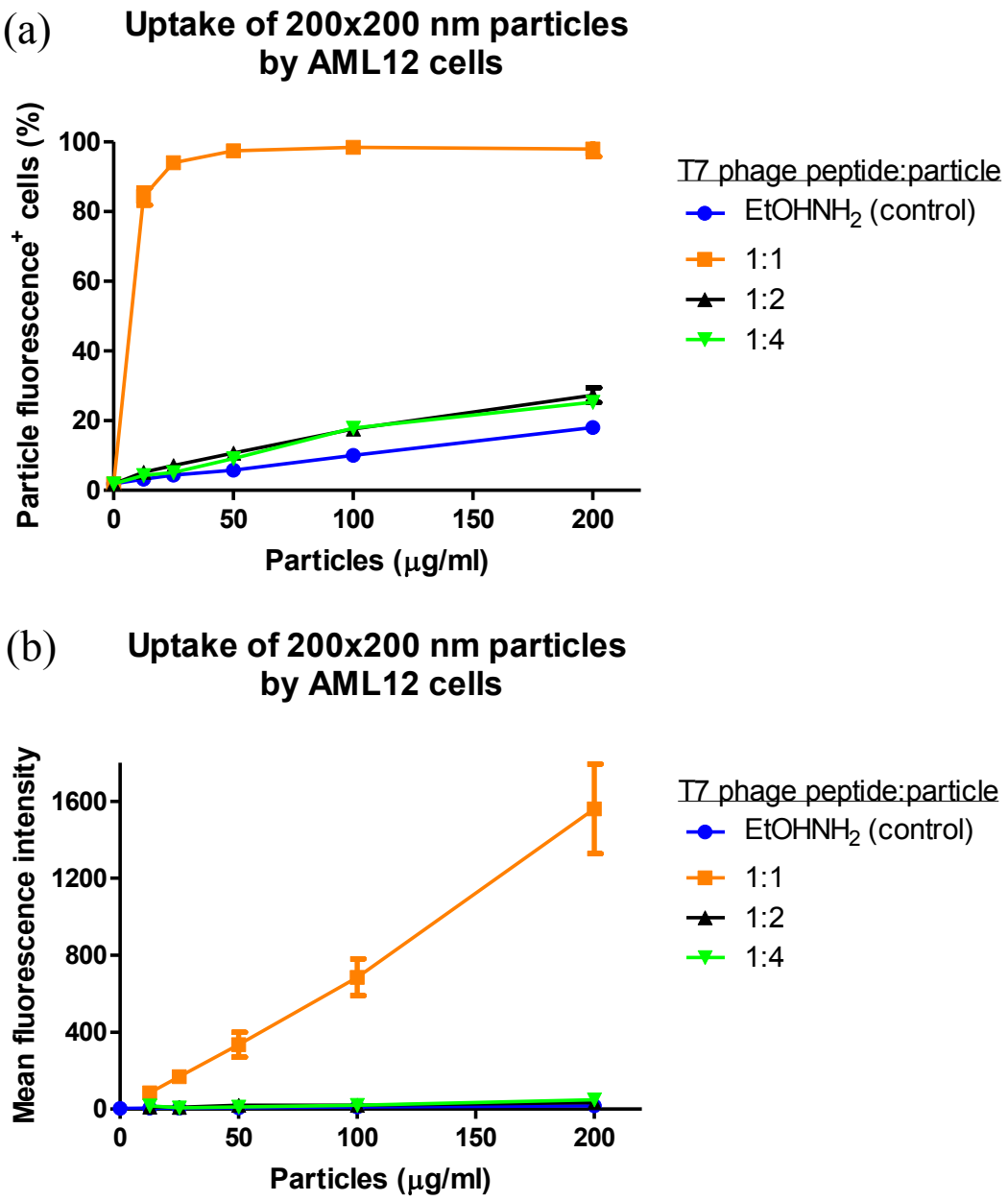

Figure 3.21 (a) AML12 cell uptake of peptide-functionalized cylindrical nanoparticles. (b) Mean fluorescence intensity of AML12 cells dosed with functionalized nanoparticles.

3.4 Targeted PRINT particles for *in vivo* delivery to hepatocytes

After establishing promising targeted delivery of lactoferrin- and p17 peptide-conjugated hydrogel nanoparticles to hepatocytes *in vitro*, the *in vivo* biodistribution and accumulation in hepatocytes was examined for functionalized hydrogels. Nanoparticle

hydrogels with different surface properties were investigated through conjugation of different ligands and quenching through covalent and electrostatic strategies.

3.4.1 Experimental

3.4.1.1 Materials

Materials used for preparing functionalized hydrogel nanoparticles were previously reported in sections 3.3.1.

3.4.1.2 Fabrication, functionalization, and analysis of particles as well as *in vitro* cell studies

Previously reported protocols in 3.2.1 and 3.3.1 were implemented for the fabrication, functionalization, and analysis of particles in addition to the *in vitro* cell uptake studies.

3.4.1.3 *In vivo* studies

Particles were administered to mice and RT-PCR was conducted as described in section 2.6.1.4.

3.4.2 Investigating the effect of covalent quenching on biodistribution of functionalized hydrogel nanoparticles

Four particle samples were prepared for administration to mice followed by liver histological analysis to determine whether particles accumulated in hepatocytes. Particles were either PEGylated or conjugated with human lactoferrin. Each particle type was divided into cationic and amine-quenched samples to determine if quenching would be necessary for targeting *in vivo*. Cationic 80x180 nm hydrogels were either reacted with SCM-mPEG$_{5K}$ or SCM-PEG$_{5K}$-maleimide. 3/5 of PEGylated particles were quenched with succinic anhydride and 2/5 were left unquenched. Maleimide-functionalized particles were then conjugated with hLTF. Quenched particles exhibited negative ζ-potentials while unquenched particles were

still positive (Table 3.8). Four particle samples were prepared for administration to mice followed by liver histological analysis to determine whether particles accumulated in hepatocytes. Particles were either PEGylated or conjugated with human lactoferrin. Each particle type was divided into cationic and amine-quenched samples to determine if quenching would be necessary for targeting *in vivo*.

Table 3.8 Zetasizer analysis of functionalized hydrogel nanoparticles.

Sample	ζ-potential (mV)	D_z (nm)
PEG, quenched	-30.9 ± 0.7	260.4 ± 2.7
PEG	+13.0 ± 1.5	235.2 ± 4.9
hLTF, quenched	-13.8 ± 0.6	226.8 ± 7.0
hLTF	+4.3 ± 0.3	226.9 ± 2.7

Significant accumulation of functionalized particles in hepatocytes was not observed. PEGylated and lactoferrin-conjugated particles that were quenched with succinic anhydride accumulated to some extent in the liver while unquenched particles were not observed notably in liver sections. Unquenched, PEGylated particles did not accumulate notably in liver tissue (Figure 3.22a,b) while quenched, PEGylated particles were observed in liver sections (Figure 3.22c,d). Unquenched, lactoferrin-conjugated particles did not accumulate notably in liver tissue (Figure 3.23a,b) while quenched, lactoferrin particles were observed in liver sections (Figure 3.23c,d). Both lactoferrin-conjugated and PEGylated, cationic particles that were not quenched were not observed notably in liver, most likely due to aggregation and clearance by the RES. Although quenched particles can be observed in liver tissue, they appear somewhat aggregated and do not seem well-dispersed and -distributed throughout hepatocytes as well as observed in previous studies with 80x320 nm, PAA-mPEG-coated nanoparticles (Figure 2.39). Therefore, PAA-based coatings may be promising for *in vivo* gene silencing. Furthermore, quenching the positive charge of functionalized particles with PAA avoids the use of small molecule anhydrides, which may damage siRNA cargo.

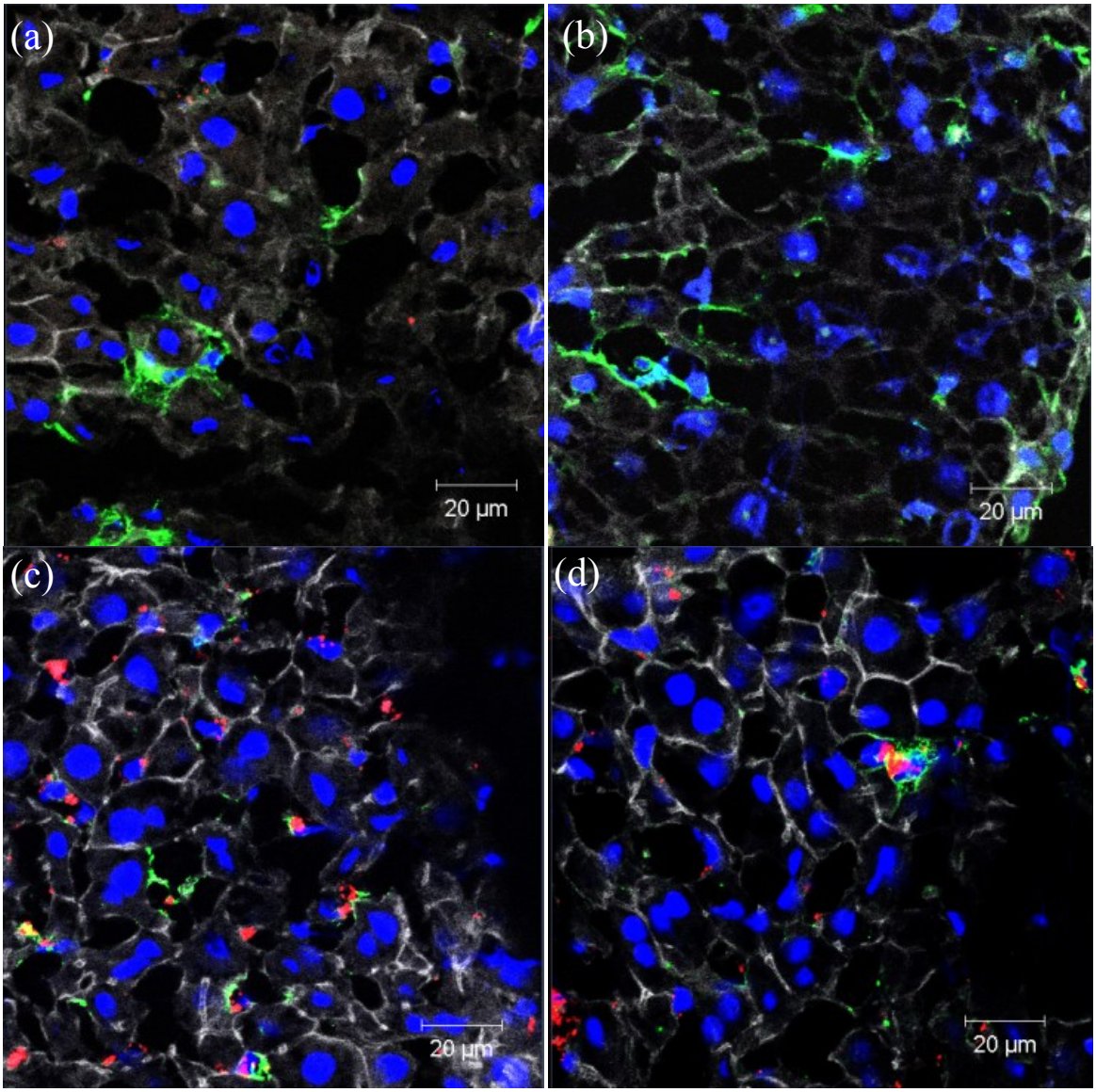

Figure 3.22 Images of liver sections from different mice dosed with 80x180 nm (a,b) unquenched, PEGylated particles, or (c,d) quenched, PEGylated particles. Nuclei were stained with DAPI (blue), actin was stained with phalloidin (Alexa Fluor 555, gray), macrophages were marked with MARCO (AlexaFluor 488, green), and particles were labeled with DyLight 680 (red).

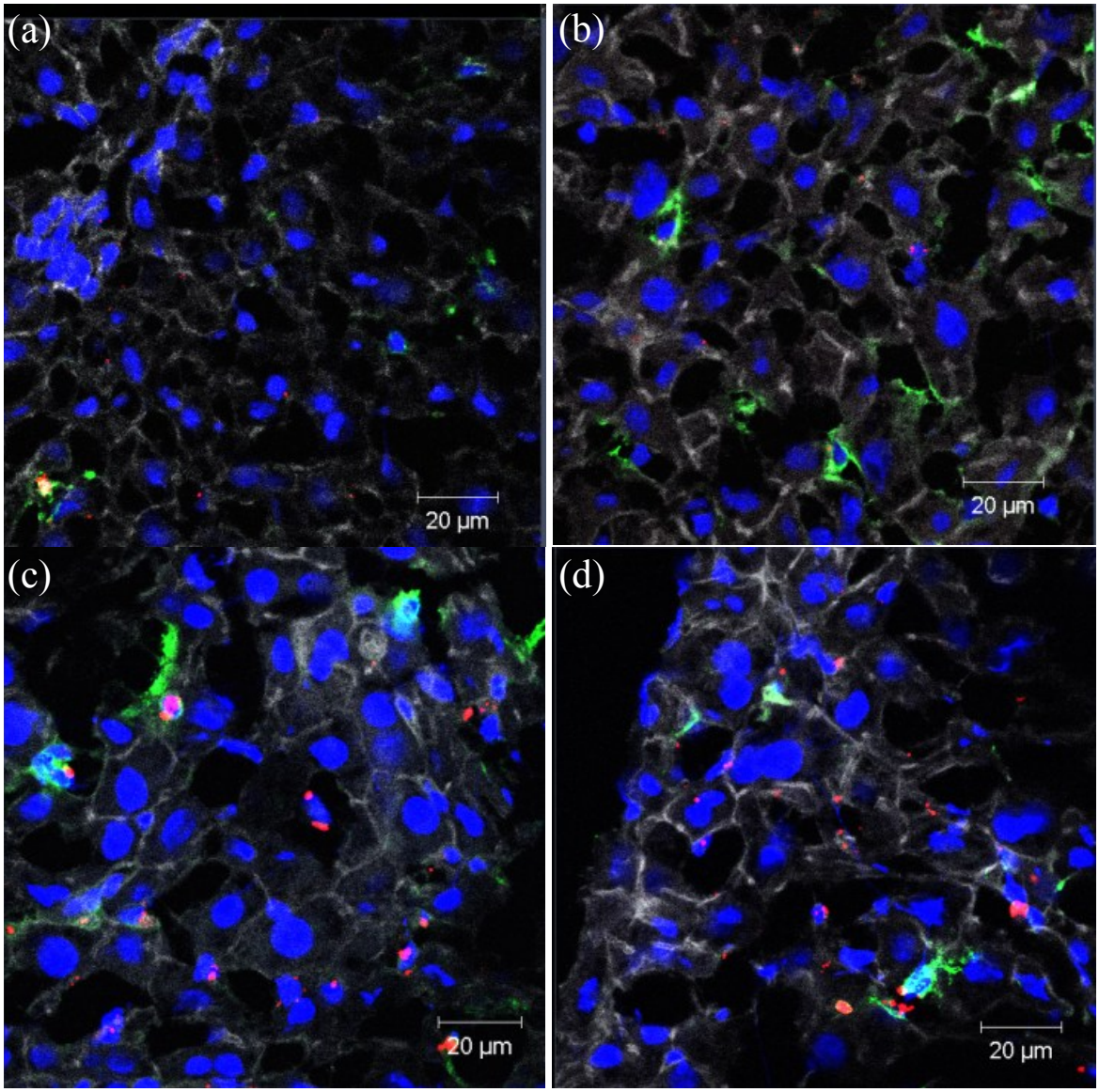

Figure 3.23 Images of liver sections from different mice dosed with (a,b) unquenched, lactoferrin-conjugated particles, or (c,d) quenched, lactoferrin-conjugated particles. Nuclei were stained with DAPI (blue), actin was stained with phalloidin (Alexa Fluor 555, gray), macrophages were marked with MARCO (AlexaFluor 488, green), and particles were labeled with DyLight 680 (red).

3.4.3 Electrostatic quenching of ligand-functionalized hydrogel nanoparticles for targeting hepatocytes

3.4.3.1 Evaluating noncovalent quenching of functionalized cationic hydrogels for targeting hepatocytes *in vitro*

Human lactoferrin- and T7 phage peptide-conjugated 200 nm hydrogel nanoparticles were tested for selective uptake by AML12 (mouse) hepatocytes relative to ethanolamine when quenching the positive charge with PAA. Previously prepared targeted particles were quenched with succinic anhydride; however, a covalent quenching approach may not be applicable for delivery of siRNA, but rather electrostatic quenching seemed appropriate to minimize damage to siRNA. Ethanolamine was not observed to behave as a negative control, i.e. ethanolamine-conjugated particles were internalized to the same degree as ligand-conjugated particles (Figure 3.24). Although PAA quenching did not yield selective uptake as seen with acylation of amines using succinic anhydride, sustained dispersion stability was noted with PAA-quenched particles.

Particles were PEGylated with SCM-PEG_{5K}-maleimide and half of the particles were incubated with PAA (30 wt eq) in PBS. Next, particles were reacted with either lactoferrin or ethanolamine ($EtOHNH_2$) in sodium borate buffer while PBS was used to conjugate T7 phage p17 peptide overnight. To the half of particles that were not previously mixed with PAA, they were subsequently mixed with PAA (30 wt eq) and washed a couple times with PBS. Zetasizer analysis of functionalized particles indicated that they all displayed a negative charge and had diameters around 300-400 nm (Table 3.9). Contrary to non-PAA coated particles previously explored, dispersion stability was noted by the absence of large

aggregate formation. After 24 h, particles quenched with PAA exhibited roughly the same diameters.

Flow cytometry analysis of AML12 cells dosed with functionalized hydrogels showed that targeting selectivity was not observed. In particular, the negative control particles (ethanolamine-conjugated) were internalized to the same degree as protein- and peptide-conjugated hydrogels (Figure 3.24). Electrostatic absorption of PAA to hydrogels does not have the same quenching effect as a covalent approach (e.g. with succinic anhydride) to provide targeting selectivity *in vitro*. However, the ζ-potential of particles was rendered negative by quenching with PAA. Ideally particles will accumulate notably in liver hepatocytes although *in vitro* selective uptake was not observed.

Table 3.9 Zetasizer analysis of functionalized 200 nm hydrogels.

Particle (ligand, PAA*)	ζ-potential (mV)	D_z (nm)	D_z (nm), 24 h
$EtOHNH_2$, A	-18.6 ± 0.7	347.1 ± 5.1	337.5 ± 1.3
Lactoferrin, A	-18.2 ± 0.6	326.1 ± 4.6	321.9 ± 9.9
Peptide, A	-14.2 ± 0.2	405.0 ± 8.0	407.2 ± 7.6
$EtOHNH_2$, B	-14.1 ± 0.8	412.6 ± 11.5	
Lactoferrin, B	-15.2 ± 0.7	373.4 ± 9.3	
Peptide, B	-14.2 ± 0.8	297.6 ± 6.5	

*A: PAA before protein conjugation; B: PAA coat after protein conjugation

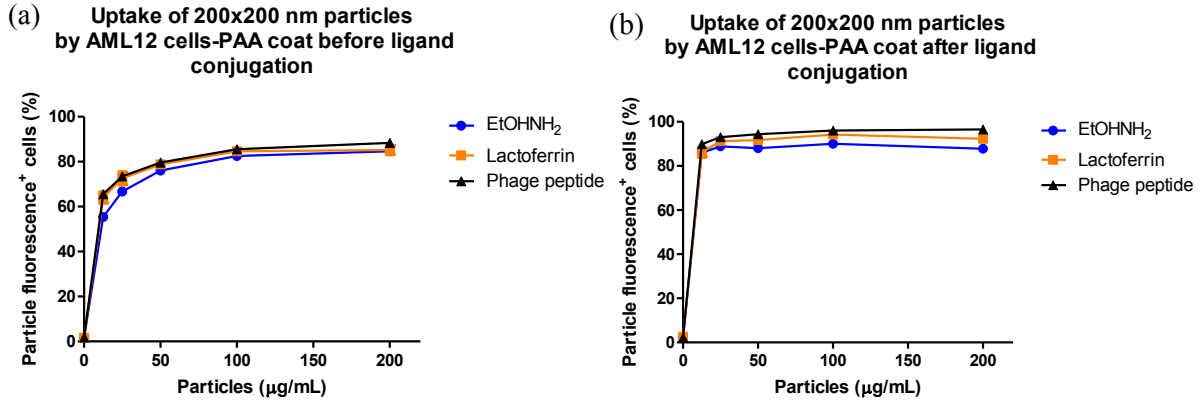

Figure 3.24 AML12 cell uptake of functionalized hydrogels coated with PAA (a) before and (b) after ligand conjugation.

3.4.3.2 Administration of hydrogel nanoparticles with different surface properties to mice to observe bioaccumulation in organs

80x320 nm hydrogels were prepared using the 30 wt% AEM-based composition with three different surface characteristics for intravenous injection in mice. The three particle samples were: (1) cationic, (2) PAA-mPEG-coated, and (3) lactoferrin-conjugated. Tissue analysis showed that all particles notably accumulated in livers while cationic particles also largely distributed to the lung. PAA-mPEG and lactoferrin-conjugated particles distributed well throughout liver tissue while cationic particles appeared more aggregated, possibly due to accumulation in Kupffer cells.

80x320 nm particles were prepared with the 30% AEM-based composition as previously tested. Particles were harvested off PET with a solution of water or PAA-mPEG-containing PBS at roughly 30 wt eq. Particles harvested in water were PEGylated with SCM-PEG_{5K}-maleimide. Next, particles were reacted with lactoferrin in sodium borate buffer. Lactoferrin-conjugated particles were then mixed with PAA (30 wt eq) and washed a couple times with PBS. All particles were ultimately re-suspended in PVA-containing PBS.

Zetasizer analysis demonstrated that all particles exhibited negative ζ-potentials with diameters around 200-250 nm. BCA analysis of lactoferrin-conjugated particles indicated there were 2.2×10^3 proteins per nanoparticle.

Table 3.10 Zetasizer and BCA analysis of nanoparticles injected into mice.

Particle	ζ-potential (mV)	D_z (nm)	Ligand density
PAA-mPEG	-9.1 ± 0.4	197.5 ± 5.1	
Lactoferrin	-13.4 ± 0.9	218.7 ± 3.4	2.2×10^3
Cationic	+14.7 ± 0.4	248.1 ± 3.7	

Compared to background fluorescence of untreated mice, livers of mice injected with all types of nanoparticles showed notable fluorescence intensity (Figure 3.25a). Also, lungs

of mice injected with cationic nanoparticles demonstrated high fluorescence intensity compared to untreated mice and those injected with PAA-coated particles. Significant differences in fluorescent intensity among untreated mice and those injected with nanoparticles were not observed in kidneys, spleen, heart, and intestine/stomach. Quantitation of fluorescence intensity (Figure 3.25b) confirms qualitative differences observed in organ imaging.

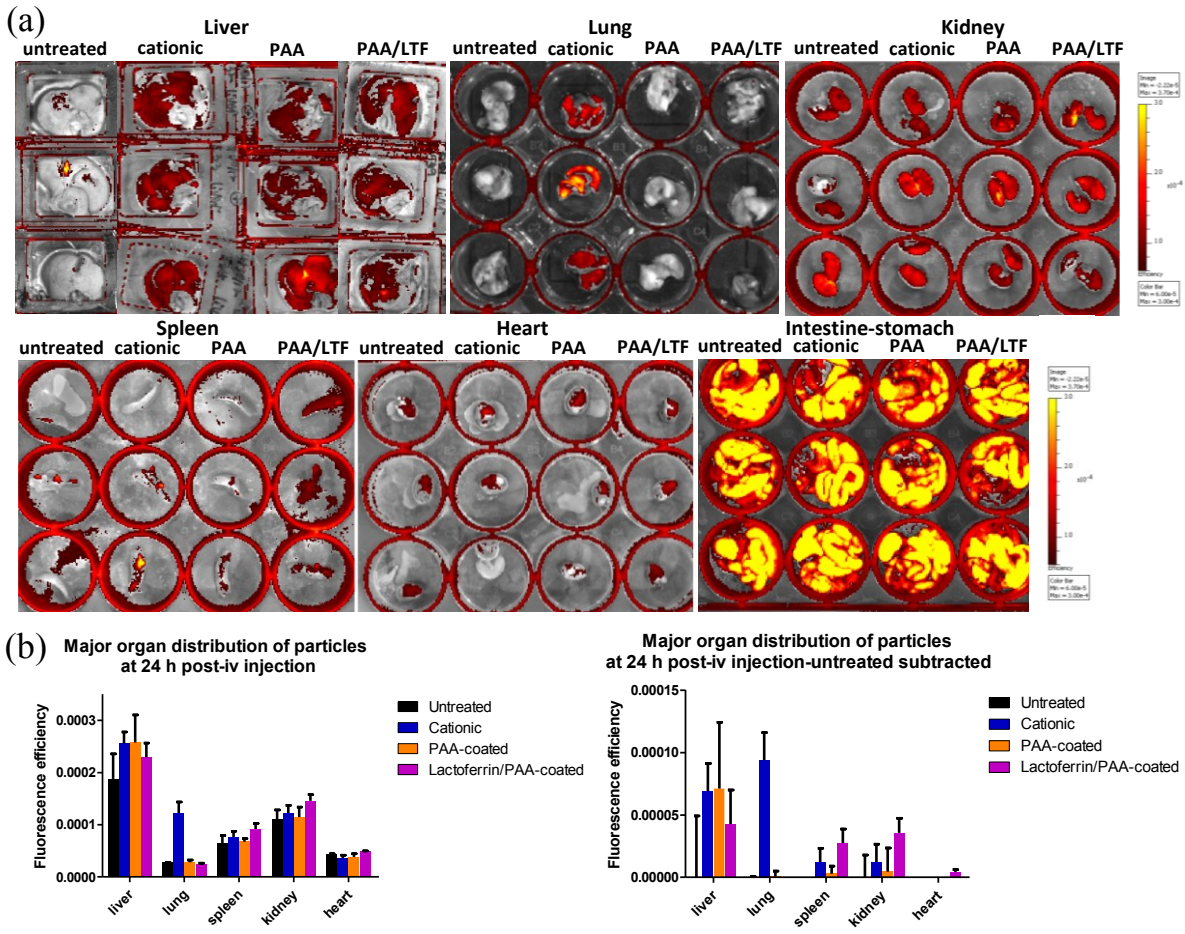

Figure 3.25 (a) Organ imaging of untreated mice and those injected with nanoparticles for biodistribution analysis. (b) Fluorescence intensity of untreated mice and those injected with nanoparticles.

Histological analysis of livers from mice injected with fluorescently-tagged cationic, PAA-mPEG-coated, and lactoferrin-conjugated, PAA-quenched particles illustrates

distribution of particles in liver tissue (Figure 3.26). 0.5 mg of particles was injected intravenously and livers were harvested 24 h post-injection and frozen. 5 µm sections were stained and imaged with confocal microscopy. Cationic particles appear aggregated to some degree in confocal images, most likely due to their charge and localization in Kupffer cells. The negative charge on functionalized and PAA-coated particles ideally enhanced their dispersion and minimized uptake by macrophages. PAA-mPEG-coated and lactoferrin-conjugated, PAA-coated particles appear to be well-distributed throughout liver tissue. Distribution of particles throughout liver tissue ideally will enable transfection with siRNA-conjugated, functionalized hydrogels.

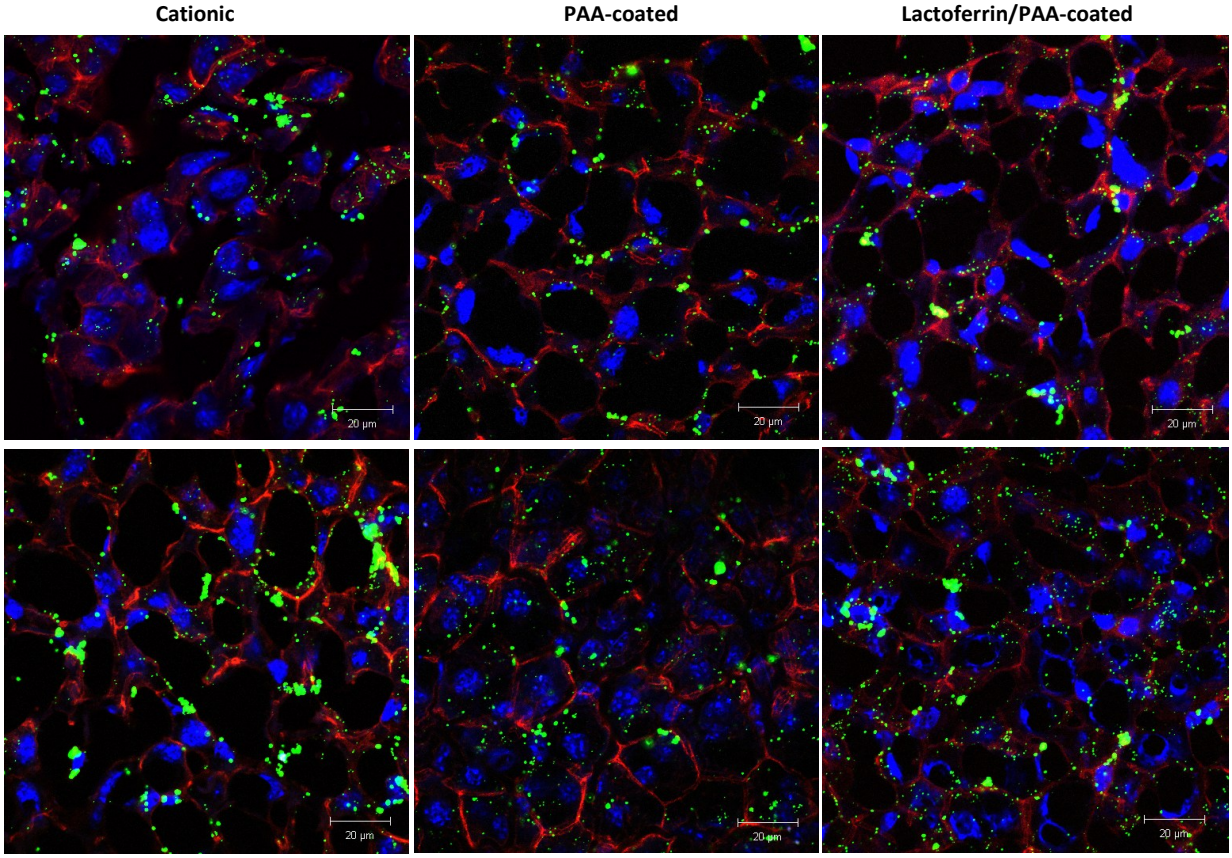

Figure 3.26 Liver histology from mice injected with cationic, PAA-mPEG-coated, and lactoferrin-conjugated, PAA-coated nanoparticles (two images per particle sample). Particles were labeled with DyLight 488 maleimide (green), cell nuclei were stained blue with DAPI, and actin was stained red with Phalloidin (AlexaFluor 555).

3.4.3.3 siRNA-conjugated hydrogel nanoparticles for *in vivo* gene silencing

80x320 nm cationic hydrogel particles were prepared with the 30 wt% AEM-based composition, charged with either FVII or ELAV siRNA, and harvested off PET with a solution of water or PAA-mPEG-containing PBS at roughly 30 wt eq. Half of the particles harvested in water were PEGylated with SCM-PEG_{5K}-maleimide. Next, particles were reacted with lactoferrin in sodium borate buffer. Lactoferrin-conjugated particles were then mixed with PAA (30 wt eq) and washed a couple times with PBS. All particles were ultimately re-suspended in PVA-containing PBS. Zetasizer analysis (Table 3.11) confirmed that cationic particles had a positive ζ-potential while PAA-mPEG-coated and lactoferrin-conjugated, PAA-quenched particles had negative ζ-potentials. BCA assay allowed for quantitation of lactoferrin conjugated to particles. Diameters of particles ranged from ca. 300 to 360 nm. Gel electrophoresis of siRNA released from particles (Figure 3.27) showed that particles had encapsulation efficiencies around 28-33%.

Table 3.11 Zetasizer and BCA analysis of pro-siRNA nanoparticles for *in vivo* gene silencing.

Particle, siRNA, sample label	ζ-potential (mV)	D_z (nm)	Ligand density (protein/particle)
PAA-mPEG, ELAV, A	-15.4 ± 0.5	303.3 ± 6.6	NA
Lactoferrin, ELAV, B	-24.2 ± 0.8	372.2 ± 4.3	4.8×10^3
Cationic, ELAV, C	+18.3 ± 3.2	292.8 ± 6.9	NA
PAA-mPEG, FVII, D	-11.3 ± 0.2	327.2 ± 11.3	NA
Lactoferrin, FVII, E	-19.4 ± 0.5	357.5 ± 3.1	6.7×10^3
Cationic, FVII, F	+23.7 ± 0.7	306.9 ± 4.7	NA

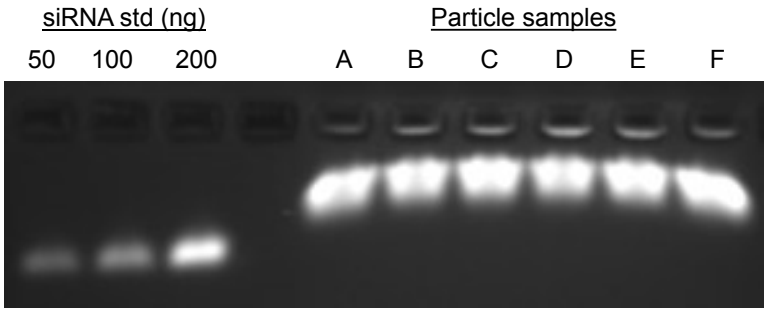

Figure 3.27 Gel electrophoresis analysis of siRNA-containing nanoparticles. Particles were incubated in 5 mM glutathione-containing 10x PBS (0.05% PVA) at 2 mg/mL for 4 h followed by isolation of supernatants for loading into the gel. Encapsulation efficiency was calculated to be 28-33% for the samples listed. Corresponding sample labels are provided in the Zetasizer table.

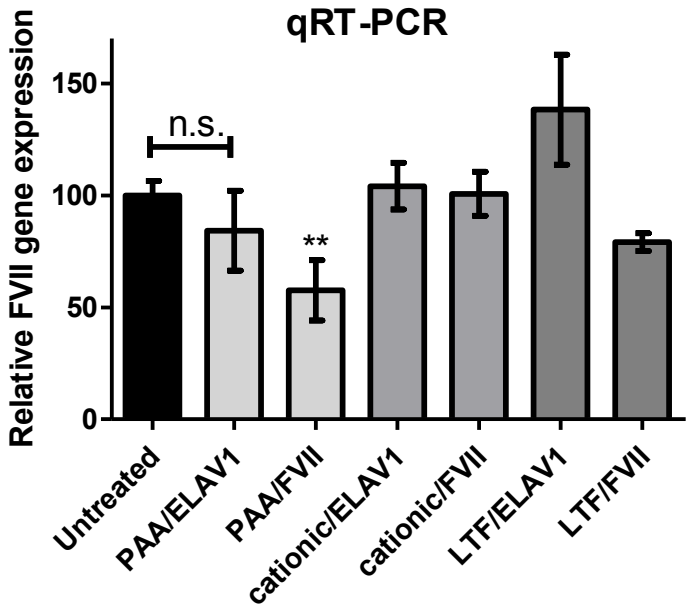

Figure 3.28 Relative FVII gene expression of mice without treatment or after administration of different hydrogel nanoparticles. n.s. not significant; $^{**}P < 0.01$; *t*-test, double-tailed, $n = 3$.

0.5 mg of particles was dosed per mouse which corresponds to ca. 0.4 mg/kg siRNA doses. FVII siRNA-conjugated hydrogel nanoparticles coated with PAA-mPEG elicited a statistically significant decrease in target FVII levels (Figure 3.28, greater than 40% knockdown). Conversely, ELAV1 siRNA-conjugated particles coated with PAA-mPEG did not significantly alter expression of FVII. Cationic particles loaded with ELAV1 or FVII siRNA did not influence expression of FVII, most likely due to inefficient accumulation in

hepatocytes. LTF-functionalized, PAA-quenched particles did not cause significant knockdown of FVII gene expression.

3.4.3.4 Targeting hepatocytes with ligand-functionalized hydrogel nanoparticles prepared with different reaction conditions

Since a notable gene silencing effect was not observed with pro-siRNA, LTF-functionalized nanoparticles *in vivo*, conjugation conditions were evaluated to maximize amine content while enabling selective cell uptake. 200 nm cationic hydrogels (30% AEM-based composition) were harvested mechanically in water, followed by functionalization with SCM-PEG_{5K}-maleimide (1 wt eq) using pyridine base in DMF overnight.

Table 3.12 Zetasizer and BCA analysis of functionalized nanoparticles.

Ligand, conditions	ζ-potential (mV)	D_z (nm)	Proteins/particle
LTF, PBS, 24 h	-11.0 ± 1.0	371.3 ± 1.9	6.8×10^3
$EtOHNH_2$, PBS, 24 h	-11.8 ± 0.6	370.2 ± 6.7	NA
LTF, pH 8.5, 1 h	-11.4 ± 0.6	385.7 ± 4.7	5.1×10^3
$EtOHNH_2$, pH 8.5, 1 h	-10.8 ± 0.7	397.6 ± 5.8	NA
LTF, pH 8.5, 4 h	-12.5 ± 0.6	324.4 ± 4.8	7.1×10^3
$EtOHNH_2$, pH 8.5, 4 h	-10.7 ± 0.2	326.5 ± 3.1	NA
LTF, pH 9.5, 1 h	-12.8 ± 1.4	334.2 ± 9.1	6.3×10^3
$EtOHNH_2$, pH 9.5, 1 h	-11.9 ± 0.8	318.8 ± 6.5	NA
LTF, pH 9.5, 4 h	-11.9 ± 0.5	316.6 ± 8.7	9.7×10^3
$EtOHNH_2$, pH 9.5, 4 h	-12.3 ± 1.2	320.2 ± 4.4	NA

NA implies that signal was not detectable in BCA analysis

Fewer equivalents of PEG were used to minimize the amount of amines reacted. Non-PEGylated amines were quenched with succinic anhydride. Lactoferrin (LTF) or ethanolamine (control, $EtOHNH_2$) were conjugated to PEGylated particles under different reaction conditions: (1) PBS for 24 h, (2) pH 8.5 buffer for 1 and 4 h, and (3) pH 9.5 buffer for 1 and 4 h. Increasingly basic conditions may result in rearrangement of AEM from amine into alcohol through intramolecular cyclization for unquenched particles; therefore, shorter reaction times and more neutral buffers were tested. Particles were washed and BCA analysis

was conducted on particle samples to determine the amount of protein conjugated to nanoparticles.

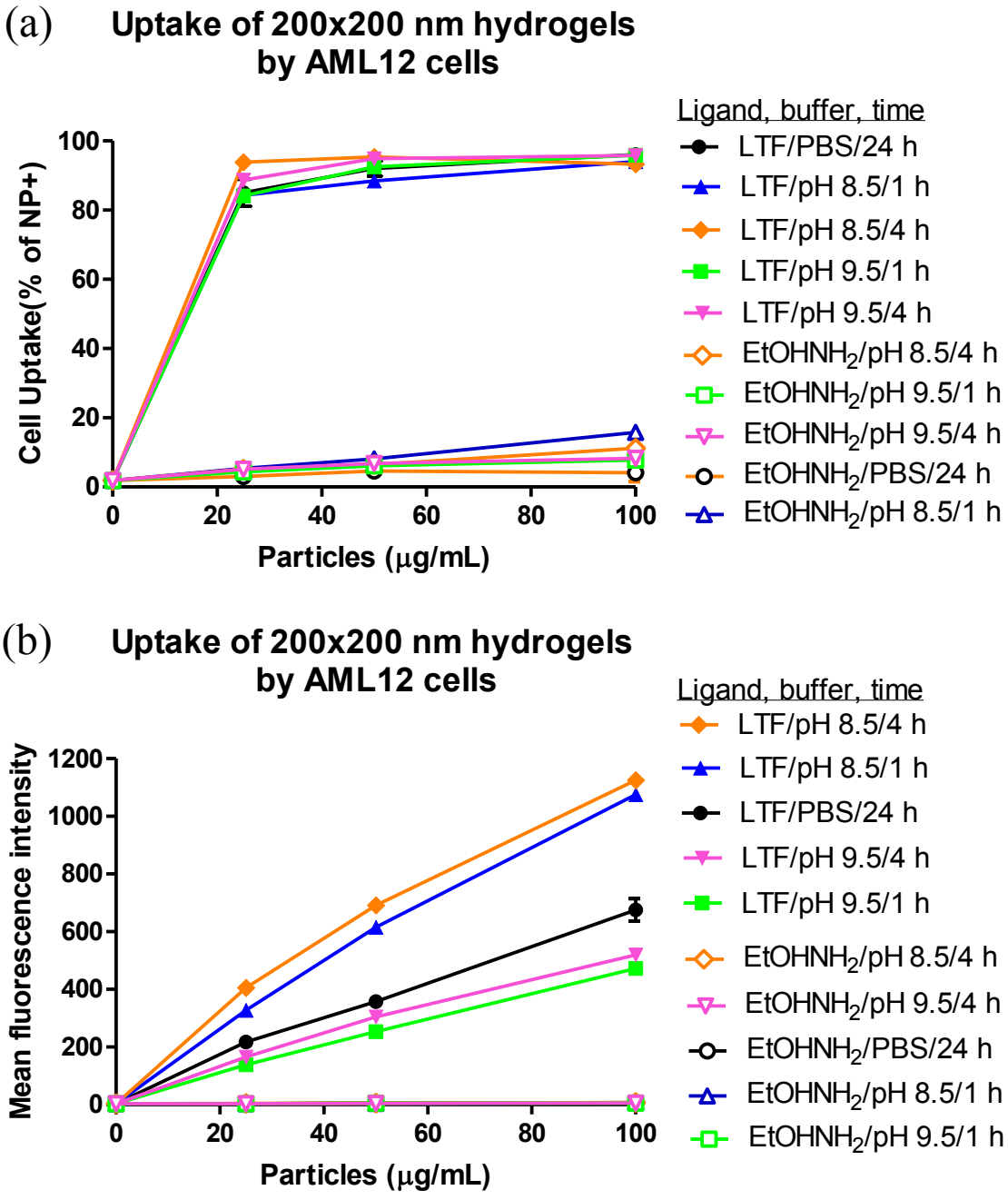

Figure 3.29 Uptake of functionalized hydrogel nanoparticles by AML12 cells shown as (a) percentage of cells with particles and (b) MFI of cells.

Selective uptake of LTF-functionalized particles by AML12 cells was observed relative to control particles for all conjugation conditions (Figure 3.29). MFI of AML12 cells shows that conjugating protein to particles in pH 8.5 buffer yielded the highest uptake, followed by pH 7.4 and then pH 9.5. Unquenched, targeted particles were prepared for conjugation of ligands in PBS for 24 h and pH 8.5 for 1 h to evaluate ζ-potential relative to bare, cationic particles. The ζ-potential of targeted particles conjugated with ligands in PBS was +14.8 ± 1.2 mV and +15.7 ± 0.5 mV for particles conjugated with ligand in pH 8.5 buffer. Unquenched, targeted particles prepared under the aforementioned conditions exhibited ζ-potentials similar to bare, cationic particles (+16.7 ± 0.5 mV). Application of these targeted particles toward *in vivo* studies at higher doses may enable complete gene silencing similar to PAA-mPEG-coated nanoparticles.

3.5 Recovery of siRNA throughout particle fabrication and pursuing scalability

To account for all of the siRNA implemented in preparing particles, excess material remaining on the delivery sheets, draw down table, and Mayer Rod was collected in addition to the sol fraction from particles for quantification. Recovered siRNA was then charged into the pre-particle solutions to prepare pro-siRNA hydrogel nanoparticles, exhibiting encapsulation efficiency similar to charging siRNA prodrug directly after synthesis.

In addition to recovering precious siRNA implemented in particle fabrication, a more scalable protocol for fabrication of particles was pursued. Specifically, a procedure that would enable rapid particle curing (in less than a minute) and avoid mechanical harvesting was desired. A UV-LED curing system was developed for quick particle curing and a sacrificial harvesting layer was used to extract particles from the mold for “bead harvesting”. A bead harvester with controlled air flow was used to create a stable water bead at the nip

that may dissolve away the harvesting layer, liberating particles into solution as the particle array-covered film passes through the nip.

3.5.1 Experimental

3.5.1.1 Materials

Materials were obtained as previously reported in previous sections. 2,4,6-trimethylbenzoyl-diphenyl-phosphineoxide (TPO) was obtained from Sigma. An LED curing system was implemented for select studies, implementing TPO as the photoinitiator. Plasdone (64 kDa) was purchased from BASF. Bead harvesters were graciously provided by Liquidia Technologies. The UV-LED setup was prepared at UNC by Sarah Mueller using StarFire MAX (150 x 20 mm, 4 W/cm^2, λ = 380-420 nm) from Phoseon Technology.

3.5.1.2 Particle fabrication and siRNA recovery methods

The 30% AEM-based composition with 5 wt% siRNA was pursued for preparation of pro-siRNA hydrogel nanoparticles as conducted through previously reported procedures. The following measures were taken for recovering siRNA implemented in pro-siRNA hydrogel fabrication: (1) after laminating the delivery sheet against the mold, remaining material was collected from the delivery sheet with a cell scraper using DEPC-treated water, (2) excess pre-particle solution drawn past PET sheet, after casting a film, was collected from the draw down table with water and a cell scraper, and (3) the Mayer rod was placed vertically on the draw down table and a few milliliters of water were dispensed on the top, letting it drip down for collection. When pro-siRNA hydrogels were washed with 10x PBS, the sol fraction was stored. All samples were concentrated through lyophilization and dialyzed (MWCO 2kDa) to remove monomers.

3.5.1.3 Fabrication of particles through scalable protocols

Compositions in Table 3.13 were used to prepare 2.5 wt% pre-particle solutions of monomers in DEPC-treated water (Hg cure) or methanol (for the LED cure). The film split technique was used to fill PRINT molds. Instead of laminating corona-treated PET to filled molds, UV curing chambers were purged with N_2, followed by quickly inserting filled molds, briefly re-purging with N_2, and curing for given times. Cured particles were then laminated against Plasdone harvesting layer at 240 ºF to adhere the sacrificial polymer to particles. After returning to room temperature, the Plasdone layer was removed, revealing an array of particles, which were then bead-harvested with water. Particles were subsequently washed with 10x PBS to remove the sol fraction.

3.5.1.4 Particle characterization and cell studies

Characterization of particles and cell studies were conducted as previously reported in in section 3.4.1.2.

3.5.2 Recovery of siRNA in the PRINT process

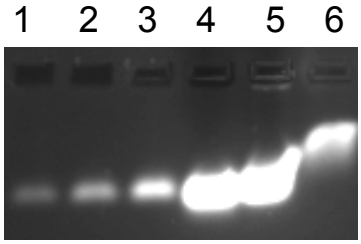

Figure 3.30 Gel electrophoresis of siRNA recovered from delivery sheet and washed from particles. (1-3) siRNA standard of 50, 100, and 200 ng; (4-5) delivery sheet contents after filling the mold; (6) sol fraction of siRNA macromer recovered in 10x PBS.

In an attempt to recover siRNA throughout particle fabrication, delivery sheets were harvested after filling the mold and non-conjugated siRNA was washed from hydrogels. 300 μL of pro-siRNA pre-particle solution containing 0.38 mg siRNA was used to prepare two delivery sheets for filling two feet of 200 nm cylindrical molds (1.7 mg particles). Collection

of delivery sheet contents with water was performed after filling molds using a cell scraper. Collected delivery sheet contents were subjected to dialysis (2 kDa MWCO membrane) to remove monomers and crosslinker. Gel analysis (Figure 3.30) shows the integrity of siRNA recovered from delivery sheets (lanes 4 and 5). UV-Vis analysis of siRNA prodrug recovered from the delivery sheet totaled 0.21 mg of siRNA (56% of the starting siRNA in the pre-particle solution). Since pro-siRNA hydrogels are subjected to washing after fabrication to remove non-conjugated siRNA, the 10x PBS washes were retained and concentrated for analysis. Lane 6 (Figure 3.27) shows siRNA washed from hydrogels (26 μg total by UV-Vis, 7% of original pre-particle solution). When combined with siRNA prodrug released from hydrogels (31 μg), the siRNA recovered totaled 15% of the starting siRNA in the pre-particle solution. Approximately 71% of the siRNA originally charged was collected.

When casting films, excess solution may be drawn past the edge of the PET sheet and could be collected for analysis. The remaining 25% may remain residually on the Mayer Rod and require addition of other solvents like EtOH to remove components efficiently while gently scraping the Mayer Rod.

Recovered siRNA was then charged into the pre-particle solution for preparing cationic pro-siRNA hydrogels (30% AEM composition). Hydrogels were thoroughly washed and then incubated in glutathione-containing 10x PBS for release of prodrug (Figure 3.31). Conversion of pro-siRNA (ca. 30%) was similar to that for pro-siRNA hydrogels prepared with prodrug directly after synthesis.

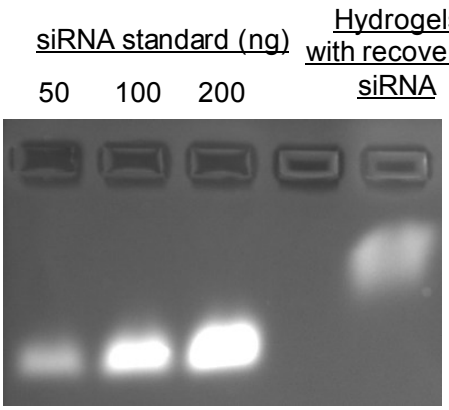

Figure 3.31 siRNA released from hydrogels charged with recovered siRNA that were incubated in GSH-containing 10x PBS for examining cargo release.

3.5.3 Scaling up pro-siRNA hydrogels of various dimensions for gene knockdown

3.5.3.1 Exploring fabrication conditions for open face curing particles

In pursuit of scalable methods to fabricate pro-siRNA hydrogels, 200 nm particles were prepared by curing molds open-face on the mercury bulb UV lamp as well as on the LED curing system. By gel electrophoresis, conversion of siRNA macromer was lower (Figure 3.32) than when curing molds closed face against PET.

Table 3.13 Compositions of pre-particle solution for fabrication of pro-siRNA hydrogels.

Component	wt% (Hg cure)	wt % (LED cure)
PEG_{700} diacrylate	5	5
HP_4A	49	59
AEM	30	30
Poly(vinyl alcohol) 2 kDa	10	0
Irgacure 2959	1	0
TPO	0	1
siRNA prodrug	5	5

The conventional composition (Table 3.13, Hg cure) was implemented in curing filled molds on the Hg bulb lamps; however, the same water-based composition was not implemented for curing molds on the LED system. The photoinitiator for the LED composition (2,4,6-Trimethylbenzoyl-diphenyl-phosphineoxide) is water-insoluble; therefore, modifications were made to the composition, including solvent (MeOH), removal

of PVA, and change of photoinitiator (Table 3.13). Cured particles were thermally transferred to PVA-coated PET, bead-harvested with DEPC-treated water, and thoroughly washed with buffer to remove the sol fraction. From Figure 3.32, conversion of siRNA appears to be roughly 5% when molds were cured on the LED for 12 sec while conversion was not attained when curing for 3 sec. Curing molds with the Hg bulb lamp enabled 18% conversion of prodrug monomer. Closed face curing molds against PET yields 35% conversion of siRNA macromer (e.g. when charging 5 wt% siRNA, 1.75 wt% siRNA is conjugated to the matrix). Longer curing times may be required for increased conversion of siRNA pro-drug macromer.

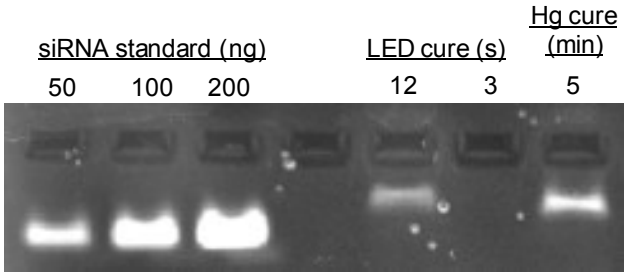

Figure 3.32 Release of siRNA from hydrogels cured under different conditions, which were incubated at 0.5 mg/mL in 10x PBS containing glutathione for 4 h at 37 °C.

3.5.3.2 Varying siRNA loading in hydrogel nanoparticles and assessing gene knockdown

siRNA pro-drug content was varied in hydrogel nanoparticles fabricated *via* a scalable protocol to optimize gene silencing efficiency. Gene silencing efficiency increased with siRNA loading. Effective gene knockdown was observed for 200 nm and 80x320 nm hydrogels charged with 5 wt% siRNA.

200x200 nm cylindrical nanoparticles were prepared from the pre-particle solution compositions listed in Table 3.14 by open-face curing molds for 30 s using the LED curing chamber, transferred to Plasdone at 240 ºF, and bead-harvested with water. Particles were then repeatedly washed in 10x PBS containing 0.05% PVA and re-suspended in 1x PBS

containing 0.05% Plasdone (for particles containing 0.1-5.0 wt% siRNA). Particles charged with 5 wt% siRNA were washed and re-suspended in DEPC-treated water to promote uptake and endosomal escape. Particles were dosed on HeLa cells for *in vitro* studies. Zetasizer analysis demonstrated that particles had similar charges and diameters (Table 3.15). Gel analysis illustrated high encapsulation efficiency of siRNA prodrugs (Figure 3.33).

Table 3.14 Compositions of LED-cured pro-siRNA hydrogels.

Component	Function	wt %
PEG_{700} diacrylate	crosslinker	10
Tetraethyleneglycol monoacrylate	hydrophile	56.9-52.0
2-aminoethyl methacrylate HCl	cationic handle	30
TPO	photoinitiator	2
DyLight 488 maleimide	fluorescent dye	1
siRNA PD	cargo	0.1-5.0

Table 3.15 Zetasizer analysis of LED-cured pro-siRNA hydrogels.

siRNA wt%	ζ-potential / mV	D_z / nm
0.1	+24.9 ± 0.9	312.5 ± 7.0
0.5	+26.2 ± 0.5	317.5 ± 3.0
1.0	+25.3 ± 3.2	307.5 ± 12.3
2.5	+25.6 ± 2.9	305.2 ± 9.6
5.0	+20.3 ± 1.4	307.5 ± 1.9

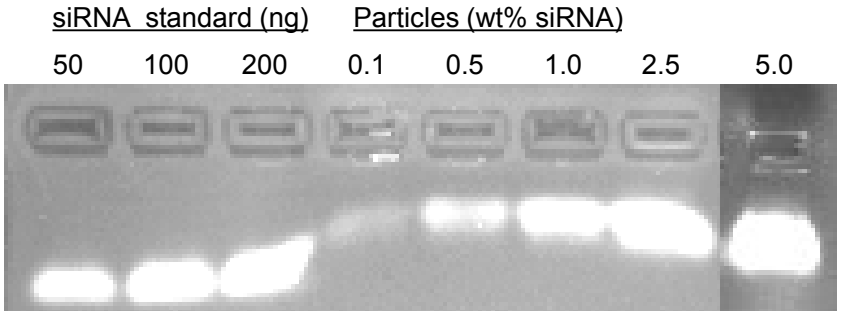

Figure 3.33 Gel analysis of particles incubated in 10x PBS (5 mM) at 37 °C for 4 h illustrates that that encapsulation efficiency appeared to be high for all samples (ca. 75% or greater except ca. 55% for 5 wt% siRNA-charged particles).

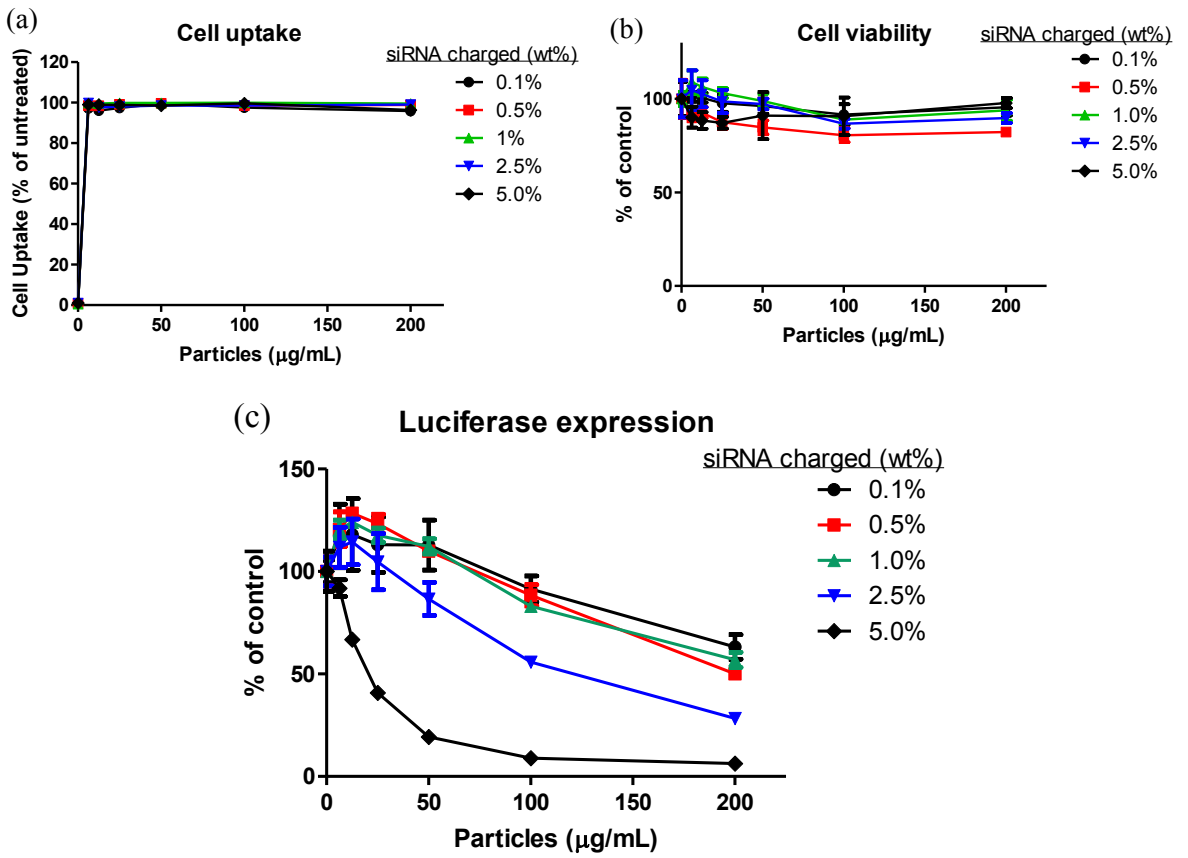

Figure 3.34 (a) HeLa cell uptake, (b) viability, and (c) luciferase expression after dosing with particles containing different siRNA loadings.

Cell uptake occurred rapidly at low doses and viability was maintained across all dosing concentrations (Figure 3.34a,b). Luciferase gene silencing efficiency increased with siRNA loading where gene knockdown was most effective for hydrogels charged with 5 wt% siRNA (Figure 3.34c).

Next, 80x320 nm hydrogel nanoparticles were evaluated for scale-up fabrication and gene silencing activity. Characterization of hydrogels through Zetasizer analysis indicated a positive ζ-potential of ca. +23 mV and a diameter around 260 nm (Table 3.16). When particles were dosed on HeLa cells, viability was maintained across all dosing concentrations (Figure 3.35a). Gene silencing was achieved notably for cells dosed with 80x320 nm hydrogels. Gene silencing efficiency of hydrogels prepared through the scalable protocol

may not be as high as for pro-siRNA particles fabricated through closed-face curing and mechanical harvesting due to difference in particle morphology and siRNA release characteristics. Combining components from the closed-face curing protocol with water-soluble LED photoinitiator may allow for equivalent transfection efficiency by particles prepared through a scalable protocol.

Table 3.16 Zetasizer analysis of LED-cured 80x320 nm hydrogel nanoparticles.

Particle dimensions (nm)	ζ-potential / mV	D_z / nm
80x320	+23.2 ± 3.9	258.8 ± 5.5

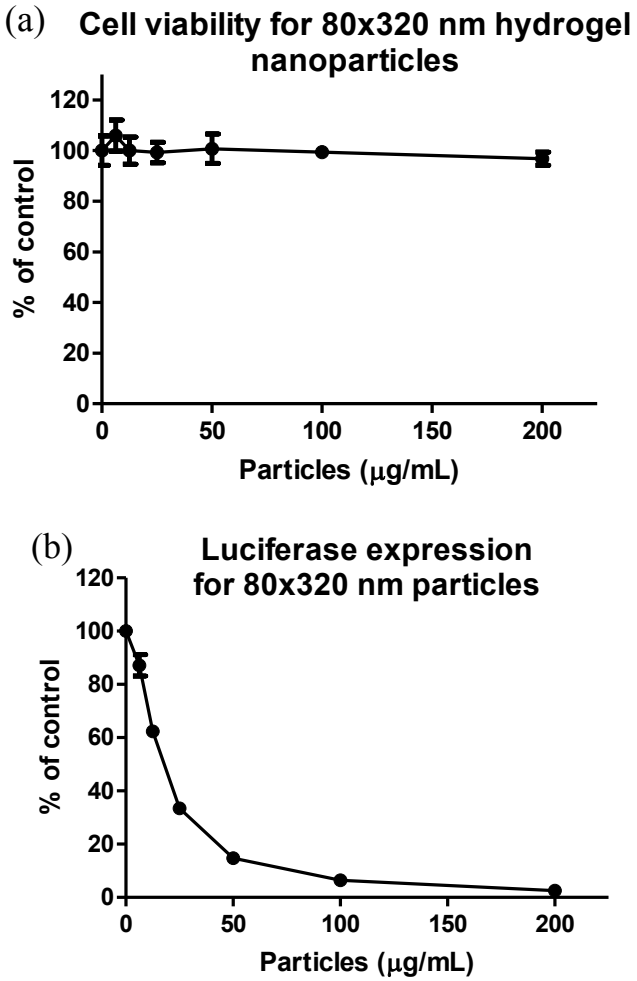

Figure 3.35 (a) Viability and (b) luciferase expression of HeLa cells dosed with rice-shaped, pro-siRNA hydrogel nanoparticles fabricated through LED curing.

3.6 Future work for siRNA-conjugated, functionalized hydrogels

Delivery of RNAi therapies *in vivo* to treat various disease targets may be pursued with well-defined particulate vectors prepared *via* PRINT technology. Derivatives of siRNA macromers containing acid-labile or enzymatically-degradable linkages may be pursued to explore different release profiles under biologically relevant conditions. Additional matrices and coatings may be explored to further enhance biocompatibility, endosomal escape, biodistribution, and targeting particular cells. Instead of polymerizing siRNA into hydrogel matrices, particles may be conjugated with siRNA post-fabrication to control surface density of siRNA on particles.

3.6.1 siRNA macromers with different degradable linkages

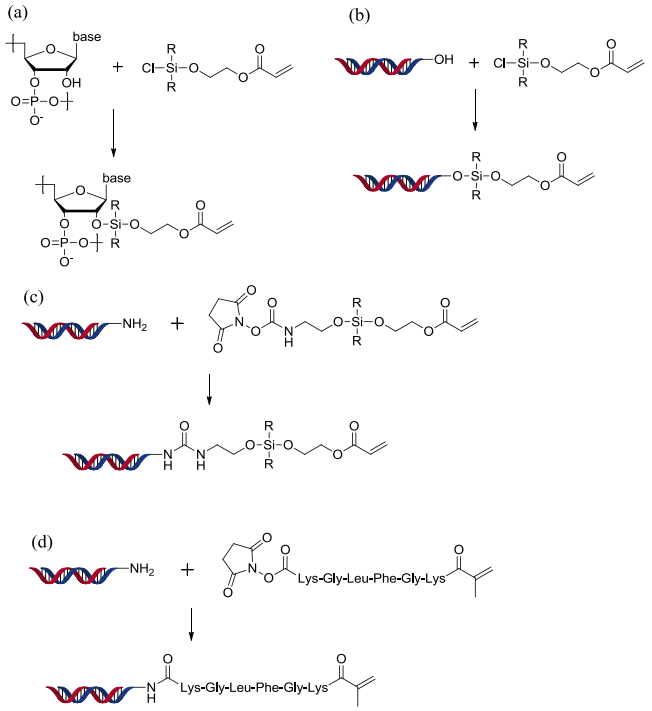

Figure 3.36 Synthetic routes to siRNA pro-drug macromers containing degradable linkages. (a) 2'-hydroxyl groups of the backbone or the (b) 5' terminal alcohol of the oligonucleotide may be reacted with acrylate-functionalized chlorosilanes. (c) Amine-terminated siRNA may be reacted with an NHS-activated chlorosilane to yield a pendant silyl ether prodrug. (d) siRNA may be end-functionalized with a NHS-activated, methacrylated Cathepsin B-cleavable peptide for use as a prodrug.

Photopolymerizable siRNA macromers bearing acid-labile or enzymatically degradable linkages may be prepared to explore the controlled release of cargo from particles under different environments. For example, native siRNA may be reacted with chlorosilane acrylates in different stoichiometric ratios to yield siRNA macromers containing silyl ether linkages from nucleobases off the backbone or at the terminal end of the oligonucleotide (Figure 3.36). Controlled terminal conjugation of siRNA with silyl ether linkages may be carried out by reacting an NHS-activated silyl ether acrylate with amine-terminated siRNA. Endosomal and lysosomal peptidases like Cathepsin B may be harnessed to cleave degradable peptide linkages installed in the siRNA macromer by linking a heterobifunctional peptide containing an NHS and methacrylate with amine-terminated siRNA.

3.6.2 Additional matrices for siRNA-conjugated hydrogels

For mucociliary transport of particles, chitosan has been demonstrated to exhibit enhanced mucociliary properties. One of the principal repeating units of chitosan is glucosamine, which may be acrylated to create a photopolymerizable monomer applicable to fabrication of hydrogels. α-alkyl acrylic acids (such as propylacrylic acid) may be used as major constituents of hydrogel matrices that are water-soluble and negatively charged at physiological pH; yet, under endosomal (acidic) conditions, poly(propyl acrylic acid) undergoes a conformational change upon protonation of carboxylates to behave endosomolytically. Amine-containing monomers such as those listed in 2.7.2 may also be used in hydrogel matrices.

Controlled radical polymerizations may afford greater conversion of siRNA macromers into the particle matrix and a well-defined network structure. ATRP and RAFT

polymerizations have been conducted to produce nanogels and may potentially be applied to PRINT given the correct fabrication conditions. Preparing particles through solution polymerizations may also enable better incorporation of siRNA macromers and enhance uniformity of network structure. Larger mold feature sizes may facilitate retention of solvent when open-face curing without taking additional steps to prevent evaporation such as chill plates or covering the filled molds. To enable UV-LED curing of filled molds from water-based solutions, a hydrophilic phosphine oxide photoinitiator may be pursued (Figure 3.37).

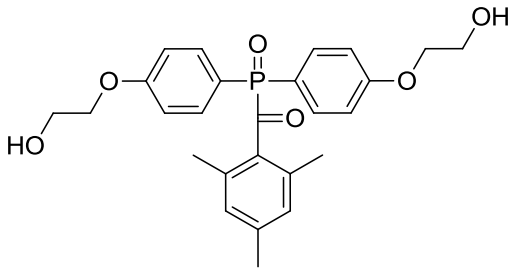

Figure 3.37 Proposed structure of water-soluble phosphine oxide photoinitiator.

3.6.3 Endosomolytic coatings on nanoparticles for gene delivery

In addition to functionalized poly(acrylic acid) derivatives mentioned in the previous chapter, poly(alkyl acrylic acid)s could be functionalized with mPEG and ligands to enable stealthing, targeting, and endosomolytic features. Poly(alkyl acrylic acid)s have demonstrated promise for endosomolysis toward delivery of biologics to the cellular cytoplasm.[33] Functional poly(glutamic acid)s may be pursued as a biodegradable polyanionic coating. Hyaluron, a carboxylic acid-containing polysaccharide, may be coated to cationic particles to provide a negative charge and act as a targeting ligand to melanoma cells.

3.6.4 Conjugation of siRNA post-particle fabrication

To avoid the need for collecting the siRNA remaining on the delivery sheet after filling molds, siRNA may be conjugated to the particle post fabrication. Conjugation strategies may be similar to nucleic acid nanostructures[6,34] where a high density of siRNA may be packed onto the surface of nanoparticles. High density of oligonucleotides conjugated to the particle surface, obtained through use of high salt concentration during conjugation reactions to minimize electrostatic repulsion, has potential to minimize nuclease degradation, provide diffusion through tissue, and enable cell uptake without posing toxicity from amine-containing species. Non-degradable conjugation strategies for siRNA to particles may entail implementing carboxylic acid-containing monomers like 2-carboxyethyl acrylate in the matrix which may be conjugated to amine-terminated siRNA through sulfo-NHS/EDC chemistry. Alkyne-containing acrylates may be implemented in particle matrices as well for conjugation with azide-terminated siRNAs through click chemistry.

To conjugate siRNA to particles through degradable linkages post-particle fabrication, heterobifunctional monomers containing degradable linkages may be pursued. For example, disulfide-containing monomers with an acrylate and a functional group may be used as illustrated in Fig 3.38. The first monomer may be synthesized by reacting 3,3'-dithiodipropionic acid with 2-aminoethylmethacrylate where this disulfide-containing monomer may be incorporated into the pre-particle solution. Subsequently, the carboxylic acid may be activated with EDC/sNHS for subsequent conjugation of amine-terminated siRNA. The second monomer may be prepared as described in section 3.2. As a control, the third monomer illustrated (an acrylamide, NHS-activated monomer) may be charged into the pre-particle solution for stable conjugation of siRNA. In case stability of the NHS carbonates

is compromised in particle fabrication, the alcohol precursors may be used as monomers followed by activation with disuccinimidyl carbonate (in large excess) post-particle fabrication for subsequent conjugation of siRNA.

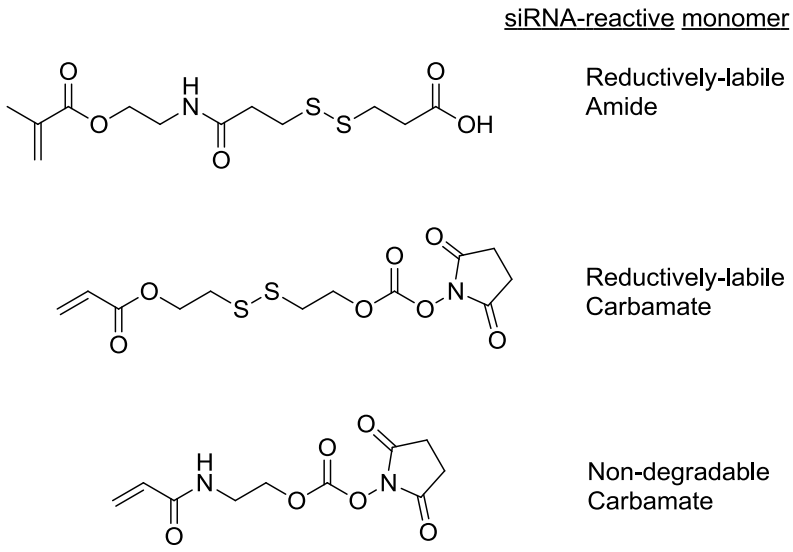

Figure 3.38 Structures of monomers that may be used to conjugate siRNA post-particle fabrication and corresponding bonds formed with siRNA.

3.6.5 Delivery targets for RNAi

Systemic delivery of siRNA through intravenous injection represents one of the most common modes of administration for liver and cancer therapies. For effective systemic delivery, generally stealthing and targeting ligands are required to passively reach the tissue and then target cell receptors for uptake. Targeting delivery vehicles to the RES (monocytes) should be easily accomplished by using ligands such as mannose to target the mannose receptor where GFP and therapeutic models may be investigated, e.g. chemokine receptor CCR2 in atherosclerosis.

Conventional systemic therapy may involve tumor targets, which feature leaky vasculature that can be harnessed in the enhanced permeability and retention effect for

increased accumulation in tumor areas. Nanoparticles may be decorated with ligands targeting the tumor endothelium, such as the RGD peptide, and loaded with siRNA against vascular endothelial growth factor (VEGF) to suppress tumor growth. In targeting tumor cells, the identity of the ligand will depend on the type of cancer, e.g. prostate specific membrane antigens may be targeted with aptamers decorated on nanoparticles containing anticancer siRNA against KIF11, which can cause cellular apoptosis. Direct intratumoral injection of delivery vectors in xenograft models may enable increased transfection relative to systemic administration. Loading magnetite (iron oxide nanoparticles) into polymeric nanoparticles may enable tissue-specific delivery of siRNA as has been demonstrated by LipoMag, an oleic acid-coated magnetic core with a cationic lipid shell[35] that is guided to tumors with a magnetic field.

Iontophoretic delivery devices may be utilized to drive charged particles into the tissue of interest with greater accumulation. Prodrug approaches to siRNA delivery could be instrumental in iontophoresis of particles due to the use of an electric field that would most likely destroy the electrostatic association of physically-entrapped siRNA with cationic particles. Microneedles may be used separately or in combination with iontophoretic delivery devices to transport siRNA to relevant tissues through topical application. Inhalation of aerosolized nanoparticles containing siRNA could provide therapeutic value in treating cystic fibrosis, asthma, influenza, or the common cold. Different modes of delivering siRNA, harnessing PRINT technology, with optimized physicochemical properties of vectors, may enable RNAi in tissues not easily accessible through traditional nanoparticle formulations or local routes of administration to treat diseases that pose many challenges for conventional therapies.

References

(1) Jeong, J. H.; Mok, H.; Oh, Y.-K.; Park, T. G. *Bioconjugate Chemistry* **2009**, *20*, 5-14.

(2) Soutschek, J.; Akinc, A.; Bramlage, B.; Charisse, K.; Constien, R.; Donoghue, M.; Elbashir, S.; Geick, A.; Hadwiger, P.; Harborth, J.; John, M.; Kesavan, V.; Lavine, G.; Pandey, R. K.; Racie, T.; Rajeev, K. G.; Röhl, I.; Toudjarska, I.; Wang, G.; Wuschko, S.; Bumcrot, D.; Koteliansky, V.; Limmer, S.; Manoharan, M.; Vornlocher, H.-P. *Nature* **2004**, *432*, 173-178.

(3) Siegwart, D. J.; Whitehead, K. A.; Nuhn, L.; Sahay, G.; Cheng, H.; Jiang, S.; Ma, M.; Lytton-Jean, A.; Vegas, A.; Fenton, P.; Levins, C. G.; Love, K. T.; Lee, H.; Cortez, C.; Collins, S. P.; Li, Y. F.; Jang, J.; Querbes, W.; Zurenko, C.; Novobrantseva, T.; Langer, R.; Anderson, D. G. *Proceedings of the National Academy of Sciences of the United States of America* **2007**, *104*, 12982-12987.

(4) Musacchio, T.; Vaze, O.; D'Souza, G.; Torchilin, V. P. *Bioconjugate Chemistry* **2010**, *21*, 1530-1536.

(5) Zhang, Y.; Zhang, Y.-F.; Bryant, J.; Charles, A.; Boado, R. J.; Pardridge, W. M. *Clinical Cancer Research* **2004**, *10*, 3667-3677.

(6) Cutler, J. I.; Zhang, K.; Zheng, D.; Auyeung, E.; Prigodich, A. E.; Mirkin, C. A. *Journal of the American Chemical Society* **2011**, *133*, 9254-9257.

(7) Singh, N.; Agrawal, A.; Leung, A. K. L.; Sharp, P. A.; Bhatia, S. N. *Journal of the American Chemical Society* **2010**, *132*, 8241-8243.

(8) Hsu, T.; Mitragotri, S. *Proceedings of the National Academy of Sciences of the United States of America* **2011**, *108*, 15816-15821.

(9) Oishi, M.; Nagasaki, Y.; Itaka, K.; Nishiyama, N.; Kataoka, K. *Journal of the American Chemical Society* **2005**, *127*, 1624-1625.

(10) Rozema, D. B.; Lewis, D. L.; Wakefield, D. H.; Wong, S. C.; Klein, J. J.; Roesch, P. L.; Bertin, S. L.; Reppen, T. W.; Chu, Q.; Blokhin, A. V.; Hagstrom, J. E.; Wolff, J. A. *Proceedings of the National Academy of Sciences of the United States of America* **2007**, *104*, 12982-12987.

(11) Lewis, C. L.; Choi, C.-hyung; Lin, Y.; Lee, C.-S.; Yi, H. *Langmuir* **2010**, *82*, 5851-5858.

(12) Pregibon, D. C.; Doyle, P. S. *Analytical Chemistry* **2009**, *81*, 4873-4881.

(13) Beaudette, T. T.; Bachelder, E. M.; Cohen, J. A.; Obermeyer, A. C.; Broaders, K. E.; Fréchet, J. M. J.; Kang, E.-S.; Mende, I.; Tseng, W. W.; Davidson, M. G.; Engleman, E. G. *Molecular Pharmaceutics* **2009**, *6*, 1160-1169.

(14) Standley, S. M.; Mende, I.; Goh, S. L.; Kwon, Y. J.; Beaudette, T. T.; Engleman, E. G.; Fréchet, J. M. J. *Bioconjugate Chemistry* **2007**, *18*, 77-83.

(15) Gillies, E. R.; Goodwin, A. P.; Fréchet, J. M. J. *Bioconjugate Chemistry* **2004**, *3*, 1254-1263.

(16) Oishi, M.; Sasaki, S.; Nagasaki, Y.; Kataoka, K. *Biomacromolecules* **2003**, *4*, 1426-1432.

(17) MacKay, J. A.; Chen, M.; McDaniel, J. R.; Liu, W.; Simnick, A. J.; Chilkoti, A. *Nature Materials* **2009**, *8*, 993-999.

(18) Chau, Y.; Tan, F. E.; Langer, R. *Bioconjugate Chemistry* **2004**, *15*, 931-41.

(19) Satchi-Fainaro, R.; Puder, M.; Davies, J. W.; Tran, H. T.; Sampson, D. A.; Greene, A. K.; Corfas, G.; Folkman, J. *Nature Medicine* **2004**, *10*, 255-261.

(20) Meng, F.; Hennink, W. E.; Zhong, Z. *Biomaterials* **2009**, *30*, 2180-2198.

(21) Schafer, F. Q.; Buettner, G. R. *Free Radical Biology & Medicine* **2001**, *30*, 1191-1212.

(22) Feener, E. P.; Shen, W. C.; Ryser, H. *Journal of Clinical Investigation* **1986**, *77*, 977-984.

(23) Kim, S. H.; Jeong, J. H.; Lee, S. H.; Kim, S. W.; Park, T. G. *Journal of Controlled Release* **2006**, *116*, 123-129.

(24) York, A. W.; Huang, F.; McCormick, C. L. *Biomacromolecules* **2010**, *11*, 505-514.

(25) Vázquez-Dorbatt, V.; Tolstyka, Z. P.; Chang, C.-W.; Maynard, H. D. *Biomacromolecules* **2009**, *10*, 2207-12.

(26) Romberg, B.; Hennink, W. E.; Storm, G. *Pharmaceutical Research* **2008**, *25*, 55-71.

(27) Harris, T. J.; Green, J. J.; Fung, P. W.; Langer, R.; Anderson, D. G.; Bhatia, S. N. *Biomaterials* **2010**, *31*, 998-1006.

(28) Lillis, A. P.; Duyn, L. B. V. A. N.; Murphy-Ullrich, J. E.; Strickland, D. K. *Physiological Reviews* **2008**, *88*, 887-918.

(29) Herz, J.; Strickland, D. K. *Journal of Clinical Investigation* **2001**, *108*, 779-784.

(30) Weeke-Klimp, A. H.; Bartsch, M.; Morselt, H. W. M.; Van Veen-Hof, I.; Meijer, D. K. F.; Scherphof, G. L.; Kamps, J. A. A. M. *Journal of Drug Targeting* **2007**, *15*, 585-594.

(31) Ludtke, J. J.; Sokoloff, A. V.; Wong, S.; Zhang, G.; Strickland, D. K.; Wolff, J. A. *Drug Delivery* **2009**, *16*, 268-273.

(32) Wong, S. C.; Wakefield, D.; Klein, J.; Monahan, S. D.; Rozema, D. B.; Lewis, D. L.; Higgs, L.; Ludtke, J.; Sokoloff, A. V.; Wolff, J. A. *Molecular Pharmaceutics* **2006**, *3*, 386-397.

(33) Jones, R. A; Cheung, C. Y.; Black, F. E.; Zia, J. K.; Stayton, P. S.; Hoffman, A. S.; Wilson, M. R. *The Biochemical Journal* **2003**, *372*, 65-75.

(35) Zheng, D.; Giljohann, D. A.; Chen, D. L.; Massich, M. D.; Wang, X.-Q.; Iordanov, H.; Mirkin, C. A.; Paller, A. S. *Proceedings of the National Academy of Sciences of the United States of America* **2012**, 1-6.

(36) Namiki, Y.; Namiki, T.; Yoshida, H.; Ishii, Y.; Tsubota, A.; Koido, S.; Nariai, K.; Mitsunaga, M.; Yanagisawa, S.; Kashiwagi, H.; Mabashi, Y.; Yumoto, Y.; Hoshina, S.; Fujise, K.; Tada, N. *Nature Nanotechnology* **2009**, *4*, 598-606.

APPENDIX

BIODEGRADABLE POLY(ESTER)-BASED RICE-SHAPED NANOPARTICLES FOR GENE SILENCING IN CANCER CELLS

A.1 Introduction to biodegradable poly(ester)s for delivery of siRNA

Polyesters present attractive qualities as a matrix in the delivery of siRNA such as biocompatibility, lack of toxicity, bioabsorption (biodegradation), and high stability. The backbone of polyesters may be degraded hydrolytically or enzymatically to produce low molecular weight fragments and ultimately small molecule acids. Hydrophobic thermoplastic polyesters are melt-processable and water-insoluble materials, whose rate of hydrolytic degradation depends on morphology. Increased crystallinity leads to a slower rate of hydrolytic degradation due to limited access of water to attack the ester backbone. Chemical structures of three common polyesters, which are all FDA-approved materials, are illustrated in Figure A.1. As homopolymers, all materials are semicrystalline with poly(ε-caprolactone) (PCL) having the slowest rate of degradation due to its longer aliphatic chain length (hydrophobicity). Combining polyester homopolymers can produce amorphous thermoplastics, e.g. poly(lactic-co-glycolic acid) (PLGA), which is a commonly used copolymer of poly(glycolic acid) and poly(lactic acid) with relevant degradation times and processing properties toward drug delivery.

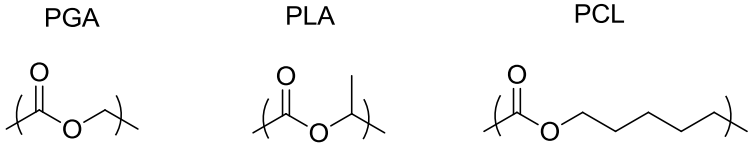

Figure A.1 Structures of poly(glycolic acid), poly(lactic acid), and poly(ε-caprolactone).

PLGA nanoparticles have been prepared in a double emulsion solvent evaporation technique with siRNA and spermine, a biological polyamine that significantly enhanced encapsulation efficiency and enabled effective gene silencing *in vitro*.[1] Steady release of siRNA from PLGA nanoparticles was observed under biologically relevant conditions and sustained gene silencing was elicited by vaginal instillation of particles into the reproductive tract of female mice. The double emulsion solvent evaporation technique has also been applied to prepare siRNA-loaded PLGA nanoparticles using acetylated bovine serum albumin to stabilize the primary emulsion and notably enhance encapsulation efficiency.[2] Slow release of siRNA from these PLGA nanoparticles was observed in buffer and released siRNA silenced gene expression *in vitro* when complexed with Lipofectamine™ 2000. Blends of polyethyleneimine, polyethylene glycol, and chitosan with PLGA and siRNA have been formulated to produce nanoparticles through nanoprecipitation to enable gene knockdown *in vitro*.[3] In contrast to the requirement for additional materials to enhance encapsulation of siRNA in PLGA particles, PRINT allows for the direct encapsulation of siRNA within the PLGA matrix. Multiple siRNAs have been delivered in lipid-coated PLGA PRINT nanoparticles toward the treatment of prostate cancer.[4]

A.2 PLGA and PCL particle matrices for gene silencing in cancer cells

Two polyester particle matrices were evaluated for their ability to transfect cells with siRNA. PLGA and PCL, with different rates of degradation, were independently tested to prepare PRINT nanoparticles for gene silencing.

A.2.1 Experimental

A.2.1.1 Materials

PLGA (85:15 lactic acid:glycolic acid, MW = 50 kDa) was purchased from Sigma Aldrich. PCL (MW = 43-50 kDa) was purchased from Polysciences. Luciferase and control siRNA sequences used in these studies are listed in section 2.2.1.1 and 2.3.1.1. DOTAP:DOPE transfection lipid was obtained from Avanti Polar Lipids, Inc. 80x320 nm molds were graciously provided by Liquidia Technologies. Krosflow® MicroKros (X1-500S-200) tangential flow filtration apparatus was obtained from Spectrum Labs.

A.2.1.2 Fabrication of siRNA-containing, lipid-coated PLGA and PCL nanoparticles

A 2 wt% solution of 95:5 (wt:wt) of PLGA or PCL:siRNA was prepared in DMF (using an aliquot of siRNA dissolved in DEPC-treated water at 50 mg/mL) from which a film was cast on a PET sheet using a #5 Mayer Rod while evaporating solvent with a heat gun. 80x320 nm Liquidia molds were filled by lamination against PCL-siRNA and PLGA-siRNA films using a heated nip laminator at 270 ºF (80 psi) and 240 ºF. After cooling to room temperature wherein vitrification of PLGA and crystallization of PCL may occur, filled molds were laminated against PVA-coated PET under the same heated nip conditions. After delaminating the mold from the harvesting layer, particles were bead-harvested with DEPC-treated water or a lipid-containing solution using 1 mL of solvent per ft of particles. Particles were subsequently purified through tangential flow filtration using ca. 15 mL of water for 2 mg of particles.

A.2.2 PLGA particles

80x320 nm PLGA particles fabricated with luciferase or control siRNA were harvested with 0.25 mg of lipid per ft of particles and washed through tangential flow

filtration (TFF). Harvested 80x320 nm particles appear rice-shaped and monodisperse (Figure A.2). Zetasizer analysis of lipid-coated siRNA particles shows that particles are positively charged with diameters around 300 nm. When lipid-coated particles were dosed on HeLa cells stably transfected with luciferase firefly gene, sequence-specific and dose-dependent gene silencing was observed. Specifically, control siRNA-loaded particles did not reduce luciferase expression significantly in comparison to luciferase-containing particles (Figure A.3). After confirming that lipid-coated particles could effectively transfect HeLa cells, PCL was evaluated as a slow-degrading particle matrix for gene silencing.

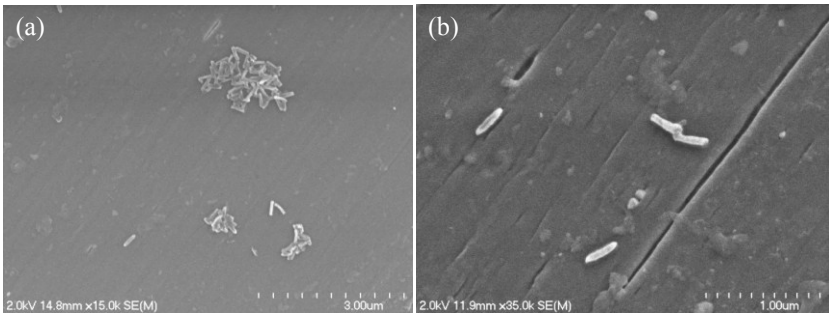

Figure A.2 SEM micrographs of (a) control and (b) anti-luciferase siRNA-loaded lipidated PLGA rice.

Table A.1 Zetasizer characterization of lipid-coated, PLGA rice.

siRNA particle	ζ-potential / mV	D_z / nm
Anti-luciferase	+8.03	314.3
Control	+10.8	307.1

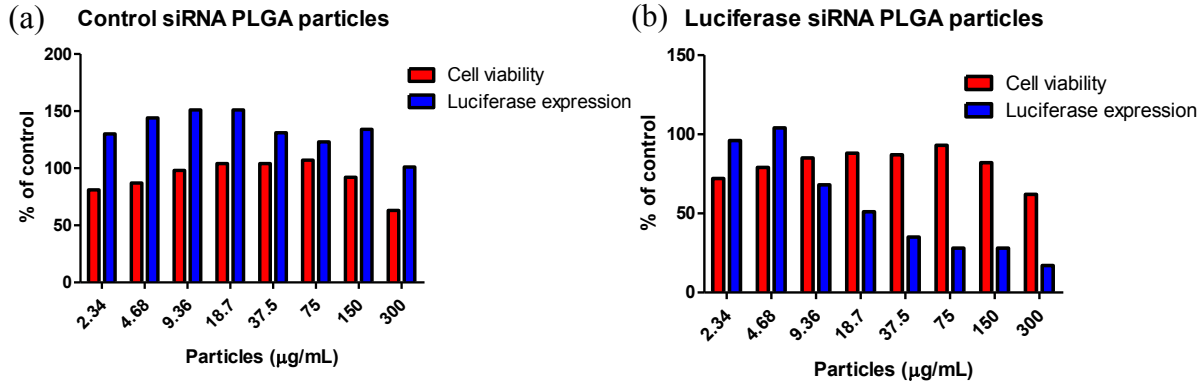

Figure A.3 Viability and luciferase expression of HeLa cells dosed with lipidated PLGA rice containing (a) control or (b) anti-luciferase siRNA for 4 h followed by 72 h incubation at 37 ºC in media.

A.2.3 PCL particles

Anti-luciferase and control siRNA-charged rice-shaped PCL nanoparticles were coated with increasing amounts of transfection lipid and purified through TFF to optimize biocompatibility and gene silencing efficiency. 80x320 nm lipid-coated particles appear monodisperse and to adopt the correct dimensions (Figure A.4). Diameters of all particles were around 220-240 nm, which is lower than PLGA particles due to the absence of a small aggregate peak (Table A.2). Lipid concentration-dependent ζ-potentials were observed for lipidated PCL rice.

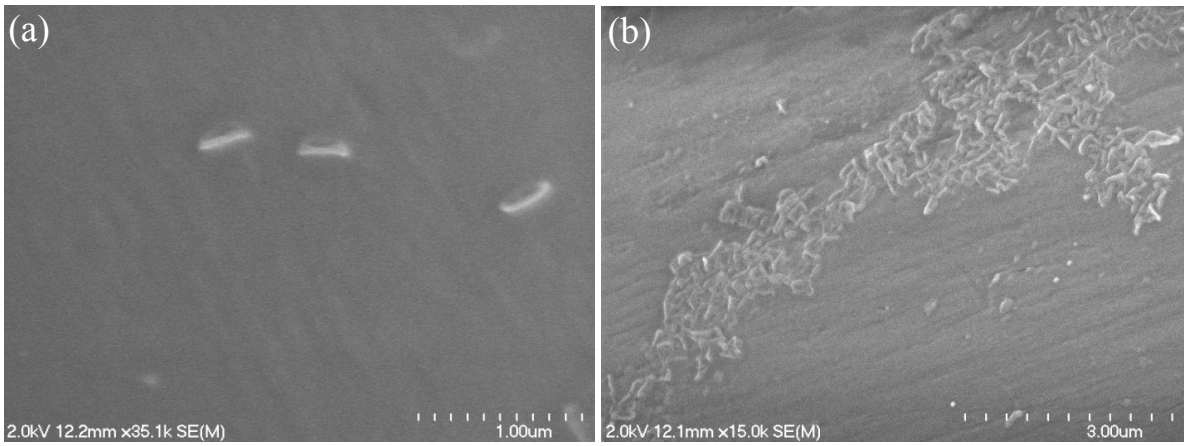

Figure A.4 SEM micrographs of (a) control and (b) anti-luciferase siRNA-containing lipidated PCL rice.

Table A.2 Zetasizer analysis of PVA-harvested and lipid-coated PCL particles.

[Lipid], siRNA*	ζ-potential / mV	D_z / nm
0 A	-3.92	233.7
0 C	-3.01	229.3
0.05 A	-1.64	228.2
0.05 C	-0.64	227.4
0.10 A	+1.00	231.9
0.10 C	+0.81	239.8
0.15 A	+8.69	230.8
0.15 C	+8.91	234.7
0.20 A	+12.7	244.7
0.20 C	+11.7	225.8

*[Lipid] represents the DOTAP:DOPE stock solution concentration (mg/mL); A and C are anti-luciferase and control siRNA.

siRNA-containing, lipid-coated particles were dosed on luciferase-transfected HeLa cells for 4 h followed by 72 h incubation. Gene silencing efficiency increased with particle dose and mostly with lipid concentration, reaching an EC_{50} of ~ 64 nM for particles coated with 0.2 mg of lipid per ft of particle based on 100% encapsulation efficiency. However, cytotoxicity was noted at high doses of particles coated with lipid at 0.2 mg/ft.

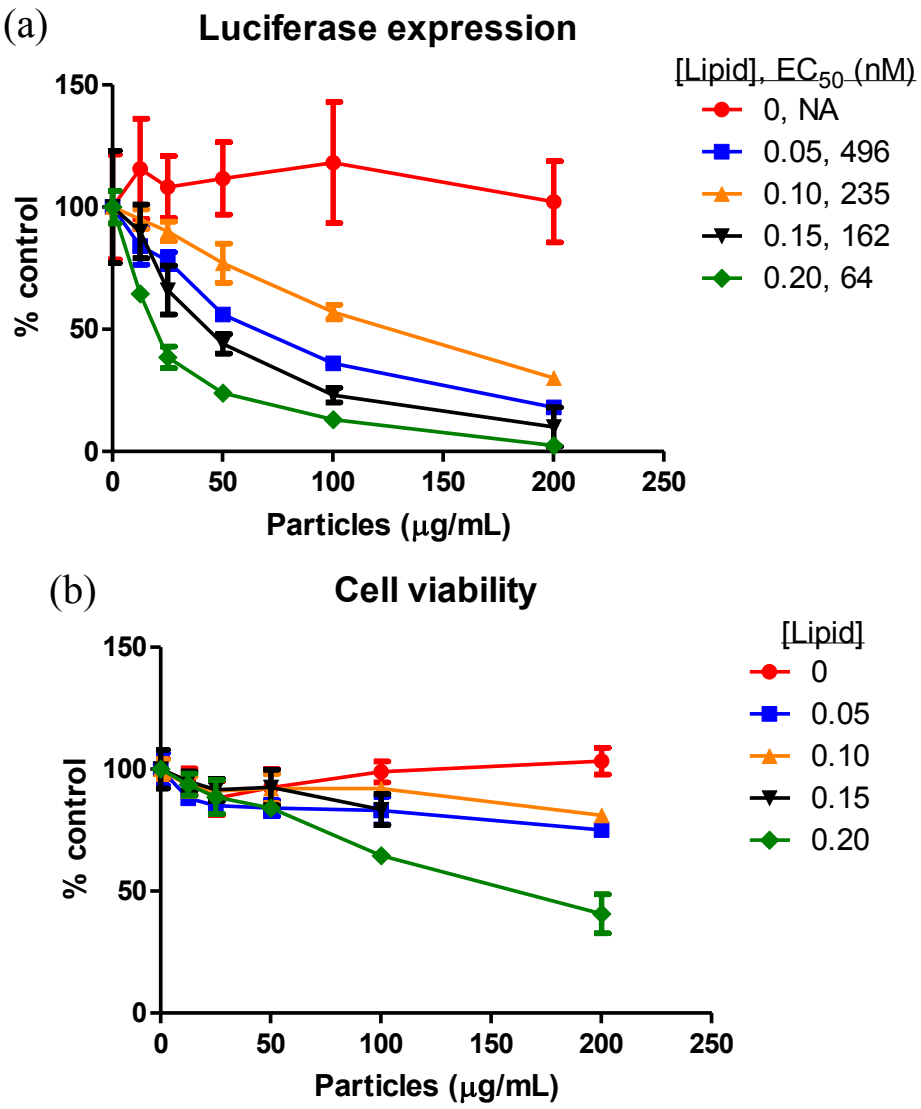

Figure A.5 (a) Luciferase expression and (b) viability of HeLa cells dosed with particles coated with increasing amounts of DOTAP:DOPE and at increasing particle concentration for 4 h followed by 72 h incubation at 37 ºC in media. EC_{50}s were calculated based on 100% encapsulation efficiency.

A.2.4 Future Work

To enable systemic delivery of PLGA nanoparticles *in vivo*, PEG lipids, e.g. 1,2-distearoyl-sn-glycero-3-phosphoethanolamine (DSPE-PEG), may be mixed into the cationic lipid harvesting solution. Cells may be targeted with nanoparticles *via* use of ligand-terminated lipids in addition to cationic and stealthing ligands. Alternatively, polyanions like poly(glutamic acid) may be electrostatically absorbed to cationic lipid-coated particles. Polyacid-tethered ligands may enable targeting to specific cellular receptors for selective internalization.

Increased encapsulation of siRNA and retention in the particle matrix may be afforded by amine-containing end groups and main chain polyesters. For example, oligomeric or low molecular weight *telechelic* PLGA (dicarboxylic acid) may be reacted with diethylenetriamine to install secondary amines and amides into the backbone. Also, diacid end groups may be reacted with a variety of amines, e.g. 2-(4-isopropylpiperazin-1-yl)ethanamine. Covalent attachment of siRNA to PCL may be achieved through acid- or reductively-labile bonds (Figure A.6).

Efficacious polyester-based siRNA delivery vehicles for systemic administration would contribute to biodegradable, non-toxic platforms using FDA-approved materials in the treatment of diseases.

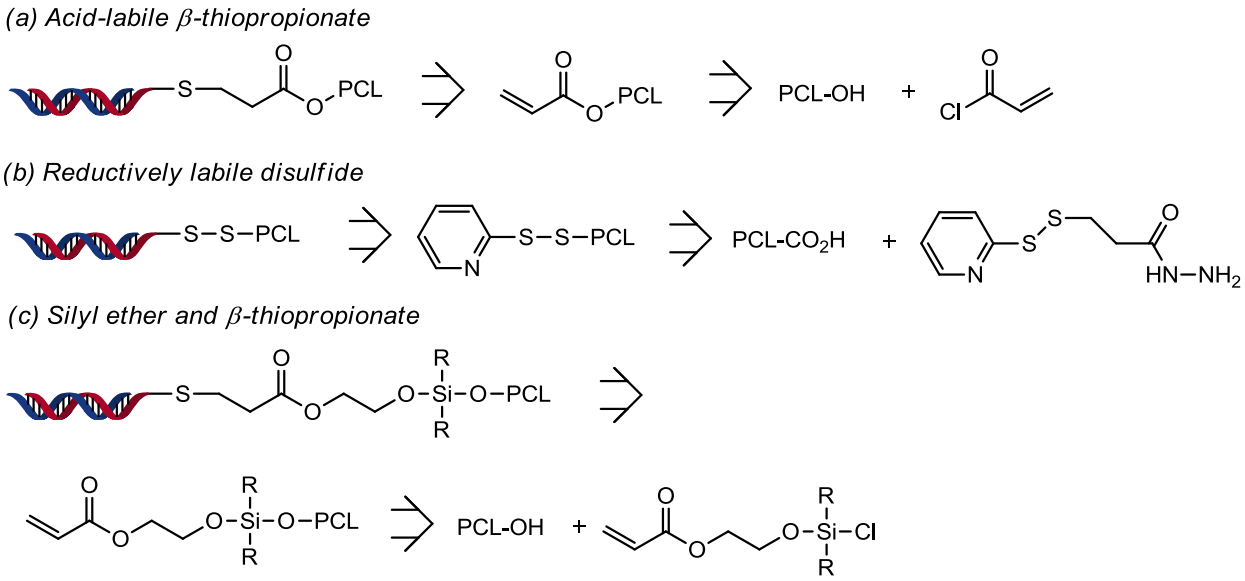

Figure A.6 Retrosynthetic schemes toward siRNA-PCL pro-drug conjugates for covalent incorporation and triggered release from the particle matrix.

References

(1) Woodrow, K. A.; Cu, Y.; Booth, C. J.; Saucier-Sawyer, J. K.; Wood, M. J.; Saltzman, W. M. *Nature Materials* **2009**, *8*, 526-533.

(2) Cun, D.; Jensen, D. K.; Maltesen, M. J.; Bunker, M.; Whiteside, P.; Scurr, D.; Foged, C.; Nielsen, H. M. *European Journal of Pharmaceutics and Biopharmaceutics* **2011**, *77*, 26-35.

(3) Wang, J.; Feng, S.-S.; Wang, S.; Chen, Z.-Y. *International Journal of Pharmaceutics* **2010**, *400*, 194-200.

(4) Hasan, W.; Chu, K.; Gullapalli, A.; Dunn, S. S.; Enlow, E. M.; Luft, J. C.; Tian, S.; Napier, M. E.; Pohlhaus, P. D.; Rolland, J. P.; DeSimone, J. M. *Nano Letters* **2012**, *12*, 287-292.